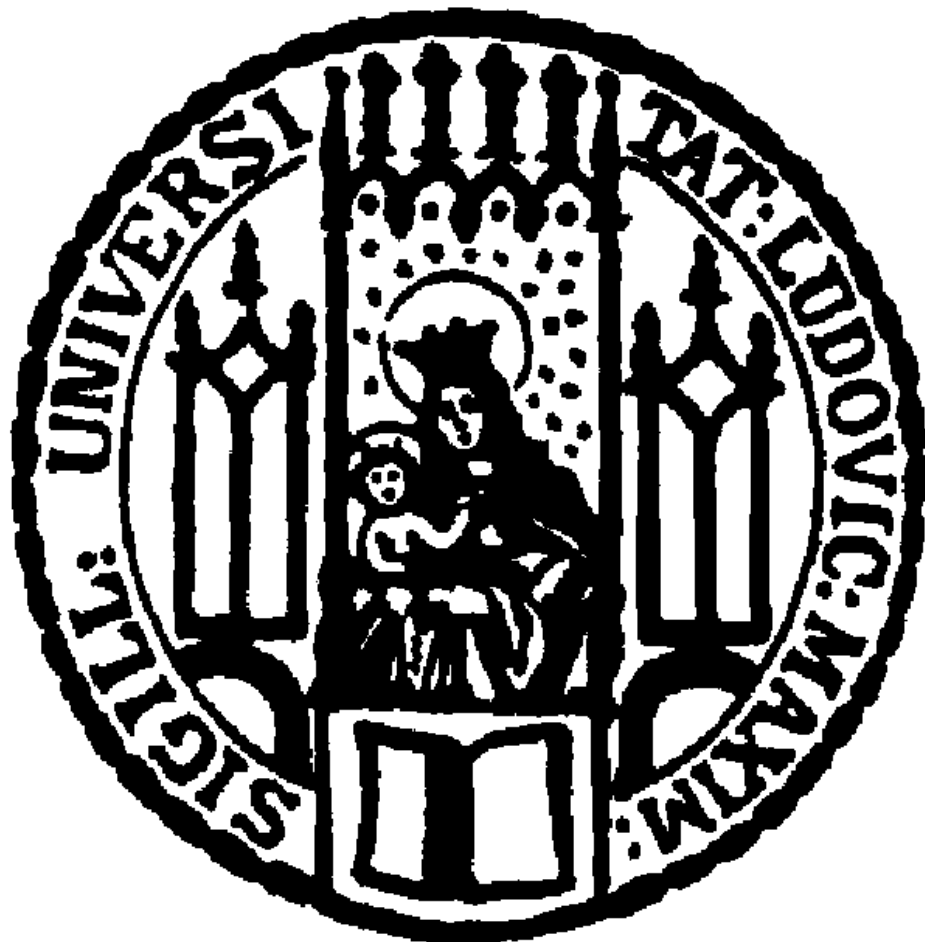


Analysis of Manganese Transporters belonging to the UPF0016 Protein Family



Dissertation

Zur Erlangung des Doktorgrades der Naturwissenschaften
an der Fakultät für Biologie
der Ludwig-Maximilians-Universität München

Natalie Marina Hoècker

München

August 2021

Diese Dissertation wurde angefertigt unter der Leitung von PD Dr. Anja Schneider im Bereich „Molekulare Pflanzenwissenschaften“ an der Fakultät für Biologie der Ludwig-Maximilians-Universität München

Datum der Abgabe: 04.08.2021

Datum der mündlichen Prüfung: 27.10.2021

Erstgutachter: PD Dr. Anja Schneider

Zweitgutachter: Prof. Dr. Hans-Henning Kunz

„Die Natur ist unerbittlich und unveränderlich, und es ist ihr gleichgültig, ob die verborgenen Gründe und Arten ihres Handelns dem Menschen verständlich sind oder nicht.“

Galileo Galilei (1564 - 1642)

Eidesstattliche Erklärung

Ich versichere hiermit an Eid statt, dass die vorgelegte Dissertation von mir selbstständig und ohne unerlaubte Hilfe angefertigt wurde. Des Weiteren erkläre ich, dass ich nicht anderweitig ohne Erfolg versucht habe, eine Dissertation einzureichen oder mich der Doktorprüfung zu unterziehen. Die folgende Dissertation liegt weder ganz noch in wesentlichen Teilen einer anderen Prüfungskommission vor.

München, 04.08.2021

M.Sc. N. Hoècker

Statutory declaration

I declare that I have authored this thesis independently and that I have not used other than the declared (re)sources. As well I declare that I have not submitted a dissertation without success and not passed the oral exam. The present dissertation (neither the entire dissertation nor parts) has not been presented to another examination board.

München, 04.08.2021

M.Sc. N. Hoècker

Content

1	Abbreviations	7
2	List of publications with declaration of contribution	9
3	Summary	11
4	Zusammenfassung	13
5	Aim of the thesis	15
6	Introduction	16
6.1	Plant Nutrition	16
6.2	Manganese and its role in cellular processes	16
6.2.1	Role of Manganese in cellular processes	17
6.2.1.1	(N)-linked glycosylation.....	17
6.2.1.2	ROS antioxidation.....	18
6.2.1.3	Manganese in chloroplasts	18
6.3	Manganese transporters in plants	19
6.4	Uncharacterized Protein Families.....	21
6.4.1	Protein topology of Uncharacterized Protein Family 0016 (UPF0016) members	21
6.4.2	Prokaryotic members of UPF0016	24
6.4.2.1	The <i>Vibrio cholerae</i> Mn ²⁺ exporter A (MneA).....	24
6.4.2.2	The <i>Synechocystis</i> sp. PCC6803 Manganese Exporter (MNX/ SynPAM71)	25
6.4.3	Eukaryotic members of UPF0016.....	25
6.4.3.1	The <i>Homo sapiens</i> Transmembrane Protein 165 (TMEM165)	25
6.4.3.2	The <i>Saccharomyces cerevisiae</i> GCR Dependent Translation Factor 1 (GDT1)	26
6.4.3.3	The <i>Chlamydomonas reinhardtii</i> Conserved in Green Lineage and Diatom 1 (CGLD1)	27
6.4.3.4	<i>Arabidopsis thaliana</i> Photosynthesis Affected Mutant 71 (PAM71).....	28
7	Results.....	30
7.1	Publication I: The Plastid Envelope CHLOROPLAST MANGANESE TRANSPORTER1 Is Essential for Manganese Homeostasis in <i>Arabidopsis</i>	30
7.2	Publication II: Homologous Proteins of the Manganese Transporter PAM71 Are Localized in the Golgi Apparatus and Endoplasmic Reticulum	46

7.3	Publication III: Gene Replacement in Arabidopsis Reveals Manganese Transport as an Ancient Feature of Human, Plant and Cyanobacterial UPF0016 Proteins	61
8	Discussion.....	77
9	References	88
10	Appendix	99
10.1	List of Protein Sequences	99
10.2	Permission for republication	100
10.2.1	Publication I: The Plastid Envelope CHLOROPLAST MANGANESE TRANSPORTER1 Is Essential for Manganese Homeostasis in <i>Arabidopsis</i>	100
10.2.2	Publication II: Homologous Proteins of the Manganese Transporter PAM71 Are Localized in the Golgi Apparatus and Endoplasmic Reticulum	100
10.2.3	Publication III: Gene Replacement in Arabidopsis Reveals Manganese Transport as an Ancient Feature of Human, Plant and Cyanobacterial UPF0016 Proteins	101
11	Acknowledgement	102

1 Abbreviations

α	alpha
aa	amino acid
Arg (R)	arginine
Asp(D)	aspartic acid
bzw.	beziehungsweise
Ca^{2+}	divalent calcium cation/ zweiwertiges Calcium Kation
cTP	chloroplast target peptide
DNA	deoxyribonucleic acid/ Desoxyribonukleinsäure
EGT	endosymbiotic gene transfer
ER	endoplasmic reticulum
Glu (E)	glutamic acid
Gly (G)	glycine
H^+	proton/ Wasserstoff Kation
HGT	horizontal gene transfer
H_2O	water/ Wasser
H_2O_2	hydrogen peroxide/ Wasserstoffperoxid
LHCII	light harvesting complex des PSII
Lys (K)	lysine
M	molarity
mg	milligram
mM	millimol
Mn^{2+}	divalent manganese cation /zweiwertiges Mangan Kation
MnO_2	manganese dioxide
OEC	oxygen evolving complex
$\text{O}_2^{\cdot -}$	superoxide anion radical
PS	photosynthesis
PSI	photosystem I
PSII	photosystem II
ROS	reactive oxygen species

Abbreviations

Ser (S)	serine
Thr(T)	threonine
TM	transmembrane
WT	wildtype
µg	microgram

2 List of publications with declaration of contribution

Publication I

Eisenhut, M., Hoecker, N., Schmidt, S. B., Basgaran, R. M., Flachbart, S., Jahns, P., Eser, T., Geimer, S., Husted, S., Weber, A. P. M., Leister, D., & Schneider, A. (2018). The Plastid Envelope CHLOROPLAST MANGANESE TRANSPORTER1 Is Essential for Manganese Homeostasis in Arabidopsis. *Mol Plant*, 11(7), 955-969. <https://doi.org/10.1016/j.molp.2018.04.008>

E.M. and **N.H.** contributed equally to this work

Conceptualization, M.E. and A.S.; Investigation, M.E., **N.H.**, S.B.S., R.M.B., S.F., P.J., T.E., S.G., and A.S.; Resources, M.E., S.H., A.P.M.W., D.L., and A.S.; Writing – Original Draft, M.E. and A.S.; Writing – Review & Editing, M.E., S.B.S., and A.S.; Visualization, A.S.; Funding Acquisition, M.E., A.P.M.W., S.B.S., D.L., and A.S., Supervision, M.E. and A.S.

Investigation performed by **N.H.**:

Photography and genotyping of plant lines, Protein isolation and analysis (*In Vivo* pulse labeling/ translation), Western blots (steady state-levels), thylakoid and intact chloroplast isolation for further MS measurements and BN-PAGE (By S.B.S)), staining of Reactive Oxygen Species, Growth phenotype under different Mn conditions on MS plates, Transcription analysis

Investigation performed by M.E.:

Subcellular localization, Promotor-GUS Staining, Measurements of photochemistry parameters, writing, conceptualization and funding acquisition

Dr. M. Eisenhut

M.Sc. N. Hoècker

Publication II

Hoecker, N., Honke, A., Frey, K., Leister, D., & Schneider, A. (2020). Homologous Proteins of the Manganese Transporter PAM71 Are Localized in the Golgi Apparatus and Endoplasmic Reticulum. *Plants*, 9(2), 239.

Conceptualization, **N.H.** and A.S.; Investigation, **N.H.**, A.H., and K.F.; Resources, D.L. and A.S.; Writing, Visualization and Supervision, A.S.; Funding Acquisition, D.L. and A.S.

Publication III

Hoecker, N., Hennecke, Y., Schrott, S., Marino, G., Schmidt, S. B., Leister, D., & Schneider, A. (2021). Gene replacement in Arabidopsis reveals manganese transport as an ancient feature of human, plant and cyanobacterial UPF0016 proteins. *Frontiers in Plant Science*, 12, 1157

Conceptualization, A.S; Investigation and Analysis of Data, **N.H.**, Y.H., S.S., G.M., and S.B.S; Resources, D.L. and A.S.; Funding acquisition, S.B.S and A.S.; Writing – Original Draft, **N.H.** and A.S.; Writing – Review and Editing, S.B.S. and A.S.; All authors contributed to manuscript revision, read, and approved the submitted version.

München, den 19.07.2021

PD. Dr. A. Schneider

M.Sc. N. Hoëcker

3 Summary

Manganese (Mn) is an essential nutrient for proper plant growth and development. It is involved in many cellular processes as antioxidation, photosynthesis and glycosylation where it can act as a cofactor or an enzyme activator. One prominent role of Mn is being a cofactor of the oxygen evolving center (OEC) of photosystem II (PSII) in the chloroplast, catalyzing the water splitting reaction. Besides its role for optimal photosynthesis performance, Mn is also required in other compartments. Therefore, Mn needs to be translocated and distributed properly within the cell to maintain Mn-dependent metabolic processes in the respecting compartments. Mn deficiency leads to severe plant growth defects including interveinal chlorosis, and excess Mn leads to the accumulation of toxic Mn oxidation products also resulting in growth defects. Consequently, to prevent intracellular toxic levels or deficiencies, plants evolved regulated Mn uptake, distribution and storage mechanisms.

There are several protein families involved in the process of Mn transport, for example the NRAMP, CAX, CCX, MTP and ECA protein families. They regulate the uptake via the root system, and the intracellular distribution among the Golgi apparatus, ER compartment, vacuole and cytosol.

A newly characterized protein family, called UPF0016, is supposed to be involved in intracellular Mn transport as well, with members in nearly all species of life. The *Homo sapiens* (human) homolog TMEM165 is important for proper Mn supply of the Golgi apparatus as patients with a defect in this protein show disrupted *N*-glycosylation causing a severe psychomotor disease called Congenital Disorders of Glycosylation defects Type II (CDGII). In *Saccharomyces cerevisiae* (yeast) the homolog GDT1 is also reported to regulate Mn homeostasis in the Golgi apparatus. Some bacterial members, *Vibrio cholerae* MneA and *Synechocystis* MNX are important for cytosol detoxification by exporting Mn either out of the cell into the periplasmic space or into the thylakoid lumen.

In *Arabidopsis thaliana*, the UPF0016 family comprises five members. Two proteins harbor a chloroplast target peptide (cTP), one a TP for the secretory pathway and two proteins lack a TP. PAM71, the thylakoid membrane localized Mn transporter of the UPF0016 family is important for Mn supply to the thylakoid lumen to ensure proper OEC formation. Its closest homolog, CMT1, we found to be localized in the inner envelope of chloroplasts, importing Mn into the chloroplast stroma. Loss of CMT1 leads to disturbed chloroplast development, reduced amounts of photosynthesis complexes as well as reduced Mn incorporation into the OEC. The reduced growth phenotype and yellowish leaves of *cmt1* mutant plants are a result of this defect which manifests itself also in a reduced amount of chlorophyll and carotenoid pigments.

The remaining three *Arabidopsis thaliana* members of the UPF0016 family we found to be localized in the ER membrane (PML4 and PML5), and the Golgi membrane (PML3), where they are also supposed to play a role in Mn homeostasis. In two independent studies, PML3 localization to the Golgi membrane was confirmed and it was shown to be required for *N*-glycosylation.

Employing cross-species complementation assays we discovered HsTMEM165, SynMNX and AtCMT1 to be able to functionally replace PAM71 in the thylakoid membrane, supporting that Mn transport activity is an ancient trait of the UPF0016 protein family. Phylogenetic analysis revealed that cyanobacterial UPF0016 members are closer related to eukaryotic members than to other prokaryotic ones.

We hypothesized that two individual events introduced UPF0016 genes into the green lineage. First, a horizontal gene transfer (HGT), generated a gene copy, which is manifested in all eukaryotes, and resulted in plants in ER and Golgi-membrane localized proteins. Second, the cyanobacterial endosymbiotic gene transfer (EGT) gave rise to the two gene copies of *PAM71* and *CMT1* and the encoded proteins localize to the thylakoid and envelope membrane of chloroplasts, respectively.

Each protein family has its own evolutionary history, we were able to contribute to a better understanding of the function and evolution of the UPF0016 protein family and we were also able to show that the manganese transport function of individual members has been conserved over millions of years.

4 Zusammenfassung

Mangan (Mn) ist ein essenzieller Nährstoff, der für ein gesundes Pflanzenwachstum und die Pflanzenentwicklung benötigt wird. Mn ist an vielen zellulären Prozessen, wie der Antioxidation, Photosynthese und Glykosylierung beteiligt und kann als Cofaktor oder Enzymaktivator wirken. Mn spielt eine sehr wichtige Rolle als Cofaktor des Sauerstoff-entwickelnden-Zentrums (OEC) im Photosystem II (PSII) in den Chloroplasten, welcher die Wasserspaltungsreaktion katalysiert. Neben seiner Rolle für eine optimale Photosynthese Leistung wird Mn auch in anderen pflanzlichen Zellkompartimenten benötigt. Daher muss Mn transloziert und verteilt werden, um Mn-abhängige Stoffwechselprozesse in den entsprechenden Kompartimenten aufrechtzuerhalten. Mn-Mangel führt zu schweren Pflanzenschädigungen, einschließlich intervenöser Chlorosen und ein Überschuss resultiert in einer Anhäufung toxischer Mn-Oxidationsprodukten, welche schließlich zu Wachstumsstörungen führen. Folglich entwickelten Pflanzen in ihrer Evolution eine regulierte Mn-Aufnahme, -Verteilung und -Speicherung, um intrazelluläre Toxizität und Mangel zu verhindern.

Es gibt verschiedene Proteinfamilien, die in diesen Prozessen des Mn-Transports beteiligt sind, zum Beispiel die NRAMP, CAX, CCX, MTP und ECA Proteinfamilien. Sie regulieren die Aufnahme über das Wurzelsystem, und die intrazelluläre Verteilung zwischen dem Golgiapparat, dem ER, der Vakuole und dem Zytosol.

Auch die neu charakterisierte Proteinfamilie, UPF0016 ist am intrazellulären Mn-Transport beteiligt und Proteine dieser Familie sind in fast allen Organismen enthalten. Das menschliche Homolog TMEM165 ist wichtig für die Mn-Versorgung des Golgiapparates, da Patienten mit einem Gendefekt eine gestörte N-Glykosylierung haben, die eine schwere psychomotorische Krankheit verursachen kann, die als kongenitale Störungen von Glykosylierungsdefekten Typ II (CDGII) bezeichnet wird. Das homologe Protein aus *Saccharomyces cerevisiae* (Hefe), GDT1, reguliert ebenfalls die Aufnahme von Mn in den Golgiapparat. Einige Mitglieder aus Bakterien, z.B. das *Vibrio cholerae* Protein MneA und das *Synechocystis* Protein MNX, sind für die Mn Entgiftung des Zytosols wichtig, indem sie Mn entweder aus der Zelle in den periplasmatischen Raum oder das Thylakoidlumen exportieren.

In *Arabidopsis thaliana* umfasst die UPF0016 Familie fünf Mitglieder, wobei zwei Proteine ein Chloroplasten-Zielpeptid (cTP) besitzen, ein Protein enthält ein TP für den Golgiapparat und zwei Proteine besitzen keine Zielpeptide. PAM71 ist ein in der Thylakoidmembran lokalisierter Mn-Transporter der UPF0016 Familie, der wichtig für die Mn-Versorgung des Thylakoidlumens ist. Dadurch wird die Wasserspaltung, die mit der Sauerstoff Entwicklung einhergeht, sichergestellt. Das am nächsten verwandte Protein von PAM71 ist CMT1, welches in der inneren Hüllmembran von Chloroplasten lokalisiert ist und Mn in das Chloroplastenstroma importiert. Der Verlust von CMT1 führt zu einer gestörten Chloroplasten Entwicklung, einer reduzierten Anzahl an Photosyntheseproteinkomplexen sowie reduziertem Mn-Gehalt im Photosystem II. Das reduzierte Wachstum und die gelblichen Blätter in der *cmt1* Mutante sind eine Folge dessen, die sich auch in einer reduzierten Chlorophyll- oder Carotinoidmenge manifestiert.

Die restlichen drei pflanzlichen Proteine der UPF0016 Familie sind in der ER Membran (PML4 und PML5), und in der Golgi Membran (PML3) lokalisiert. Es wird angenommen, dass sie dort ebenfalls eine wichtige Rolle bei der Mn-Homöostase spielen. In zwei unabhängigen Studien wurde bestätigt, dass PML3 in der Golgi Membran lokalisiert ist, sowie eine Rolle bei der N-Glykosylierung spielt.

Mit Hilfe von speziesübergreifenden Komplementationsassays haben wir festgestellt, dass HsTMEM165, SynMNX und AtCMT1 in der Lage sind, PAM71 in der Thylakoidmembran funktionell zu ersetzen. Dadurch wird die Annahme unterstützt, dass die Mn-Transportaktivität das ursprüngliche Merkmal dieser Proteinfamilie ist. Unsere phylogenetischen Analysen ergaben, dass cyanobakterielle UPF0016 Proteine näher mit eukaryotischen Proteinen verwandt sind als mit anderen prokaryotischen Proteinen.

Wir stellten die Hypothese auf, dass zwei unabhängige Ereignisse die UPF0016-Gene in Pflanzen bzw. photosynthetische Eukaryonten eingeführt haben. Es wird vermutet, dass ein horizontaler Gentransfer (HGT) die Genkopie(n), die in allen Eukaryonten und somit auch in photosynthetischen Eukaryonten enthalten sind, erzeugt hat. Daraus resultierten in Pflanzen, die Golgi Membran und ER lokalisierten Proteine. In einem zweiten Schritt führte der endosymbiontische Gentransfer (EGT), nachdem ein Cyanobakterium von einer eukaryotischen Wirtszelle aufgenommen wurde, zu den beiden Genkopien von *PAM71* und *CMT1*. Die entsprechenden Proteine erhielten im Laufe der Evolution eine chloroplastidäre Zielsequenz, sodass sie in die Thylakoid- bzw. Hüllmembran des Chloroplasts geleitet werden können.

Jede Proteinfamilie hat ihre eigene evolutionäre Geschichte, wir konnten dazu beitragen, dass die Funktion und Evolution der UPF0016 Proteinfamilie besser verstanden wird und konnten zudem zeigen, dass die Mn-Transportfunktion einzelner Mitglieder über Jahrtausende konserviert geblieben ist.

5 Aim of the thesis

The UPF0016 protein family harbors members in nearly every species of life, however not much was known about the function and evolution of this family in *Arabidopsis thaliana*. The predicted protein topology of all eukaryotic members is described by two clusters of three transmembrane (TM) domains. The two clusters are oppositely orientated in the membrane and linked via an acidic loop. The proteins contain two highly conserved motifs in TM1 and TM4 which are supposed to play an important role in cation binding. Human and yeast homologs are characterized as important Mn transporters in the Golgi membrane and bacterial homologs reside in the plasma membrane and/or thylakoid membrane of photosynthetic species. In *Arabidopsis thaliana*, there are five members present, including two proteins with a chloroplast target peptide (cTP), one protein with a Golgi apparatus targeting peptide TP and two proteins without a TP. The best characterized protein is the thylakoid membrane localized Mn transporter PAM71, importing Mn into the thylakoid lumen (Schneider et al., 2016).

This thesis is aimed to investigate the closest homolog of PAM71, which is named CMT1. The localization of CMT1 and its ability to function as a Mn transporter were analyzed. Additionally, an examination of the respective knock-out phenotype in *Arabidopsis thaliana* and its underlying defects was conducted to gain more information about the function of UPF0016 members in chloroplast Mn homeostasis.

Besides that, the subcellular localization of the three remaining proteins, named PML3, PML4 and PML5, the expression of the respective genes and knock-out mutant plants were investigated.

To gain further insights into the UPF0016 protein family evolution and the conservation of the mode of Mn transport cross-species complementation assays were performed. The similarities in the protein topology suggested a conserved mode of Mn transport. The aim was to functionally complement the *Arabidopsis thaliana* mutant *pam71* with the human, *Synechocystis* and *Arabidopsis thaliana* homologs HsTMEM165, SynMNX and AtCMT1, respectively.

Taken together further examination of UPF0016 protein members manifested their influence on Mn homeostasis.

6 Introduction

6.1 Plant Nutrition

Plants are sessile organisms that have to cope with and adapt to different environmental conditions. Generating crop plants capable of withstanding challenging environmental changes like droughts, floods, intensifying temperature ranges, as well as varying nutrient availability is of big interest due to an increasing human population. Research on understanding the underlying cellular processes, like metal uptake, distributions and protection mechanisms to nutrient excess or limitation are from utmost importance to face the impact of climate changes on plants.

For proper plant growth, development and reproduction essential micro - and macronutrients are required (Barker et al., 2007). The classification into micro - and macronutrient is done according to their concentration in plants. Micronutrients are found to be below ≤ 100 mg/kg dw (milligram per kilogram dry weight) while macronutrients are above that value (Barker & Pilbeam, 2015). Classified macronutrients are for example nitrogen (N), phosphorus (P), potassium (K), calcium (Ca), magnesium (Mg), and sulphur (S), which are taken up from the soil (Eppstein, 1972). Hydrogen (H), oxygen (O) and carbon (C) are nonmineral elements - also classified as macronutrients but are obtained from water and carbon dioxide. Manganese (Mn), iron (Fe), sodium (Na), copper (Cu) are examples for micronutrients which are all acquired from the soil (Eppstein, 1972). Macronutrients are mostly used to build cellular components like nucleic acids or proteins and are therefore required in higher amounts while some micronutrients like Mn are often found to be cofactors for enzymes.

6.2 Manganese and its role in cellular processes

Mn is a transition metal with a wide range of different oxidation states from +2 to +7. In biological systems Mn^{2+} , Mn^{3+} and Mn^{4+} are predominantly present in redox cycles, with Mn^{4+} being the least stable one (Marschner & Marschner, 2012). The most usable form for plants is the divalent cation Mn^{2+} (Marschner & Marschner, 2012). The different oxidation states of Mn are influenced by the pH value of the soil. In acidic soils, Mn^{2+} is preferentially present while in more neutral or high pH and partial O_2 pressure (pO_2) soil the oxidation states +3 and +4 as well as insoluble forms like manganese dioxide (MnO_2) are found (Broadley et al., 2012; Lynch & Clair, 2004; Marschner & Marschner, 2012; Rengel, 2000). Those forms are not accessible for plants. Excess of other minerals like Fe, Mg, Ca and P can lead to Mn deficiency as they compete and interfere with Mn uptake (Lynch & Clair, 2004; Marschner & Marschner, 2012) by blocking transport proteins that transport not only Mn. Microorganisms can affect Mn availability for plants as well as they can either reduce or oxidize the occurring Mn states into more soluble ones (Geszvain et al., 2012; Lovley et al., 2011).

6.2.1 Role of Manganese in cellular processes

Mn is an essential micronutrient and therefore the regulated uptake, distribution and storage is crucial for proper plant development, growth and biomass production (Marschner, 1995). Mn deficiency or excess can cause severe toxicity related alterations. Symptoms of Mn deficiency in plants can be interveinal chlorosis in younger leaves and prolonged deficiency leads to necrosis of older leaves (Schmidt et al., 2016). Inhibited growth caused by Mn deficiency and the consequential reduced net photosynthesis rate and chlorophyll content, results in decreased biomass. Mn is involved in several cellular processes like antioxidation, protein glycosylation and photosynthesis either as a catalytic activator integral in clusters or as a cofactor of enzymes. In plants, around 300 proteins have been identified being activated by Mn^{2+} or are having a Mn binding site (The UniProt Knowledgebase, <http://www.uniprot.org>, accessed 30 May 2021), such as the oxalate oxidase and the Mn-dependent superoxide dismutase. The most important function of Mn is driving the water splitting reaction during photosynthesis. Mn^{2+} as a cofactor is also required for multiple steps during carbohydrate, lipid and lignin biosynthesis in plants (Engelsma, 1972; Köllner et al., 2008; Marschner & Marschner, 2012), but also during purine and urea catabolism (Cao et al., 2010; Werner et al., 2008), DNA repair (Szurmak et al., 2008; Takahashi et al., 2007) and phospholipid biosynthesis (Collin et al., 1999; Nowicki et al., 2005).

6.2.1.1 (N)-linked glycosylation

N-Glycosylation of proteins is an essential co- and post-translational modification of membrane and secretory pathway localized proteins (Strasser, 2016). It has been shown that the activity of several enzymes involved in this process are dependent on Mn^{2+} . Protein modifications are important for proteome homeostasis as protein folding, stability and protein-protein interactions are regulated by them (Hebert et al., 2014). *N*-Glycosylation processing starts in the ER with the transfer of a preassembled oligosaccharide precursor of a lipid carrier to the asparagine residue of the sequence aspartate-X-serine/threonine (Asn-X-Thr/Ser where X can be any amino acid except Pro) of a polypeptide (Strasser, 2016). After that, the *N*-glycan is processed by α -glucosidases and/or α -mannosidases (AtMNS1-AtMNS5) which cleave off glucose or mannose residues, respectively (Liebminger et al., 2009; Strasser, 2014). The ER localized AtMNS4 and AtMNS5 are involved in the degradation of misfolded proteins while the remaining three are localized in the Golgi apparatus and are important for further processing the properly folded secretory glycoproteins (Hüttner et al., 2014; Liebminger et al., 2009). All AtMNS enzymes require divalent cations like Mn^{2+} for activation (Liebminger et al., 2009). *N*-glycans themselves affect the activity of enzymes, for example the endoglucanase RSW2, which plays an important role in cellulose biosynthesis (Lane et al., 2001; Liu et al., 2018). Additionally, the activity of the two types of glycosyltransferases (xyloglucan glucosyltransferase and arabinosyltransferase), which are involved in proper cell wall polysaccharides biosynthesis, are activated/ stimulated by Mn^{2+} (Nunan & Scheller, 2003; Romero & Herscovics, 1989; White et al., 1993). Besides its activating role for glycosyltransferases and *N*-glycan processing in the ER and Golgi apparatus, Mn plays an important role in the antioxidation process in mitochondria.

6.2.1.2 ROS antioxidation

Reactive oxygen species (ROS) can cause severe damage to DNA/RNA and can lead to protein oxidation (Mittler, 2017). Therefore, antioxidation mechanisms focusing to reduce and prevent ROS induced damage are present in nearly all compartments of a cell. The Mn-dependent superoxide dismutase (MnSOD) is a prominent enzyme with Mn as integral part and it is mainly localized in mitochondria (Bowler et al., 1994; Corpas et al., 2017). It catalyzes the detoxification of dangerous ROS which occur as a by-product of plant metabolism. The MnSOD transmutes two superoxide anions (O_2^-) into oxygen (O_2) and hydrogen peroxide (H_2O_2) (Schmidt et al., 2016). Mn^{2+} is bound to SOD and oxidized into Mn^{3+} -SOD which is the resting state of the enzyme (Irving & Williams, 1948; Schmidt & Husted, 2019). By transferring one electron from the superoxide radical onto Mn^{3+} -SOD it is reduced back to Mn^{2+} -SOD and generates O_2 . Mn^{2+} -SOD is supposed to be oxidized back to Mn^{3+} -SOD by another superoxide anion which is then processed to hydroperoxyl anion (HOO^-) and protonation finally forms H_2O_2 (Borgstahl et al., 1992; Zhu & Richards, 2017).

In plants, Mn deficiency causes reduced MnSOD activity, which leads to increased levels of ROS and tissue necrosis (Socha & Guerinot, 2014). In *Chlamydomonas* it was shown that the activity of MnSOD was reduced before that of the oxygen evolving complex (OEC) to ensure enough Mn for the water splitting reaction. This underlines the importance of Mn for proper photosynthesis performance (Allen et al., 2007).

6.2.1.3 Manganese in chloroplasts

Mn plays a crucial role in photosynthesis - more precisely in the light driven reaction. The wide range of oxidation states of Mn makes it optimal for sequential redox reactions during photochemistry.

The light dependent reaction during photosynthesis takes place in the thylakoid membrane/lumen where all the participating complexes, photosystem I (PSI), photosystem II (PSII), cytochrome *b₆f* (Cyt*b₆f*), and the single protein plastocyanin (PC) are localized. The linear electron transfer through all these complexes relies on the three transition metals Fe, Cu and Mn (Merchant, 2007; Schmidt et al., 2020). The PSII contains a luminal orientated Mn_4CaO_5 cluster that is called OEC. The light induced oxidation of H_2O into O_2 in the OEC of PSII extracts four electrons and protons from water molecules (Schmidt & Husted, 2019). The reaction catalyzed by the Mn_4CaO_5 cluster therefore passes five S_i (redox) states from 0-4 (Schmidt & Husted, 2019) to accumulate four electrons to build O_2 . The Kok cycle describes the different oxidation steps of the four Mn ions in the OEC and the preferred redox states (Mn^{3+} and Mn^{4+}) (Kok et al., 1970), which is depicted in Figure 1. Four light flashes are needed to oxidize Mn ions inside the OEC and to release electrons from H_2O which are reducing the tyrosin-161 (Y_2) residue of D1 - a PSII core protein - which then reduces $P680^+$ and starts the linear electron flow.

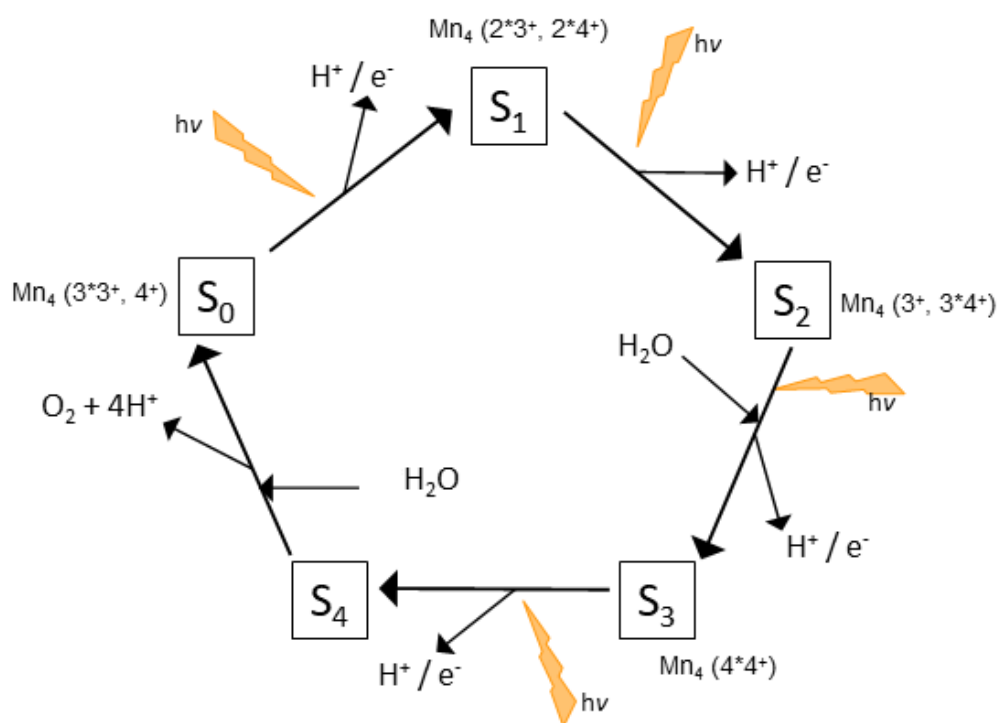


Figure 1 Schematic illustration of the Kok-Joliot-Cycle. The Mn₄CaO₅ cluster passes five different transition states after each illumination. Electrons are released in each step by oxidation of one Mn element of the cluster. Transition from state S₄ to S₀ reduces three Mn ions back to Mn³⁺. Modified from (Kern et al., 2018).

During the OEC cluster assembly, the Mn²⁺ are stepwise attached and become the catalytically active form Mn₄ (3*3⁺, 4⁺) through photooxidation (Burnap, 2004; Dasgupta et al., 2008). Accordingly, Mn deficiency in plants has detrimental effects on PSII activity (Schmidt et al., 2016) and downstream reactions. Besides the catalytic activity of Mn in the OEC, a binuclear Mn²⁺ center is indirectly regulating energy distribution between PSII and PSI as it is involved in the recognition of two proteins (TAP38 and phosphorylated Lhcb1) during state transition (Pribil et al., 2010; Wei et al., 2015).

Besides its prominent role in photosynthesis, Mn²⁺ is required in the chloroplast stroma for the activation of enzymes in the histidine biosynthesis (Ingle, 2011; Rawson et al., 2018) and the shikimate pathway (Entus et al., 2002). Therefore, Mn is especially important for chloroplast-located metabolic pathways.

6.3 Manganese transporters in plants

Mn can be found in most organs and compartments in plant cells and needs to pass several membranes to reach its final destinations. Hence, Mn²⁺ specific transport proteins are needed because Mn concentration is low compared to other divalent cations. As of yet, only a handful of Mn²⁺-specific transporters have been identified in plants (Socha & Guerinot, 2014), as most of the transporters have a broad specificity to other divalent cations as well, e.g. Fe²⁺, Zn²⁺ and

Ca^{2+} . In *Arabidopsis thaliana* around 7% (1800 out of 25000) of all proteins count as transport proteins (Lanquar et al., 2010; Schwacke et al., 2003).

Mn uptake starts with the absorption of Mn^{2+} over the root surface. Afterwards, the high affinity Mn^{2+} NRAMP1 transporter, which is located in the plasma membrane of cortex cells and the epidermis of the roots (Cailliatte et al., 2010; Castaings et al., 2016), imports Mn^{2+} into the cytosol. NRAMP1 additionally regulates Fe uptake (Curie et al., 2000). Furthermore Mn uptake is also mediated by IRT1, a transporter with a broad affinity for other divalent cations, like Fe (Castaings et al., 2016). Then, Mn needs to be transported to the different plant organs through the vascular system - specifically the xylem. The mechanism of Mn loading into the xylem is not described yet for *Arabidopsis thaliana* (Alejandro et al., 2020), but members of the YSL protein family are hypothesized to be involved (Waters et al., 2006).

Through the xylem, Mn can be transported to all tissues inside the plant and is then distributed adequately to the cellular compartments. To prevent cytosolic toxification, Mn^{2+} can be stored in the vacuole (Lanquar et al., 2010). Vacuole loading with Mn^{2+} in the cells of the epidermis or cortex of roots and the mesophyll cells of the areal part is for example performed by MTP8 (Chu et al., 2017; Eroglu et al., 2017) and members of the CAX family (CAX2, CAX4 and CAX5) (Edmond et al., 2009; Koren'kov et al., 2007; Pittman et al., 2004). NRAMP3 (Thomine et al., 2003) and NRAMP4 (Lanquar et al., 2005) are involved in the release of Mn from the vacuole into the cytosol in photosynthetic tissue and their expression is only affected by changing Fe^{2+} levels (Lanquar et al., 2010). Their importance in Mn homeostasis is suggested, as the growth of the double mutant *nramp3nramp4* is inhibited under Mn deficiency due to reduced photosynthesis performance, a consequence of Mn shortage in the OEC (Lanquar et al., 2010).

Another family member, the NRAMP2, is described as a *trans*-Golgi network (TGN)-localized transporter, allocating Mn intracellularly (Alejandro et al., 2017; Gao et al., 2018). Transportation of Mn into endomembrane compartments is facilitated for example by ECA1 into the ER compartment and ECA3 (Huda et al., 2013) into the Golgi apparatus. MTP11 is a putatively double localized transporter in the Golgi membrane and the prevacuolar compartment membrane (PVC) and is therefore suspected to avoid Mn accumulation by loading it into the vacuole via PVCs or secretion into the apoplast via vesicles (Delhaize et al., 2007; Peiter et al., 2007).

How Mn is imported into mitochondria and chloroplast stroma was not known at the beginning of this thesis. The first chloroplast localized Mn transporter, the thylakoid membrane protein PAM71, was described in 2016 (Schneider et al., 2016) and belongs to the Uncharacterized Protein Family 0016 (UPF0016), which is described in detail in the next paragraphs.

6.4 Uncharacterized Protein Families

Proteins that share a common evolutionary origin may have related functions and are grouped into protein families according to similarities in their sequence and/or structure. Since genome sequencing was developed, the number of protein families increased rapidly. The similarity in the protein structure and/or sequence can help identifying new protein functions of the family it belongs to. However, there are some protein families where the function of their members was not yet described. Those families are called Uncharacterized Protein Families (UPFs).

6.4.1 Protein topology of Uncharacterized Protein Family 0016 (UPF0016) members

The Protein Family 0016 (UPF0016, Pfam PF01169, TCDB number: 2.A.106) was described in 2014 with members found in nearly all species of life (eukaryotes, prokaryotes and archaea) with only two exceptions, the prokaryotic phyla Lactobacillales and Bacillales (Demaegd et al., 2014). The UPF0016 belongs to the LysE superfamily of transport proteins that include heavy metal ion transporter (Tsu & Saier Jr, 2015). Different bioinformatic phylogenetic analysis of the UPF0016 revealed twelve subgroups from eukaryotic (VII-XII) and prokaryotic (I-VI) organisms, which are depicted in Figure 2 (Demaegd et al., 2014). Several approaches of alignment tools displayed a slight variation in the layout of the subgroups to each other while two major groups remained (see Figure 2). The members of cyanobacteria subgroup VI seems to be more closely related to eukaryotic proteins than to other prokaryotic proteins (Demaegd et al., 2014).

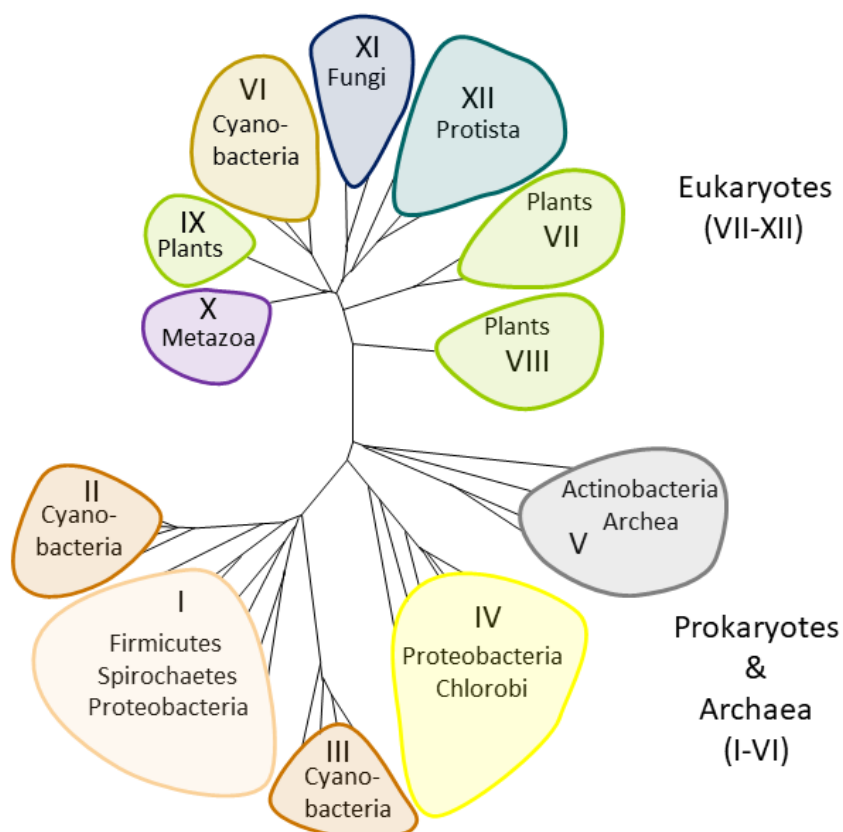


Figure 2: Simplified schematic illustration of the UPF0016 Phylogenetic tree modified from (Demaegd et al., 2014). Representative members from several prokaryotes and eukaryotes were chosen, which resulted in twelve subgroups of two major groups - one including prokaryotes and archaea (lower part) and the other one including eukaryotes and the group of cyanobacteria with two-cluster protein topology (6 TM domains) (Subgroup VI, upper part). The groups I, II and III include only single-cluster proteins (3 TM domains). This indicates two-cluster proteins of cyanobacteria are closer related to eukaryotes than to other prokaryotes.

The overall structure of functional UPF0016 proteins consists of six transmembrane (TM) domains, which are composed of two antiparallel orientated clusters of 3 TM domains. A singleton gene can encode for such a cluster of 3 TM domains which then composes a homodimer (resulting in 6 TMs). Gene pairs, being adjacent on the chromosome, encoding two 3 TM domain clusters compose a heterodimeric protein consisting of 6 TM domains. Another option is the formation of a fusion gene (from two genes), which is directly coding for a 6 TM domain protein. Bacterial members of the UPF0016 are common in nearly all phyla and they are mostly encoded by singleton genes or a fusion gene (Demaegd et al., 2014). Gene pairs, finally assembling into a heterodimeric protein have only been found to be present in cyanobacteria subgroup II and III in Figure 2 (Demaegd et al., 2014). Eukaryotic members (subgroups VII-XII) as well as the members of cyanobacteria subgroup VI are encoded by a fusion gene (Demaegd et al., 2014) linked with a highly acidic loop (Hoecker et al., 2017).

Analyzing the orientation of the proteins in the membrane can be performed by measuring the amount of positive (arginine or lysine) and negative (aspartic acid or glutamic acid) charged residues in the odd and even (orientated the same as the N-terminus) hydrophilic loops. According to the positive inside rule by Heijne (von Heijne, 2006), cytosolic orientation occurs if the amount of arginine and lysine is smaller on one side than on the other,

consequently the cytosolic side being more acidic and therefore negatively charged. If the numbers are equivalent, there is no preferred orientation leading to dual topology. This can lead to homodimer formation. Applying this rule to the UPF0016 members, singleton-encoded proteins are equally likely to be inserted in both directions into the membrane forming homodimers, while fusion proteins have a highly acidic central loop which faces the cytosol (Demaegd et al., 2014). In gene pairs, the one closer to the 5' end encodes a highly acidic N-terminus, while the other one features a longer acidic C-terminus - both are facing the cytosol and are supposed to associate to the central loop composing the heterodimer (Demaegd et al., 2014).

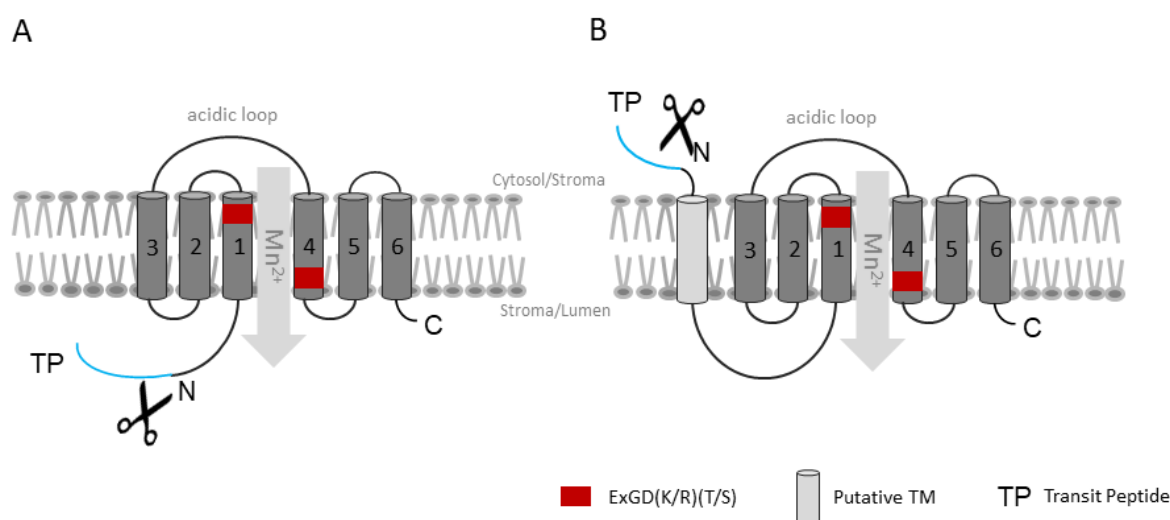


Figure 3 Predicted protein topology of eukaryotic members of the UPF0016. The protein consists of two homologous clusters of 3 TM domains with a highly conserved amino acid pattern in TM1 and TM4, which are supposed to build the pore of the transporter. A) depicts the topology consistent of 6 TM domains and shorter N-terminus, facing the stroma side of the membrane, like the C-terminus. B) shows a prolonged N-terminus version with a putative 7th TM domain. This flips the N-terminus to the opposite of the membrane compared to the C-terminus. B is supposed to be the topology of some eukaryotic members of UPF0016, namely PAM71 and CMT1 (Hoecker et al., 2017). Modified from (Thines et al., 2020)

Taken together, in eukaryotes, the conserved protein topology consists of two clusters of 3 TM domains. These clusters are integrated in an antiparallel manner and linked by a central acidic loop which is facing the cytosol (Figure 3A), while the N- and C-termini are facing the lumen (Demaegd et al., 2014). This common structure could indicate an important role in protein folding, stability, localization and/or activity of the proteins. The highest similarity can be found in the highly conserved Glu-x-Gly-Asp-(Lys/Arg)-(Thr/Ser) ((ExGD(K/R)(T/S)) consensus motif which is present in TM1 and TM4 (Figure 3). X can be any hydrophobic residue (Demaegd et al., 2014). This motif contains two negatively charged (aspartic acid and glutamic acid), one positively charged (arginine or lysine) and an hydroxyl containing (serine or threonine) residue which provides a fitting environment for cations (Waight et al., 2013) and it is supposed to build the pore of the transport proteins.

A further layer of diversity of UPF0016 proteins is found in plants, as they possess at least four members, while other non-photosynthetic eukaryotic organisms mostly have single ones - if different splicing variants are not considered (Demaegd et al., 2014; Hoecker et al., 2017).

There is one subgroup (VII) in plants that has an elongated N-terminus with an additional putative TM domain (Figure 3B), leading to a new orientation of the N-terminus in these proteins (Demaegd et al., 2014). The N-terminal region of all proteins is found to show the highest diversity (Demaegd et al., 2014; Hoecker et al., 2017) indicating that the transport function of the proteins does not depend on the N-terminus but it could play an important role in their localization (Hoecker et al., 2017) and/or regulation. These variations can be observed in several other protein families as well, e.g. the *Arabidopsis thaliana* members of the cation exchanger family (CaCA) contain an N-terminal autoinhibitory tail which is missing in the yeast ortholog (Pittman, 2011). According to the consensus motifs and the similarities in the topology to the cation/ Ca^{2+} exchangers superfamily, the members of the UPF0016 are supposed to be involved in divalent cation transporting (Cai & Lytton, 2004). The number of 6 TM domains, and the antiparallel orientation of the two clusters which is linked by a highly acidic loop are common features in divalent cation transporters (Vinothkumar & Henderson, 2010).

6.4.2 Prokaryotic members of UPF0016

6.4.2.1 The *Vibrio cholerae* Mn^{2+} exporter A (MneA)

As single-cell organisms, bacteria, especially as pathogens, must be able to cope with environmental changes and stresses. Mammalian cells invaded by these bacteria try to hold back essential metals to disturb the pathogens maintenance and therefore destroying their pathogenicity (Hood & Skaar, 2012; Lisher & Giedroc, 2013). Intracellular Mn levels in *Vibrio cholerae* are mostly regulated via import and export proteins (Fisher et al., 2016).

The *Vibrio cholerae* homolog of UPF0016, the Mn^{2+} exporter A (MneA) is such a Mn level regulating exporter (Fisher et al., 2016). The $\Delta mneA$ mutant displays a Mn^{2+} sensitive phenotype when grown on media containing high levels of Mn^{2+} (Fisher et al., 2016). The reduced Mn^{2+} export in this mutant leads to high intracellular Mn^{2+} levels and supports the role of MneA in conferring Mn resistance (Fisher et al., 2016). That function is supported by heterologous expression of MneA in the *E. coli* $\Delta mntP$ mutant. MntP is a non-homolog Mn^{2+} exporter preventing Mn^{2+} accumulation in the cytosol (Waters et al., 2011). *Vibrio cholerae* MneA is able to functionally complement the $\Delta mntP$ Mn sensitive phenotype by decreasing intracellular Mn^{2+} levels (Fisher et al., 2016; Zeinert et al., 2018), therefore corroborating its Mn export function. Loss of MneA leads to high cytosolic Mn^{2+} levels that influence antioxidation mechanisms. The $\Delta mneA$ mutant has increased resistance to oxidative stress induced by H_2O_2 , which is supposed to result from the high availability of Mn^{2+} for Mn-dependent MnSOD (Fisher et al., 2016). *In silico* analysis revealed the eukaryotic-like topology of MneA (Demaegd et al., 2014; Zeinert et al., 2018), with the difference of lacking a signal peptide (Petersen et al., 2011).

6.4.2.2 The *Synechocystis* sp. PCC6803 Manganese Exporter (MNX/ SynPAM71)

The cyanobacteria model organism *Synechocystis* sp. PCC6803 (from now on mentioned as *Synechocystis*) also harbors an ortholog of MneA, named MNX (manganese exporter) or SynPAM71. The characterized protein is localized in the plasma membrane and thylakoid membrane (Brandenburg et al., 2017; Gandini et al., 2017). Mutants lacking MNX are Mn^{2+} sensitive and display a Mn specific phenotype (Brandenburg et al., 2017; Gandini et al., 2017). Mn^{2+} specific transport is highlighted, as MNX is able to suppress the Mn^{2+} sensitivity of the yeast mutant $\Delta pmr1$ (Brandenburg et al., 2017). The yellowish-green phenotype of Δmnx is caused by reduced chlorophyll *a* amounts (only up to 60%) and photosynthesis complexes - mostly PSI (Gandini et al., 2017). The disturbed photochemistry of PSII is supposed to be solely caused by toxic accumulation of Mn^{2+} in the thylakoid lumen, where it is concentrated around PSII complexes and the membrane itself (Brandenburg et al., 2017; Gandini et al., 2017). MNX is assumed to transport Mn^{2+} from the cytosol into the thylakoid lumen for proper Mn^{2+} supply during the repair of PSII and into the periplasmic space to prevent toxic accumulation in the cytosol (Brandenburg et al., 2017; Gandini et al., 2017). The first role is important under high light stress, correlating with the fact that Δmnx growth is reduced as a result of impaired photoprotection/repair mechanism (Brandenburg et al., 2017; Gandini et al., 2017). Also, the MNX's predicted topology is similar to that described for other UPF0016 proteins (Gandini et al., 2017), and, similar to MneA, lacking a signal peptide. Taken together, the severe Mn^{2+} sensitive phenotype of the Δmnx mutant strains and the Mn^{2+} transport function of the protein supports a role of MNX in Mn^{2+} homeostasis in cyanobacteria.

6.4.3 Eukaryotic members of UPF0016

6.4.3.1 The *Homo sapiens* Transmembrane Protein 165 (TMEM165)

The interest in members of the UPF0016 family arose in 2012. Mutations in the human gene encoding the Transmembrane Protein 165 (TMEM165) protein were shown to result in glycosylation defects in the Golgi compartment, leading to a disease called congenital disorders of glycosylation type II (CDG-II) (Foulquier et al., 2012). Defects in protein glycosylation (*N*-glycosylation, *O*-glycosylation, and both) (Foulquier, 2009; Jaeken et al., 2009; Jaeken & Matthijs, 2007; Schachter & Freeze, 2009) can lead to severe psychomotor retardations and growth disorders. Proper protein glycosylation depends on intact pH and ion homeostasis, cellular Mn^{2+} levels, as well as proper Golgi trafficking (Foulquier et al., 2012; Foulquier et al., 2007; Foulquier et al., 2006; Kornak et al., 2008; Potelle et al., 2017; Reynnders et al., 2011; Reynnders et al., 2009; Wu et al., 2004).

TMEM165 is mainly localized in the trans-Golgi membrane system (Foulquier et al., 2012; Rosnoblet et al., 2013). The topology of TMEM165 is like the predicted one of UPF0016 proteins - two clusters of 3 TM domains with an antiparallel orientation, linked by an acidic loop facing the cytosol, apart from that TMEM165 possesses an extended N-terminus with an additional putative TM domain (Potelle et al., 2017) or a secretory pathway signal peptide sequence (Hoecker et al., 2017).

TMEM165 is not directly affecting *N*-glycosylation but plays an important role in Golgi morphology and glycosylation maintenance (Foulquier et al., 2012) as TMEM165 depletion caused glycosylation defects can be rescued by adding Mn^{2+} (Potelle et al., 2016). Only the import of Mn^{2+} into the Golgi lumen allows Mn^{2+} -dependent glycosyltransferases to function properly. Since TMEM165 is able to complement the yeast $\Delta gdt1$ Mn^{2+} sensitivity, its role in Mn^{2+} homeostasis is solidified (Stribny et al., 2020). Nevertheless, it cannot be ruled out that TMEM165 has an additional transport activity for Ca^{2+} (Demaegd et al., 2013; Reinhardt et al., 2014). HeLa cells expressing TMEM165 show decreased membrane currents in the presence of a Ca^{2+} chelating agent (EGTA), hence supporting a possible role of TMEM165 in Ca^{2+} transport. In lactating mammary tissue the expression of *TMEM165* increases and as the secretion of Golgi luminal stored Ca^{2+} into milk is linked to that expression, TMEM165 may contribute as Ca^{2+} transporter (Reinhardt et al., 2014).

The highly conserved ELGDK (Glu-Leu-Gly-Asp-Lys) motif in TM1, which is facing the cytosol, is supposed to be Mn^{2+} sensitive and possibly plays a role in the functionality and regulation of TMEM165, as high Mn^{2+} levels lead to a degradation of TMEM165 in the lysosomes (Potelle et al., 2017). The degradation of TMEM165 as a response to high Mn^{2+} levels can act as detoxification mechanisms to avoid overloading of Mn^{2+} into the Golgi lumen (Potelle et al., 2017).

As TMEM165 is supposed to play an important role in Mn^{2+} homeostasis and maybe in Ca^{2+} homeostasis it is hypothesized that TMEM165 can either act as Mn^{2+} importer with an antiport of Ca^{2+} (Potelle et al., 2017) or it is co-transporting Mn^{2+} or Ca^{2+} in an antiport mechanism with protons. Consequently, TMEM165 would be additionally responsible for pH homeostasis in the Golgi compartment (Dulavy et al., 2017; Lebredonchel et al., 2019). If TMEM165 is supposed to antiport Ca^{2+} and Mn^{2+} , it could eventually change the direction of transport under high cytosolic Mn^{2+} concentrations (Potelle et al., 2017).

6.4.3.2 The *Saccharomyces cerevisiae* GCR Dependent Translation Factor 1 (GDT1)

The *Saccharomyces cerevisiae* GCR1 Dependent Translation Factor 1 (GDT1) is the yeast member of the UPF0016 family and like the human ortholog localizes in the *cis* and *medial* Golgi membrane (Demaegd et al., 2013). Beside their localizations the human TMEM165 and yeast GDT1 share the predicted topology of UPF0016 proteins with an additional putative TM domain at the N-terminus, or alternatively a signal peptide for Golgi membrane targeting (Demaegd et al., 2013; Hoecker et al., 2017; Potelle et al., 2016). The similarities strengthen the hypothesis of GDT1 being able to transport Ca^{2+}/Mn^{2+} as well. Therefore, to investigate its functionality, the $\Delta gdt1$ yeast mutant was compared to the yeast mutant lacking PMR1, which is a well described Golgi membrane localized Ca^{2+}/Mn^{2+} P-type ATPase.

The glycosylation defects of $\Delta pmr1$ are completely due to Mn^{2+} deficiency in the Golgi compartment (Durr et al., 1998). This indicates an important role of PMR1 in Mn^{2+} supply for proper protein glycosylation in the Golgi (Durr et al., 1998). Beside its role in Mn homeostasis its role for Ca^{2+} import is proven as expressing other Ca^{2+} transporters rescues the $\Delta pmr1$ mutant growth defect under Ca^{2+} deficiency (Durr et al., 1998).

GDT1 also plays a role in coping with Ca^{2+} stress, as the $\Delta gdt1$ mutant displays slight growth deficiencies under high Ca^{2+} concentrations [750 mM] compared to WT strains yet growth of $\Delta pmr1$ is more affected than the one of $\Delta gdt1$ (Demaegd et al., 2013). The growth of $\Delta gdt1\Delta pmr1$ decreases drastically under higher Ca^{2+} concentrations [400 mM] as well as under Ca^{2+} limitation, while the growth of $\Delta gdt1$ resembles the WT strain and $\Delta pmr1$ is only slightly impaired in this condition (Colinet et al., 2016; Demaegd et al., 2013; Rudolph et al., 1989).

The imbalances of Ca^{2+} and mainly Mn^{2+} levels in the Golgi lumen of $\Delta gdt1$ affect protein glycosylation under high Ca^{2+} levels (Dulary et al., 2018; Potelle et al., 2016). This effect can be rescued by adding Mn^{2+} to the growth media (Potelle et al., 2017; Potelle et al., 2016) which explains the observation that glycosylation defects under high Ca^{2+} levels are the result of Ca^{2+} competing with Mn^{2+} , eventually leading to Mn^{2+} deficiency inside the Golgi lumen (Potelle et al., 2016). GDT1 is essentially regulating cellular Mn^{2+} pools, as it is important for resistance to high Mn^{2+} concentrations (Thines et al., 2018). Regulating Mn^{2+} homeostasis, GDT1 directly impacts the activity of Mn^{2+} -dependent enzymes (Thines et al., 2018).

Similar to TMEM165 in the human body, the yeast GDT1 is hypothesized to either antiport $\text{Mn}^{2+}/\text{Ca}^{2+}$ while Mn^{2+} is imported into the Golgi and Ca^{2+} is exported (Dulary et al., 2018; Lebretonchel et al., 2019; Thines et al., 2020) or to import Mn^{2+} and Ca^{2+} in antiport with H^+ (Colinet et al., 2016; Thines et al., 2020). The antiport of $\text{Mn}^{2+}/\text{Ca}^{2+}$ would prevent cytosolic accumulation of Mn and provides Mn^{2+} as cofactor for glycosyltransferases and contributes to Ca^{2+} homeostasis. On the other hand, an antiport of $\text{Mn}^{2+}\text{-Ca}^{2+}/\text{H}^+$ would also prevent Ca^{2+} accumulation in the cytosol and would regulate the proton load of the Golgi compartment (Thines et al., 2020).

As a truncated version of human TMEM165 is able to rescue the $\Delta gdt1$ Mn-sensitive phenotype, it was concluded that GDT1 and TMEM165 are evolutionary conserved Mn^{2+} transporters of the Golgi compartment (Stribny et al., 2020).

6.4.3.3 The *Chlamydomonas reinhardtii* Conserved in Green Lineage and Diatom 1 (CGLD1)

CGLD1 is the *Chlamydomonas* homolog belonging to the UPF0016 proteins. To date, two *cgl1* mutants in different wildtype backgrounds of *Chlamydomonas* have been described (Schneider et al., 2016; Xing et al., 2017). In both mutant strains, reduced photoautotrophic growth and photosystem II performance can be observed. Reduced quantum maximum yield of PSII (F_v/F_m) values of *cgl1* mutants can be restored by supplementing Mn^{2+} (Schneider et al., 2016; Xing et al., 2017). This suggests CGLD1 to be involved in Mn^{2+} homeostasis of *Chlamydomonas* with a proposed conserved function in Mn^{2+} transport (Schneider et al., 2016). In contrast to the *Vibrio cholerae* MneA mutant, the *cgl1* mutant is more sensitive to oxidation stress induced by H_2O_2 (Xing et al., 2017).

6.4.3.4 *Arabidopsis thaliana* Photosynthesis Affected Mutant 71 (PAM71)

Various numbers of homologs of UPF0016 members are present in plants (Demaegd et al., 2014). In *Arabidopsis thaliana* there are five proteins belonging to this protein family (Demaegd et al., 2014; Hoecker et al., 2017; Schneider et al., 2016). The first protein which was described and characterized was called PAM71, which stands for Photosynthesis Affected Mutant AFFECTED MUTANT71 and later it was also named CCHA1 for Chloroplast $\text{Ca}^{2+}/\text{H}^{+}$ Antiporter 1 and BICAT1 for Bivalent Cation Transporter 1 (Frank et al., 2019; Schneider et al., 2016; Wang et al., 2016).

The predicted protein topology of PAM71 (Figure 3B) depicts the conserved 6 TM domains with the highly conserved consensus motif in TM1 and TM4 as well as a prolonged N-terminal region with an additional TM domain and a chloroplast target peptide (cTP) sequence (Frank et al., 2019; Schneider et al., 2016; Wang et al., 2016). Accordingly, the PAM71 protein is localized in the chloroplast, more precisely, in the thylakoid membrane (Schneider et al., 2016).

PAM71 knock out mutants are characterized as pale green and small growing plants with drastically reduced PSII performance (Frank et al., 2019; Schneider et al., 2016; Wang et al., 2016). Reduced chlorophyll contents and reduced PSII protein levels explain the pale green phenotype as well as the reduced electron transport of PSII (Schneider et al., 2016; Wang et al., 2016). The ability of PAM71 to rescue the yeast $\Delta pmr1$ Mn^{2+} -sensitive phenotype demonstrated PAM71 to transport Mn^{2+} (Schneider et al., 2016). Two other studies mentioned the impact of PAM71 on cellular Ca^{2+} levels and accordingly a Ca^{2+} transport function (Frank et al., 2019; Wang et al., 2016). Schneider et al. (2016) hypothesized mainly a Mn^{2+} transport function of PAM71 from the chloroplast stroma into the thylakoid lumen, since only Mn^{2+} supplementation, but not Ca^{2+} , to the growth media was able to rescue the *pam71* photosynthetic phenotype back to WT levels. The reduced protein levels of PSII core proteins and the OEC complex are most probably a consequence of the lack of Mn^{2+} in the thylakoid lumen (Schneider et al., 2016). Additionally, decreased levels of Mn incorporated into PSII complexes are found in the *pam71* mutant (Schneider et al., 2016). In the absence of PAM71, low affinity systems (LAS) are supposed to transport small amounts of Mn into the thylakoid lumen, resulting in a few proper assembled PSII super complexes (Figure 4) which keep *pam71* alive (Schneider et al., 2016). All these findings strengthen the hypothesis of PAM71 being a thylakoid localized Mn^{2+} transporter, rather than a Ca^{2+} transporter (Schneider et al., 2016).

The closest homolog of PAM71 is PAM71-HL/CMT1 (encoded by *At4g31590*), which harbors a different chloroplast target peptide (cTP) (Hoecker et al., 2017; Schneider et al., 2016), is supposed to be localized in the chloroplast envelope membrane according to proteomic studies (Ferro et al., 2010; Ferro et al., 2003; Simm et al., 2013). The remaining three homologs in *Arabidopsis thaliana* are encoded by the genes *At5g36290* (*GDT1-like 3*), *At1g22520* (*GDT1-like 4*) and *At1g68650* (*GDT1-like 5*) (Hoecker et al., 2017). The encoded proteins share the topology with PAM71, with differences in the N-terminal regions, e.g. lacking an N-terminal region (*GDT1-like 4* and *GDT1-like 5*) or containing a shorter N-terminal region, putatively coding for a signal peptide directing the protein to the secretory pathway (*GDT1-like 3*) (Hoecker et al., 2017). The genes *At1g22520* and *At1g68650* are supposed to

have evolved through a segmental chromosome duplication event in a progenitor of *Arabidopsis thaliana* and are in contrast to PAM71 and CMT1 not strictly conserved as a homologous pair in other plant species (Hoecker et al., 2017).

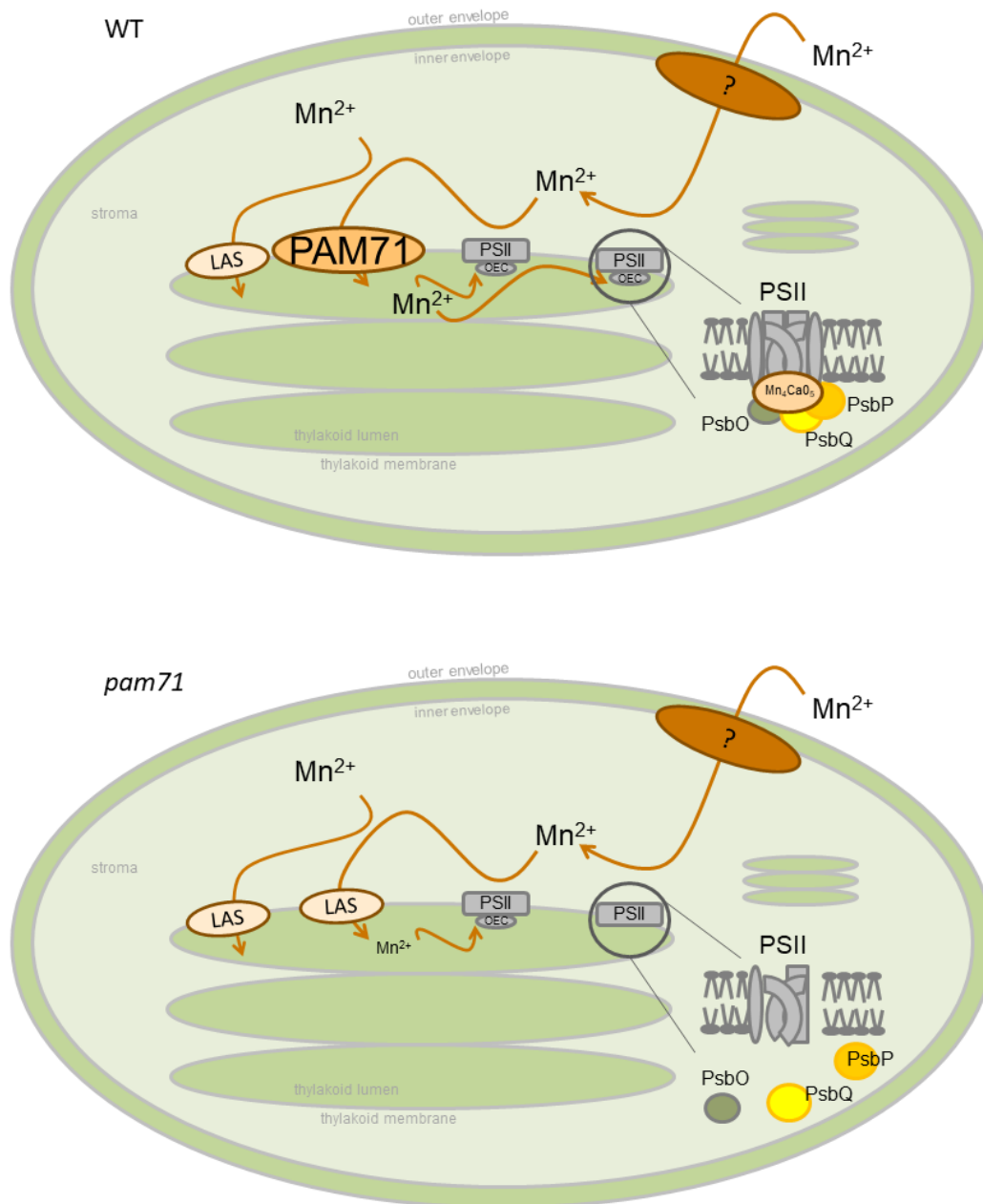


Figure 4 Schematic model for PAM71 in WT and *pam71* mutant. In WT plants, PAM71 transports Mn^{2+} from the stroma into the thylakoid lumen where it is integrated into the OEC. In *pam71* mutants, low affinity systems are supposed to import small amounts of Mn^{2+} (depicted as smaller written Mn^{2+}) into the thylakoid lumen and only a few proper PSII super complexes (PSII SC) including the OEC are built. Mn deficiency restricts the assembly of PSII SC and results in rapid disassembly. LAS (Low Affinity System) is expected to transport small amounts of Mn^{2+} into the thylakoid lumen, especially when PAM71 is missing. *Modified from* (Hoecker et al., 2017; Schmidt et al., 2020; Zhang et al., 2018)

7 Results

7.1 Publication I: The Plastid Envelope CHLOROPLAST MANGANESE TRANSPORTER1 Is Essential for Manganese Homeostasis in *Arabidopsis*

Marion Eisenhut¹, **Natalie Hoecker**¹, Sidsel Birkelund Schmidt, Rubek Merina Basgaran, Samantha Flachbart, Peter Jahns, Tabea Eser, Stefan Geimer, Søren Husted, Andreas P M Weber, Dario Leister, Anja Schneider

Mol Plant.2018 Jul 2;11(7):955-969

1: Marion Eisenhut and Natalie Hoecker both contributed equally to this work.

Supplementary data available under:

<https://www.sciencedirect.com/science/article/pii/S1674205218301588>

The Plastid Envelope CHLOROPLAST MANGANESE TRANSPORTER1 Is Essential for Manganese Homeostasis in *Arabidopsis*

Marion Eisenhut^{1,5,*}, Natalie Hoecker^{2,5}, Sidsel Birkelund Schmidt³, Rubek Merina Basgaran¹, Samantha Flachbart¹, Peter Jahns¹, Tabea Eser², Stefan Geimer⁴, Søren Husted³, Andreas P.M. Weber¹, Dario Leister² and Anja Schneider^{2,*}

¹Biochemie der Pflanzen, Cluster of Excellence on Plant Science (CEPLAS), Heinrich-Heine-Universität Düsseldorf, 40225 Düsseldorf, Germany

²Molekularbiologie der Pflanzen (Botanik), Department Biologie I, Ludwig-Maximilians-Universität München, 82152 Martinsried, Germany

³Department of Plant and Environmental Sciences and Copenhagen Plant Science Centre (CPSC), Faculty of Science, University of Copenhagen, 1871 Frederiksberg, Denmark

⁴Zellbiologie/Elektronenmikroskopie NW I/B1, Universität Bayreuth, 95447 Bayreuth, Germany

⁵These authors contributed equally to this article.

*Correspondence: Marion Eisenhut (m.eisenhut@uni-duesseldorf.de), Anja Schneider (anja.schneider@lrz.uni-muenchen.de)

<https://doi.org/10.1016/j.molp.2018.04.008>

ABSTRACT

The transition metal manganese (Mn) is indispensable for photoautotrophic growth since photosystem II (PSII) employs an inorganic Mn_4CaO_5 cluster for water splitting. Here, we show that the *Arabidopsis* membrane protein CHLOROPLAST MANGANESE TRANSPORTER1 (CMT1) is involved in chloroplast Mn homeostasis. CMT1 is the closest homolog of the previously characterized thylakoid Mn transporter PHOTOSYNTHESIS-AFFECTED MUTANT71 (PAM71). In contrast to PAM71, CMT1 resides at the chloroplast envelope and is ubiquitously expressed. Nonetheless, like PAM71, the expression of CMT1 can also alleviate the Mn-sensitive phenotype of yeast mutant $\Delta pmr1$. The *cmt1* mutant is severely suppressed in growth, chloroplast ultrastructure, and PSII activity owing to a decrease in the amounts of pigments and thylakoid membrane proteins. The importance of CMT1 for chloroplast Mn homeostasis is demonstrated by the significant reduction in chloroplast Mn concentrations in *cmt1-1*, which exhibited reduced Mn binding in PSII complexes. Moreover, CMT1 expression is downregulated in Mn-surplus conditions. The *pam71 cmt1-1* double mutant resembles the *cmt1-1* single mutant rather than *pam71* in most respects. Taken together, our results suggest that CMT1 mediates Mn^{2+} uptake into the chloroplast stroma, and that CMT1 and PAM71 function sequentially in Mn delivery to PSII across the chloroplast envelope and the thylakoid membrane.

Key words: manganese, transporter, envelope, chloroplast, photosynthesis, *Arabidopsis*

Eisenhut M., Hoecker N., Schmidt S.B., Basgaran R.M., Flachbart S., Jahns P., Eser T., Geimer S., Husted S., Weber A.P.M., Leister D., and Schneider A. (2018). The Plastid Envelope CHLOROPLAST MANGANESE TRANSPORTER1 Is Essential for Manganese Homeostasis in *Arabidopsis*. *Mol. Plant*. **11**, 955–969.

INTRODUCTION

The transition metal manganese (Mn) is a trace element required for growth of all known living organisms. In plants, Mn is integral to physiological functions including photosynthesis, redox processes (e.g., as a catalytic metal ion in oxalate oxidase of barley, *Hordeum vulgare*) (Whittaker et al., 2007), and scavenging of reactive oxygen species (ROS). With respect to the latter function, plant mitochondria possess a highly conserved Mn superoxide dismutase (MnSOD) catalyzing the dismutation of two superoxide radicals to H_2O_2 and oxygen (Fridovich, 1995; Kliebenstein et al.,

1998). MnSOD has been reported to play an important role in plant growth (Morgan et al., 2008), especially during embryo sac development and fertilization (Martin et al., 2013).

A further essential function of Mn relates to photosynthetic electron transport, which takes place in thylakoid membranes found in cyanobacteria and in chloroplasts of plants and algae.

Thylakoid membranes harbor the four major protein complexes photosystem I (PSI), photosystem II (PSII), Cytochrome-*b₆/f* complex (Cytb₆f), and ATP synthase, which make use of light energy to drive electron transport from water (at the donor side of PSII) to NADP⁺ (at the acceptor side of PSI) and to generate an electrochemical proton gradient that is utilized for ATP synthesis. PSII comprises the oxygen-evolving complex (OEC), an inorganic Mn₄CaO₅ cluster, which is ligated to the PSII core proteins D1 and CP43 (Ferreira et al., 2004; Kawakami et al., 2011; Umena et al., 2011). In higher plants, a set of three extrinsic non-ligating proteins (PsbO, PsbP, and PsbQ) protect and stabilize the Mn₄CaO₅ cluster (Suorsa and Aro, 2007). Using T-DNA insertional mutagenesis in *Arabidopsis*, it was shown that at least one of these extrinsic proteins, the PsbP1 isoform, is essential for photoautotrophic growth (Allahverdiyeva et al., 2013).

The fundamental role of Mn in photosynthesis and as a co-factor for MnSOD was underlined by a study analyzing Mn deficiency in *Chlamydomonas reinhardtii* (Allen et al., 2007). Interestingly, MnSOD activity decreased before that of PSII, suggesting the intracellular regulation of Mn supply in *Chlamydomonas* to preferentially support PSII function in chloroplasts over MnSOD function (Allen et al., 2007). Mn-deficient plants typically show retarded growth and decreased biomass. Most frequently Mn deficiency results from oxidation of plant-available Mn²⁺ to unavailable forms, caused by alkaline soil conditions. In contrast, soil acidity increases the Mn²⁺ concentration to levels that might induce Mn toxicity. Interestingly, excess Mn causes minimal changes in PSII photochemical efficiency and targets mostly PSI in *Arabidopsis* (Millaleo et al., 2013).

Arabidopsis relies on a high-affinity Mn uptake system under conditions of low Mn availability, which is represented by the divalent metal transporter NATURAL RESISTANCE ASSOCIATED MACROPHAGE PROTEIN1 (NRAMP1) (Cailliatte et al., 2010). The corresponding gene is expressed in roots, and consistent with its function, NRAMP1 localizes to the plasma membrane. It has been shown that a naturally occurring accession containing a histidine to tyrosine substitution in NRAMP1 is severely compromised in photosynthetic performance at chilling temperatures due to Mn deficiency (Ihnatowicz et al., 2014). Two homologous transporters, NRAMP3 and NRAMP4, play an important role in the vacuolar export of Mn in mesophyll cells of rosette leaves (Lanquar et al., 2010). The impaired Mn release from mesophyll vacuoles in *nramp3 nramp4* double-mutant plants was associated with reduced plant growth and a less functional PSII under Mn deficiency, yet the mitochondrial MnSOD activity was maintained. The authors suggested Mn transit through the vacuole prior to import into chloroplasts (Lanquar et al., 2010). Besides taking part in Mn homeostasis, the NRAMP1, NRAMP3, and NRAMP4 proteins are also involved in Fe homeostasis (Curie et al., 2000; Lanquar et al., 2005). Recently, a critical function for NRAMP2 in intracellular Mn distribution was demonstrated. NRAMP2 resides in the membrane of the trans-Golgi network and affects the cytoplasmic Mn pool, from which Mn is recruited to the organelles where it functions in fighting oxidative stress and in photosynthesis (Alejandro et al., 2017; Gao et al., 2018). Mn²⁺ loading into the vacuole is mediated by members of the CATION EXCHANGER (CAX) family, CAX2, CAX4, and CAX5, which are constitutively expressed at low levels in all tissues of

Arabidopsis (Hirschi et al., 2000; Cheng et al., 2002; Edmond et al., 2009). *Arabidopsis cax2* mutants accumulate significantly less vacuolar Mn than wild-type (WT) plants (Pittman et al., 2004) but do not display an obvious phenotype, presumably due to functional redundancy. Several other transporters have been implicated in Mn transport across the plasma membrane, into or out of the vacuole, and into the endoplasmic reticulum/Golgi apparatus, and most of them have the ability to transport other cations as well (Socha and Gueriot, 2014).

Despite its essential role in mitochondria and chloroplasts, little is known about how Mn is taken up into and further handled in these organelles. Recently the transporter PHOTOSYNTHESIS-AFFECTED MUTANT71 (PAM71) was shown to be required for efficient uptake of Mn²⁺ into the thylakoid lumen of *Arabidopsis* chloroplasts (Schneider et al., 2016). In *pam71* mutant plants the OEC of PSII was specifically affected and thus PSII photochemical efficiency significantly dropped, resulting in reduced growth and biomass production. The requirement of PAM71/putative CHLOROPLAST LOCALIZED CA²⁺/H⁺ ANTIporter1 (CCHA1) for PSII function was also observed by Wang et al. (2016). Consistent with its function, the PAM71 protein localizes to the thylakoid membrane of *Arabidopsis* (Schneider et al., 2016). PAM71 belongs to the ubiquitous UPF0016 family, and shares homology with GCR1 DEPENDENT TRANSLATION FACTOR1 (GDT1) in yeast (*Saccharomyces cerevisiae*) and TRANSMEMBRANE PROTEIN165 (TMEM165) in human (*Homo sapiens*) (Demaegd et al., 2014; Hoecker et al., 2017). Furthermore, one homologous protein, designated Mn EXPORTER (MNX) (Brandenburg et al., 2017) or SynPAM71 (Gandini et al., 2017), exists in the cyanobacterium *Synechocystis* sp. PCC 6803 and is encoded by the gene *slr0615*. The Δmnx and $\Delta SynPAM71$ strains display increased sensitivity toward externally supplied Mn and Mn toxicity symptoms caused by increased intracellular Mn accumulation (Brandenburg et al., 2017; Gandini et al., 2017). Thus, it was hypothesized that MNX/SynPAM71 is involved in the export of Mn from the cytoplasm into the luminal and periplasmic compartments. Accordingly, this protein was localized to the thylakoid membrane (Brandenburg et al., 2017; Gandini et al., 2017) and the plasma membrane (Gandini et al., 2017).

In most eukaryotes and bacteria, only single members of the UPF0016 family are present. In *Arabidopsis*, this protein family comprises five members, including PAM71 and its closest homolog PAM71HL (Schneider et al., 2016; Hoecker et al., 2017). In the course of this study we found that PAM71HL also contributes to Mn homeostasis, and therefore we renamed this protein CHLOROPLAST MANGANESE TRANSPORTER1 (CMT1). In an independent study, the importance of CMT1 for chloroplast Mn homeostasis was also demonstrated (Zhang et al., 2018). In this report, we describe analysis of the *Arabidopsis cmt1* single-mutant and *pam71 cmt1* double-mutant lines. Both lines were strongly impaired in chloroplast Mn homeostasis. The double mutant *pam71 cmt1* resembled the *cmt1* single mutant rather than the *pam71* single mutant, indicating that these proteins have different and non-overlapping functions and that the CMT1 protein operates upstream of PAM71. This observation is in line with the proposed function of CMT1 as a plastid Mn importer, transporting Mn²⁺ from the cytosol into the chloroplast stroma.

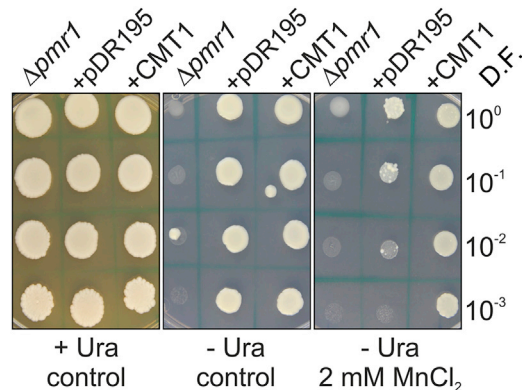


Figure 1. Characterization of CMT1.

AT4G13590 (= CMT1) expression suppresses the MnCl_2 sensitivity of the P-type $\text{Ca}^{2+}/\text{Mn}^{2+}$ -ATPase ($\Delta pmr1$) yeast mutant. Untransformed yeast cells and yeast cells transformed with the empty vector pDR195 (+pDR195) or with a vector expressing CMT1 (+CMT1) were dropped on different media. Undiluted yeast cells (10^0) correspond to an $\text{OD}_{600} = 3.0$. Photographs were taken after 4 days at 30°C . D.F., dilution factor.

RESULTS

CMT1 Facilitates Mn Transport

The protein AT4G13590 belongs to the UPF0016 family, which contains five members in *Arabidopsis* (Hoecker et al., 2017) (Supplemental Table 1). It is the closest homolog of the thylakoid Mn transporter PAM71 (AT1G64150) with 49% identity and 64% similarity at the amino acid sequence level. Accordingly, we tested the ability of AT4G13590 to facilitate Mn transport. To this end, AT4G13590 was cloned into the yeast expression vector pDR195 and introduced into the yeast (*S. cerevisiae*) strain $\Delta pmr1$. This strain is defective in pumping Mn^{2+} and Ca^{2+} into the Golgi and is hence sensitive to high concentrations of Mn in the growth medium (Dürr et al., 1998). Transformation of $\Delta pmr1$ with the empty vector control conferred uracil auxotrophy but could not attenuate the negative effect of high Mn concentrations on the growth of the strain (Figure 1). In contrast, when $\Delta pmr1$ was transformed with the plasmid for AT4G13590 expression, growth of the resulting strain was unaffected by elevated Mn concentrations (Figure 1). We propose that chloroplast-localized (see below) AT4G13590 functions as a Mn transporter, and we thus named this protein CHLOROPLAST MANGANESE TRANSPORTER1 or CMT1 (Supplemental Table 1).

CMT1 Localizes to the Chloroplast Envelope and is Ubiquitously Expressed

The protein sequence of CMT1 possesses an N-terminal chloroplast transit peptide. In contrast to PAM71, which was detected in the thylakoid membrane (Schneider et al., 2016), CMT1 was found to be enriched in the chloroplast envelope fraction of *Arabidopsis* (Ferro et al., 2003, 2010) and absent in the thylakoid membrane fraction (Ferro et al., 2010). CMT1 was also identified in *Pisum sativum* (pea) chloroplast envelope membranes in other proteome analyses (Bräutigam et al., 2008; Bräutigam and Weber, 2009; Simm et al., 2013). To verify its subcellular localization, CMT1 was fused N-terminally to YFP and transiently expressed in tobacco leaves. Confocal

microscopy of isolated protoplasts demonstrated that the CMT1:YFP signal surrounded the chloroplasts, whereas the chlorophyll fluorescence was equally distributed within the chloroplasts (Figure 2A). In accordance with the proteomic data mentioned above, this result indicates that CMT1 resides in the chloroplast envelope, most likely in the inner envelope membrane. In fractions derived from pea chloroplasts, the two envelope membranes can be separated into inner and outer envelopes, and indeed CMT1 was assigned to the inner envelope membrane in pea (Simm et al., 2013).

To determine the tissue-specific expression pattern of CMT1, we fused the promoter of CMT1 to the reporter gene β -glucuronidase (GUS). We found GUS staining in cotyledons (Figure 2B), true leaves, and roots of seedlings (Figure 2B) and in mature plants (Supplemental Figure 1). Thus, CMT1 is ubiquitously expressed within the plant.

Knockout Alleles of CMT1 Affect Plant Growth and Development

To study the physiological role of CMT1, we analyzed mutant lines carrying T-DNA insertions in AT4G13590. In total, three independent alleles, named *cmt1-1* to *cmt1-3* (Supplemental Figure 2A), were isolated. The three mutants showed similar phenotypes, including strongly reduced growth rates, drastically reduced leaf size, pale-green leaf coloration, and late flowering (Figure 3A, 3B, and 3C and Supplemental Figure 2B). The defective phenotype of *cmt1-1* could be complemented by introducing a cDNA copy of CMT1 under the control of the *UBIQUITIN10* promoter. The resulting line was named *cmt1-1_{PUB10:CMT1}* (Figure 3A).

The distinct leaf phenotype of the mutant prompted us to investigate leaf cross-sections via transmission electron microscopy. In WT and the complemented line the palisade and spongy layers were clearly distinguishable (Figure 3D). In *cmt1-1* it was impossible to distinguish between the palisade and spongy parenchyma. Nevertheless, it was possible to identify chloroplasts with an ordered thylakoid structure composed of grana stacks and stroma lamellae (Figure 3D). In contrast to WT and *cmt1-1_{PUB10:CMT1}*, where nearly all chloroplasts contained starch granules, almost all chloroplasts of *cmt1-1* examined were missing these granules. In addition, *cmt1-1* contained abnormal chloroplasts (Figure 3E). Indeed, only 20% of analyzed chloroplasts resembled WT chloroplasts (Figure 3F). Furthermore, the phenotype of abnormal chloroplasts in *cmt1-1* was not homogeneous. We found some *cmt1-1* chloroplasts where the lamellae were totally or partially relaxed and some chloroplasts with hyperstacked grana membranes (Figure 3E). Interestingly, the chloroplast ultrastructure in *pam71* was nearly unaffected (Schneider et al., 2016). Thus, we conclude that the function of CMT1 is linked to chloroplast development and that individual chloroplasts respond in an autonomous manner.

The *cmt1-1* Mutant Displays Defects in PSII and PSI Performance

To examine whether the lack of CMT1 affects photosynthesis, we monitored chlorophyll a fluorescence and P_{700} redox kinetics in WT, *cmt1-1*, and *cmt1-1_{PUB10:CMT1}*. PSII functionality (F_v/F_m)

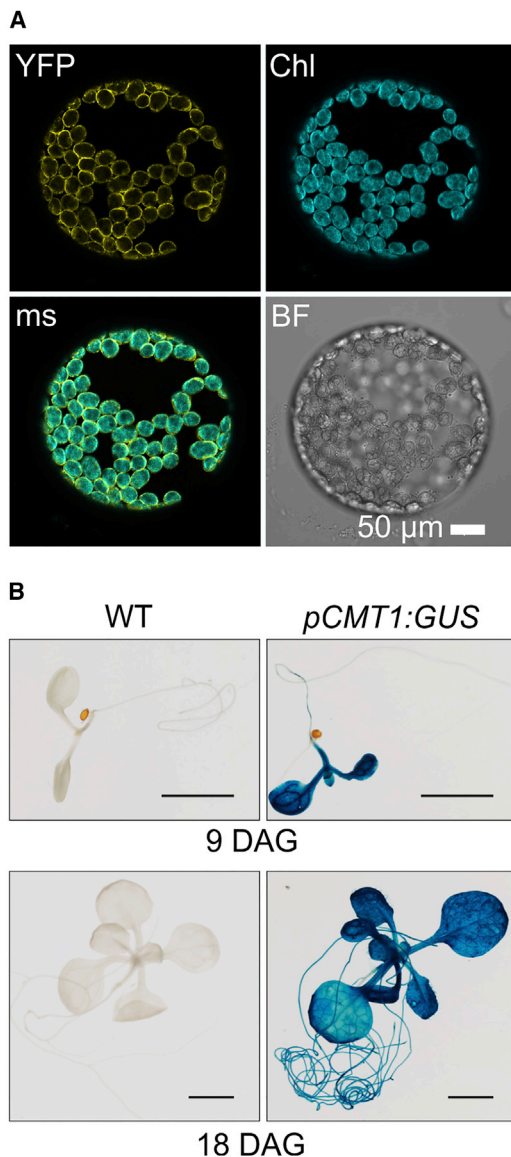


Figure 2. Subcellular Localization of CMT1 and CMT1 Promoter Analysis.

(A) Envelope localization of the CMT1:YFP fusion protein. *Nicotiana benthamiana* leaves were infiltrated with an appropriate *Agrobacterium* strain, protoplasts were isolated after 48 h, and localization of the fusion protein was analyzed by confocal microscopy. YFP fluorescence was excited at 488 nm and emission recorded at 505–550 nm. Chlorophyll autofluorescence (Chl) was excited at 488 nm and emission was recorded at 650 nm. Signals were merged (ms), and a bright-field (BF) image was taken to show protoplast intactness.

(B) Tissue-specific gene expression analysis of CMT1 in seedlings using a promoter:GUS reporter. Transgenic plants carrying *pCMT1:GUS* were assayed for CMT1 promoter activity by staining for GUS at the indicated days after germination (DAG). Plants were grown under a 12-h/12-h light/dark cycle at 22°C/18°C at 90 $\mu\text{mol photons m}^{-2} \text{s}^{-1}$. As a negative control, WT seedlings were used. Scale bars, 5 mm.

and effective quantum yield (Φ_{II}) were significantly reduced in the *cmt1-1* mutant (Table 1 and Supplemental Figure 3A). However, the overall chlorophyll a fluorescence profile was similar in all three genotypes (Supplemental Figure 3A). In addition, P_{700}

redox kinetic studies revealed that the $\Delta A/\Delta A_{\text{max}}$ value was significantly increased in *cmt1-1*, indicating that electron flow toward PSI was reduced (Table 1, Supplemental Figure 3B), which might be a direct consequence of the reduced Φ_{II} .

To investigate the photosynthetic performance in response to different light intensities, we recorded light curves. Electron transport rates of PSI (ETR_I) and PSII (ETR_{II}) were strongly reduced in *cmt1-1*, with ETR_{II} being more affected (Figure 4A and 4B). In agreement with the increased $\Delta A/\Delta A_{\text{max}}$ values, the *cmt1-1* mutant already showed higher non-photochemical PSI quantum yield of donor side limitation, Y(ND), under low light intensities (Supplemental Figure 4A), supporting the assumption that PSII activity is reduced and does not provide sufficient electrons for re-reduction of P_{700} . ETR_{II} of *cmt1-1* decreased at light intensities higher than the growth light intensity of 90 $\mu\text{mol photons m}^{-2} \text{s}^{-1}$ (Figure 4B), indicating the pronounced susceptibility of PSII to high light in *cmt1-1*. This sensitivity to high light was not related to impaired heat dissipation of excess light energy, since under low light intensities *cmt1-1* plants showed an even higher yield of regulated non-photochemical quenching, Y(NPQ), than WT plants (Figure 4C and 4D). However, this regulatory mechanism was not sufficient in *cmt1-1*, as the photosynthetic phenotype was accompanied by high quantum yield of non-regulated energy dissipation, Y(NO) (Supplemental Figure 4B). Importantly, in all measurements the complemented line behaved like the WT. These results together indicate that the loss of CMT1 results in severely reduced photosynthetic activity and markedly enhanced susceptibility to high light.

Reduced Transcription and Translation of Chloroplast Proteins

The results so far suggest that CMT1 has an important function in photosynthesis and also in chloroplast development. We therefore inspected the expression of plastid encoded genes. Northern blot analysis was performed with RNA isolated from leaf tissues of WT, *cmt1-1*, and *cmt1-1 PUB10:CMT1*. For detection, we used radiolabeled probes corresponding to transcripts coding for representative subunits of PSI (*psaA*) and PSII (*psbA*, *psbB*, *psbC*, and *psbD*, which code for D1, CP47, CP43, and D2 respectively), and *Cytb₆f* (*petB*, which codes for *Cytb₆*), and for the large subunit of Rubisco (*rbcl*). A probe recognizing the nuclear encoded transcript for *Lhcb2* was also included (Figure 5A). Transcript levels of *psaA*, *psbA*, *psbB*, *psbC*, *psbD*, and *rbcl* were reduced to about 50% of WT levels in *cmt1-1*, whereas the levels of *petB* and *Lhcb2* transcripts were less affected (Figure 5A). Accordingly, the translation rates of PsaA/B, RbcL, and D1/D2 in *cmt1-1* were less than 50% of WT rates (Figure 5B).

The defects in transcription and translation in *cmt1-1* presumably cause changes in the steady-state level of the various proteins. Therefore, steady-state protein levels were examined by immunoblot analysis (Figure 5C). Accumulation of PSII subunits (D1, CP47, CP43, D2, PsbO, PsbP), PSI subunits (PsaA, PsaD), and RbcL were reduced to approximately 50% of WT levels in *cmt1-1*. Interestingly, steady-state levels of subunits of the intersystem electron transport chain (*Cytb₆*, *Cytf*, and plastocyanin) were reduced to less than 50% of WT levels, despite the nearly unchanged mRNA levels of *petB* (Figure 5A).

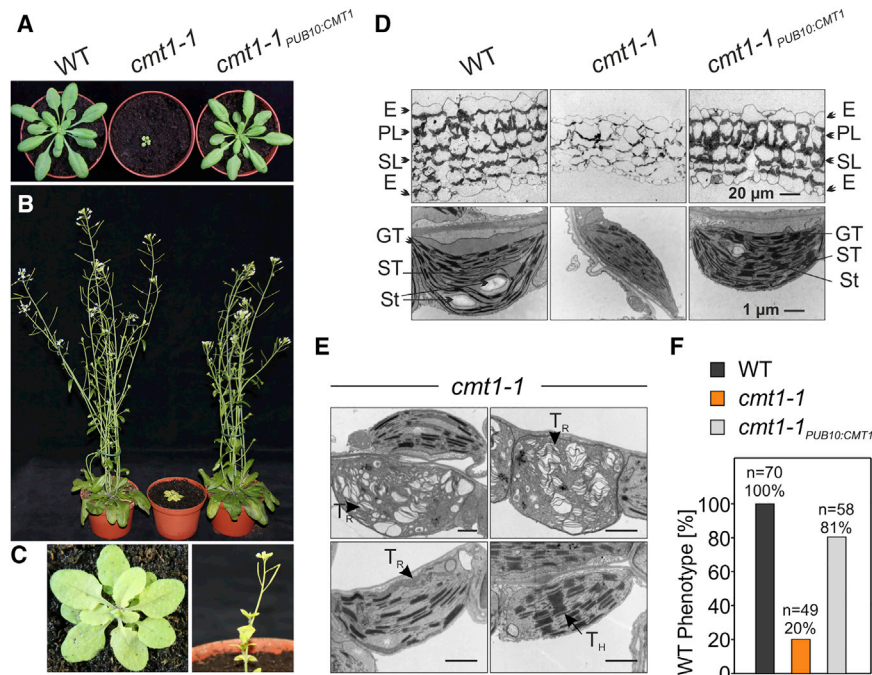


Figure 3. Growth Phenotype of *cmt1-1*, Complementation of *cmt1-1*, and Ultrastructural Analysis.

(A) Plants were grown for 4 weeks under a 12-h/12-h light/dark cycle at 22°C/18°C and at 90 $\mu\text{mol photons m}^{-2} \text{s}^{-1}$ and then transferred to a temperature-controlled greenhouse for flowering and seed production.

(B) Plants at an age of 8 weeks are shown.

(C) Top view of the *cmt1-1* plant shown in (B) (left panel). Flowering of the *cmt1-1* mutant at an age of 10 weeks (right panel).

(D) Electron micrographs of 2-week-old plants. Leaf sections (top panel) and individual normal chloroplasts (bottom panel) of each genotype are depicted. Epidermis (E), palisade layer (PL), spongy layer (SL), starch (St), grana thylakoids (GT), and stroma thylakoids (ST) are indicated.

(E) Ultrastructural alterations in *cmt1-1* chloroplasts range from strongly to moderately affected. Loosely appressed (= relaxed) thylakoid stacks are indicated by the arrowhead (T_R) and hyperstacking of thylakoids (T_H) is indicated by an arrow. Scale bars, 1 μm .

(F) Quantification of the chloroplast phenotype. Ten cells of each genotype were analyzed, and the number (*n*) of inspected chloroplasts is given. The percentage of chloroplasts with a nearly WT phenotype, as shown in (D), is given.

Only the steady-state level of Lhcb2 was unaffected, and the amount of the ATP synthase β subunit (AtpB) was only marginally decreased (Figure 5C). These results suggest that the reduced steady-state levels of thylakoid proteins in *cmt1-1* are partially due to reduced chloroplast transcription and translation. In this regard, *cmt1-1* clearly differs from the *pam71* mutant. In *pam71* the chloroplast transcription and translation machinery was unaffected and the reduction in PSII and PSI subunit accumulation appeared to occur at the post-translational level (Schneider et al., 2016).

Decreased Mn Concentrations in *cmt1-1* Shoots and Chloroplasts Result in Reduced Mn Binding in PSII

The impact of CMT1 on Mn homeostasis in leaves and chloroplasts was investigated. The analysis of Mn concentrations in leaf tissue revealed significant reductions in *cmt1-1*, ~60% compared with WT (Figure 6A). In addition, the concentrations of iron (Fe) and other elements relevant to photosynthesis were analyzed to determine whether the loss of CMT1 had element-specific or more general effects on metal homeostasis. Interestingly, the Fe concentration was nearly doubled in *cmt1-1* leaves compared with WT leaves (Figure 6A), whereas the Fe concentration in *cmt1-1* chloroplast fractions was decreased to ~56% of that in WT (Figure 6B). The latter result is consistent with the reduced abundance of PSI subunits in *cmt1-1* (Figure 5C). Importantly, the Mn concentration in intact chloroplasts was reduced to ~30% compared with WT, indicating that CMT1 loss of function specifically affects this metal (Figure 6B). In leaves of *cmt1-1*^{PUB10:CMT1} the Mn and Fe concentrations almost reached WT levels, but in chloroplasts the concentrations of both metals recovered to WT levels (Figure 6A and 6B). In addition to analyzing Mn and Fe

contents in chloroplasts, other elements such as Mg, Cu, P, and Zn were analyzed (Supplemental Figure 5). Only the concentration of Mg in chloroplasts was significantly reduced in *cmt1-1* (~57% of the WT concentration), consistent with the observed chlorotic phenotype of the mutant.

Next, Mn and Fe binding in various photosynthetic complexes were investigated according to the method developed by Schmidt et al. (2015). Isolated and solubilized thylakoid membrane complexes were fractionated by blue-native PAGE or size-exclusion chromatography (SEC). Although several bands corresponding to the different photosynthetic complexes could be identified (Figure 6C), only the abundance of the LHCII trimer complex was similar in all three genotypes. The abundance of various PSII complexes (PSII supercomplexes, PSII monomer complexes, and PSII complex without CP43) and the PSII dimer/PSI monomer fractions were markedly reduced in *cmt1-1* compared with WT (Figure 6C), in line with the lower steady-state levels of thylakoid proteins in the *cmt1-1* mutant (Figure 5C). The solubilized thylakoid membrane complexes were further analyzed by SEC combined with inductively coupled plasma mass spectrometry (SEC-ICP-MS) to determine the ion intensities of sulfur (S), Mn, and Fe in the fractionated photosynthetic complexes. A pronounced decrease in the ion intensity of S was observed in *cmt1-1* compared with WT (Figure 6D and 6E), reflecting the lower protein abundance in this mutant (Figure 6C). Moreover, the reduced abundance of PSII and PSI complexes was further supported by reduced ion intensity signals for Mn and Fe (Figure 6D and 6E). The stoichiometric ratios of Mn/S and Fe/S were analyzed to determine the relative amount of Mn and Fe incorporation per unit of S (proxy for protein) in PSII and in PSI, respectively. Clear differences in PSII and PSI intactness were

	WT	<i>cmt1-1</i>	<i>cmt1-1^{PUB10k:CMT1}</i>
F_v/F_m	0.81 ± 0.01	$0.57 \pm 0.06^{***}$	$0.78 \pm 0.01^{**}$
Φ_{II}	0.53 ± 0.03	$0.37 \pm 0.07^{**}$	$0.49 \pm 0.03^*$
$\Delta A/\Delta A_{max}$	0.13 ± 0.08	$0.52 \pm 0.20^{**}$	0.20 ± 0.08

Table 1. Spectroscopic Analysis of the WT, Mutant, and Complementation Line.

Plants were dark-adapted for 30 min and F_v/F_m was determined. Yield of PSII (Φ_{II}) was recorded following exposure for 5 min to 125 $\mu\text{mol photons m}^{-2} \text{ s}^{-1}$ photosynthetically active radiation. $\Delta A/\Delta A_{max}$ was calculated from P_{700} absorption changes. Ten different plants were measured and mean values \pm SD are presented. Asterisks indicate the statistical significance of differences between WT and mutant plants (*t*-test): *** $P < 0.0001$, ** $P < 0.001$, * $P < 0.01$.

found (Figure 6F). In *cmt1-1*, much less Mn was loaded into PSII super- and subcomplexes compared with WT, while Fe incorporation in PSI monomers was unaltered (Figure 6F). Taken together, these findings indicate the specifically reduced incorporation of Mn into PSII, indicating lower amounts of functional PSII complexes in the mutant, whereas the reduction in Fe signal intensities (Figure 6E) is the result of overall decreased PSI levels in *cmt1-1* and not loss of PSI functionality.

The *pam71 cmt1-1* Double Mutant Resembles *cmt1-1*

We were very interested in the phenotype of the *pam71 cmt1-1* double mutant. Due to the different membrane localization of the respective proteins—CMT1 in the envelope membrane (this study) and PAM71 in the thylakoid membrane (Schneider et al., 2016)—we expected that the two proteins were not redundant in function. A homozygous double mutant was generated by crossing, and we verified that *pam71 cmt1-1* possessed knockout alleles for both genes (Supplemental Figure 6A and 6B). The phenotypic appearance of *pam71 cmt1-1* plants more closely resembled that of *cmt1-1* plants than that of *pam71* plants, and hence confirmed our assumption (Figure 7A and 7B). The increase in minimal chlorophyll *a* fluorescence (F_0) and concomitant decrease in F_v/F_m in *pam71 cmt1-1* (Figure 7C) indicated profound defects in electron transfer within PSII comparable with *cmt1-1* (Table 1 and Figure 4). Moreover, transcription and translation of chloroplast genes, steady-state protein levels (Supplemental Figure 6C–6E), and effects on Mn and Fe homeostasis (Supplemental Figure 7) in *pam71 cmt1-1* and *cmt1-1* were similar, and CMT1 defects could be restored in an independent complemented line *cmt1-1^{P35S:CMT1}* (Supplemental Figures 6 and 7). Interestingly, the double mutant behaved slightly better than *cmt1-1*. The phenotypes of *cmt1-1*, *pam71* and the double mutant based on visual inspection were very consistent with those determined from the analysis of pigment composition. The contents of chlorophyll and carotenoids decreased slightly in *pam71*, strongly in *pam71 cmt1-1*, and decreased the most in *cmt1-1* compared with WT (Figure 7D). In addition, we monitored the production of ROS in all three mutants and WT. *In situ* staining with nitroblue tetrazolium (NBT) or diaminobenzidine (DAB) revealed the accumulation of superoxide anion ($\text{O}_2^{\cdot-}$), but not H_2O_2 in *cmt1-1*, *pam71*, and the double mutant (Figure 7E), presumably as a direct consequence of defective photosynthetic electron transport rates.

Furthermore, we monitored the steady-state level of mitochondrial MnSOD. Levels of this enzyme decreased to ~50% of WT levels in *cmt1-1* and *pam71 cmt1-1* (Supplemental Figure 8), perhaps in response to the decreased leaf Mn concentration in *cmt1-1* (Figure 6A) and *pam71 cmt1-1* (Supplemental Figure 7A). In the *pam71* single mutant, the steady-state level of MnSOD remained unchanged compared with WT (Supplemental Figure 8).

CMT1 Expression Is Reduced and F_v/F_m Value Is Enhanced in *cmt1-1* and *pam71 cmt1-1* under Mn-Excess Conditions

To examine the response of CMT1 and PAM71 to excess Mn at the transcriptional level, we grew WT plants on medium supplemented with different concentrations of MnSO_4 (Figure 8A). It turned out that transcript levels, as evaluated by qRT-PCR, of PAM71 remained nearly unchanged under all conditions, whereas the expression of CMT1 was downregulated ~0.4-fold under Mn excess compared with standard-Mn conditions in leaves of WT plants (Figure 8A). Reduction in CMT1 promoter activity was likewise observed for *pCMT1:GUS* plants grown on 500 μM MnSO_4 (Supplemental Figure 9). Finally, we cultivated *cmt1-1* and *pam71 cmt1-1* plants under Mn-standard and Mn-excess conditions. The mutant *pam71* was included in this feeding experiment as a control (Figure 8B). The overall fitness of all genotypes was diminished in the presence of high (1 mM) MnSO_4 . However, the photosynthetic activity of PSII, monitored as F_v/F_m value, was unaffected under the different conditions (Figure 8B and 8C). The expected drop in F_v/F_m in all three mutants compared with WT was evident under standard-Mn conditions (Figure 8C). In *pam71* the F_v/F_m value increased to that of WT on 500 μM MnSO_4 and thus confirmed earlier studies (Schneider et al., 2016). Although the F_v/F_m value of *cmt1-1* and *pam71 cmt1-1* did not reach that of WT, neither on 500 μM nor on 1 mM MnSO_4 , it was significantly increased under 1 mM MnSO_4 compared with 50 μM MnSO_4 conditions (Figure 8C). This result confirmed that *pam71 cmt1-1* behaves almost the same as *cmt1-1* and not like *pam71*, and that the diminished PSII function in *cmt1-1* caused by Mn depletion in chloroplasts (Figure 6B) can be alleviated by increasing the Mn availability to the plant.

DISCUSSION

Mn is a metal co-factor for the OEC and essential for oxygenic photosynthesis. Despite its importance, it remains unknown how Mn is imported into the chloroplast to fulfill its function. In this study, we found evidence that the protein CMT1 is a plastid envelope Mn transporter in *Arabidopsis*, presumably facilitating the uptake of Mn^{2+} into the chloroplast stroma.

CMT1 Facilitates Mn Transport

CMT1 belongs, together with its closest homolog PAM71, to the UPF0016 family of membrane proteins, which is widely distributed among prokaryotes and eukaryotes (Demaegd et al., 2014), and members of this family in oxygenic photosynthetic organisms were demonstrated to function in Mn^{2+} transport (Schneider et al., 2016; Brandenburg et al., 2017; Gandini et al., 2017). In accordance, we found that expression of CMT1 in *Δpmr1* yeast cells suppressed their Mn sensitivity (Figure 1).

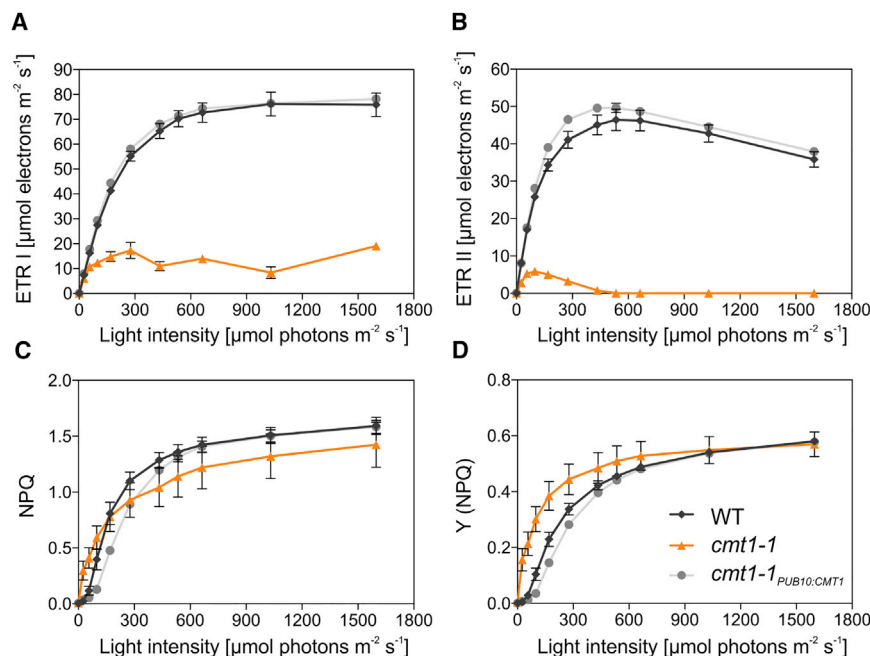


Figure 4. Light-Dependent Photosynthetic Performance in WT, *cmt1-1*, and *cmt1-1*^{PUB10:CMT1}

Electron transfer rates of PSI (ETR I) (A), electron transfer rates of PSII (ETR II) (B), non-photochemical quenching (NPQ) (C), and quantum yield of energy dissipation by NPQ (Y(NPQ)) (D) were measured in pre-illuminated leaves of plants grown at 90 $\mu\text{mol photons m}^{-2} \text{s}^{-1}$. Shown are average datasets (\pm SE) of six measurements per plant line.

consequence of Mn deficiency in chloroplasts, Mn binding in PSII complexes (Figure 6D) and consequently PSII functionality (Table 1; Figures 4 and 6F; Supplemental Figures 3 and 4) were strongly reduced in *cmt1-1*. In the case of Mn toxicity we would have expected increased Mn concentrations in leaves and/or chloroplasts and a stronger negative impact on PSI than PSII activity (Millaleo et al., 2013). Moreover, the Mn deficiency in *cmt1-1* was found to be

This finding indicates that CMT1 may also function as a Mn transporter. We further demonstrated that CMT1 resides in the envelope membrane of chloroplasts (Figure 2A; Ferro et al., 2003, 2010). Thus, we hypothesized that CMT1 functions as a Mn^{2+} transporter at the chloroplast envelope. However, the direction of Mn transport mediated by CMT1, i.e., whether it is involved in import or export of Mn, required closer inspection.

The *cmt1* Mutant Displays a Pleiotropic Mn-Deficiency Phenotype

To determine whether CMT1 acts as a plastid Mn importer or exporter, we analyzed *Arabidopsis* plants defective in CMT1 for symptoms related to Mn limitation and toxicity, respectively. The *cmt1* mutant plants showed severe growth defects, having only one-tenth of the rosette diameter of WT plants at the same developmental stage (Figure 3A and 3B; Supplemental Figure 2B). In fact, the phenotype of *cmt1* already appeared under standard growth conditions, whereas other *Arabidopsis* mutant lines defective in Mn transporters/homeostasis often display either hypersensitivity to Mn stress (MTP11, Peiter et al., 2007; ECA1, Wu et al., 2002) or reduced growth under Mn deficiency (NRAMP3/4, Lanquar et al., 2010), or confer Mn tolerance (MTP8, Eroglu et al., 2017). Interestingly, the phenotype of *cmt1* was slightly less severe in the *pam71* background as evidenced by the phenotype of the double mutant *pam71 cmt1-1* (Figure 7, Supplemental Figures 6 and 7), perhaps due to activation of low-affinity transport systems only in the *pam71* background. Despite this, the Mn content in leaves and—more importantly—in chloroplasts of *cmt1-1* was reduced significantly compared with WT levels (Figure 6A and 6B). The deficiency of Mn in chloroplasts of *cmt1-1* was very prominent; the Mn concentration in *cmt1-1* was only 30% of that in WT. In fact, the growth defects of the *cmt1* mutants resembled those of *Arabidopsis* plants grown in Mn-free medium (Rodríguez-Celma et al., 2016). As a

accompanied by an increased Fe concentration in leaves (Figure 6A), a feature readily observed in earlier studies of *Arabidopsis* plants grown under Mn deficiency (Yang et al., 2008). In contrast, Fe concentrations in *cmt1-1* chloroplasts dropped to about 56% of those in WT (Figure 6B), confirming the overall decreased PSI levels in *cmt1-1*. It was previously found that under Mn deficiency many robustly downregulated nuclear genes (at the transcript level as well as protein abundance) were related to photosynthesis, e.g., coding for subunits of PSII and PSI (Rodríguez-Celma et al., 2016). This finding was nicely reflected in this study. Indeed, transcription and translation of chloroplast genes was downregulated in *cmt1-1* (Figure 5A and 5B). Diminished transcription and translation of plastid genes eventually resulted in reduced protein content in *cmt1-1* (Figure 5C). Defects in chloroplast gene transcription (and RNA maturation) as well as protein translation have a great impact on chloroplast biogenesis and development (Chi et al., 2008; Pogson and Albrecht, 2011; Huang et al., 2013; Pyo et al., 2013; Schneider et al., 2014; Zhang et al., 2016). It was therefore not surprising that there were several abnormalities in chloroplast ultrastructure in *cmt1-1* plants (Figure 3D–3F). Disorganization of the thylakoid membrane system with, e.g., fully relaxed grana membranes (Figure 3E) has been described earlier as an effect of Mn deficiency in spinach chloroplasts (Mercer et al., 1962). The *cmt1-1* mutant chloroplasts showed varying degrees of defects, ranging from WT-like to aberrant. This variation might be caused by variable rates of Mn depletion within single chloroplasts. In line with the disrupted chloroplast structure, we observed high susceptibility of the photosynthetic apparatus in *cmt1-1* mutants, and at light intensities higher than growth light (i.e., above 90 $\mu\text{mol photons m}^{-2} \text{s}^{-1}$), *cmt1-1* plants were completely inhibited in PSII activity (Figure 4B). The low functionality of photochemical quenching was counteracted as the mutant plants already boosted light energy dissipation under low light intensities in the form of NPQ (Figure 4C and

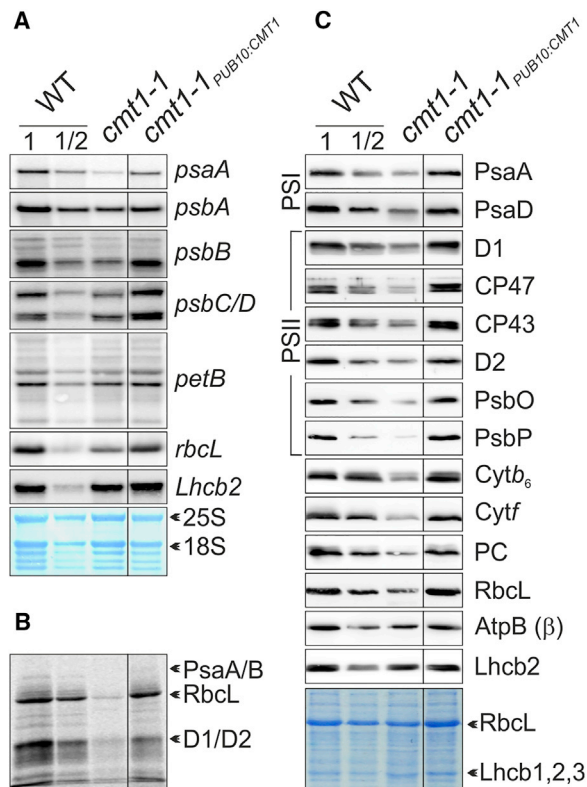


Figure 5. Transcription, Translation, and Steady-State Levels of Chloroplast Proteins.

(A) Transcription of chloroplast encoded proteins. In all lanes 15 μ g of total leaf RNA was loaded, except in the lane WT 1/2, where only 7.5 μ g of RNA was loaded. RNA gel blots were hybridized with radiolabeled probes specific for the indicated transcripts. As a loading control, blots were stained with methylene blue, and bands corresponding to 25S and 18S rRNA are indicated.

(B) Incorporation of [35 S]Met into chloroplast-encoded proteins. Pulse-labeling was performed for 20 min in the presence of cycloheximide to inhibit cytosolic translation. In all lanes 100 000 cpm were loaded, except in the lane WT 1/2, where only 50 000 cpm were loaded. The translated products RbcL, D1 and D2, and PsaA and PsaB are indicated.

(C) Immunodetection of chloroplast proteins using antibodies raised against PSI subunits, PSII subunits, Cytb₆f subunits, chloroplast ATP synthase subunit β , plastocyanin (PC), Rubisco large subunit (RbcL), and Lhcb2. Samples equivalent to 30 μ g of protein were loaded in all lanes, except those marked WT 1/2 where only 15 μ g of protein was loaded. As a loading control, proteins were visualized by Coomassie blue staining, and bands corresponding to Lhcb1, Lhcb2, and Lhcb3 (constituting the LHCII complex), as well as RbcL are indicated. In **(A)** to **(C)**, two lanes have been omitted (complete set shown in Supplemental Figure 6).

4D). However, this protective mechanism was not sufficient since the *cmt1-1* mutant already showed high non-regulated energy quenching (Supplemental Figure 4B) and accumulated superoxide anion ($O_2^{\cdot-}$) under growth light (Figure 7E). It is very likely that $O_2^{\cdot-}$ is derived from defective photosynthesis in *cmt1-1* (and in *pam71 cmt1-1* and *pam71*); more precisely, $O_2^{\cdot-}$ is generated mainly at the acceptor side of PSI via the Mehler reaction (Dietz et al., 2016 and references therein). However, the possibility that $O_2^{\cdot-}$ might, in addition, be of mitochondrial origin caused by reduced MnSOD abundance in *cmt1-1* (and *pam71 cmt1-1*) (Supplemental Figure 8) cannot be

excluded. Intracellular Mn trafficking and distribution to various organelles must be tightly regulated and is mediated by NRAMP2 (Alejandro et al., 2017; Gao et al., 2018), NRAMP3, and NRAMP4 (Lanquar et al., 2010). It has been suggested that maintaining mitochondrial Mn homeostasis and MnSOD activity is a higher priority for the plant cell (Alejandro et al., 2017) than for green algae, which preserves PSII activity upon Mn deficiency (Allen et al., 2007).

In summary, we conclude that the retarded growth phenotype of *cmt1-1* results from Mn deficiency in the chloroplast, allowing us to propose that CMT1 functions as a plastid Mn importer. Due to Mn deficiency in chloroplasts, transcription, translation, protein abundance, and Mn loading of thylakoid protein complexes were strongly affected in *cmt1-1* and also in *pam71 cmt1-1* (Supplemental Figures 6 and 7), resulting in impaired chloroplast development and photosynthetic performance, and increased light sensitivity.

Interplay of CMT1 and PAM71

The CMT1 protein possesses the typical features of UPF0016 proteins, namely six conserved transmembrane domains, including two highly conserved E-x-G-D-(KR)-(TS) motifs in transmembrane domains 1 and 4 and an acidic loop between transmembrane domains 3 and 4 (Schneider et al., 2016; Wang et al., 2016). The closest homolog of CMT1 in plants, PAM71, and its homolog in *Synechocystis*, MNX/SynPAM71, were suggested to function as Mn^{2+}/H^+ antiporters, since the direction of Mn^{2+} transport is into an acidic compartment (Schneider et al., 2016; Brandenburg et al., 2017; Gandini et al., 2017). The molecular mechanism of Mn^{2+} import via CMT1 into the chloroplast stroma remains to be elucidated, since a H^+ coupled antiport mechanism across the chloroplast envelope seems less likely (Hohner et al., 2016).

Despite this, the question arose as to how CMT1 and PAM71 may cooperate in Mn homeostasis. To this end we constructed a *pam71 cmt1-1* double-mutant line (Figure 7, Supplemental Figure 6A). The phenotype of *pam71 cmt1-1* plants was similar to the phenotype of *cmt1-1* plants in many respects: for example, transcription/translation of chloroplast-encoded proteins was downregulated in *cmt1-1* and *pam71 cmt1-1* compared with WT (Supplemental Figure 6C–6E), but was unaltered in *pam71-1* (Schneider et al., 2016); *cmt1-1* and *pam71 cmt1-1* plants had similar pigment compositions (Figure 7C); and there was only partial rescue of the photosynthetic phenotype in both mutants by externally supplied Mn (Figure 8B and 8C). The phenotypic data for the *cmt1* single and *pam71 cmt1-1* double mutants allowed us to conclude that CMT1 is the limiting step in Mn delivery to the chloroplast, i.e., CMT1 functions upstream of PAM71. This conclusion is supported by the localization of CMT1 at the chloroplast envelope membrane (Figure 2A, Ferro et al., 2003, 2010, Bräutigam et al., 2008, Bräutigam and Weber, 2009, Simm et al., 2013), and we propose that CMT1 and PAM71 function sequentially in Mn^{2+} uptake over the chloroplast envelope membrane and thylakoid membrane, respectively. We previously proposed a back-up system for Mn uptake at the thylakoid membrane. In contrast, there seems to be only a rudimentary back-up system for Mn uptake at the envelope membrane based on the severe phenotype of *cmt1* mutants and the—only—low

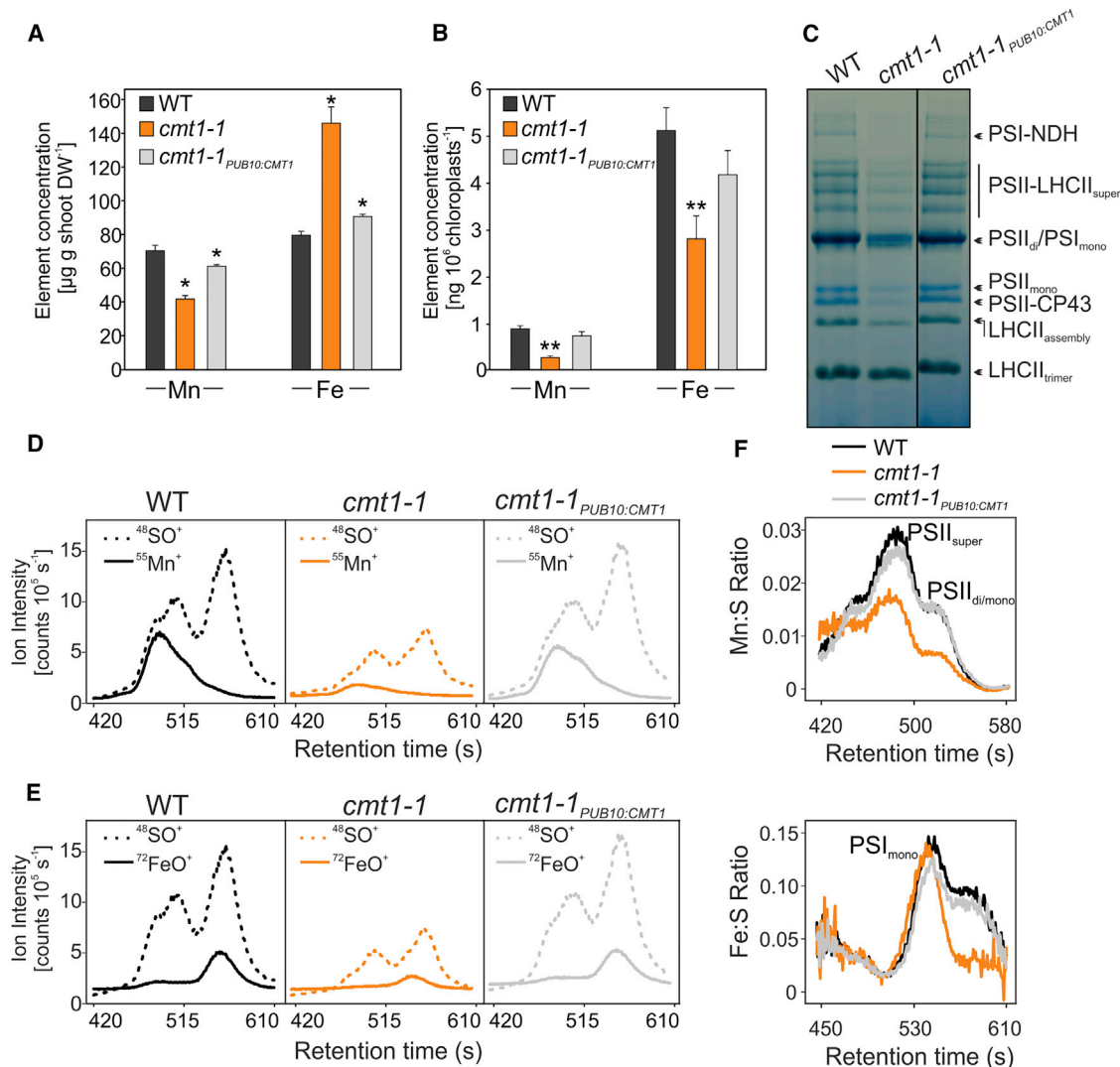


Figure 6. Manganese and Iron Homeostasis and Impact on Thylakoid Membrane Complexes in WT, *cmt1-1*, and *cmt1-1*^{PUB10:CMT1}.

(A) Total element concentrations of Mn and Fe in shoots. Element concentrations were quantified by inductively coupled plasma-optical emission spectrometry (ICP-OES) and are given on a dry-weight (DW) basis. Mean values (\pm SE) are based on four to five biological replicates. Asterisks indicate significant differences between WT and mutant lines (Mann–Whitney test, $*P < 0.05$).

(B) Total element analysis of Mn and Fe in chloroplast fractions. Element concentrations were quantified by ICP-QQQ-MS and normalized based on chloroplast numbers. Data represent one experiment (similar results were obtained in four independently grown batches of plants). Mean values (\pm SE) are based on four (WT and *cmt1-1*^{PUB10:CMT1}) or eight (*cmt1-1*) technical replicates. Asterisks indicate significant differences between WT and mutant lines (Mann–Whitney test, $**P < 0.01$).

(C) Accumulation of thylakoid photosynthetic complexes. Thylakoid membranes (equivalent to 18 μ g of protein) were solubilized with 1% (w/v) α -dodecyl maltoside, and protein complexes were fractionated by blue-native gel electrophoresis (3–12% [w/v] acrylamide). The protein complexes LHCII_{trimer}, LHCII_{assembly}, PSII without CP43 (PSII-CP43), PSII monomer (PSII_{mono}), PSII dimer (PSII_{di}), PSI monomer (PSI_{mono}), PSII-LHCII supercomplexes (PSII-LHCII_{super}), and PSI-NDH are indicated. Note that two lanes have been omitted (complete set shown in Supplemental Figure 7C).

(D) Size-exclusion profiles recorded for ⁵⁵Mn⁺ together with ⁴⁸SO⁺ in the different genotypes reported as ion intensities. Solubilization was performed as in (C). Fifty micrograms of total protein was loaded onto the size-exclusion column for each sample.

(E) Size-exclusion profiles recorded for ⁷²FeO⁺ together with ⁴⁸SO⁺ in the different genotypes reported as ion intensities. Solubilization was performed as in (C). Fifty micrograms of total protein was loaded onto the size-exclusion column for each sample.

(F) Quantification of the Mn/S (upper panel) and the Fe/S (lower panel) stoichiometric ratios are shown for samples analyzed in (D) and (E), respectively. Individual ⁵⁵Mn⁺ fractions and the first eluting ⁷²FeO⁺ fraction were assigned according to Schmidt et al. (2015). In total, five to six independent thylakoid preparations were analyzed, and data for one representative sample is shown.

degree of rescue of the photosynthetic phenotype upon the supply of additional Mn (Figure 8B and 8C). We speculate that this rudimentary back-up system might be slightly activated in the *pam71* mutant background.

CMT1 presumably is part of the cellular Mn homeostasis network, e.g., Mn content in leaves is reduced in *cmt1-1* and *pam71 cmt1-1* (Figure 6A and Supplemental Figure 7A) but not in *pam71* (Schneider et al., 2016), and CMT1 expression is

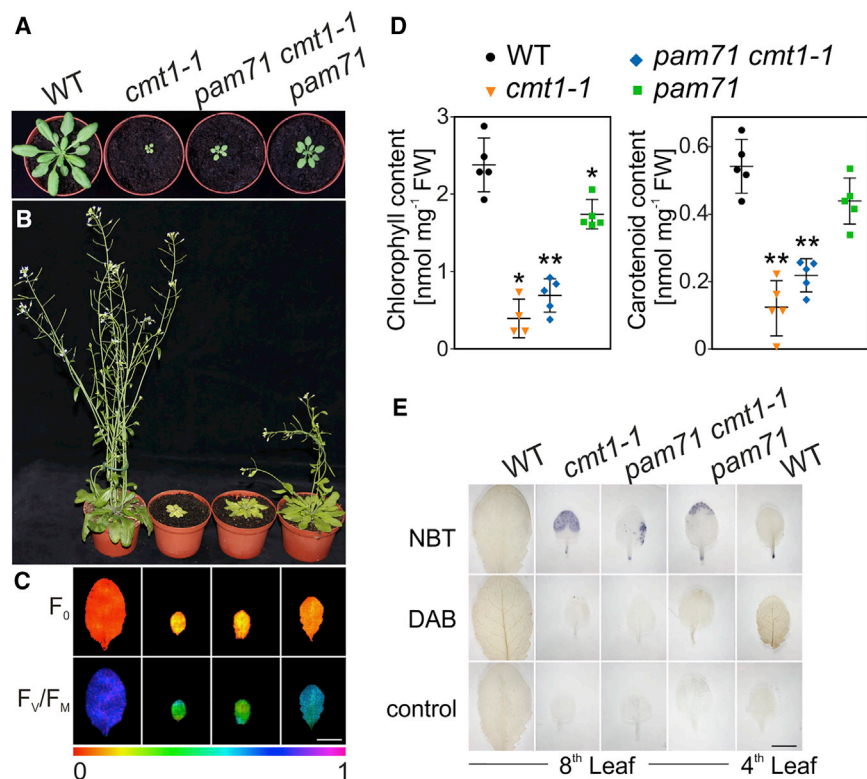


Figure 7. Characterization of the Double Mutant *pam71 cmt1-1* in Comparison with WT, *cmt1-1*, and *pam71*.

(A) Plants were grown for 4 weeks under a 12-h/12-h light/dark cycle at 22°C/18°C and at 90 $\mu\text{mol photons m}^{-2} \text{s}^{-1}$ and then transferred to a temperature-controlled greenhouse for flowering and seed production. Note that the WT and *cmt1-1* plants are identical to the plants shown in Figure 3A.

(B) Plants at an age of 8 weeks are shown.

(C) Minimal chlorophyll *a* fluorescence (F_0) and maximum quantum yield of PSII (F_v/F_m) were recorded from leaves of 4-week-old plants. The color scale at the bottom indicates the signal intensities. Scale bar, 12.5 mm.

(D) Chlorophyll and carotenoid content was determined from plants grown for 3 weeks on $\frac{1}{2}$ MS with 1% sucrose. Given are average values (\pm SD) of four (*cmt1-1*) and five (WT, *pam71 cmt1-1*, *pam71*) biological replicates. Asterisks indicate the statistical significance of differences between WT and mutant plants (Mann–Whitney test, ** $P < 0.01$, * $P < 0.05$). FW, fresh weight.

(E) NBT ($\text{O}_2^{\cdot-}$) and DAB (H_2O_2) staining of younger (4th rosette leaf, counted from the top) and older leaves (8th rosette leaf) from 4-week-old plants. As a control, leaves were incubated in buffer without dye. Scale bar, 10 mm.

regulated by Mn-feeding (Figure 8A and Supplemental Figure 9). Reduced transcription of *CMT1* under Mn-excess conditions might prevent detrimental overaccumulation of Mn^{2+} in the chloroplast. Moreover, *CMT1* might function in Mn homeostasis in non-green plastids because it is ubiquitously expressed (Figure 2B and Supplemental Figure 1). To date only a limited number of metal transporters in chloroplast membranes have been described (Szabo and Spetea, 2017), and understanding how they affect cellular and/or organellar metal homeostasis may aid the development of crop plants with improved nutrient-use efficiency in the future.

METHODS

Plant Material and Complementation Line Construction

Arabidopsis thaliana cmt1 mutants were identified in the SALK collection (*cmt1-1* SALK_129037 N629037; *cmt1-3* SALKseq_61 850 N926448) (Alonso et al., 2003) and in the Wisconsin DsLox T-DNA collection (*cmt1-2* WiscDsLox434C5 N855634). Seeds were provided by NASC, the European *Arabidopsis* Stock Center. Genotyping of all lines was performed using PCR with appropriate primer combinations (Supplemental Table 2), and PCR products were sequenced. For all experiments *cmt1-1* was used. This mutant line was crossed with *pam71-1* (Schneider et al., 2016) and in the F_2 generation a double mutant was identified and named *pam71 cmt1-1*. WT plants were accession Columbia-0.

For cloning of pPUB10:CMT1, the full-length *CMT1* coding sequence was PCR-amplified from *Arabidopsis* cDNA with gene-specific primers (SK141/SK142; Supplemental Table 2), subcloned into pJET1.2 (Thermo Fisher Scientific), and the insert verified by sequencing. The *CMT1* coding sequence was then cut out by double-digest with *Bam*HI and *Ap*al and ligated into the binary T-DNA vector pUTKan (Fendrych et al., 2014) in which expression of *CMT1* is under the control of the

UBIQUITIN10 promoter. The cloning of pP35S:CMT1 began with amplification of full-length *CMT1* with PCR primers (Supplemental Table 2) from *Arabidopsis* first-strand cDNA. The amplified full-length *CMT1* cDNA was ligated into pENTR-TOPO (Life Technologies) and subsequently recombined into pB2WG7 (Karimi et al., 2002) yielding plasmid pP35S:CMT1.

The two constructs were stably introduced into *cmt1-1* by floral dip transformation (Clough and Bent, 1998). Individual transgenic plants were selected on the basis of their resistance to kanamycin (50 $\mu\text{g ml}^{-1}$) and BASTA (100 mg l^{-1} ammonium glufosinate), respectively. One complemented plant per construct was chosen for further analysis and named *cmt1-1*^{PUB10:CMT1} and *cmt1-1*^{P35S:CMT1}.

Plant Growth Conditions

Unless stated otherwise, plants were grown for 4–5 weeks in a growth chamber equipped with 17-W cool white fluorescent lamps (CLF Plant Climatics) under a 12-h/12-h day/night cycle at 90 $\mu\text{mol photons m}^{-2} \text{s}^{-1}$. For individual experiments, the mutant lines (*cmt1* and *pam71 cmt1-1*) were pre-cultivated for 2 weeks to ensure an equal number of leaves at the time of harvesting. Plants were cultivated on standard soil substrate A210 (Stender) without further fertilization and watered with tap water. *Arabidopsis* plants used for kanamycin and hygromycin (33.3 $\mu\text{g ml}^{-1}$) selection, microscopy, and pigment analysis were surface sterilized and grown on half-strength Murashige and Skoog ($\frac{1}{2}$ MS) medium including 1% (w/v) sucrose, with or without antibiotic. $\frac{1}{2}$ MS medium contains 50 μM MnSO_4 , and excess Mn conditions were generated by supplementing MnSO_4 to a final concentration of 500 μM or 1000 μM MnSO_4 . Sterile *Arabidopsis* plants were cultivated at 90 $\mu\text{mol photons m}^{-2} \text{s}^{-1}$ under a 16-h/8-h day/night cycle. *Arabidopsis* plants used for crosses, transformation, BASTA selection, and seed propagation were grown in a temperature-controlled greenhouse. *Nicotiana benthamiana* plants for transient expression analysis were grown for 4 weeks in a temperature-controlled greenhouse.

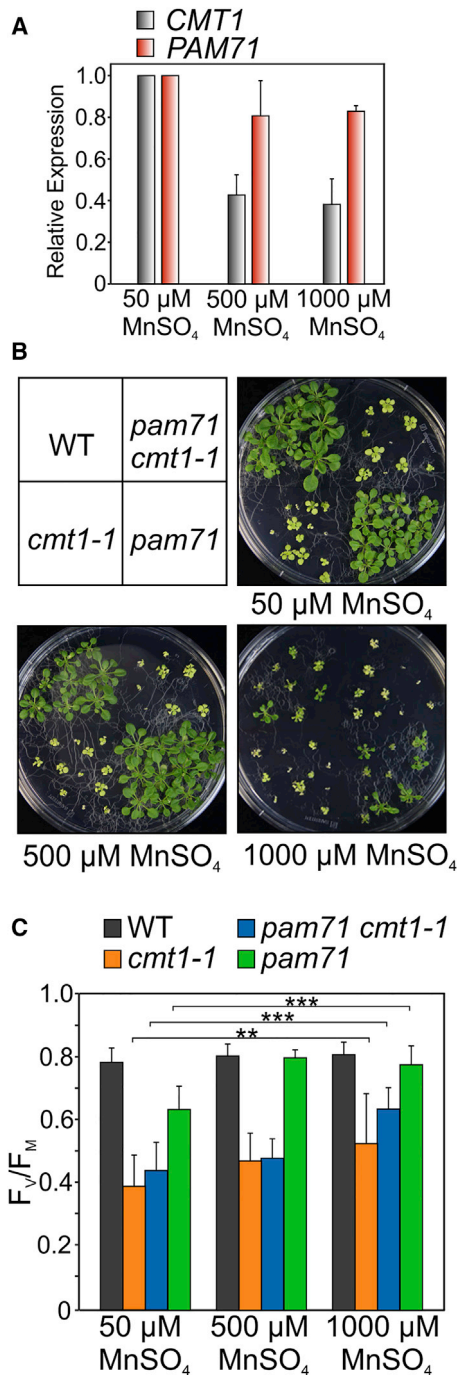


Figure 8. Expression of CMT1 and PAM71 and Rescue of Photosynthesis in *pam71*, *cmt1-1*, and *pam71 cmt1-1* under Mn-Excess Conditions.

(A) Expression levels of CMT1 and PAM71 in WT plants were determined by real-time qPCR. Expression levels are relative values based on the expression level in WT plants grown on standard $\frac{1}{2}$ MS medium (50 μ M MnSO₄). Mean values (\pm SD) are based on four biological replicates.

(B) Seeds of the indicated genotypes were surface sterilized and grown for 3 weeks on standard $\frac{1}{2}$ MS medium (50 μ M MnSO₄) and $\frac{1}{2}$ MS medium supplemented with MnSO₄ concentrations as indicated.

(C) F_v/F_m values are given for WT, *cmt1-1*, *pam71 cmt1-1*, and *pam71* grown as in **(B)**. Error bars represent mean values (\pm SD) of individual plants ($n = 15$). Asterisks indicate the statistical significance of differences between growth conditions (t -test, *** $P < 0.001$, ** $P < 0.01$).

Subcellular Localization of CMT1:YFP Fusion Protein

For subcellular localization studies, the coding sequence (without stop codon) of CMT1 was PCR-amplified from *Arabidopsis* cDNA with gene-specific primers (ME182/ME183; Supplemental Table 2), subcloned into pJET1.2 (Thermo Fisher Scientific), cut out by double-digest with BamHI and SalI, and ligated into the pNL3 vector (Linka et al., 2008) to obtain a C-terminal fusion of CMT1 to YFP, driven by the 35S promoter. The fusion construct CMT1:YFP in pNL3 was verified by sequencing. The *Agrobacterium tumefaciens* strain GV3101 was transformed with the plasmid and infiltrated into *N. benthamiana* leaves for transient expression of CMT1:YFP fusion proteins. After 48 h, protoplasts were isolated for localization studies with a confocal laser scanning microscope (Zeiss LSM 510) as described by Breuers et al. (2012).

Heterologous Expression of CMT1 in Yeast

The coding sequence of CMT1 was PCR-amplified from *Arabidopsis* cDNA using appropriate primers (Supplemental Table 2). After restriction digestion with XhoI and BamHI, the PCR fragment was cloned into yeast expression vector pDR195 (Rentsch et al., 1995), yielding plasmid pDR195-CMT1, and sequenced. The yeast mutant $\Delta pmr1$, which carries a defect in the P-type Ca²⁺/Mn²⁺-ATPase (Dürr et al., 1998), was transformed with pDR195-CMT1 and the empty vector pDR195 according to Gietz and Schiestl (1991), and individual colonies were analyzed as described by Schneider et al. (2016).

Promoter Activity Analysis

To test for tissue-specific promoter activity, we PCR-amplified a 1500-bp fragment upstream of the CMT1 coding sequence (excluding the start codon) from *Arabidopsis* genomic DNA with specific primers (ME108/ME110; Supplemental Table 2). This fragment was subcloned into pJET1.2 (Thermo Fisher Scientific), cut out by double-digest with SalI and PstI, and ligated into the pCAMBIA1381 vector (Cambia, <http://www.cambia.org/daisy/cambia/home.html>) upstream of the reporter gene *gusA*. The generated plasmid containing the *pCMT1:GUS* fusion was introduced into *Arabidopsis* WT plants as described above.

For the GUS assay, plants were placed in appropriate containers and immersed in GUS staining solution (50 mM NaH₂PO₄ [pH 7.0], 10 mM EDTA, 5 mM K₃Fe(CN)₆, 0.1% Triton X-100, 0.1% Tween 20, 1 mM 5-bromo-4-chloro-3-indolyl glucuronide [X-Gluc]). After overnight incubation at 37°C, the tissue was fixed by incubating in fixation solution (50% ethanol, 5% glacial acetic acid, 3.7% formaldehyde) for 10 min at 65°C. The samples were treated with 80% ethanol at 37°C to remove chlorophyll and stored in 80% ethanol until photographic documentation.

Chlorophyll a Fluorescence and P₇₀₀ Absorption Measurements

Chlorophyll a fluorescence was recorded using the Dual-PAM (Walz) (Steinberger et al., 2015) or the Imaging-PAM (Walz). Plants were dark-adapted for 30 min, and single leaves were exposed briefly (10 s) to measuring light, followed by a saturating light pulse (10 000 μ mol photons m⁻² s⁻¹, 800 ms). Actinic light was switched on for 5 min (125 μ mol photons m⁻² s⁻¹), and this was followed by a saturating light pulse (10 000 μ mol photons m⁻² s⁻¹, 800 ms). Parameters were calculated as follows: maximum quantum yield of PSII $F_v/F_m = (F_m - F_0)/F_m$; effective quantum yield of PSII $\Phi_{II} = (F_m' - F_0')/F_m'$; where F_m and F_m' represent the maximal fluorescence of dark-adapted or actinic light-adapted samples, and F_0 and F_0' represent the minimal fluorescence of dark-adapted or actinic light-adapted samples.

P₇₀₀ absorption measurements were performed using the Dual-PAM, and $\Delta A/\Delta A_{max}$ was determined according to Meurer et al. (1996). Single leaves were light-adapted for 5 min at 100 μ mol photons m⁻² s⁻¹ followed by a 25-s dark incubation. To determine maximal absorption of P₇₀₀ at 830 nm, we exposed leaves to far-red light (720 nm, 260 μ mol photons m⁻² s⁻¹) for 30 s.

Molecular Plant

Light curves were recorded with pre-illuminated plants grown at 90 $\mu\text{mol photons m}^{-2} \text{ s}^{-1}$ using the Dual-PAM/F (Walz). Light intensities were held for 3 min each and increased stepwise up to 1600 $\mu\text{mol photons m}^{-2} \text{ s}^{-1}$. The parameters ETR I, ETR II, NPQ, Y(NPQ), Y(NO), and Y(ND) were calculated by the Dual-PAM 100 software according to the equations by Kramer et al. (2004).

Leaf Pigment Analysis

Plant material was frozen in liquid N_2 . After homogenization, pigments were extracted with acetone and analyzed by reversed-phase high-performance liquid chromatography according to Färber et al. (1997).

Protein Analysis

For isolation of thylakoid proteins, leaf samples (5 g fresh weight) were homogenized in 0.4 M sucrose, 10 mM NaCl, 5 mM MgCl_2 , 20 mM tricine (pH 7.9), 10 mM ascorbate, and 10 mM NaF. The suspension was filtered through two layers of Miracloth and centrifuged at 6000 g for 10 min at 4°C. The pellet was resuspended in 5 mM tricine (pH 7.9) and 10 mM NaF, and centrifuged at 11 200 g for 10 min at 4°C. The resulting thylakoid pellet was resuspended in storage puffer (0.4 M sucrose, 10 mM NaCl, 5 mM MgCl_2 , 20 mM tricine, 10 mM NaF, and 20% [v/v] glycerol) and protein concentration was determined using the Pierce BCA Protein Assay (Thermo Fisher Scientific). For isolation of total proteins, leaf samples (two to three leaves) were frozen and homogenized in 100 mM tricine (pH 7.5), 10 mM KCl, 1 mM MgCl_2 , 1 mM EDTA, 10% (w/v) sucrose, 2% (w/v) Triton X-100, and 1 mM DTT supplemented with protease inhibitor cocktail (Roche) and incubated for 10 min at 4°C. The homogenate was centrifuged at 6000 g for 10 min at 4°C, and the supernatant was subsequently used for determination of the protein concentration. Protein samples were adjusted to 30 μg in 45 mM Tris-HCl (pH 6.8), 50 mM DTT, 0.1% (w/v) SDS, 0.1% (v/v) glycerol, and 0.01% (w/v) bromophenol blue, incubated at 80°C for 5 min, and fractionated on Tris-tricine SDS gels (12% acrylamide).

Individual proteins of interest were detected using antibodies raised against D1 (Agrisera 05 084, 1:10 000), PsbO (Agrisera 06 142-33, 1:4000), PsbP (Agrisera 06 142-23, 1:4000), Lhcb2 (Agrisera 01 003, 1:5000), PsbA (Agrisera 06 172, 1:1000), PsbD (Agrisera 04 064, 1:4000), Cytb₆ (Agrisera 03 034, 1:10 000), Cyt f (Agrisera 08 306, 1:5000), AtpB (β) (Agrisera 05 085, 1:4000), RbcL (Agrisera 03 037, 1:5000), plastocyanin (Agrisera 06 141, 1:2000), MnSOD (Agrisera AS 09 524, 1:4000) D2, CP43, and CP47 in combination with α -rabbit immunoglobulin G horseradish peroxidase (Sigma-Aldrich A9169, 1:25 000) and the Pierce enhanced chemiluminescence system (Thermo Fisher Scientific).

The thylakoid membrane complexes were isolated from the thylakoid pellet in storage buffer (see above). Samples, equivalent to 18 μg protein, were solubilized in the presence of 1% (w/v) α -dodecyl-maltoside for 10 min on ice in darkness. Solubilized thylakoid membrane complexes were complemented by adding Novex BN-PAGE sample buffer (Invitrogen) and separated by non-denaturing BN-PAGE (3%–12% acrylamide) for 3 h 15 min.

For *in vivo* labeling, four to five leaves were incubated in 1 mCi of [^{35}S]Met for 20 min in the presence of 20 $\mu\text{g ml}^{-1}$ cycloheximide at 60 $\mu\text{mol photon m}^{-2} \text{ s}^{-1}$. Thylakoid and stroma proteins were prepared and fractionated on denaturing gradient Tris-glycine SDS gels (8–12% acrylamide), and radioactive signals were detected using a Typhoon imager (GE Healthcare).

Transcription Analysis

Total RNA was isolated from leaves of *Arabidopsis* lines using TRIzol reagent (Invitrogen). Expression of *CMT1*, *PAM71*, and *Actin2* was analyzed by 30 cycles of PCR using appropriate primer combinations (Supplemental Table 2) and first-strand cDNA as the template. The absence or presence of a PCR product was verified using DNA gel

CMT1 Is Required for Manganese Homeostasis

electrophoresis. For real-time qRT-PCR, SYBR Green Supermix (Bio-Rad) was used, and PCR was performed with the iQ5 multicolor real-time PCR detection system (Bio-Rad) using appropriate primer combinations (Supplemental Table 2). Quantification of relative expression levels was performed using the comparative C_t method (Schmittgen and Livak, 2008). Expression of various chloroplast-located genes was determined using RNA gel-blot analysis and standard protocols. Probe generation was performed using PCR-amplified sequenced products (for primer combinations see Supplemental Table 2) and [^{32}P]dCTP labeling. Hybridization was conducted under stringent conditions at 65°C overnight and radioactive signals were detected using a Typhoon imager (GE Healthcare).

Determination of Total Element Concentrations in Leaves and Intact Chloroplasts

The element concentrations in leaves and in intact chloroplast fractions were determined using inductively coupled plasma-optical emission spectrometry (ICP-OES) (Agilent 5100 ICP-OES) or triple quadrupole inductively coupled plasma mass spectrometry (ICP-QQQ-MS) for leaf and chloroplast digests, respectively. Harvested leaves were freeze-dried and homogenized, and a representative sample (~40 mg) was digested in ultra-pure acids (2.5:1 70% HNO_3 and 30% H_2O_2) using a pressurized microwave digestion system (UltraWAVE) (Hansen et al., 2013).

For isolation of intact chloroplasts, leaf samples (10 g fresh weight) were homogenized in 0.4 M sorbitol, 20 mM tricine-NaOH (pH 8.4), 10 mM EDTA, 0.1% (w/v) BSA, 5 mM NaHCO_3 , 1 mM MgCl_2 , and 1 mM MnCl_2 using a blender (Waring laboratory). The extract was filtered through two layers of Miracloth and concentrated at 1500 g for 5 min. The pellet was resuspended in 80 mM sorbitol, 4 mM tricine-NaOH (pH 8.4), 0.5 mM EDTA, and 1 mM MgCl_2 and layered onto a discontinuous 40% (w/v)/80% (w/v) Percoll gradient. After centrifugation for 15 min at 7000 g , intact chloroplasts were recovered from the interphase and washed two times. The integrity of the chloroplasts was verified by microscopy, and the number of chloroplasts was estimated by counting with a Neubauer chamber. An equal number of chloroplasts were pelleted, and the individual chloroplast samples were digested using the microwave system described above. The accuracy and precision of the measurements were estimated by analyzing certified reference material (apple [*Malus domestica*] leaf, NIST 1515, National Institute of Standards and Technology).

SEC-ICP-MS Measurements

Thylakoid membranes were isolated and solubilized as described above in the Protein Analysis section and fractionated by SEC as described previously (Schmidt et al., 2015; Schneider et al., 2016). The outlet of the column was coupled to a triple quadrupole ICP-MS (Agilent 8800 ICP-QQQ-MS) for online detection of metal binding in the size-fractionated thylakoid complexes. The ICP-QQQ-MS was operated in MS/MS scan mode with oxygen as the reaction gas, which allowed for ultrasensitive and simultaneous detection of all elements of interest (Schmidt et al., 2015). The integration time was 0.1 s per element. Quantification of the Mn/S and Fe/S stoichiometric ratios in PSII and PSI complexes, respectively, was performed by external calibration (Schmidt et al., 2015).

Transmission Electron Microscopy

Leaves of agar-grown *Arabidopsis* lines used for transmission electron microscopy were processed as previously described (Breuers et al., 2012) with the following exceptions. As fixative, 2% glutaraldehyde and 4% formaldehyde in 100 mM sodium phosphate buffer (pH 7.4) was used. Osmication was performed in 1% osmium tetroxide and 1.5% potassium ferricyanide in 100 mM sodium phosphate buffer (pH 7.4) for 70 min at 4°C. En bloc staining of the samples by incubation in 2% uranyl acetate at 4°C overnight was omitted. Sections were viewed using a JEM-1400 Plus transmission electron microscope (JEOL) operated at 80 kV. Micrographs were taken using a 3.296 \times 2.472

charge-coupled device camera (Ruby, JEOL) equipped with appropriate software (JEOL TEM Center software) and manually inspected for the status of individual chloroplasts.

Staining of Reactive Oxygen Species

Leaves of *Arabidopsis* lines were stained for ROS according to Ramel et al. (2009). For staining of H₂O₂, leaves were vacuum infiltrated for 10 min in 4 ml 3,3'-diaminobenzidine (DAB) staining solution (1 mg ml⁻¹ DAB, 0.01 M Na₂HPO₄, 0.05% [v/v] Tween 20 [pH 3.8]) and incubated in darkness for 4 h at room temperature. For staining of superoxide anion (O₂⁻), leaves were vacuum infiltrated for 10 min in 4 ml of nitroblue tetrazolium (NBT) staining solution (0.5 mg ml⁻¹ NBT, 10 mM K₂HPO₄, 10 mM Na₃N) and incubated in darkness for 1 h at room temperature. Stained leaves were then bleached in acetic acid/glycerol/ethanol (1/1/3) (v/v/v) solution at 95°C for 5 min, and photographs were taken. H₂O₂ was visualized as a brown color due to DAB polymerization. O₂⁻ was visualized as blue color produced by NBT precipitation.

ACCESSION NUMBERS

The *Arabidopsis* Genome Initiative identifiers for the genes described in this article are as follows: *CMT1* (At4g13590) and *PAM71* (At1g64150).

SUPPLEMENTAL INFORMATION

Supplemental Information is available at *Molecular Plant Online*.

FUNDING

This research was supported by the German Science Foundation (EI 945/3-1 to M.E., EXC 1028 to A.P.M.W., SCHN 560/4-1 to A.S.) and by the Independent Research Fund Denmark – Technology and Production Sciences (grant no. DFF-5054-00042 to S.B.S.).

AUTHOR CONTRIBUTIONS

Conceptualization, M.E. and A.S.; Investigation, M.E., N.H., S.B.S., R.M.B., S.F., P.J., T.E., S.G., and A.S.; Resources, M.E., S.H., A.P.M.W., D.L., and A.S.; Writing – Original Draft, M.E. and A.S.; Writing – Review & Editing, M.E., S.B.S., and A.S.; Visualization, A.S.; Funding Acquisition, M.E., A.P.M.W., S.B.S., D.L., and A.S.; Supervision, M.E. and A.S. All authors read and approved the final version of the manuscript.

ACKNOWLEDGMENTS

We thank Gabi Burkhard, Reinhild Rode, and Maria Graf for their excellent technical assistance, Steffen Köhler for photography support, Jasmin Weber and Tatjana Goss for support during cloning and plant growth, and Nadine Polster and Yvonne Hennecke as undergraduate students taking part in this project. We also acknowledge the European Stock Center NASC and the Salk Institute for seed distribution, and R. Barbato for D2, CP43, and CP47 antibodies. No conflict of interest declared.

Received: November 30, 2017

Revised: April 26, 2018

Accepted: April 27, 2018

Published: May 4, 2018

REFERENCES

- Alejandro, S., Cailliatte, R., Alcon, C., Dirick, L., Domergue, F., Correia, D., Castaings, L., Briat, J.F., Mari, S., and Curie, C. (2017). Intracellular distribution of manganese by the trans-Golgi network transporter NRAMP2 is critical for photosynthesis and cellular redox homeostasis. *Plant Cell* **29**:3068–3084.
- Allahverdiyeva, Y., Suorsa, M., Rossi, F., Pavesi, A., Kater, M.M., Antonacci, A., Tadini, L., Pribil, M., Schneider, A., Wanner, G., et al. (2013). *Arabidopsis* plants lacking PsbQ and PsbR subunits of the oxygen-evolving complex show altered PSII super-complex organization and short-term adaptive mechanisms. *Plant J.* **75**: 671–684.
- Allen, M.D., Kropat, J., Tottey, S., Del Campo, J.A., and Merchant, S.S. (2007). Manganese deficiency in *Chlamydomonas* results in loss of photosystem II and MnSOD function, sensitivity to peroxides, and secondary phosphorus and iron deficiency. *Plant Physiol.* **143**: 263–277.
- Alonso, J.M., Stepanova, A.N., Leisse, T.J., Kim, C.J., Chen, H., Shinn, P., Stevenson, D.K., Zimmerman, J., Barajas, P., Cheuk, R., et al. (2003). Genome-wide insertional mutagenesis of *Arabidopsis thaliana*. *Science* **301**:653–657.
- Brandenburg, F., Schoffman, H., Kurz, S., Kramer, U., Keren, N., Weber, A.P., and Eisenhut, M. (2017). The *Synechocystis* manganese exporter Mnx is essential for manganese homeostasis in cyanobacteria. *Plant Physiol.* **173**:1798–1810.
- Bräutigam, A., Shrestha, R.P., Whitten, D., Wilkerson, C.G., Carr, K.M., Froehlich, J.E., and Weber, A.P. (2008). Low-coverage massively parallel pyrosequencing of cDNAs enables proteomics in non-model species: comparison of a species-specific database generated by pyrosequencing with databases from related species for proteome analysis of pea chloroplast envelopes. *J. Biotechnol.* **136**:44–53.
- Bräutigam, A., and Weber, A.P. (2009). Proteomic analysis of the proplastid envelope membrane provides novel insights into small molecule and protein transport across proplastid membranes. *Mol. Plant* **2**:1247–1261.
- Breuers, F.K., Brautigam, A., Geimer, S., Welzel, U.Y., Stefano, G., Renna, L., Brandizzi, F., and Weber, A.P. (2012). Dynamic remodeling of the plastid envelope membranes—a tool for chloroplast envelope in vivo localizations. *Front. Plant Sci.* **3**:7.
- Cailliatte, R., Schikora, A., Briat, J.F., Mari, S., and Curie, C. (2010). High-affinity manganese uptake by the metal transporter NRAMP1 is essential for *Arabidopsis* growth in low manganese conditions. *Plant Cell* **22**:904–917.
- Cheng, N.H., Pittman, J.K., Shigaki, T., and Hirschi, K.D. (2002). Characterization of CAX4, an *Arabidopsis* H(+)/cation antiporter. *Plant Physiol.* **128**:1245–1254.
- Chi, Y.H., Moon, J.C., Park, J.H., Kim, H.S., Zulfugarov, I.S., Fanata, W.I., Jang, H.H., Lee, J.R., Lee, Y.M., Kim, S.T., et al. (2008). Abnormal chloroplast development and growth inhibition in rice thioredoxin m knock-down plants. *Plant Physiol.* **148**:808–817.
- Clough, S.J., and Bent, A.F. (1998). Floral dip: a simplified method for *Agrobacterium*-mediated transformation of *Arabidopsis thaliana*. *Plant J.* **16**:735–743.
- Curie, C., Alonso, J.M., Le Jean, M., Ecker, J.R., and Briat, J.F. (2000). Involvement of NRAMP1 from *Arabidopsis thaliana* in iron transport. *Biochem. J.* **347** (Pt 3):749–755.
- Demaegd, D., Colinet, A.S., Deschamps, A., and Morsomme, P. (2014). Molecular evolution of a novel family of putative calcium transporters. *PLoS One* **9**:e100851.
- Dietz, K.J., Turkan, I., and Krieger-Liszky, A. (2016). Redox- and reactive oxygen species-dependent signaling into and out of the photosynthesizing chloroplast. *Plant Physiol.* **171**:1541–1550.
- Dürr, G., Strayle, J., Plemper, R., Elbs, S., Klee, S.K., Catty, P., Wolf, D.H., and Rudolph, H.K. (1998). The medial-Golgi ion pump Pmr1 supplies the yeast secretory pathway with Ca²⁺ and Mn²⁺ required for glycosylation, sorting, and endoplasmic reticulum-associated protein degradation. *Mol. Biol. Cell* **9**:1149–1162.
- Edmond, C., Shigaki, T., Ewert, S., Nelson, M.D., Connorton, J.M., Chalova, V., Noordally, Z., and Pittman, J.K. (2009). Comparative analysis of CAX2-like cation transporters indicates functional and regulatory diversity. *Biochem. J.* **418**:145–154.
- Eroglu, S., Giehl, R.F.H., Meier, B., Takahashi, M., Terada, Y., Ignatyev, K., Andresen, E., Kupper, H., Peiter, E., and von

- Wiren, N. (2017). Metal tolerance protein 8 mediates manganese homeostasis and iron reallocation during seed development and germination. *Plant Physiol.* **174**:1633–1647.
- Färber, A., Young, A.J., Ruban, A.V., Horton, P., and Jahns, P. (1997). Dynamics of xanthophyll-cycle activity in different antenna subcomplexes in the photosynthetic membranes of higher plants (the relationship between zeaxanthin conversion and nonphotochemical fluorescence quenching). *Plant Physiol.* **115**:1609–1618.
- Fendrych, M., Van Hautegeem, T., Van Durme, M., Olvera-Carrillo, Y., Huysmans, M., Karimi, M., Lippens, S., Guerin, C.J., Krebs, M., Schumacher, K., et al. (2014). Programmed cell death controlled by ANAC033/SOMBRERO determines root cap organ size in *Arabidopsis*. *Curr. Biol.* **24**:931–940.
- Ferreira, K.N., Iverson, T.M., Maghlaoui, K., Barber, J., and Iwata, S. (2004). Architecture of the photosynthetic oxygen-evolving center. *Science* **303**:1831–1838.
- Ferro, M., Brugiere, S., Salvi, D., Seigneurin-Berny, D., Court, M., Moyet, L., Ramus, C., Miras, S., Mellal, M., Le Gall, S., et al. (2010). AT_CHLORO, a comprehensive chloroplast proteome database with subplastidial localization and curated information on envelope proteins. *Mol. Cell Proteomics* **9**:1063–1084.
- Ferro, M., Salvi, D., Brugiere, S., Miras, S., Kowalski, S., Louwagie, M., Garin, J., Joyard, J., and Rolland, N. (2003). Proteomics of the chloroplast envelope membranes from *Arabidopsis thaliana*. *Mol. Cell Proteomics* **2**:325–345.
- Fridovich, I. (1995). Superoxide radical and superoxide dismutases. *Annu. Rev. Biochem.* **64**:97–112.
- Gandini, C., Schmidt, S.B., Husted, S., Schneider, A., and Leister, D. (2017). The transporter SynPAM71 is located in the plasma membrane and thylakoids, and mediates manganese tolerance in *Synechocystis* PCC6803. *New Phytol.* **215**:256–268.
- Gao, H., Xie, W., Yang, C., Xu, J., Li, J., Wang, H., Chen, X., and Huang, C.F. (2018). NRAMP2, a trans-Golgi network-localized manganese transporter, is required for *Arabidopsis* root growth under manganese deficiency. *New Phytol.* **217**:179–193.
- Gietz, R.D., and Schiestl, R.H. (1991). Applications of high efficiency lithium acetate transformation of intact yeast cells using single-stranded nucleic acids as carrier. *Yeast* **7**:253–263.
- Hansen, T.H., de Bang, T.C., Laursen, K.H., Pedas, P., Husted, S., and Schjoerring, J.K. (2013). Multielement plant tissue analysis using ICP spectrometry. *Methods Mol. Biol.* **953**:121–141.
- Hirschi, K.D., Korenkov, V.D., Wilganowski, N.L., and Wagner, G.J. (2000). Expression of *Arabidopsis* CAX2 in tobacco. Altered metal accumulation and increased manganese tolerance. *Plant Physiol.* **124**:125–133.
- Hoecker, N., Leister, D., and Schneider, A. (2017). Plants contain small families of UPF0016 proteins including the PHOTOSYNTHESIS AFFECTED MUTANT71 transporter. *Plant Signal. Behav.* **12**:e1278101.
- Hohner, R., Aboukila, A., Kunz, H.H., and Venema, K. (2016). Proton gradients and proton-dependent transport processes in the chloroplast. *Front. Plant Sci.* **7**:218.
- Huang, C., Yu, Q.B., Lv, R.H., Yin, Q.Q., Chen, G.Y., Xu, L., and Yang, Z.N. (2013). The reduced plastid-encoded polymerase-dependent plastid gene expression leads to the delayed greening of the *Arabidopsis* fln2 mutant. *PLoS One* **8**:e73092.
- Ihnatowicz, A., Siwinska, J., Meharg, A.A., Carey, M., Koornneef, M., and Reymond, M. (2014). Conserved histidine of metal transporter AtNRAMP1 is crucial for optimal plant growth under manganese deficiency at chilling temperatures. *New Phytol.* **202**:1173–1183.
- Karimi, M., Inze, D., and Depicker, A. (2002). GATEWAY vectors for *Agrobacterium*-mediated plant transformation. *Trends Plant Sci.* **7**:193–195.
- Kawakami, K., Umena, Y., Kamiya, N., and Shen, J.R. (2011). Structure of the catalytic, inorganic core of oxygen-evolving photosystem II at 1.9 Å resolution. *J. Photochem. Photobiol. B* **104**:9–18.
- Kliebenstein, D.J., Monde, R.A., and Last, R.L. (1998). Superoxide dismutase in *Arabidopsis*: an eclectic enzyme family with disparate regulation and protein localization. *Plant Physiol.* **118**:637–650.
- Kramer, D.M., Johnson, G., Kiirats, O., and Edwards, G.E. (2004). New fluorescence parameters for the determination of QA redox state and excitation energy fluxes. *Photosynth. Res.* **79**:209.
- Lanquar, V., Lelievre, F., Bolte, S., Hames, C., Alcon, C., Neumann, D., Vansuyt, G., Curie, C., Schroder, A., Kramer, U., et al. (2005). Mobilization of vacuolar iron by AtNRAMP3 and AtNRAMP4 is essential for seed germination on low iron. *EMBO J.* **24**:4041–4051.
- Lanquar, V., Ramos, M.S., Lelievre, F., Barbier-Brygoo, H., Krieger-Liszka, A., Kramer, U., and Thomine, S. (2010). Export of vacuolar manganese by AtNRAMP3 and AtNRAMP4 is required for optimal photosynthesis and growth under manganese deficiency. *Plant Physiol.* **152**:1986–1999.
- Linka, N., Theodoulou, F.L., Haslam, R.P., Linka, M., Napier, J.A., Neuhaus, H.E., and Weber, A.P. (2008). Peroxisomal ATP import is essential for seedling development in *Arabidopsis thaliana*. *Plant Cell* **20**:3241–3257.
- Martin, M.V., Fiol, D.F., Sundaresan, V., Zabaleta, E.J., and Pagnussat, G.C. (2013). oiwa, a female gametophytic mutant impaired in a mitochondrial manganese-superoxide dismutase, reveals crucial roles for reactive oxygen species during embryo sac development and fertilization in *Arabidopsis*. *Plant Cell* **25**:1573–1591.
- Mercer, F.V., Nittim, M., and Possingham, J.V. (1962). The effect of manganese deficiency on the structure of spinach chloroplasts. *J. Cell Biol.* **15**:379–381.
- Meurer, J., Meierhoff, K., and Westhoff, P. (1996). Isolation of high-chlorophyll-fluorescence mutants of *Arabidopsis thaliana* and their characterisation by spectroscopy, immunoblotting and northern hybridisation. *Planta* **198**:385–396.
- Millaleo, R., Reyes-Diaz, M., Alberdi, M., Ivanov, A.G., Krol, M., and Huner, N.P. (2013). Excess manganese differentially inhibits photosystem I versus II in *Arabidopsis thaliana*. *J. Exp. Bot.* **64**:343–354.
- Morgan, M.J., Lehmann, M., Schwarzlander, M., Baxter, C.J., Sienkiewicz-Porzućek, A., Williams, T.C., Schauer, N., Fernie, A.R., Fricker, M.D., Ratcliffe, R.G., et al. (2008). Decrease in manganese superoxide dismutase leads to reduced root growth and affects tricarboxylic acid cycle flux and mitochondrial redox homeostasis. *Plant Physiol.* **147**:101–114.
- Peiter, E., Montanini, B., Gobert, A., Pedas, P., Husted, S., Maathuis, F.J., Blaudez, D., Chalot, M., and Sanders, D. (2007). A secretory pathway-localized cation diffusion facilitator confers plant manganese tolerance. *Proc. Natl. Acad. Sci. USA* **104**:8532–8537.
- Pittman, J.K., Shigaki, T., Marshall, J.L., Morris, J.L., Cheng, N.H., and Hirschi, K.D. (2004). Functional and regulatory analysis of the *Arabidopsis thaliana* CAX2 cation transporter. *Plant Mol. Biol.* **56**:959–971.
- Pogson, B.J., and Albrecht, V. (2011). Genetic dissection of chloroplast biogenesis and development: an overview. *Plant Physiol.* **155**:1545–1551.
- Pyo, Y.J., Kwon, K.C., Kim, A., and Cho, M.H. (2013). Seedling Lethal1, a pentatricopeptide repeat protein lacking an E/E+ or DYW domain in *Arabidopsis*, is involved in plastid gene expression and early chloroplast development. *Plant Physiol.* **163**:1844–1858.

- Ramel, F., Sulmon, C., Bogard, M., Couee, I., and Gouesbet, G. (2009). Differential patterns of reactive oxygen species and antioxidative mechanisms during atrazine injury and sucrose-induced tolerance in *Arabidopsis thaliana* plantlets. *BMC Plant Biol.* **9**:28.
- Rentsch, D., Laloi, M., Rouhara, I., Schmelzer, E., Delrot, S., and Frommer, W.B. (1995). NTR1 encodes a high affinity oligopeptide transporter in *Arabidopsis*. *FEBS Lett.* **370**:264–268.
- Rodriguez-Celma, J., Tsai, Y.H., Wen, T.N., Wu, Y.C., Curie, C., and Schmidt, W. (2016). Systems-wide analysis of manganese deficiency-induced changes in gene activity of *Arabidopsis* roots. *Sci. Rep.* **6**:35846.
- Schmidt, S.B., Persson, D.P., Powikrowska, M., Frydenvang, J., Schjoerring, J.K., Jensen, P.E., and Husted, S. (2015). Metal binding in photosystem II super- and subcomplexes from barley thylakoids. *Plant Physiol.* **168**:1490–1502.
- Schmittgen, T.D., and Livak, K.J. (2008). Analyzing real-time PCR data by the comparative C-T method. *Nat. Protoc.* **3**:1101–1108.
- Schneider, A., Steinberger, I., Herdean, A., Gandini, C., Eisenhut, M., Kurz, S., Morper, A., Hoecker, N., Ruhle, T., Labs, M., et al. (2016). The evolutionarily conserved protein PHOTOSYNTHESIS AFFECTED MUTANT71 is required for efficient manganese uptake at the thylakoid membrane in *Arabidopsis*. *Plant Cell* **28**:892–910.
- Schneider, A., Steinberger, I., Strissel, H., Kunz, H.H., Manavski, N., Meurer, J., Burkhard, G., Jarzombski, S., Schunemann, D., Geimer, S., et al. (2014). The *Arabidopsis* tellurite resistance C protein together with ALB3 is involved in photosystem II protein synthesis. *Plant J.* **78**:344–356.
- Simm, S., Papatotiriou, D.G., Ibrahim, M., Leisegang, M.S., Muller, B., Schorge, T., Karas, M., Mirus, O., Sommer, M.S., and Schleiff, E. (2013). Defining the core proteome of the chloroplast envelope membranes. *Front. Plant Sci.* **4**:11.
- Socha, A.L., and Guerinot, M.L. (2014). Mn-euvering manganese: the role of transporter gene family members in manganese uptake and mobilization in plants. *Front. Plant Sci.* **5**:106.
- Steinberger, I., Egidi, F., and Schneider, A. (2015). Chlorophyll fluorescence measurements in *Arabidopsis* wild-type and photosystem II mutant leaves. *Bio-Protocol* **5**:e1532.
- Suorsa, M., and Aro, E.M. (2007). Expression, assembly and auxiliary functions of photosystem II oxygen-evolving proteins in higher plants. *Photosynth Res.* **93**:89–100.
- Szabo, I., and Spetea, C. (2017). Impact of the ion transportome of chloroplasts on the optimization of photosynthesis. *J. Exp. Bot.* **68**:3115–3128.
- Umena, Y., Kawakami, K., Shen, J.R., and Kamiya, N. (2011). Crystal structure of oxygen-evolving photosystem II at a resolution of 1.9 Å. *Nature* **473**:55–60.
- Wang, C., Xu, W., Jin, H., Zhang, T., Lai, J., Zhou, X., Zhang, S., Liu, S., Duan, X., Wang, H., et al. (2016). A putative chloroplast-localized Ca(2+)/H(+) antiporter CCHA1 is involved in calcium and pH homeostasis and required for PSII function in *Arabidopsis*. *Mol. Plant* **9**:1183–1196.
- Whittaker, M.M., Pan, H.Y., Yukl, E.T., and Whittaker, J.W. (2007). Burst kinetics and redox transformations of the active site manganese ion in oxalate oxidase: implications for the catalytic mechanism. *J. Biol. Chem.* **282**:7011–7023.
- Wu, Z., Liang, F., Hong, B., Young, J.C., Sussman, M.R., Harper, J.F., and Sze, H. (2002). An endoplasmic reticulum-bound Ca(2+)/Mn(2+) pump, ECA1, supports plant growth and confers tolerance to Mn(2+) stress. *Plant Physiol.* **130**:128–137.
- Yang, T.J., Perry, P.J., Ciani, S., Pandian, S., and Schmidt, W. (2008). Manganese deficiency alters the patterning and development of root hairs in *Arabidopsis*. *J. Exp. Bot.* **59**:3453–3464.
- Zhang, Z., Tan, J., Shi, Z., Xie, Q., Xing, Y., Liu, C., Chen, Q., Zhu, H., Wang, J., Zhang, J., et al. (2016). Albino Leaf1 that encodes the sole octotricopeptide repeat protein is responsible for chloroplast development. *Plant Physiol.* **171**:1182–1191.
- Zhang, B., Zhang, C., Liu, C., Jing, Y., Wang, Y., Jin, L., Yang, L., Fu, A., Shi, J., Zhao, F., et al. (2018). Inner envelope Chloroplast Manganese Transporter 1 supports manganese homeostasis and phototrophic growth in *Arabidopsis*. *Mol. Plant* **11**:943–954.

7.2 Publication II: Homologous Proteins of the Manganese Transporter PAM71 Are Localized in the Golgi Apparatus and Endoplasmic Reticulum

Natalie Hoecker, Anna Honke, Katharina Frey, Dario Leister, Anja Schneider

Plants (Basel). 2020 Feb 13;9(2):239

Supplementary data available under:

<https://www.mdpi.com/2223-7747/9/2/239>

Article

Homologous Proteins of the Manganese Transporter PAM71 Are Localized in the Golgi Apparatus and Endoplasmic Reticulum

Natalie Hoecker, Anna Honke, Katharina Frey , Dario Leister  and Anja Schneider * 

Molekularbiologie der Pflanze (Botanik), Department Biologie I, Ludwig-Maximilians-Universität München, 82152 Martinsried, Germany; Natalie.Hoecker@campus.lmu.de (N.H.); anna.honke@campus.lmu.de (A.H.); Ka.Frey@campus.lmu.de (K.F.); leister@lmu.de (D.L.)

* Correspondence: anja.schneider@lrz.uni-muenchen.de; Tel.: +49-89-2180-74696

Received: 13 December 2019; Accepted: 11 February 2020; Published: 13 February 2020



Abstract: Chloroplast manganese transporter 1 (CMT1) and photosynthesis-affected mutant 71 (PAM71) are two membrane proteins that function sequentially to mediate the passage of manganese across the chloroplast envelope and the thylakoid membrane. CMT1 and PAM71 belong to a small five-member protein family in *Arabidopsis thaliana*. The other three, photosynthesis-affected mutant 71 like 3 (PML3), PML4 and PML5 are not predicted to reside in chloroplast membranes. In this study, the subcellular localization of PML3:GFP, PML4:GFP and PML5:GFP was determined using transient and stable expression assays. PML3:GFP localizes to the Golgi apparatus, whereas PML4:GFP and PML5:GFP are found in the endoplasmic reticulum. We also examined patterns of *PML3*, *PML4* and *PML5* promoter activity. Although the precise expression pattern of each promoter was unique, all three genes were expressed in the leaf vasculature and in roots. Greenhouse grown single mutants *pml3*, *pml4*, *pml5* and the *pml4/pml5* double mutant did not exhibit growth defects, however an inspection of the root growth revealed a difference between *pml3* and the other genotypes, including wild-type, in 500 μ M manganese growth conditions. Strikingly, overexpression of PML3 resulted in a stunted growth phenotype. Putative functions of PML3, PML4 and PML5 are discussed in light of what is known about PAM71 and CMT1.

Keywords: manganese transporter; UPF0016 protein family; PAM71; CMT1; Arabidopsis

1. Introduction

Plants, like all other living organisms, require manganese (Mn) as an activator of enzymes or as an integral component of protein complexes. The translocation of Mn from the soil into the aerial parts of plants requires the concerted action of a number of Mn transporters, which mediate uptake of Mn into root cells and facilitate subsequent Mn translocation from root to shoot [1,2]. At the cellular level, stably bound Mn is found in various locations, including the photosystem II (PSII) in chloroplasts, oxalate oxidase in cell walls, and Mn superoxide dismutase in mitochondria. Mn is also present in the Golgi apparatus (e.g., glycosyltransferases are activated by Mn^{2+}), in the endoplasmic reticulum and in the vacuole. Indeed, the vacuole serves as an intracellular sink when Mn is in excess and as a source when the Mn supply is limited [3]. The most prominent role of Mn is its involvement in the oxygen-evolving complex of PSII, which splits water into oxygen, protons and electrons. The electrons released from water in PSII are eventually transferred to $NADP^+$ via the cytochrome b_6/f complex, plastocyanin, photosystem I and ferredoxin. Detailed analysis over the past several years has elucidated the structural basis for water oxidation and oxygen evolution in PSII by the catalytic Mn_4CaO_5 cluster [4–7].

To reach its destination in the oxygen-evolving complex of PSII in the thylakoid lumen, Mn must cross all three chloroplast membranes (the outer and inner envelopes and the thylakoid membrane). The outer envelope membrane is non-selectively permeable to most ions, while the inner envelope and the thylakoid membrane possess specific transport proteins. At the inner envelope membrane, chloroplast manganese transporter 1 (CMT1) represents the first candidate for the long-sought Mn import protein [8,9]. CMT1 transports Mn from the cytosol into the chloroplast stroma. The Arabidopsis mutant *cmt1* exhibits severe growth retardation, disruption of chloroplast ultrastructure and reduction of PSII activity, in association with a significant drop in the level of Mn in this organelle [8]. The protein responsible for the transport of Mn from the chloroplast stroma into the thylakoid lumen is photosynthesis-affected mutant 71 (PAM71) [10]. PAM71 resides in the thylakoid membrane and in *pam71* mutants PSII function is specifically impaired at the oxygen-evolving complex. The Mn transport function of CMT1 and PAM71 is conserved among homologous proteins from oxygenic photosynthetic organisms, e.g., cyanobacteria and green algae [10–12].

The presence of manganese in the Golgi apparatus, in the endoplasmic reticulum and in the vacuole means that transporter proteins of the endomembrane system and the tonoplast are important for the distribution of Mn in the cell [2]. Mn that is sequestered into the vacuole by members of the cation exchanger and calcium cation exchanger protein families is remobilized upon Mn deficiency by natural resistance-associated macrophage protein 3 (NRAMP3) and NRAMP4 in Arabidopsis mesophyll cells [2,13]. Another vacuolar Mn transporter, metal tolerance protein 8 (MTP8), participates in Mn homeostasis during seed development and germination in Arabidopsis plants [14,15]. A second member of the MTP family, MTP11, is found in Golgi-like and/or in pre-vacuolar compartments [16,17]. The *MTP11* gene is most highly expressed in leaf hydathodes and root tips and the protein could be involved in the exocytosis of excess Mn in these secretory tissues [16]. Two P-type ATPases, ER-type calcium ATPase 1 (ECA1) and ECA3 (which are localized to the endoplasmic reticulum and the Golgi membrane, respectively) are expressed in all major organs, and are involved in Mn pumping into these organelles [18–20]. Remobilization of Mn from the trans-Golgi compartment is mediated by NRAMP2 [21,22] which helps to build up/maintain the cytosolic Mn pool.

In addition to PAM71 and CMT1, the Arabidopsis genome encodes three other members of the uncharacterized protein family 0016 (UPF0016) [23], which we refer here as PML for PAM71-like proteins: PML3 (encoded by *At5g36290*), PML4 (encoded by *At1g25520*) and PML5 (encoded by *At1g68650*). According to the Transporter Classification Database (TCDB) [24] this protein family (classification number 2.A.106 in the TCDB) belongs to the LysE superfamily, this superfamily contains no other Mn transporters from plants. The three proteins PML3, PML4, and PML5 are predicted as substrates of the secretory pathway [10,23]. In the present study, we determined their subcellular localization and isolated insertion alleles. Moreover, we analyzed the spatial and temporal expression patterns by monitoring their activity of promoter fusions.

2. Results

2.1. PML3, PML4 and PML5 Are Predicted Substrates of the Secretory Pathway

The UPF0016 family of membrane proteins comprises five members in Arabidopsis, and a sequence alignment is shown in Figure 1. PAM71 and CMT1 each contain a chloroplast-targeting signal (cTP) [8,10,23], whereas PML3 contains an N-terminal extension, which is predicted to be a secretory signal peptide (SP) [23] (Figure 1) and is notably lacking in PML4 and PML5 (Figure 1). The five proteins each possess six conserved transmembrane domains and share two highly conserved E-x-G-D-(KR)-(TS) motifs in transmembrane domain TM1 and TM4. In all five proteins, the central loop between transmembrane domain TM3 and TM4 is enriched in negatively charged acidic residues (Figure 1). Based on this sequence analysis, we concluded that PML3, PML4 and PML5 belong to the conserved group of Mn/Ca transporters, which are evolutionary conserved [23,25].

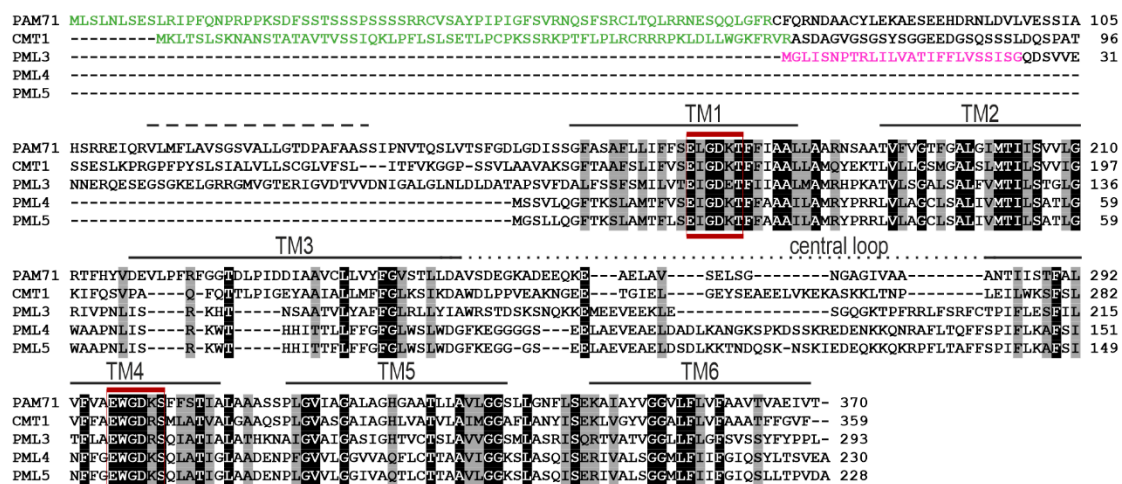


Figure 1. Protein sequence alignment of chloroplast manganese transporter 1 (CMT1), photosynthesis-affected mutant 71 (PAM71) and related proteins in Arabidopsis. Annotations were made as described previously [10]. Black and grey boxes indicate identical residues and conservative exchanges. Six putative transmembrane domains are indicated from TM1 to TM6, with the putative additional TM domain of CMT1 and PAM71 indicated by a dashed line. The conserved motifs E-x-G-D-(KR)-(TS) are highlighted by red lines, and the central loops are indicated by a dotted line. The putative chloroplast transit peptides are indicated by green letters and the putative secretory pathway transit peptide is indicated by magenta letters.

2.2. PML3 Localizes to the Golgi, and PML4 and PML5 Are Found in the Endoplasmic Reticulum

In order to determine the subcellular localization of PML3, PML4 and PML5, the open reading frames of the respective cDNAs were amplified and subsequently cloned upstream of the *GFP* reporter gene and downstream of the 35S promoter. The resulting constructs were then transiently expressed in *Nicotiana benthamiana* leaves (Figure 2 and Figure S1). In none of these cases was the GFP signal found to overlap with chlorophyll autofluorescence (Figure 2). Thus, a chloroplast localization for PML3, PML4 and PML5 can be excluded, as already suggested by the *in silico* analysis (Figure 1). The pattern of PML3:GFP fluorescence displayed predominantly dot-like signals resembling those of the fluorescent Golgi marker GmMAN1:mCherry [26]. Indeed, when simultaneously expressed, fluorescence signals from both proteins PML3:GFP and GmMAN1:mCherry overlapped, thus indicating that PML3:GFP is targeted to the Golgi apparatus (Figure 2A, Figure S1A). We also determined the subcellular localization of PML4:GFP and PML5:GFP. The GFP fluorescence of both protein fusions was distributed in a pattern resembling that of the ER marker AtWAK2:mCherry [26] and coincided exactly with the red fluorescence of this marker (Figure 2B,C, Figure S1B), indicating that both proteins are targeted to the endoplasmic reticulum. We verified that the GFP fluorescence of PML5:GFP did not overlap with the red fluorescence of GmMAN:mCherry, effectively excluding the possibility of a dual localization (Figure S1C).

To further confirm these findings, we generated stably transformed Arabidopsis lines expressing *PML3:GFP*, *PML4:GFP* and *PML5:GFP* under the control of the 35S promoter and named these individual lines *Pro35S::PML3:GFP* #1, *Pro35S::PML4:GFP* #1 and *Pro35S::PML5:GFP* #1, respectively (Figure S2). Microsomal fractions from leaves of the three lines were subjected to centrifugation on sucrose-density gradients (Figure 2D–F). Fractions 6 to 22 were subjected to immunoblot analysis employing three antibodies, including the GFP antibody. Antibodies against sterol methyltransferase 1 (SMT1), an integral membrane protein specific to the endoplasmic reticulum [27], and ADP-ribosylation factor 1 (ARF1), a protein that is found in both the Golgi and the trans-Golgi network [28], were used to detect endogenous proteins of the respective compartment (Figure 2D,F). PML3:GFP was found in the same fractions as the ARF1 signal (Figure 2D), while the GFP fusions expressed in the lines

Pro35S::PML4:GFP and *Pro35S::PML5:GFP* were both found to comigrate with the SMT1 protein (Figure 2E,F). These observations confirm the localization of PML3 to the Golgi apparatus and the assignments of PML4 and PML5 to the endoplasmic reticulum.

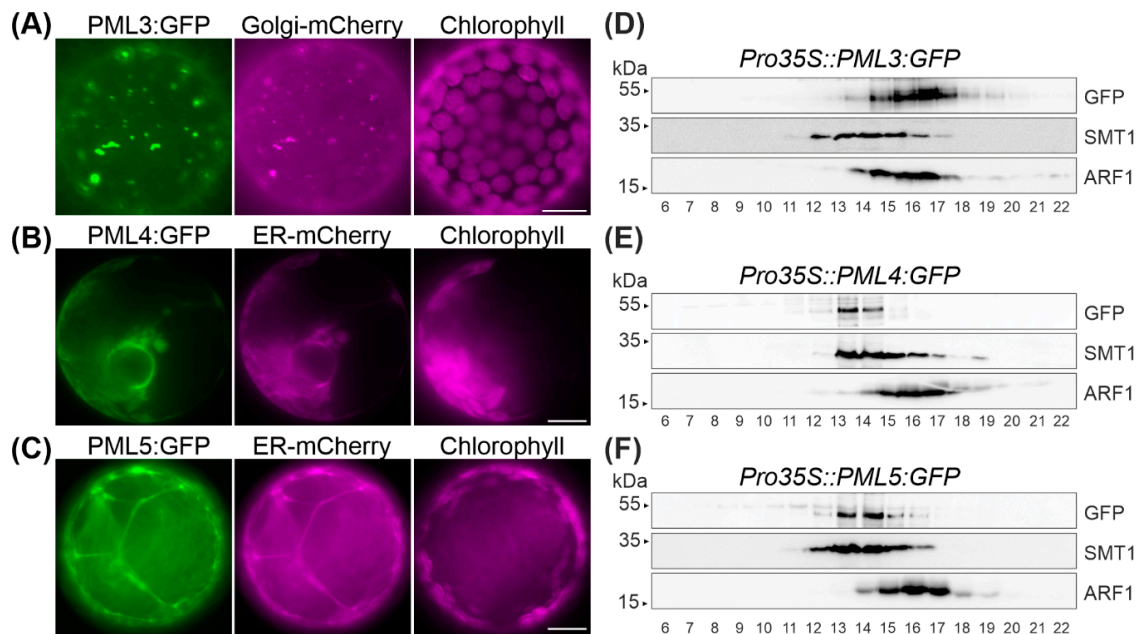


Figure 2. Fluorescence analysis of *Nicotiana benthamiana* protoplasts and immunoblot analysis of stable transformed Arabidopsis lines. (A) *N. benthamiana* leaves were infiltrated with pPro35S::PML3:GFP and pG-rk (=Golgi-mCherry); a second focus layer and corresponding overlay and bright field photographs are shown in Figure S1. (B) *N. benthamiana* leaves were infiltrated with pPro35S::PML4:GFP and pER-rk (=ER-mCherry); a second protoplast with overlay and bright field photographs is shown in Figure S1. (C) *N. benthamiana* leaves were infiltrated with pPro35S::PML5:GFP and pER-rk (=ER-mCherry). (A–C) GFP fluorescence of the indicated fusion protein is depicted in green, mCherry fluorescence and chlorophyll autofluorescence are depicted in magenta. Scale bar = 10 μm. (D–F) Separation of isolated microsomes of the indicated stable transformed Arabidopsis line by sucrose density centrifugation (20% to 50%). Top-down aliquots of fractions as indicated, were separated by SDS-PAGE and analyzed by immunodetection using anti-GFP, anti-sterol methyltransferase 1 (SMT1) and anti-ADP-ribosylation factor 1 (ARF1) antibodies. The individual lines used for this experiment were *Pro35S::PML3:GFP* #1, *Pro35S::PML4:GFP* #1 and *Pro35S::PML5:GFP* #1, as indicated in Figure S2.

2.3. Transgenic Arabidopsis Lines Expressing PML3:GFP Show a Stunted Growth Phenotype

The stably transformed Arabidopsis lines *Pro35S::PML4:GFP* #1 and *Pro35S::PML5:GFP* #1 possessed a wild-type-like phenotype (Figure 3A), however *Pro35S::PML3:GFP* #1 showed an interesting leaf phenotype. The rosette of *Pro35S::PML3:GFP* #1 was much smaller than a wild-type rosette of the same developmental stage (Figure 3B), and individual leaves exhibited a prominent constraint and bent morphology (Figure 3C,D). A rather simple explanation for this growth phenotype could be that the transgene caused a mutation by its random insertion into the genome of Arabidopsis. To exclude this possibility, we searched for independent transgenic *Pro35S::PML3:GFP* lines that exhibited GFP expression. To this end, we isolated three further lines, named *Pro35S::PML3:GFP* #2, #3, and #4 (Figure S2). All lines were grown at the same time and visually inspected for their leaf phenotype. It turned out that they were smaller than wild-type of the same age; thus, it is likely that expression of *PML3:GFP* evokes the stunted growth phenotype. Moreover, two lines, *Pro35S::PML3:GFP* #2 and #3, displayed a similar curvature of individual leaves in agreement with observations made in *Pro35S::PML3:GFP* #1 (Figure 3). It should be noted that not all leaves are equally affected and therefore it is maybe not surprising that *Pro35S::PML3:GFP* #4 did not show curvature of individual leaves (Figure 3).

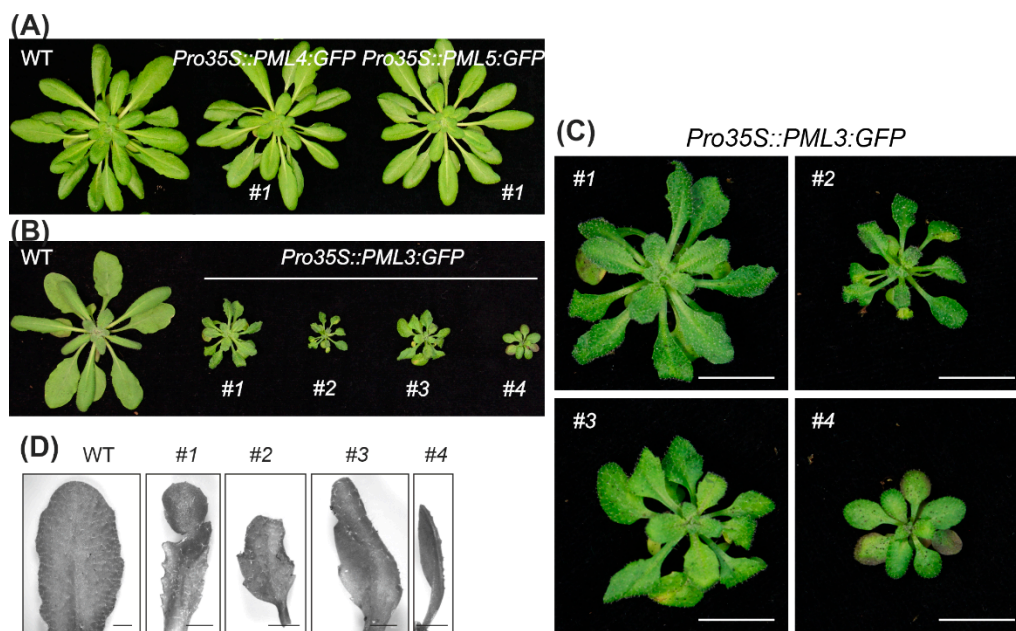


Figure 3. Photographs of stably transformed Arabidopsis lines. (A) *Pro35S::PML4::GFP* and *Pro35S::PML5::GFP* plants in comparison to a wild-type plant are shown. (B) WT and transgenic lines *Pro35S::PML3::GFP* #1, #2, #3, #4 were grown for 3 weeks under a 12 h/12 h light–dark cycle and 2 weeks in the greenhouse. (C) Magnified images of plants shown in (B), Scale bar = 1 cm. (D) Magnified images of individual leaves taken from the plants shown in (B) and (C), Scale bar = 2 mm.

2.4. Expression Patterns of PML3, PML4 and PML5 in Arabidopsis Tissues

From the results so far, we concluded that PML4 and PML5 localize to the same compartment and thus might have redundant functions in the cell. The expression pattern revealed that *PML4* and *PML5*, as well as *PML3*, are expressed in photosynthetic and in non-photosynthetic tissues (Figure 4A and Figure S3). To define the expression patterns more specifically, promoter-driven reporter gene constructs were assembled by fusing a 1.3-kb fragment upstream of the *PML3* coding sequence and 1.2-kb segments of the upstream regions of *PML4* and *PML5*, respectively, to the *uidA* reporter gene. The constructs were designed to exclude the ATG of the endogenous genes; more precisely, the *PML3* fragment comprises −1021 bp to +315 bp from the transcription initiation site, the *PML4* fragment comprises −971 bp to +237 bp from the transcription initiation site, and the *PML5* fragment comprises −1116 bp to +94 bp from the transcription initiation site (sequences of the fragments are shown in Table S1). Transgenic lines harboring the individual constructs were generated and named *ProPML3::GUS*, *ProPML4::GUS* and *ProPML5::GUS*. We found β-Glucuronidase (GUS) activity in rosette leaves and in roots of the transgenic line *ProPML3::GUS*, *PML3* promoter-driven GUS expression was strong in lateral roots, throughout the leaf and particularly in the vasculature and in anthers (Figure 4B). Both *ProPML4::GUS* and *ProPML5::GUS* lines showed similar yet distinct GUS activity patterns. In both lines, GUS activity was found in roots and leaves; however, *PML4*-driven GUS expression was found mainly in minor veins, and *PML5*-driven GUS expression was predominantly detected in the main veins of adult leaves (Figure 4C,D). The *ProPML4::GUS* line expressed GUS particularly in root hairs, while in line *ProPML5::GUS*, the GUS activity was found in the root stele (Figure 4C,D). Moreover, the patterns of *PML4* and *PML5* promoter expression differed from each other in flower tissues (Figure 4C,D). Only weak GUS activity in the receptacle tissue of *ProPML5::GUS* was detected, whereas petals of *ProPML4::GUS* displayed strong GUS activity. Taken together, this analysis shows that *PML4* and *PML5* are expressed in distinct tissues of roots, leaves and flowers, which suggests that they might have partially redundant functions in plants.

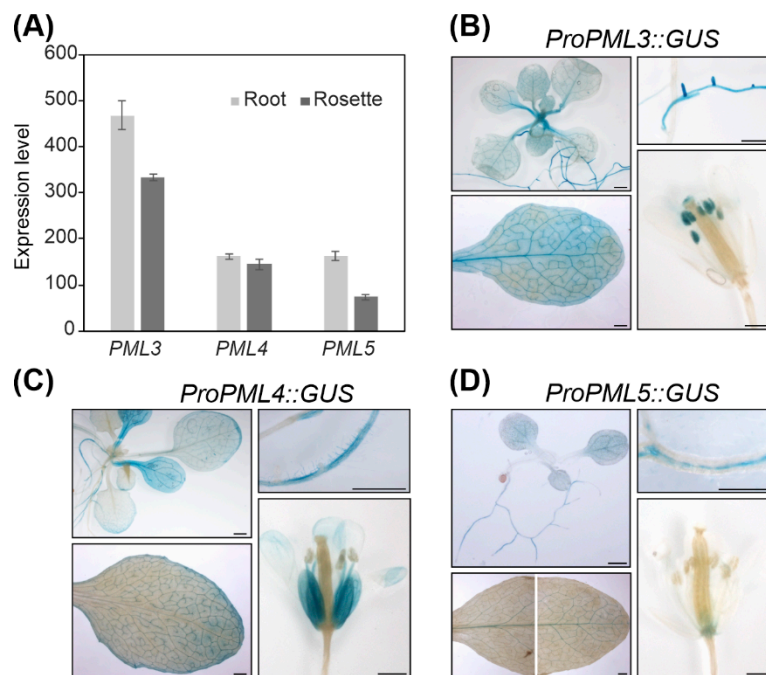


Figure 4. Analysis of *PML3*, *PML4*, and *PML5* expression. (A) Expression levels were derived from the developmental map of the Arabidopsis Browser Database [29]. (For promotor analysis, various tissues of Arabidopsis line *ProPML3::GUS* (B), *ProPML4::GUS* (C), and *ProPML5::GUS* (D) were incubated in staining solution and analyzed for a blue precipitate of chloro-bromindigo indicating β -Glucuronidase (GUS) activity. Please note that the leaf photograph in (D) is composed of two single photographs. Scale bar = 1 mm.

2.5. Root Elongation in *pml3* Is Distinct from Other Genotypes in 500 μ M MnSO_4

We isolated the insertion alleles *pml3*, *pml4* and *pml5* (Figure S4), and named the mutant lines accordingly. From our observations so far, we also aimed to generate a double mutant *pml4/pml5* to test whether *PML4* and *PML5* have a redundant function. Single and double mutant plants grown in the greenhouse did not display differences compared to wild-type plants (Figure S4). Thus, we examined the mutants at an earlier stage, with a focus on roots, because *PML3*, *PML4* and *PML5* expression is higher in roots than in rosette leaves (Figure S3). Seeds of wild-type, *pml3*, *pml4*, *pml5*, and *pml4/pml5* were sterilized and grown for ten days to inspect for a rosette-leaf phenotype and for root phenotype. The five genotypes were grown on medium containing 5 μ M MnSO_4 , 50 μ M MnSO_4 , and 500 μ M MnSO_4 (Figure 5A).

As a read-out for a rosette-leaf phenotype, we determined chlorophyll content. The chlorophyll content of the five genotypes is subjected to little fluctuation when plants were grown in 5 μ M and 50 μ M MnSO_4 , indicating that Arabidopsis can grow well within a certain range of Mn. The overall chlorophyll content went down when plants were subjected to 500 μ M MnSO_4 and a comparison between the five genotypes revealed that they behave similarly (Figure 5B, Table S2). As a read-out for a root phenotype, we determined the length of the primary root and observed that this parameter is also subjected to little fluctuation when plants were grown in 5 μ M and 50 μ M MnSO_4 (Figure 5A,C). The overall root length increased when plants were subjected to 500 μ M MnSO_4 (Figure 5C); in another study, this tendency was observed when Arabidopsis plants were treated with 1250 μ M MnSO_4 [30]. Interestingly, a comparison of the root length revealed that roots of *pml3* grown in 500 μ M MnSO_4 were significantly more elongated than roots of wild-type, *pml4*, *pml5* and *pml4/pml5* (Figure 5C, Table S3) in 500 μ M MnSO_4 and in any other condition. To investigate whether this effect can be inverted, plants were grown on medium with the MnSO_4 concentration set to 50 nM (Figure S5). Plant growth was not drastically impaired, indicating that internal Mn stores possibly support plant growth to a

certain degree. The overall root length decreased slightly in this condition (Table S3), in agreement with a trend described by Gruber et al. [31]. However, we could not detect any difference between the genotypes regarding root length and chlorophyll content (Figure S5). Taken together, we concluded that the 500 μM MnSO_4 treatment caused an intracellular excess of Mn which influences root elongation and that PML3 is involved in this process. Consistent with other results, this finding indicates that the functionality of PML3 is distinct from that of PML4 and PML5.

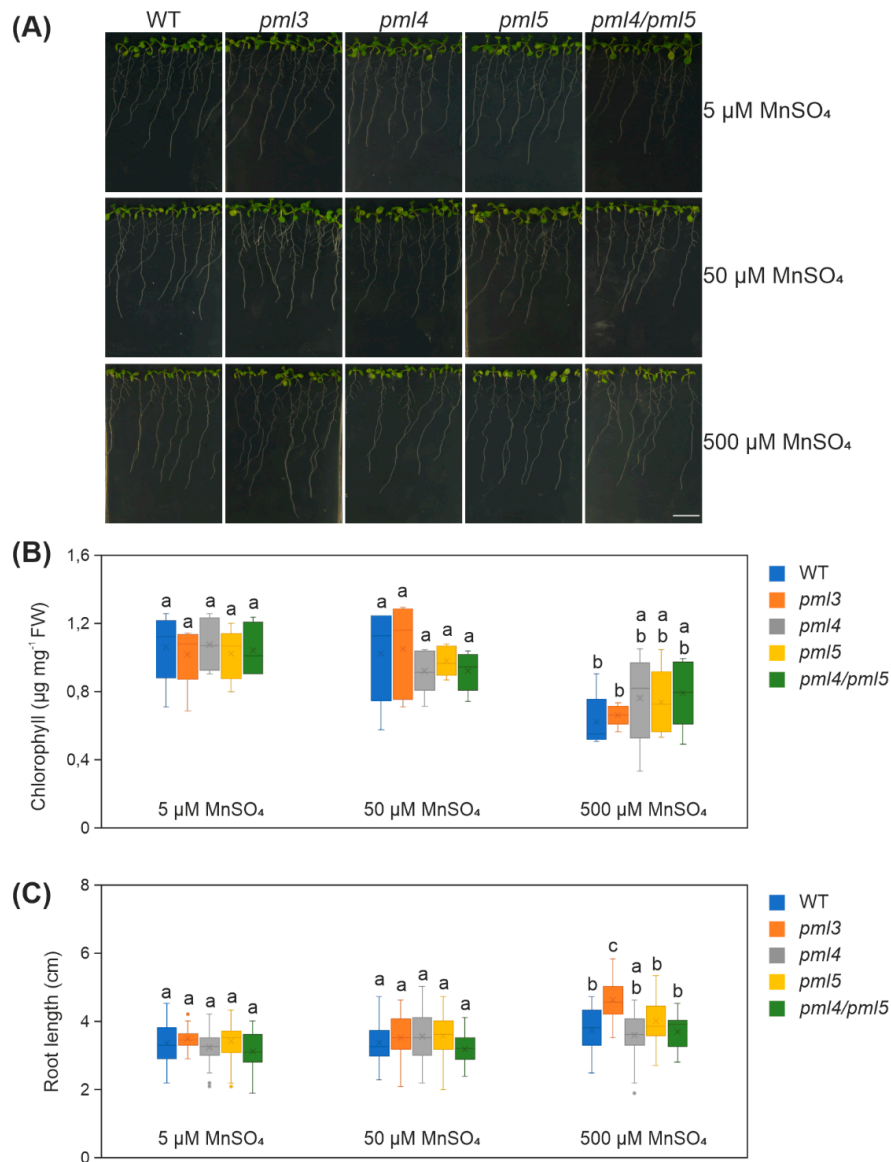


Figure 5. Analysis of wild-type, *pml3*, *pml4*, *pml5* and *pml4/pml5* grown under different Mn regimes (A) Photographs were taken from representative samples. Plants were grown in the indicated Mn condition, in a vertical position under a 16 h/8 h light–dark cycle at $100 \mu\text{mol photons m}^{-2} \text{s}^{-1}$ for 10 days. Scale bar = 1 cm (B) Five to six plants per genotype and condition were combined for one chlorophyll extraction and at least five extractions were prepared. Data are depicted as boxplots representing the range of values, the exclusive median and the mean, indicated as \times ($n \geq 5$). FW = fresh weight. (C) The length of the primary root of all plants are depicted as boxplots representing the range of values, the exclusive median and mean, indicated as \times ($n \geq 35$ per genotype and condition). Outliers are indicated as dots. (B,C): different letters indicate statistical significance according to ANOVA ($p < 0.05$, Tukey’s honestly significant difference (HSD) test). Mean values and standard deviations are given in Tables S2 and S3. Poorly germinated seeds were excluded from the analysis.

3. Discussion

The genome of *Arabidopsis* contains three sequences that code for proteins with high similarity to PAM71 and CMT1, two previously characterized Mn transporters localized in distinct chloroplast membranes [8–10]. Like PAM71 and CMT1, the three predicted protein sequences contain the two highly conserved E-x-G-D-(KR)-(TS) motifs, with two negatively charged acidic residues in TM1 and TM4, which provide a suitable environment for the passage of Mn^{2+} ions and maybe other cations through membranes. The greatest diversity within this protein family is found in their N-terminal regions (Figure 1), which were proposed to be responsible for targeting the respective protein to the correct membrane [23]. In the present study, we were able to localize PML3, PML4 and PML5 in the endomembrane system of *Arabidopsis*.

The PML3 protein sequence contains an N-terminal region predicted to serve as signal peptide for the secretory pathway (Figure 1), and indeed PML3 could be localized to the Golgi apparatus (Figure 2, Figure S1), most likely in the Golgi membrane. PML3, together with its homologs, belongs to the UPF0016 family of membrane proteins, and the yeast and human members of this family were found to be located in the Golgi membrane as well [32]. Recent findings support a role for the human member transmembrane protein 165 (TMEM165) in Ca^{2+}/Mn^{2+} import into the Golgi. Indeed, Mn^{2+} is known to be an essential cofactor for many Golgi-localized glycosyltransferases [33] and glycosylation abnormalities have been described in humans with mutations in TMEM165, which result in a rare genetic condition called Congenital Disorder(s) of Glycosylation [34]. Plant glycosyltransferases with functions in glycoprotein biosynthesis are also present in the Golgi [35,36]. In addition, glycosyltransferases in plants are involved in the biosynthesis of non-cellulosic polysaccharides of the cell wall [35], and some of them have been shown to depend on Mn^{2+} [37]. It is perhaps not surprising that the *pml3* insertion line does not show a drastic altered phenotype compared to wild-type (Figure 5, Figure S4), as at least one other protein, the P-type ATPase ECA3, is known to be located in the Golgi membrane and possibly plays a role in the transport of Mn into this organelle [19]. ECA3 is expressed in all major organs, and particularly in the vasculature of primary and lateral roots, as well as in leaves and flowers [19,20]. Its expression thus overlaps with PML3 expression, which was found in all major organs, especially in the vasculature of leaves and in roots (Figure 4). The growth of the *eca3* mutant is impaired when grown in Mn deficiency [19,20], whereas in *pml3*, only a subtle root phenotype appeared (Figure 5). It appears that primary root elongation in *pml3* plants is induced more in 500 μM $MnSO_4$ conditions (Figure 5). Because the root length of *pml3* plants was not changed in comparison to wild-type in lower $MnSO_4$ concentrations, we assume that PML3 is involved in specific processes during Mn excess, perhaps loading Mn into the Golgi. It is believed that Mn stored in the Golgi can be remobilized by NRAMP2 in Mn deficient conditions [21,22]. In addition, an interesting phenotype was observed when PML3:GFP was overexpressed. A stunted growth phenotype occurred in PML3:GFP over-expressor lines (Figure 3), with some leaves being out of shape. The underlying molecular mechanism evoking this phenotype is unknown, however one speculation is that massive Mn content in the Golgi apparatus of the over-expressor lines might alter glycosylation reactions, which eventually affects leaf shape and plant growth. Although highly speculative, this hypothesis certainly deserves deeper investigation in the future.

The subcellular localization of PML4 and PML5 was also determined and, unlike PML3, both proteins were found to reside in the endoplasmic reticulum (Figure 2, Figure S1). The importance of the endoplasmic reticulum in N-glycosylation of glycoproteins and in the biosynthesis of glycans for the cell wall matrix is well known [38,39]. Furthermore, the peptidyl serine O- α -galactosyltransferase (SGT1), which is involved in O-glycosylation, localizes to the endoplasmic reticulum, and was shown to require Mn^{2+} as a cofactor [40]. Mn transport into the endoplasmic reticulum is mediated by ECA1, and the *eca1* mutant showed increased sensitivity towards high Mn; in fact, it failed to elongate the root hairs under these conditions, presumably through impairment in growth tip processes [18]. We propose that PML4 and PML5 might act to fine tune Mn allocation into the endoplasmic reticulum of specific cell types, e.g., those of the root hair (PML4) or root stele (PML5) (Figure 4), as they are

dispensable for primary metabolism. The interplay of various Mn transporters within single cells as well as on different tissue levels is complicated by the fact that some of them also transport other cations like calcium, or indirectly act on calcium homeostasis. Thus, the challenge of future work will be to elucidate the precise substrate specificity of PML3, PML4 and PML5 and perhaps other Mn transporters by employing heterologous expression and reconstitution assays. Furthermore, it will be interesting to learn more about the sophisticated network of Mn transporters, perhaps through the generation of triple or even higher order mutant lines.

4. Materials and Methods

4.1. Plasmid Construction and Plant Material

For subcellular localization studies, the sequences encoding PML4 and PML5 were amplified using specific primer combinations (Table S4) and single-stranded Arabidopsis cDNAs. The amplified cDNAs were ligated into pENTR-TOPO (Life Technologies, Carlsbad, CA, USA), and recombined into pB7FWG2 [41], yielding the plasmids pPro35S::PML4:GFP and pPro35S::PML5:GFP. The plasmid pPro35S::PML3:GFP was constructed from appropriate primers (Table S4), the backbone of pB7FWG2 and a template cDNA using the Gibson Assembly Cloning Kit (catalog number E5510S, New England Biolabs, Ipswich, MA, USA) in accordance with the manufacturer's instructions.

For study promoter activities, fragments located upstream of the *PML3*, *PML4* and *PML5* coding regions (Table S3) were amplified from Arabidopsis genomic DNA using specific primer combinations (Table S4) and ligated into pENTR-TOPO. The entry clones were subsequently recombined into pKGWFS7 [41] upstream of the *uidA* reporter gene, yielding the plasmids pProPML3::GUS, pProPML4::GUS and pProPML5::GUS. Thus, the constructs were designed to use the ATG of the *uidA* reporter gene.

All plasmids were transformed into *Agrobacterium tumefaciens* strain GV3101. *Agrobacterium* strains harboring pPro35S::PML3:GFP, pPro35S::PML4:GFP or pPro35S::PML5:GFP were either infiltrated into *N. benthamiana* leaves or used for stable transformation of Arabidopsis by the floral dip method. Individual transgenic Arabidopsis plants were selected on the basis of their resistance to ammonium glufosinate (100 mg L^{-1}). *Agrobacterium* strains harboring pProPML3::GUS, pProPML4::GUS or pProPML5::GUS were also used for stable transformation of Arabidopsis. In this case, individual transgenic Arabidopsis plants were selected on the basis of their resistance to kanamycin ($50 \text{ } \mu\text{g mL}^{-1}$).

Arabidopsis mutant lines were obtained from the European Arabidopsis Stock Centre (NASC) and named *pml3* (N402563=GK-027F07), *pml4* (N664220=SALK_143524) and *pml5* (N438509=GK-402B01), respectively. Genotyping of all lines was performed using PCR with appropriate primer combinations (Table S3). Expression of *PML3*, *PML4* and *PML5* in the different genotypes was analyzed by RT-PCR using an appropriate primer combination (Table S4), first strand cDNA and 30 PCR cycles.

Arabidopsis wild-type plants (accession Columbia-0) were used for stable transformation by the floral dip method [42] and as controls. Unless stated otherwise, Arabidopsis lines and *N. benthamiana* were cultivated in a temperature-controlled greenhouse with additional lighting up to 16 h to reach at least $140 \text{ } \mu\text{mol photons m}^{-2} \text{ s}^{-1}$. Surface-sterilized Arabidopsis seeds were germinated on half-strength Murashige and Skoog medium ($\frac{1}{2}$ MS) including 1% (*w/v*) sucrose, with or without antibiotic, and grown for two weeks before individual plants were transferred to the greenhouse. For growth on media with different Mn concentrations, the macro and micro elements of $\frac{1}{2}$ MS were mixed according to the Murashige and Skoog medium composition (Duchefa M0222), with the exception of MnSO_4 : $0.00845 \text{ mg L}^{-1}$, 0.845 mg L^{-1} , 8.45 mg L^{-1} or 84.5 mg L^{-1} of $\text{MnSO}_4 \times \text{H}_2\text{O}$ were added in 1 L of medium to give a final concentration of 50 nM, 5 μM , 50 μM or 500 μM MnSO_4 , respectively. Plant agar (Duchefa P1001) was used for solidification.

4.2. Protoplast Isolation and Fluorescence Microscopy

Agrobacterium-mediated infiltration of *N. benthamiana* was performed as described [43]. Protoplasts were isolated from leaf tissue 48 h after infiltration [43] and fluorescent signals were detected using an Axio-Imager fluorescence microscope (Carl Zeiss, Oberkochen, Germany). Two plasmids expressing marker proteins for either the Golgi (pG-rk expressing GmMAN1:mCherry) or the endoplasmic reticulum (pER-rk expressing AtWAK2:mCherry) were chosen for co-infiltration, because their specificity is well established [26,44]. The GFP fluorescence was excited at 470 ± 40 nm and the emission recorded at 525 ± 50 nm. Chlorophyll autofluorescence was excited at 450–490 nm, and emission was recorded at >515 nm. The mCherry fluorescence of the marker proteins was excited at 560 ± 40 nm and the emission recorded at 630 ± 75 nm. The fluorescence signals obtained in the different channels were overlaid using ImageJ (version 1.51j).

4.3. Microsomal Preparation and Western Blot Analysis

For the isolation of microsomal fractions, transgenic Arabidopsis lines were grown for 4–5 weeks in a growth chamber under a 12 h/12 h light–dark cycle at $100 \mu\text{mol photons m}^{-2} \text{s}^{-1}$ and $22^\circ\text{C}/18^\circ\text{C}$. Leaf homogenization and microsomal fraction enrichment by differential centrifugation was performed as previously described [45]. Isolated microsomal fractions were layered on top of a continuous 20–50% (*w/v*) sucrose density gradient and centrifuged for 16 h at 4°C and $100,000\times g$. After centrifugation, 500 μL fractions were collected from the top of the tube and analyzed by SDS-PAGE and Western blotting [45]. Individual proteins were detected using antisera raised against GFP (Life Technologies A6455, 1:2000 dilution), SMT1 (Agrisera AS07 266, Vannas, Sweden; 1:500 dilution) and ARF1 (Agrisera AS08 325, 1:1000 dilution) in combination with anti-rabbit IgG horseradish peroxidase (HRP) (Sigma Aldrich, St. Louis, MO, USA 1:25,000 dilution) and the Pierce Enhanced Chemiluminescence System (Thermo Fisher Scientific, Waltham, MA, USA).

4.4. Promotor Activity Analysis and Light Microscopy

To monitor tissue-specific promoter activity, transgenic Arabidopsis lines were assayed for β -glucuronidase (GUS) activity. After overnight incubation in staining solution (100 mM NaH_2PO_4 pH 7.0, 10 mM ethylenediaminetetraacetic acid (EDTA), 0.1% (*v/v*) Triton X-100, and 0.5 mg mL^{-1} 5-bromo-4-chloro-3-indolyl glucuronide (X-Gluc)) at 37°C , tissues were cleared in 70% (*v/v*) ethanol and analyzed with a stereoscope (SteREO Lumar.V12, Carl Zeiss) equipped with an AxioCam color camera.

4.5. Real-time PCR Analysis

Total RNA was isolated from the root and shoot systems of Arabidopsis wild-type plants using TRIzol reagent (Invitrogen). For real time qRT-PCR, SYBR Green Supermix (Bio-Rad) was used, and PCR was performed with the iQ5 multi-color real-time PCR detection system (Bio-Rad). Quantification of relative expression levels was performed using the comparative cycle threshold (C_T) method [46].

4.6. Sequence Analysis and Statistical Analysis

Alignments were generated using Clustal Omega [47]. Putative secretory pathway signal peptides (SP) were predicted with TargetP [48] and transmembrane helix predictions were obtained from the Aramemnon database [49,50] with manual adjustments. Arabidopsis sequence data were obtained from the National Center for Biotechnology Information [51] under the following accession numbers: NP_564825.1 (PAM71, At1g64150); NP_193095.2 (CMT1, At4g13590); NP_568535.1 (PML3, At5g36290); NP_173923.1 (PML4, At1g25520); NP_177032.1 (PML5, At1g68650).

Boxplots were generated in Excel 2016 and a one-way ANOVA with post-hoc Tukey HSD test was performed [52].

5. Conclusions

The main goal of the present study was to determine the subcellular localization(s) of the three PAM71 homologs: PML3, PML4 and PML5. The localization of PML3 to the Golgi, and of PML4 and PML5 to the endoplasmic reticulum, is clearly different from the chloroplast localizations of PAM71 and CMT1 in a leaf cell. Logically, PAM71 and CMT1 must both be present in chloroplast membranes at the same time. In contrast, the functions of the other three proteins do not necessarily have to be coordinated within individual cells. In agreement with their subcellular localization in the endomembrane system, expression of *PML3*, *PML4* and *PML5* is not restricted to photosynthetic cells, e.g., they are also expressed in non-photosynthetic cells of roots or flowers. The three proteins do not seem to be essential for plant growth and development, however a subtle root growth phenotype was observed in the *pml3* mutant. Overall, root length increased in plants exposed to 500 μ M Mn, and this phenomenon is boosted in *pml3*. Taken together, the cellular function of PML3 is distinct from that of PML4 and PML5 and is also evident from the leaf phenotype of the *PML3* over-expressor line. We suspect that PML3 at the Golgi membrane plays a role in balancing excess manganese.

Supplementary Materials: The following are available online at <http://www.mdpi.com/2223-7747/9/2/239/s1>, Figure S1: Fluorescence analysis of PML3:GFP, PML4:GFP and PML5:GFP in *N. benthamiana* protoplasts upon leaf infiltration. Figure S2: Selection of stable transformed Arabidopsis lines *Pro35S::PML3:GFP*, *Pro35S::PML4:GFP* and *Pro35S::PML5:GFP*. Figure S3: Analysis of *PML3*, *PML4*, and *PML5* expression. Figure S4: Arabidopsis T-DNA mutant analysis. Figure S5: Analysis of the five genotypes grown under an external supply of 50 nM MnSO₄. Table S1: Fragments used for promotor analysis. Table S2: Mean values \pm standard deviation of chlorophyll contents of the five genotypes grown under different Mn regimes. Table S3: Mean values \pm standard deviation of root length of the five genotypes grown under different Mn regimes. Table S4: Primers used in this study.

Author Contributions: Conceptualization, N.H. and A.S.; Investigation, N.H., A.H., and K.F.; Resources, D.L. and A.S.; Writing, Visualization and Supervision, A.S.; Funding Acquisition, D.L. and A.S.; All authors have read and agreed to the published version of the manuscript.

Funding: This research was funded by the German Science Foundation (DFG) grant number SCHN 560/4-1.

Acknowledgments: We thank Sabine Jarzombski for her excellent technical assistance, and Yvonne Hennecke and Karina Dadrich taking part in this project as graduate and undergraduate students. We also acknowledge the European Stock Center NASC and the Salk Institute for seed distribution, and Paul Hardy for critical reading of the manuscript.

Conflicts of Interest: The authors declare no conflict of interest.

References

1. Milner, M.J.; Seamon, J.; Craft, E.; Kochian, L.V. Transport properties of members of the ZIP family in plants and their role in Zn and Mn homeostasis. *J. Exp. Bot.* **2013**, *64*, 369–381. [CrossRef]
2. Socha, A.L.; Guerinot, M.L. Mn-euvering manganese: The role of transporter gene family members in manganese uptake and mobilization in plants. *Front. Plant Sci.* **2014**, *5*, 106. [CrossRef] [PubMed]
3. Pittman, J.K. Managing the manganese: Molecular mechanisms of manganese transport and homeostasis. *New Phytol.* **2005**, *167*, 733–742. [CrossRef] [PubMed]
4. Umena, Y.; Kawakami, K.; Shen, J.R.; Kamiya, N. Crystal structure of oxygen-evolving photosystem II at a resolution of 1.9 Å. *Nature* **2011**, *473*, 55–60. [CrossRef] [PubMed]
5. Shen, J.R. The Structure of Photosystem II and the Mechanism of Water Oxidation in Photosynthesis. *Annu. Rev. Plant Biol.* **2015**, *66*, 23–48. [CrossRef] [PubMed]
6. Wei, X.; Su, X.; Cao, P.; Liu, X.; Chang, W.; Li, M.; Zhang, X.; Liu, Z. Structure of spinach photosystem II-LHCII supercomplex at 3.2 Å resolution. *Nature* **2016**, *534*, 69–74. [CrossRef]
7. Su, X.; Ma, J.; Wei, X.; Cao, P.; Zhu, D.; Chang, W.; Liu, Z.; Zhang, X.; Li, M. Structure and assembly mechanism of plant C2S2M2-type PSII-LHCII supercomplex. *Science* **2017**, *357*, 815–820. [CrossRef]
8. Eisenhut, M.; Hoecker, N.; Schmidt, S.B.; Basgaran, R.M.; Flachbart, S.; Jahns, P.; Eser, T.; Geimer, S.; Husted, S.; Weber, A.P.M.; et al. The Plastid Envelope CHLOROPLAST MANGANESE TRANSPORTER1 Is Essential for Manganese Homeostasis in Arabidopsis. *Mol. Plant* **2018**, *11*, 955–969. [CrossRef]

9. Zhang, B.; Zhang, C.; Liu, C.; Jing, Y.; Wang, Y.; Jin, L.; Yang, L.; Fu, A.; Shi, J.; Zhao, F.; et al. Inner Envelope CHLOROPLAST MANGANESE TRANSPORTER 1 Supports Manganese Homeostasis and Phototrophic Growth in Arabidopsis. *Mol. Plant* **2018**, *11*, 943–954. [\[CrossRef\]](#)
10. Schneider, A.; Steinberger, I.; Herdean, A.; Gandini, C.; Eisenhut, M.; Kurz, S.; Morper, A.; Hoecker, N.; Ruhle, T.; Labs, M.; et al. The Evolutionarily Conserved Protein PHOTOSYNTHESIS AFFECTED MUTANT71 Is Required for Efficient Manganese Uptake at the Thylakoid Membrane in Arabidopsis. *Plant Cell* **2016**, *28*, 892–910. [\[CrossRef\]](#)
11. Brandenburg, F.; Schoffman, H.; Kurz, S.; Kramer, U.; Keren, N.; Weber, A.P.; Eisenhut, M. The Synechocystis Manganese Exporter Mnx Is Essential for Manganese Homeostasis in Cyanobacteria. *Plant. Physiol.* **2017**, *173*, 1798–1810. [\[CrossRef\]](#) [\[PubMed\]](#)
12. Gandini, C.; Schmidt, S.B.; Husted, S.; Schneider, A.; Leister, D. The transporter SynPAM71 is located in the plasma membrane and thylakoids, and mediates manganese tolerance in Synechocystis PCC6803. *New Phytol.* **2017**, *215*, 256–268. [\[CrossRef\]](#) [\[PubMed\]](#)
13. Lanquar, V.; Ramos, M.S.; Lelievre, F.; Barbier-Brygoo, H.; Krieger-Liszkay, A.; Kramer, U.; Thomine, S. Export of vacuolar manganese by AtNRAMP3 and AtNRAMP4 is required for optimal photosynthesis and growth under manganese deficiency. *Plant. Physiol.* **2010**, *152*, 1986–1999. [\[CrossRef\]](#) [\[PubMed\]](#)
14. Eroglu, S.; Meier, B.; von Wiren, N.; Peiter, E. The Vacuolar Manganese Transporter MTP8 Determines Tolerance to Iron Deficiency-Induced Chlorosis in Arabidopsis. *Plant. Physiol.* **2016**, *170*, 1030–1045. [\[CrossRef\]](#) [\[PubMed\]](#)
15. Eroglu, S.; Giehl, R.F.H.; Meier, B.; Takahashi, M.; Terada, Y.; Ignatyev, K.; Andresen, E.; Kupper, H.; Peiter, E.; von Wiren, N. Metal Tolerance Protein 8 Mediates Manganese Homeostasis and Iron Reallocation during Seed Development and Germination. *Plant. Physiol.* **2017**, *174*, 1633–1647. [\[CrossRef\]](#)
16. Peiter, E.; Montanini, B.; Gobert, A.; Pedas, P.; Husted, S.; Maathuis, F.J.; Blaudez, D.; Chalot, M.; Sanders, D. A secretory pathway-localized cation diffusion facilitator confers plant manganese tolerance. *Proc. Natl. Acad. Sci. USA* **2007**, *104*, 8532–8537. [\[CrossRef\]](#)
17. Delhaize, E.; Gruber, B.D.; Pittman, J.K.; White, R.G.; Leung, H.; Miao, Y.; Jiang, L.; Ryan, P.R.; Richardson, A.E. A role for the AtMTP11 gene of Arabidopsis in manganese transport and tolerance. *Plant J.* **2007**, *51*, 198–210. [\[CrossRef\]](#)
18. Wu, Z.; Liang, F.; Hong, B.; Young, J.C.; Sussman, M.R.; Harper, J.F.; Sze, H. An endoplasmic reticulum-bound $\text{Ca}^{2+}/\text{Mn}^{2+}$ pump, ECA1, supports plant growth and confers tolerance to Mn^{2+} stress. *Plant. Physiol.* **2002**, *130*, 128–137. [\[CrossRef\]](#)
19. Mills, R.F.; Doherty, M.L.; Lopez-Marques, R.L.; Weimar, T.; Dupree, P.; Palmgren, M.G.; Pittman, J.K.; Williams, L.E. ECA3, a Golgi-localized P2A-type ATPase, plays a crucial role in manganese nutrition in Arabidopsis. *Plant. Physiol.* **2008**, *146*, 116–128. [\[CrossRef\]](#)
20. Li, X.; Chanroj, S.; Wu, Z.; Romanowsky, S.M.; Harper, J.F.; Sze, H. A distinct endosomal $\text{Ca}^{2+}/\text{Mn}^{2+}$ pump affects root growth through the secretory process. *Plant. Physiol.* **2008**, *147*, 1675–1689. [\[CrossRef\]](#)
21. Alejandro, S.; Cailliatte, R.; Alcon, C.; Dirick, L.; Domergue, F.; Correia, D.; Castaings, L.; Briat, J.F.; Mari, S.; Curie, C. Intracellular Distribution of Manganese by the Trans-Golgi Network Transporter NRAMP2 Is Critical for Photosynthesis and Cellular Redox Homeostasis. *Plant Cell* **2017**, *29*, 3068–3084. [\[CrossRef\]](#) [\[PubMed\]](#)
22. Gao, H.; Xie, W.; Yang, C.; Xu, J.; Li, J.; Wang, H.; Chen, X.; Huang, C.F. NRAMP2, a trans-Golgi network-localized manganese transporter, is required for Arabidopsis root growth under manganese deficiency. *New Phytol.* **2018**, *217*, 179–193. [\[CrossRef\]](#) [\[PubMed\]](#)
23. Hoecker, N.; Leister, D.; Schneider, A. Plants contain small families of UPF0016 proteins including the PHOTOSYNTHESIS AFFECTED MUTANT71 transporter. *Plant Signal. Behav.* **2017**, *12*, e1278101. [\[CrossRef\]](#) [\[PubMed\]](#)
24. Available online: <http://www.tcdb.org/> (accessed on 12 February 2020).
25. Demaegd, D.; Colinet, A.S.; Deschamps, A.; Morsomme, P. Molecular evolution of a novel family of putative calcium transporters. *PLoS ONE* **2014**, *9*, e100851. [\[CrossRef\]](#)

26. Nelson, B.K.; Cai, X.; Nebenfuhr, A. A multicolored set of in vivo organelle markers for co-localization studies in Arabidopsis and other plants. *Plant J.* **2007**, *51*, 1126–1136. [\[CrossRef\]](#)
27. Boutte, Y.; Frescatada-Rosa, M.; Men, S.; Chow, C.M.; Ebine, K.; Gustavsson, A.; Johansson, L.; Ueda, T.; Moore, I.; Jurgens, G.; et al. Endocytosis restricts Arabidopsis KNOLLE syntaxin to the cell division plane during late cytokinesis. *EMBO J.* **2010**, *29*, 546–558. [\[CrossRef\]](#)
28. Matheson, L.A.; Suri, S.S.; Hanton, S.L.; Chatre, L.; Brandizzi, F. Correct targeting of plant ARF GTPases relies on distinct protein domains. *Traffic* **2008**, *9*, 103–120. [\[CrossRef\]](#)
29. Available online: <http://bbc.botany.utoronto.ca> (accessed on 12 February 2020).
30. Leskova, A.; Giehl, R.F.H.; Hartmann, A.; Fargasova, A.; von Wiren, N. Heavy Metals Induce Iron Deficiency Responses at Different Hierarchic and Regulatory Levels. *Plant. Physiol.* **2017**, *174*, 1648–1668. [\[CrossRef\]](#)
31. Gruber, B.D.; Giehl, R.F.; Friedel, S.; von Wiren, N. Plasticity of the Arabidopsis root system under nutrient deficiencies. *Plant. Physiol.* **2013**, *163*, 161–179. [\[CrossRef\]](#)
32. Demaegd, D.; Foulquier, F.; Colinet, A.S.; Gremillon, L.; Legrand, D.; Mariot, P.; Peiter, E.; Van Schaftingen, E.; Matthijs, G.; Morsomme, P. Newly characterized Golgi-localized family of proteins is involved in calcium and pH homeostasis in yeast and human cells. *Proc. Natl. Acad. Sci. USA* **2013**, *110*, 6859–6864. [\[CrossRef\]](#)
33. Potelle, S.; Morelle, W.; Dulary, E.; Duvet, S.; Vicogne, D.; Spriet, C.; Krzewinski-Recchi, M.A.; Morsomme, P.; Jaeken, J.; Matthijs, G.; et al. Glycosylation abnormalities in Gdt1p/TMEM165 deficient cells result from a defect in Golgi manganese homeostasis. *Hum. Mol. Genet.* **2016**, *25*, 1489–1500. [\[CrossRef\]](#) [\[PubMed\]](#)
34. Foulquier, F.; Amyere, M.; Jaeken, J.; Zeevaert, R.; Schollen, E.; Race, V.; Bammens, R.; Morelle, W.; Rosnoble, C.; Legrand, D.; et al. TMEM165 deficiency causes a congenital disorder of glycosylation. *Am. J. Hum. Genet.* **2012**, *91*, 15–26. [\[CrossRef\]](#) [\[PubMed\]](#)
35. Driouich, A.; Follet-Gueye, M.L.; Bernard, S.; Kousar, S.; Chevalier, L.; Vire-Gibouin, M.; Lerouxel, O. Golgi-mediated synthesis and secretion of matrix polysaccharides of the primary cell wall of higher plants. *Front. Plant Sci.* **2012**, *3*, 79. [\[CrossRef\]](#) [\[PubMed\]](#)
36. Hansen, S.F.; Harholt, J.; Oikawa, A.; Scheller, H.V. Plant Glycosyltransferases Beyond CAZy: A Perspective on DUF Families. *Front. Plant Sci.* **2012**, *3*, 59. [\[CrossRef\]](#)
37. Nunan, K.J.; Scheller, H.V. Solubilization of an arabinan arabinosyltransferase activity from mung bean hypocotyls. *Plant. Physiol.* **2003**, *132*, 331–342. [\[CrossRef\]](#)
38. Strasser, R. Plant protein glycosylation. *Glycobiology* **2016**, *26*, 926–939. [\[CrossRef\]](#)
39. Amos, R.A.; Mohnen, D. Critical Review of Plant Cell Wall Matrix Polysaccharide Glycosyltransferase Activities Verified by Heterologous Protein Expression. *Front. Plant Sci.* **2019**, *10*, 915. [\[CrossRef\]](#)
40. Saito, F.; Suyama, A.; Oka, T.; Yoko, O.T.; Matsuoka, K.; Jigami, Y.; Shimma, Y.I. Identification of Novel Peptidyl Serine alpha-Galactosyltransferase Gene Family in Plants. *J. Biol. Chem.* **2014**, *289*, 20405–20420. [\[CrossRef\]](#)
41. Karimi, M.; Inze, D.; Depicker, A. GATEWAY vectors for Agrobacterium-mediated plant transformation. *Trends Plant Sci.* **2002**, *7*, 193–195. [\[CrossRef\]](#)
42. Clough, S.J.; Bent, A.F. Floral dip: A simplified method for Agrobacterium-mediated transformation of Arabidopsis thaliana. *Plant J.* **1998**, *16*, 735–743. [\[CrossRef\]](#)
43. Schweiger, R.; Schwenkert, S. Protein-protein interactions visualized by bimolecular fluorescence complementation in tobacco protoplasts and leaves. *J. Vis. Exp.* **2014**, *85*, e51327. [\[CrossRef\]](#) [\[PubMed\]](#)
44. Schweiger, R.; Muller, N.C.; Schmitt, M.J.; Soll, J.; Schwenkert, S. AtTPR7 is a chaperone-docking protein of the Sec translocon in Arabidopsis. *J. Cell Sci.* **2012**, *125 Pt 21*, 5196–5207. [\[CrossRef\]](#)
45. Ruge, H.; Flösdorff, S.; Ebersberger, I.; Chigri, F.; Voithknecht, U.C. The calmodulin-like proteins AtCML4 and AtCML5 are single-pass membrane proteins targeted to the endomembrane system by an N-terminal signal anchor sequence. *J. Exp. Bot.* **2016**, *67*, 3985–3996. [\[CrossRef\]](#)
46. Schmittgen, T.D.; Livak, K.J. Analyzing real-time PCR data by the comparative C(T) method. *Nat. Protoc.* **2008**, *3*, 1101–1108. [\[CrossRef\]](#) [\[PubMed\]](#)
47. Available online: <https://www.ebi.ac.uk/Tools/msa/clustalo/> (accessed on 12 February 2020).
48. Available online: <http://www.cbs.dtu.dk/services/TargetP> (accessed on 12 February 2020).
49. Schwacke, R.; Schneider, A.; van der Graaff, E.; Fischer, K.; Catoni, E.; Desimone, M.; Frommer, W.B.; Flugge, U.I.; Kunze, R. ARAMEMNON, a novel database for Arabidopsis integral membrane proteins. *Plant. Physiol.* **2003**, *131*, 16–26. [\[CrossRef\]](#) [\[PubMed\]](#)

50. Available online: <http://aramemnon.uni-koeln.de/> (accessed on 12 February 2020).
51. Available online: <https://www.ncbi.nlm.nih.gov/> (accessed on 12 February 2020).
52. Available online: https://astatsa.com/OneWay_Anova_with_TukeyHSD/ (accessed on 12 February 2020).



© 2020 by the authors. Licensee MDPI, Basel, Switzerland. This article is an open access article distributed under the terms and conditions of the Creative Commons Attribution (CC BY) license (<http://creativecommons.org/licenses/by/4.0/>).

7.3 Publication III: Gene Replacement in Arabidopsis Reveals Manganese Transport as an Ancient Feature of Human, Plant and Cyanobacterial UPF0016 Proteins

Natalie Hoecker, Yvonne Hennecke, Simon Schrott, Giada Marino, Sidsel Birkelund Schmidt, Dario Leister and Anja Schneider

Front Plant Sci, 2021 Jun 14;12:697848.

Supplementary data available under:

<https://www.frontiersin.org/articles/10.3389/fpls.2021.697848/full>



Gene Replacement in *Arabidopsis* Reveals Manganese Transport as an Ancient Feature of Human, Plant and Cyanobacterial UPF0016 Proteins

Natalie Hoecker¹, Yvonne Hennecke¹, Simon Schrott¹, Giada Marino^{1,2}, Sidsel Birkelund Schmidt³, Dario Leister¹ and Anja Schneider^{1*}

¹ Molekularbiologie der Pflanzen (Botanik), Fakultät für Biologie, Ludwig-Maximilians-Universität München, Martinsried, Germany, ² Massenspektrometrie von Biomolekülen an der LMU (MSBioLMU), Fakultät für Biologie, Ludwig-Maximilians-Universität München, Martinsried, Germany, ³ Department of Plant and Environmental Sciences, Faculty of Science, University of Copenhagen, Frederiksberg, Denmark

OPEN ACCESS

Edited by:

Alistair McCormick,
University of Edinburgh,
United Kingdom

Reviewed by:

Pierre Morsomme,
UCLouvain, Belgium
Greg B. Moorhead,
University of Calgary, Canada

*Correspondence:

Anja Schneider
anja.schneider@lrz.uni-muenchen.de

Specialty section:

This article was submitted to
Plant Physiology,
a section of the journal
Frontiers in Plant Science

Received: 20 April 2021

Accepted: 20 May 2021

Published: 14 June 2021

Citation:

Hoecker N, Hennecke Y,
Schrott S, Marino G, Schmidt SB,
Leister D and Schneider A (2021)
Gene Replacement in *Arabidopsis*
Reveals Manganese Transport as an
Ancient Feature of Human, Plant
and Cyanobacterial UPF0016
Proteins. *Front. Plant Sci.* 12:697848.
doi: 10.3389/fpls.2021.697848

The protein family 0016 (UPF0016) is conserved through evolution, and the few members characterized share a function in Mn^{2+} transport. So far, little is known about the history of these proteins in Eukaryotes. In *Arabidopsis thaliana* five such proteins, comprising four different subcellular localizations including chloroplasts, have been described, whereas non-photosynthetic Eukaryotes have only one. We used a phylogenetic approach to classify the eukaryotic proteins into two subgroups and performed gene-replacement studies to investigate UPF0016 genes of various origins. Replaceability can be scored readily in the *Arabidopsis* UPF0016 transporter mutant *pam71*, which exhibits a functional deficiency in photosystem II. The N-terminal region of the *Arabidopsis* PAM71 was used to direct selected proteins to chloroplast membranes. Transgenic *pam71* lines overexpressing the closest plant homolog (CMT1), human TMEM165 or cyanobacterial MNX successfully restored photosystem II efficiency, manganese binding to photosystem II complexes and consequently plant growth rate and biomass production. Thus AtCMT1, HsTMEM165, and SynMNX can operate in the thylakoid membrane and substitute for PAM71 in a non-native environment, indicating that the manganese transport function of UPF0016 proteins is an ancient feature of the family. We propose that the two chloroplast-localized UPF0016 proteins, CMT1 and PAM71, in plants originated from the cyanobacterial endosymbiont that gave rise to the organelle.

Keywords: PAM71, manganese transporter, *Arabidopsis*, UPF0016 evolution, endosymbiosis, gene replacement, *Synechocystis*

INTRODUCTION

Cross-species replacement of genes in model organisms is a powerful tool with which to investigate whether the corresponding proteins retain their ancestral functions over a billion years of evolution. There are several examples in which human genes have been shown to supply the functions of their orthologous counterparts in plants (Jha et al., 2018; Huber et al., 2020), and plant genes can

frequently be replaced by the cyanobacterial ortholog or vice versa (Savidge et al., 2002; Sattler et al., 2003; Lv et al., 2009; Armbruster et al., 2013; Proctor et al., 2018; Yoon et al., 2019). These examples of pairwise replacements can be expanded further with multiple replacement assays to gain insight into the history and evolution of gene families. Gene duplication and subsequent divergence is a major driver of evolution, and each gene/protein family has its own evolutionary history.

The uncharacterized protein family 0016 (UPF0016), also referred to as the Gcr1-dependent translation factor1 (GDT1) family (Thines et al., 2020), is a highly conserved membrane transporter family with members in many lineages of the tree of life (Demaegd et al., 2014). One prominent member, which is responsible for the alternative family name just mentioned, is the Golgi-localized Gdt1p, originally identified as a $\text{Ca}^{2+}/\text{H}^{+}$ antiporter in *Saccharomyces cerevisiae* (Demaegd et al., 2013; Colinet et al., 2016). A second, the human transmembrane protein 165 (TMEM165), attracted much interest when its involvement in the rare condition known as congenital disorders of glycosylation (CDG) was demonstrated in 2012 (Foulquier et al., 2012; Rosnoblet et al., 2013; Zeevaert et al., 2013; Bammens et al., 2015; Potelle et al., 2016; Schulte Althoff et al., 2016; Krzewinski-Recchi et al., 2017; Morelle et al., 2017). Several studies have hypothesized that TMEM165 is a Golgi-localized Mn^{2+} and/or Ca^{2+} transporter (Demaegd et al., 2013; Potelle et al., 2016; Stribny et al., 2020).

In the model plant *Arabidopsis thaliana*, the chloroplast manganese transporter1 (CMT1) and photosynthesis-affected mutant71 (PAM71) proteins were found to transport Mn^{2+} across the chloroplast envelope and the thylakoid membrane, respectively (Schneider et al., 2016; Eisenhut et al., 2018; Zhang et al., 2018). Two additional members of the family are located in the endoplasmic reticulum (ER) compartment (Hoecker et al., 2020) and a third, pam71-like3 (PML3), found in the Golgi membrane, facilitates Mn^{2+} import under conditions of Mn deficiency (Yang et al., 2021).

It has been shown that, in bacteria, members of UPF0016 are located in the plasma membrane, where their main function is the export of excess Mn^{2+} to prevent Mn toxicity. One prominent example is the manganese exporter A (MneA), a UPF0016 protein found in *Vibrio cholerae* (Fisher et al., 2016; Zeinert et al., 2018). Cyanobacteria, such as *Synechocystis*, possess additional internal membranes, at which photosynthesis takes place. Here, the manganese exporter (MNX) protein presumably needs to be targeted to both the thylakoid and the plasma membrane in order to perform its physiological function and prevent accumulation of toxic levels of Mn^{2+} in the cytosol (Brandenburg et al., 2017; Gandini et al., 2017; Eisenhut, 2019).

Eukaryotic proteins of the UPF0016 family share a conserved overall structure, comprising two regions consisting of three transmembrane (TM) domains each, which are connected by an acidic loop, and contain a highly conserved Glu-x-Gly-Asp-(Arg/Lys)-(Ser/Thr) motif in TM1 and TM4, respectively (Demaegd et al., 2014; Hoecker et al., 2017; Thines et al., 2020). This type—with six TM domains—is also found in many prokaryotes, while some others harbor one or two genes coding for a version that consists of only three TM domains,

which are assumed to form homo- or heterodimers (Demaegd et al., 2014). Besides the high degree of conservation, eukaryotic representatives of the UPF0016 family exhibit additional features, among them high sequence diversity within their N-terminal segments (Hoecker et al., 2017). While the ER-localized proteins lack an N-terminal extension, ScGdt1p, HsTMEM165 and AtPML3 all have an N-terminal signal peptide that directs them to the Golgi membrane (Foulquier et al., 2012; Demaegd et al., 2013; Hoecker et al., 2020; Yang et al., 2021). The chloroplast-targeting peptide (cTP) sequences of Arabidopsis PAM71 and CMT1 direct these proteins to the thylakoid and inner-envelope membranes, respectively (Schneider et al., 2016; Eisenhut et al., 2018; Zhang et al., 2018).

In this study, we set out to define the ancestor(s) of eukaryotic members of the UPF0016 family and determine whether individual members have retained the ancestral function. We performed a phylogenetic analysis to identify appropriate candidates. We selected MNX of *Synechocystis* (Brandenburg et al., 2017; Gandini et al., 2017), human TMEM165 and Arabidopsis CMT1 (Eisenhut et al., 2018; Zhang et al., 2018) and directed the proteins to the thylakoid membrane of the Arabidopsis *pam71* knock-out line. Appropriate control constructs were generated and transgenic *pam71* plants were analyzed for complementation of growth deficiencies as a measure of the degree to which these transporters have retained the ancestral mode of action.

MATERIALS AND METHODS

Phylogenetic Analysis

Protein sequences were retrieved by protein Blast searches at NCBI¹ using *Arabidopsis thaliana* PAM71 or *Vibrio cholerae* MneA as query sequences. Target organisms either represent ten eukaryotic model species or were manually selected from a list of 393 prokaryotes (Hanikenne and Baurain, 2013). Evolutionary analyses were conducted in MEGA X (Kumar et al., 2018) using the maximum-likelihood method and the Le_Gascuel_2008 model (Le and Gascuel, 2008). Initial tree(s) were obtained automatically by first applying Neighbor-Join and BioNJ algorithms to a matrix of pairwise distances estimated using a JTT model, and then selecting the topology with the superior log likelihood value. A discrete Gamma distribution was used to model evolutionary rate differences among sites (+G). Estimates of evolutionary divergence between sequences were obtained by using a pairwise distance calculation that assumes uniform rates among sites. All positions with less than 95% site coverage were eliminated; i.e., fewer than 5% alignment gaps, missing data, and ambiguous bases were allowed at any position (partial deletion option).

Generation of Arabidopsis Lines

The mutants *pam71* or *cmt1* were stably transformed by the floral-dip method (Clough and Bent, 1998) using Silwet L-77 (Lehle Seeds, Round Rock, TX, United States) as the detergent.

¹<https://blast.ncbi.nlm.nih.gov/Blast.cgi>

Both mutations are in the Colombia-0 background. The first step employed primer pairs 1/2 or 16/17 (see **Supplementary Table 1**), and first-strand cDNA of *Arabidopsis* for cloning of the cTP sequences into the pENTR vector (Thermo-Fisher Scientific/Invitrogen, Waltham, MA, United States), yielding pENTR-cTP_(PAM71) and pENTR-cTP_(CMT1). The Phusion High-Fidelity DNA polymerase (New England Biolabs, Frankfurt, Germany) was used for this and all subsequent steps, and all further primer sequences are listed in **Supplementary Table 1**. The plasmids pENTRcTP_(PAM71) and pENTR-PAM71 were used as templates for the amplification of two PCR products using primers 1/2 and primers 3/4, respectively. The two PCR products were then digested with *XhoI* (New England Biolabs), ligated with T4 DNA ligase (New England Biolabs), and a second PCR was performed using primers 1/4. The resulting PCR product was cloned into pENTR, yielding the plasmid pENTR-cTP_(PAM71):PAM71_{core}. The plasmid pENTR-cTP_(PAM71):CMT1_{core} was assembled in an analogous manner, using primers 1/2 with pENTRcTP_(PAM71) and primers 6/7 with pENTR-CMT1 as templates for the first PCR, and primers 1/7 for the second PCR. The plasmid pENTR-cTP_(PAM71):TMEM165 was assembled in the same way, using primers 1/2 with pENTRcTP_(PAM71) and primers 8/9 with pDNR-LIP-TMEM165 (transOMIC technologies, Huntsville, AL, United States) as templates for the first PCR and primers 1/9 for the second PCR. Plasmid pENTR-PAM71_{core} was created using primers 5/4 and pENTR-PAM71 as a template. Plasmids pENTR-cTP_(CMT1):CMT1_{core} and pENTR-cTP_(CMT1):PAM71 were constructed accordingly. All plasmids were sequenced and recombined into the destination vector pB2GW7 (Karimi et al., 2002) using the LR Clonase Gateway system (Thermo-Fisher Scientific/Invitrogen). Plasmid pB2GW7p35S:cTP_{extended(PAM71)}:MNX was assembled using three PCR products and the Gibson assembly cloning kit (New England Biolabs). The three PCR products were obtained with primer pairs 10/11, 12/13, and 14/15, and pENTR-PAM71, *Synechocystis* sp. PCC6803 genomic DNA (Gandini et al., 2017) and pB2GW7, respectively, as templates. The final construct was then sequenced. All plasmids harboring the pB2GW7 backbone were transformed into *Agrobacterium* and plated on media containing Rif/Gent/Spec. Individual colonies were selected, verified and used to transform *Arabidopsis*. Transgenic T₁ plants were selected by spraying seedlings twice with BASTA at a final concentration of 100 mg L⁻¹ glufosinate-ammonium. T₂ plants were assayed for segregation by genotyping, and appropriate homozygous T₃ seed stocks were generated.

Growth Conditions

Arabidopsis seeds were stratified for 3 days at 4°C to synchronize germination, and plants were grown for 4–5 weeks in growth chambers on a 12–12 h light-dark cycle at 18–22°C and 100 μmol photons m⁻² s⁻¹ during the light period. The *Arabidopsis* plants used for transformation and seed production, and *Nicotiana benthamiana* plants were grown in a temperature-controlled greenhouse with additional lighting for up to 16 h to reach a fluence of at least 140 μmol photons m⁻² s⁻¹.

Plant growth was analyzed on the basis of leaf area, which was determined from photographs taken at different times after germination and quantified using the ImageJ software (Schneider et al., 2012).

Transient Expression

The plasmids pENTR-cTP_(PAM71) and pENTR-cTP_(CMT1) were recombined into the destination vector pB7FWG2 (Karimi et al., 2002), resulting in pB7FWG2p35S:cTP_(PAM71):GFP and pB7FWG2p35S:cTP_(CMT1):GFP, respectively, which were then transformed into *Agrobacterium*. *Agrobacterium*-mediated infiltration of 4-week-old *N. benthamiana* leaves and protoplast isolation were performed as described (Schweiger and Schwenkert, 2014). In brief, 48 h after infiltration, protoplasts were released from leaf tissue by incubation in the dark for 4 h, with mild shaking at 40 rpm, in an enzyme solution (osmolarity: 550 mOsm) containing 1% (w/v) cellulase (Duchefa Biochemie, Haarlem, Netherlands) and 0.3% (w/v) macerozyme (Duchefa Biochemie). The protoplasts were then filtered through a 100 μm gauze filter and washed with W5 buffer [150 mM NaCl, 125 mM CaCl₂, 5 mM KCl, 2 mM MES (pH 5.7), 550–580 mOsm], then centrifuged at 100 g for 1 min and resuspended in W5 buffer. The fluorescence signals were recorded with a confocal laser-scanning microscope (Leica microsystems TCS SP5, Leica Microsystems, Wetzlar, Germany) with a 63x objective. The argon laser was set to 30%, GFP fluorescence was excited at 488 nm and the emission was recorded with a PMT detector at 515 nm. Chlorophyll autofluorescence was detected at 650–705 nm with a second PMT detector. The gain settings for both PMT detectors were chosen within the interval 760–900 to reduce background noise. Z-stacking images were generated with a maximum of 0.5 μm distance between each layer.

Chlorophyll *a* Fluorescence Measurements

The photosynthetic performance of PSII was quantified by measuring chlorophyll *a* fluorescence using a Dual PAM fluorometer (Walz, Effeltrich, Germany). Plants were dark-adapted for 30 min and single leaves were exposed to probe light (3–4 μmol photons m⁻² s⁻¹) for 30 s to measure minimal chlorophyll *a* fluorescence (F₀). A light pulse of 10,000 μmol photons m⁻² s⁻¹ was then applied for 800 ms to determine the maximum chlorophyll *a* fluorescence (F_m). Quantitative information was obtained by calculating the maximum quantum yield of PSII as F_v/F_m = (F_m - F₀)/F_m (Maxwell and Johnson, 2000). *In vivo* chlorophyll *a* fluorescence was captured as a photograph by the Imaging PAM fluorometer (Walz, Effeltrich, Germany). Plants were dark-adapted for 30 min and whole plants exposed to blue probe light (3–4 μmol photons m⁻² s⁻¹) for 30 s, followed by a light pulse of 2,800 μmol photons m⁻² s⁻¹ for 800 ms.

Real-Time PCR Analysis

Total RNA was isolated from *Arabidopsis* leaves using the Monarch Total RNA Miniprep Kit including the on-column DNase digest, and cDNA was synthesized according to the

instructions supplied with the iScript cDNA Synthesis Kit (Bio-Rad, Hercules, CA, United States). For quantitative real-time (qRT) PCR, SYBR Green Supermix (Bio-Rad) was used and PCR was performed with the CFX light cycler (Bio-Rad). Selected regions of the *cTP_(PAM71)* sequence (primers 30/31) or the *PAM71_(core)* sequence (primers 32/33) were used to record expression of the target gene and the reference gene *Actin* (primers 28/29). Relative transcript levels were quantified according to the comparative cycle threshold (C_T) method (Schmittgen and Livak, 2008): $\Delta C_T = C_T(\text{Gene}_{\text{TransgenicLine}}) - C_T(\text{Actin}_{\text{TransgenicLine}})$ or $\Delta C_T = C_T(\text{Gene}_{\text{Col-0}}) - C_T(\text{Actin}_{\text{Col-0}})$; $\Delta \Delta C_T(\text{TransgenicLine}) = \Delta C_T(\text{Gene}_{\text{TransgenicLine}}) - \Delta C_T(\text{Gene}_{\text{Col-0}})$ and $2^{-\Delta \Delta C_T}$ calculated. Expression in Col-0 is: $\Delta \Delta C_T(\text{Col-0}) = \Delta C_T(\text{Gene}_{\text{Col-0}}) - \Delta C_T(\text{Gene}_{\text{Col-0}}) = 0$ and $2^0 = 1$.

Blue-Native PAGE and SEC-ICP-MS Analysis

For the isolation of thylakoid membrane-protein complexes, leaf samples (5 g fresh weight) were homogenized in 0.4 M sucrose, 10 mM NaCl, 5 mM MgCl_2 , 20 mM Tricine (pH 7.9), 10 mM ascorbate and 10 mM NaF, then filtered through two layers of Miracloth (GE Healthcare, Chicago, IL, United States) and centrifuged at 5,000 g for 10 min at 4°C. The pellet was dissolved in 5 mM Tricine (pH 7.9) and 10 mM NaF, and centrifuged at 10,000 g for 10 min at 4°C. The resulting thylakoid membranes were dissolved in storage buffer [0.4 M sucrose, 10 mM NaCl, 5 mM MgCl_2 , 20 mM Tricine (pH 7.9), 20% (v/v) glycerol, 10 mM NaF] and the protein concentration was determined using the Pierce BCA Protein Assay (Thermo-Fisher Scientific/Invitrogen, Waltham, MA, United States). Samples were stored at −80°C. For Blue-Native PAGE analysis, samples equivalent to 18 µg protein were solubilized in the presence of 1% (w/v) β-dodecyl-maltoside (Sigma-Aldrich, St. Louis, MO, United States) for 10 min on ice in the dark. Native-PAGE sample buffer was then added and protein complexes were separated by non-denaturing Bis-Tris gel electrophoresis (3–12% acrylamide gradient, Thermo-Fisher Scientific/Invitrogen) for 3.5 h. For SEC-ICP-MS analysis, samples equivalent to 50 µg protein were solubilized in the presence of 1% (w/v) α-dodecyl-maltoside (Biomol, Hamburg, Germany) for 10 min on ice in the dark. Solubilized protein complexes were filtered through a 0.45-µm nylon membrane and applied to a size-exclusion column (BioBasic SEC1000, a silica-based high-pressure steel column; Thermo-Fisher Scientific/Invitrogen) using an inert HPLC system. Protein elution was performed with 25 mM Bis-Tris (pH 7.0) and 0.03% (w/v) α-dodecyl-maltoside as the mobile phase at a flow rate of 1 mL min^{−1}. The outlet of the column was coupled to a triple quadrupole ICP-MS (Agilent 8800 ICP-QQQ-MS, Agilent, Santa Clara, CA, United States) for online detection of Mn binding in the size-fractionated PSII complexes. The ICP-QQQ-MS was operated in MS/MS scan mode with oxygen as the reaction gas, which allowed for simultaneous detection of manganese as the parent ion (⁵⁵Mn⁺) and sulfur as the oxide product ion (⁴⁸SO⁺). The external calibration for quantification of the stoichiometric ratios of Mn to S in

photosynthetic complexes was carried out using flow-injection analysis (Schmidt et al., 2015).

Proteome Analysis

For the isolation of chloroplasts, leaf samples (12 g fresh weight) were homogenized in a mixture of 0.4 M sorbitol, 20 mM Tricine-NaOH (pH 8.4), 10 mM EDTA, 0.1% (w/v) BSA, 5 mM NaHCO_3 , 1 mM MgCl_2 and 1 mM MnCl_2 . The extract was filtered through two layers of Miracloth (GE Healthcare) and concentrated by centrifugation for 5 min at 1,500 g. The pellet was resuspended in 80 mM sorbitol, 4 mM Tricine-NaOH (pH 8.4), 0.5 mM EDTA, 1 mM MgCl_2 and then layered onto a discontinuous 40% (w/v)/80% (w/v) Percoll gradient (GE Healthcare). Intact chloroplasts were isolated from the interphase after centrifugation for 15 min at 7,000 g. To separate envelope and thylakoid membranes, the chloroplasts were lysed in 10 mM HEPES-KOH (pH 7.6) and 5 mM MgCl_2 by incubation on ice for 10 min, then layered onto a discontinuous sucrose gradient consisting of 1.2 M, 1.0 M, and 0.46 M sucrose, and centrifuged at 58,000 g for 2 h. The stroma in the top fraction was discarded, the envelopes were collected from the middle fraction, and the thylakoids were recovered as a pellet. The envelope fraction was further concentrated by centrifugation at 135,200 g for 1 h at 4°C. Both fractions were stored in TMK buffer [10 mM Tris-HCl pH 6.8, 10 mM MgCl_2 , 20 mM KCl including protease inhibitor cocktail (Roche, Basel, Switzerland)] at −80°C.

Thylakoid and envelope fractions were resuspended in 200-µl aliquots of guanidine-HCl, and incubated at 60°C for 30 min. Samples were then disrupted by applying two 10-s bursts of sonication using a Branson Sonifier B-12 (Branson Ultrasonics, Brookfield, CT, United States). After removing cell debris by centrifugation at 10,000 g for 15 min, samples were loaded onto a Microcon-30 kDa filter. On-column reduction, alkylation and tryptic digestion were performed as previously described (Janowski et al., 2018). After elution, the peptide mixtures were acidified to pH ≤ 3 using formic acid, desalted with home-made C18 stage tips (Rappsilber et al., 2003), vacuum dried to near dryness and stored at −80°C until further use.

LC-MS/MS was performed on an Ultimate 3000 RSLCnano HPLC system (Thermo-Fisher Scientific/Invitrogen), coupled online to an Impact II Ultra-High Resolution Qq-Time-Of-Flight (Bruker Daltonics, Billerica, MA, United States). The nano-LC system (Thermo-Fisher Scientific/Invitrogen) was operated in a two-column setup with an Acclaim Pepmap nano-trap column (C18, 100 Å, 100 µm × 2 cm) and an Acclaim Pepmap RSLC analytical column (C18, 100 Å, 75 µm × 50 cm). The columns were kept at 50°C throughout the run. The peptide mixtures were separated at a constant flow rate of 250 nl/min, using a linear gradient 3–30% solvent B (0.1% formic acid in acetonitrile) over 60 min, followed by a linear increase from 30 to 45% solvent B within 15 min. Full MS scans in the mass range 200–2,000 m/z were acquired at a rate of 3 Hz, and the 18 most intense peaks were selected for MS2 analysis using an intensity-dependent spectrum acquisition rate of between 4 and 16 Hz. To minimize repeated sequencing, the dynamic exclusion duration was set to 30 s.

The raw MS files were processed using the MaxQuant software (Cox and Mann, 2008). Peak lists were searched against the Arabidopsis reference proteome (Uniprot, version April 2019) using the built-in Andromeda search engine (Cox et al., 2011). The database was modified to include the sequences of the chimeric constructs. The search parameters were set as follows: Cysteine carbamidomethylation as fixed modification, methionine oxidation and acetylation of protein N-termini as variable modifications. The specific protease was set to trypsin (Thermo-Fisher Scientific/Invitrogen), allowing a maximum of two missed cleavage sites. The false-discovery rate at the protein and PSM level was set to 1%. The match-between-runs option was disabled, whereas the intensity-based-absolute-quantification (iBAQ) (Schwanhauser et al., 2011) option was enabled. Downstream data analysis was performed using Microsoft Excel. Potential contaminants, reverse hits and proteins identified only by site modification were removed. The protein group iBAQ values were then normalized to the sum of all iBAQ values within one sample, generating relative iBAQ (riBAQ) values. To compare the thylakoid and envelope fractions of single chloroplast preparations, the abundances of a given protein group were expressed as relative percentages of the total riBAQ values. Data were analyzed from three independent biological replicates.

Data and Code Availability

The mass spectrometry proteomics data have been deposited with the ProteomeXchange consortium <http://proteomecentral.proteomexchange.org> via the PRIDE partner repository (Vizcaino et al., 2016) under the accession number PXD022763.

RESULTS

Phylogenetic Analysis of UPF0016 Proteins

The family was first described in 2014 (Demaegd et al., 2014) and members have now been identified in more than 2,800 species across all three domains of life (**Supplementary Figure 1**). We were particularly interested in examining the ancestry of plant UPF0016 proteins, which are encoded by small gene families (Hoecker et al., 2017). In order to embed plant UPF0016 proteins in a broader context, proteins of prokaryotic and eukaryotic origins were retrieved and subjected to a phylogenetic analysis. A dataset of 33 proteins was selected from 33 prokaryotic organisms, which were chosen from a taxonomically representative set of phyla (Hanikenne and Baurain, 2013), taking into account phyla that appear to encompass many species that code for UPF0016 proteins (**Supplementary Figure 1**). This set was supplemented by 24 eukaryotic proteins obtained from 10 species, representing both photosynthetic and non-photosynthetic model organisms. Clear phylogenies could not be identified within prokaryotic phyla, except for those proteins of α -Proteobacteria that displayed a bootstrap value of 100%, indicating that these could be monophyletic (**Figure 1**). Intriguingly, cyanobacterial proteins were found to be closely

related to eukaryotic proteins (as indicated by a single branch supported by a bootstrap value of 100%) and were clearly separated from all other prokaryotic phyla. Closer inspection of the members of Viridiplantae confirmed the previous findings (Hoecker et al., 2017) that chloroplast-localized members and Golgi/ER-localized members form separate subgroups (**Figure 1**). The latter subgroup comprises members found in all Eukaryotes, including Metazoa and Fungi, and was named subgroup one. The chloroplast-localized proteins were named subgroup two. These proteins presumably arose separately, because they form a single defined monophyletic group. Next, we extracted the well characterized proteins of Arabidopsis, Synechocystis and human, and estimated the evolutionary divergence between these seven sequences by pairwise comparisons. In terms of their amino-acid sequences, PAM71 and AtPML4 are most dissimilar, while AtPML4 and AtPML5 display the highest similarity (**Figure 2**). HsTMEM165 shows less resemblance to SynMNX, AtPAM71, and AtCMT1 than to the three AtPML proteins, or in other words SynMNX, AtPAM71, and AtCMT1 form a cluster. Taken together, these observations allow us to conclude that the gene(s) encoding the chloroplast-localized proteins PAM71 and CMT1 are derived from the cyanobacterial endosymbiosis that gave rise to chloroplasts. Because the gene(s) encoding Golgi/ER-localized proteins have close counterparts in non-photosynthetic Eukaryotes, this clade must have arisen prior to the cyanobacterial endosymbiosis.

The Arabidopsis Mutant *pam71* as a Platform for UPF0016 Gene-Replacement Studies

To test the hypothesis that UPF0016 proteins share an ancient functionality, we chose the *pam71* Arabidopsis mutant for a gene-replacement study. We selected AtCMT1 and HsTMEM165 as representative members of each subgroup and SynMNX as the cyanobacterial representative. The nucleus-encoded PAM71 protein is equipped with a chloroplast-targeting signal peptide at the N-terminus, which is predicted to be cleaved at amino acid position 74 (Schneider et al., 2016; Hoecker et al., 2017) during uptake into the organelle from the cytoplasm. To verify that the cTP is sufficient to direct proteins of interest into this plant organelle, we cloned the first 255 bp of the PAM71 ORF upstream of the GFP sequence and transiently expressed the fusion protein in *Nicotiana benthamiana* leaves (**Figure 3A**). Indeed, the GFP fluorescence signal was found to coincide precisely with the red autofluorescence emitted by chlorophyll *a* molecules in isolated protoplasts. Next, a series of chimeric constructs was generated (**Figure 3B**), including a positive control containing the native PAM71 sequence and a negative control containing a truncated version of PAM71 lacking the first 255 bp at the 5' end. Furthermore, we linked the PAM71 cTP sequence to the full-length TMEM165 sequence and replaced the original cTP sequence of CMT1. An extended cTP sequence was used to generate the MNX construct, in order to increase the size of the protein (**Supplementary Figure 2**), as the naturally occurring MNX/SynPAM71 is smaller than any of the other three proteins (Thines et al., 2020). The

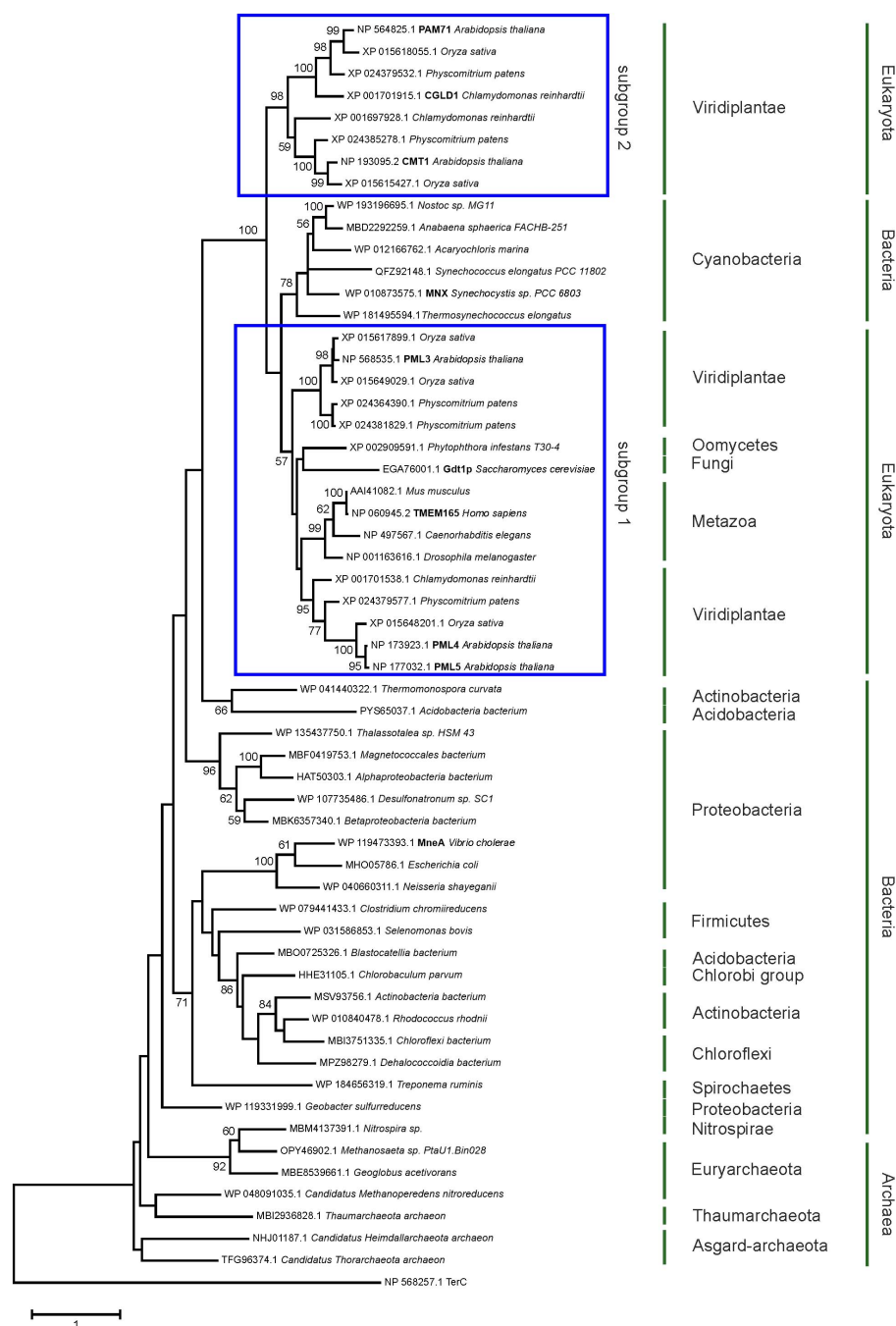


FIGURE 1 | Evolutionary analysis of UPF0016 members using the maximum-likelihood method. Protein sequences were retrieved by protein BLAST search using AtPAM71 as query sequence, except for those from *Alphaproteobacterium bacterium*, *Vibrio cholera*, *Escherichia coli*, *Neisseria shayegani*, and *Treponema ruminis*, which were identified using MneA of *Vibrio cholera* as query sequence. The tree with the highest log likelihood is shown. The percentage (>50%) of trees in which the taxa grouped together is also shown (bootstrap values based on 500 replicates). The tree is drawn to scale with branch lengths measured in numbers of substitutions per site. The tree is rooted on *Arabidopsis thaliana* TerC. The TerC and UPF0016 families form part of the LysE transporter superfamily (http://pfam.xfam.org/clan/CL0292). NCBI accession numbers are indicated and proteins mentioned throughout the text are highlighted.

five constructs were introduced into *Agrobacterium* cells and successfully transformed into the *pam71* background. The *pam71* mutant is characterized by a reduced growth rate and a lower maximum quantum yield of photosystem II (PSII) (Fv/Fm,

Figures 3C,D) (Schneider et al., 2016; Wang et al., 2016). Several independent transgenic lines per construct were selected based on their resistance to glufosinate, assayed for the presence of the transgene in the homozygous *pam71* background and

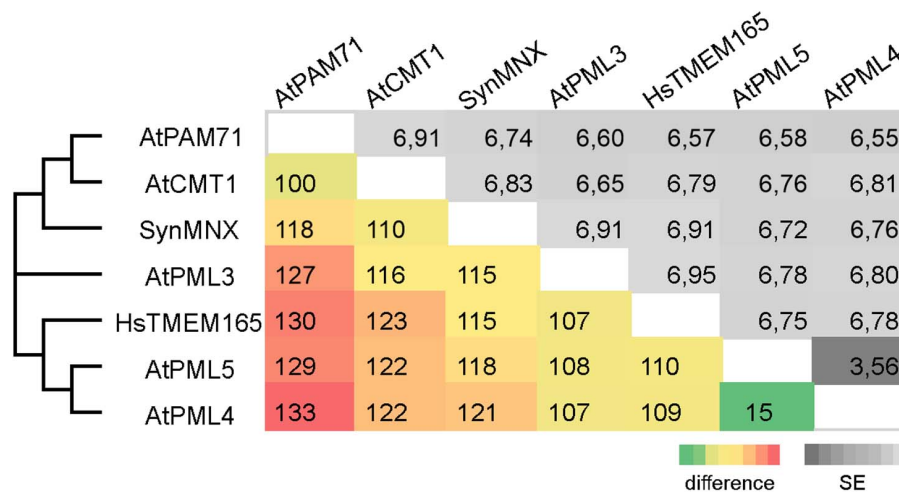


FIGURE 2 | Pairwise comparison of UPF0016 members of Arabidopsis, Synechocystis and human. The numbers of amino-acid differences between the indicated sequences are shown. Standard-error (SE) estimates are shown above the diagonal and were obtained by a bootstrap procedure (1,000 replicates). The consensus tree in which the associated proteins clustered together is indicated on the left.

characterized with respect to their Fv/Fm values. Transgenic lines were named as follows: *cP* refers to *cTP_{PAM71}* and *pos* and *neg* indicate presence or absence of *cTP_{PAM71}* respectively, followed by the protein name. Fv/Fm was significantly reduced in the twelve *cP_{neg}PAM71* lines relative to the twenty-five *cP_{pos}PAM71* control lines (Figure 3D), indicating that the presence of a cTP is required for functional complementation. Interestingly, the Fv/Fm values of the thirty-four selected *cP:CMT1* lines were comparable to those of the positive control lines (Figure 3D). However, it is worth noting that the endogenous proteins PAM71 and CMT1 have non-redundant functions in chloroplasts (Eisenhut et al., 2018; Zhang et al., 2018; Frank et al., 2019; Schmidt et al., 2020). Moreover, it was found that the thirty-four *cP:TMEM165* lines and the thirty-four selected *cP:MNX* lines have significantly increased Fv/Fm values in comparison to the negative control lines and *cP:TMEM165* lines are significantly improved in comparison to *pam71* (Figure 3D). Both groups (*cP:TMEM165* lines and *cP:MNX* lines) showed a wide range of Fv/Fm values, for instance from 0.4 to 0.8 in the *cP:MNX* lines, maybe due to very different levels of expression of the respective non-plant transgene across the populations. Taken together, these results suggested that the approach is feasible, and we proceeded to analyze individual lines in more detail.

In Transgenic Lines Both the Quantum Yield of Photosystem II and Growth Rate Are Enhanced

To select suitable lines for detailed investigations, two criteria were applied: T1 plants should exhibit an increased Fv/Fm value and harbor a single-locus transgene insertion, because this is less likely to cause (post)-transcriptional gene silencing in subsequent generations. We selected two lines that met these criteria from each group (Supplementary Figure 3). Single-locus insertion events were identified based on a segregation analysis

of T2 plants, assuming a 3:1 mode of dominant inheritance of the transgene (Supplementary Figure 3). Furthermore, we confirmed that the phenotypes of positive *cP_{pos}PAM71* and negative *cP_{neg}PAM71* control plants were close to wild-type and *pam71* plants, respectively (Supplementary Figure 4A). All selected transgenic lines were grown side by side, and on visual inspection just before the transition to the reproductive state, the rosette diameter was found to be larger in all cases than in either of the negative control lines (Figure 4A). Growth recovery to almost control levels was observed in the *cP:CMT1*, *cP:TMEM165*, and *cP:MNX* lines (Figure 4B). Furthermore, Fv/Fm values in both *cP_{pos}PAM71* lines reached almost 0.8, indicative of optimal PSII efficiency and photosynthesis, while both *cP_{neg}PAM71* lines had Fv/Fm values around 0.6 (Figure 4C). These results are similar to those of wild-type and *pam71* plants respectively (Supplementary Figure 4B). Optimal PSII efficiency was also observed in the two *cP:CMT1* lines, in one of the *cP:TMEM165* lines (#39) and in both *cP:MNX* lines (Figure 4C). The second *cP:TMEM165* line #13 did not quite reach the control value (Figure 4C), but this can probably be explained by variation in the levels of transgene expression. Based on wild-type *cTP* expression, in fact, an approximately twofold higher transgene expression was observed in *cP:TMEM165* #13 (Figure 4D), whereas transgene expression was increased by at least 10-fold in the two positive control lines, in *cP:CMT1* #16 and #27, in *cP:TMEM165* #39, and in *cP:MNX* #1 and #34 (Figure 4D). Notably, we also found transgene expression in the negative control lines to be well above the *pam71* level, which can be attributed to the use of the 35S promoter (Supplementary Figure 4C). Overall, we concluded that transgene overexpression in the *cP_{pos}PAM71*, *cP:CMT1*, *cP:MNX* and *cP:TMEM165* lines resulted in the restoration of optimal PSII efficiency, and consequently boosted plant growth and biomass production. It is worth pointing out here that no leaf abnormalities were detected in any of the lines (Figure 4A). In contrast, overexpression

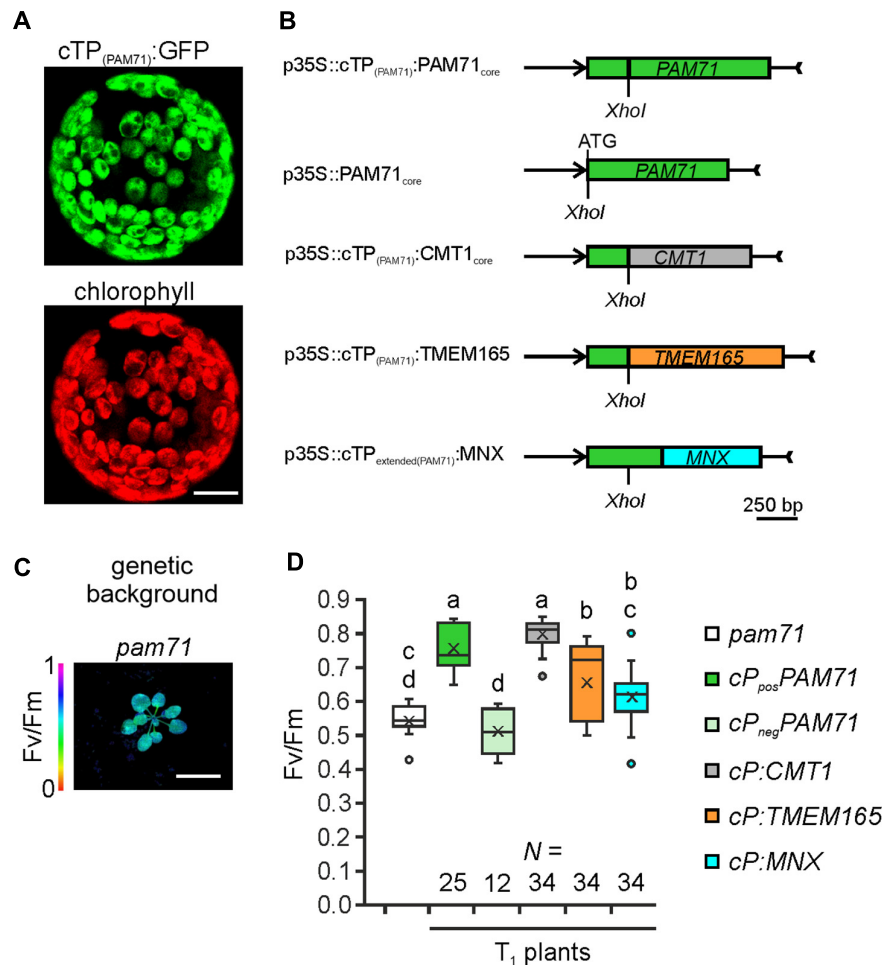


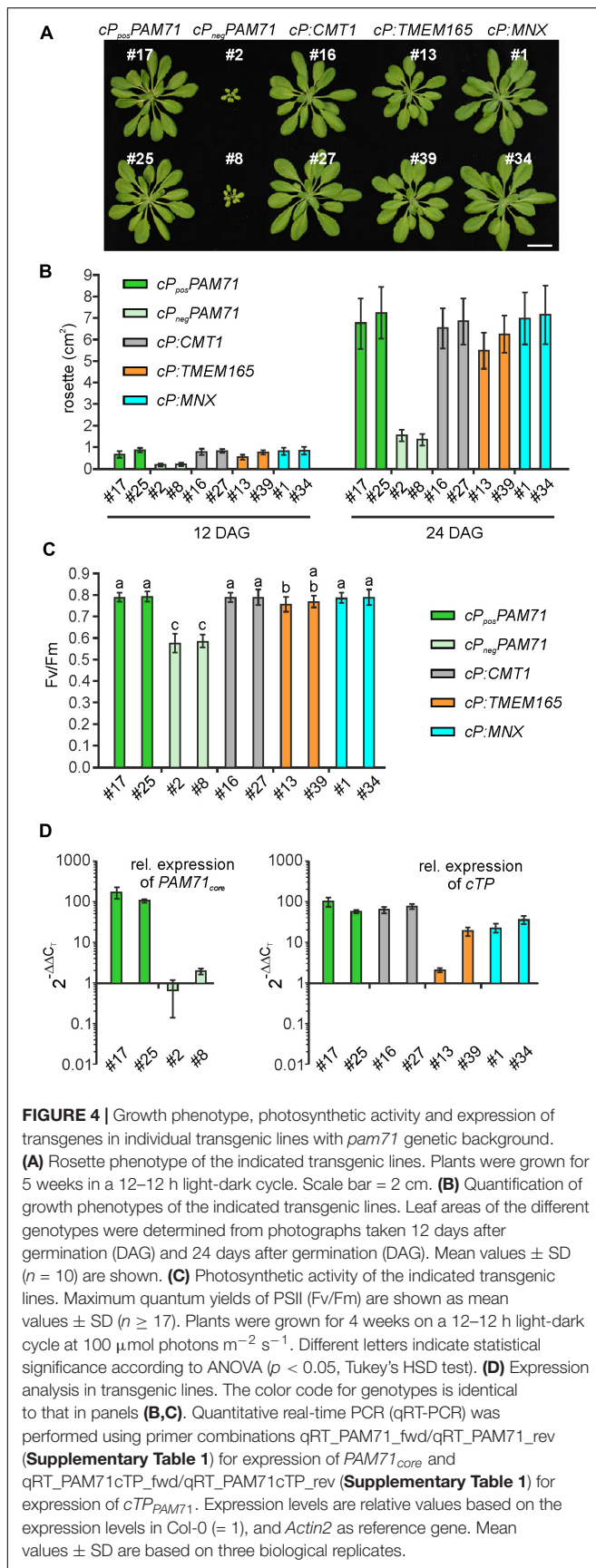
FIGURE 3 | Experimental setup for gene replacement assays. **(A)** Verification of the N-terminal PAM71 sequence as a chloroplast-targeting peptide. *Nicotiana benthamiana* leaves were infiltrated with the *Agrobacterium* strain containing p35S::cTP_(PAM71):GFP; protoplasts were isolated after 48 h and analyzed by confocal microscopy. Scale bar = 12.5 μ m. **(B)** Scheme depicting the chimeric constructs used for transformation of *pam71*. **(C)** The *pam71* mutant as genetic background. The maximum quantum yield of PSII (Fv/Fm) of a 4-week-old plant is shown. Scale bar = 1 cm. **(D)** Photosynthetic activity of BASTA-resistant T₁ transgenic plants in comparison to *pam71*. The maximum quantum yields of PSII (Fv/Fm) of T₁ plants are depicted as box plots representing the range of values, the exclusive median and the mean, indicated as x. The number of independent individuals is given (N). Outliers are indicated as dots. Different letters indicate statistical significance based on ANOVA ($p < 0.01$, Tukey's honestly significant difference (HSD) test).

of the UPF0016 transporter *PML3* in the Golgi apparatus of *Arabidopsis* was accompanied by stunted plant growth and a curled leaf morphology (Hoecker et al., 2020).

Human TMEM165, Plant CMT1, and Cyanobacteria MNX All Facilitate Incorporation of Manganese Into the Photosynthetic Complexes in the Thylakoid Membrane

To unequivocally demonstrate the subcellular localization of cP:TMEM165, cP:CMT1 and cP:MNX in the *pam71* mutant background, proteomic analysis was employed. In this approach, envelope and thylakoid membrane fractions were isolated from purified chloroplasts, and several membrane proteins with known localizations were chosen as marker proteins

for quality control. All selected marker proteins could be assigned to the correct fraction in wild-type chloroplasts (Supplementary Table 2), including the endogenous CMT1 protein, whereas the endogenous PAM71 was not detectable. We also verified that PAM71, TMEM165 and MNX were all undetectable in the negative control line, and only the endogenous CMT1 protein was found to be enriched in the envelope fraction (Supplementary Table 2). Chloroplasts were isolated from cP_{pos}PAM71 #25, cP:CMT1 #27, cP:TMEM165 #39, and cP:MNX #1, and the envelope and thylakoid fractions were analyzed for the presence of the respective test proteins and marker proteins (Figure 5A). PAM71 was found to be equally enriched in both fractions in cP_{pos}PAM71 plants, as was the MNX protein in cP:MNX plants (Figure 5A and Supplementary Tables 3, 4). The majority of the TMEM165 protein was found in the envelope fraction in



cP:TMEM165 plants, but a small portion was also present in the thylakoid membrane (Figure 5A and Supplementary Table 5). Owing to the presence of the endogenous CMT1 protein, *cP:CMT1* is difficult to quantify accurately, but nearly 40% of all CMT1 could be assigned to the thylakoid fraction of *cP:CMT1* plants (Figure 5A and Supplementary Tables 6, 7). This result differs from the distribution of endogenous CMT1 in the other genotypes, which had about 19% in their thylakoid enriched fractions (Supplementary Table 7). Thus, we concluded that overexpression of *cP:TMEM165*, *cP:MNX* or *cP:CMT1* in the *pam71* mutant background enables the production of significant amounts of the corresponding proteins, which were eventually inserted into the thylakoid membrane.

One physiological consequence of the *PAM71* knock-out mutation is a marked decrease in the amounts of photosynthetic complexes, for instance PSII dimer, PSI monomer and PSII LHCII supercomplexes (Schneider et al., 2016; Wang et al., 2016). Thus, we tested the ability of *cP:CMT1*, *cP:TMEM165* and *cP:MNX* plants to enhance levels of photosynthetic membrane complexes. To this end, we employed Blue-Native PAGE analysis to determine the amounts of these complexes in the transgenic lines relative to wild-type and *pam71*. As expected, the steady-state levels of PSII_{di}/PSII_{mono} and PSII-LHCII_{super} were reduced in the negative control line (*cP_{neg}PAM71*) to quantities comparable to those in *pam71* (Figure 5B). On the other hand, steady-state levels of these protein complexes were restored to wild-type amounts in *cP_{pos}PAM71*, *cP:CMT1*, and *cP:MNX* and almost to wild-type levels in *cP:TMEM165* plants. In the *pam71* mutant, inadequate amounts of Mn are bound in PSII complexes (Schneider et al., 2016) and, as expected, the same effect was observed in the negative control line (Figures 5C,D and Supplementary Figure 4D). In contrast, the levels of Mn bound in PSII complexes in *cP:CMT1*, in *cP:TMEM165* and in *cP:MNX* plants matched those seen in the positive control (Figure 5C), as determined by SEC-ICP-MS analysis. Moreover, the Mn:S ratios (the relative amount of Mn incorporated into PSII per unit of S, used here as a proxy for protein) in these three lines were indistinguishable from that in *cP_{pos}PAM71* (Figure 5D), indicating sufficient transport of Mn²⁺ into the thylakoid lumen.

CMT1 of Arabidopsis Cannot Be Replaced by PAM71

Following the observation that overexpression of *CMT1* can complement the *pam71* phenotype, we also investigated the reverse configuration. First, we verified that the *cTP* of *CMT1* was able to direct GFP into the chloroplast (Figure 6A). Next, a fusion construct consisting of the *cTP* of *CMT1* (designated as *cC*) and the core sequence of *PAM71* (Figure 6B) was assembled. This construct and a positive control (*cTP* of *CMT1* fused to the *CMT1* core sequence) were introduced into the *cmt1* genetic background, and several independent transgenic lines per construct were selected (Figure 6C). Comparison of the Fv/Fm values for both groups of plants revealed that, in contrast to *cC_{pos}CMT1* lines, the Fv/Fm ratios in *cC:PAM71*

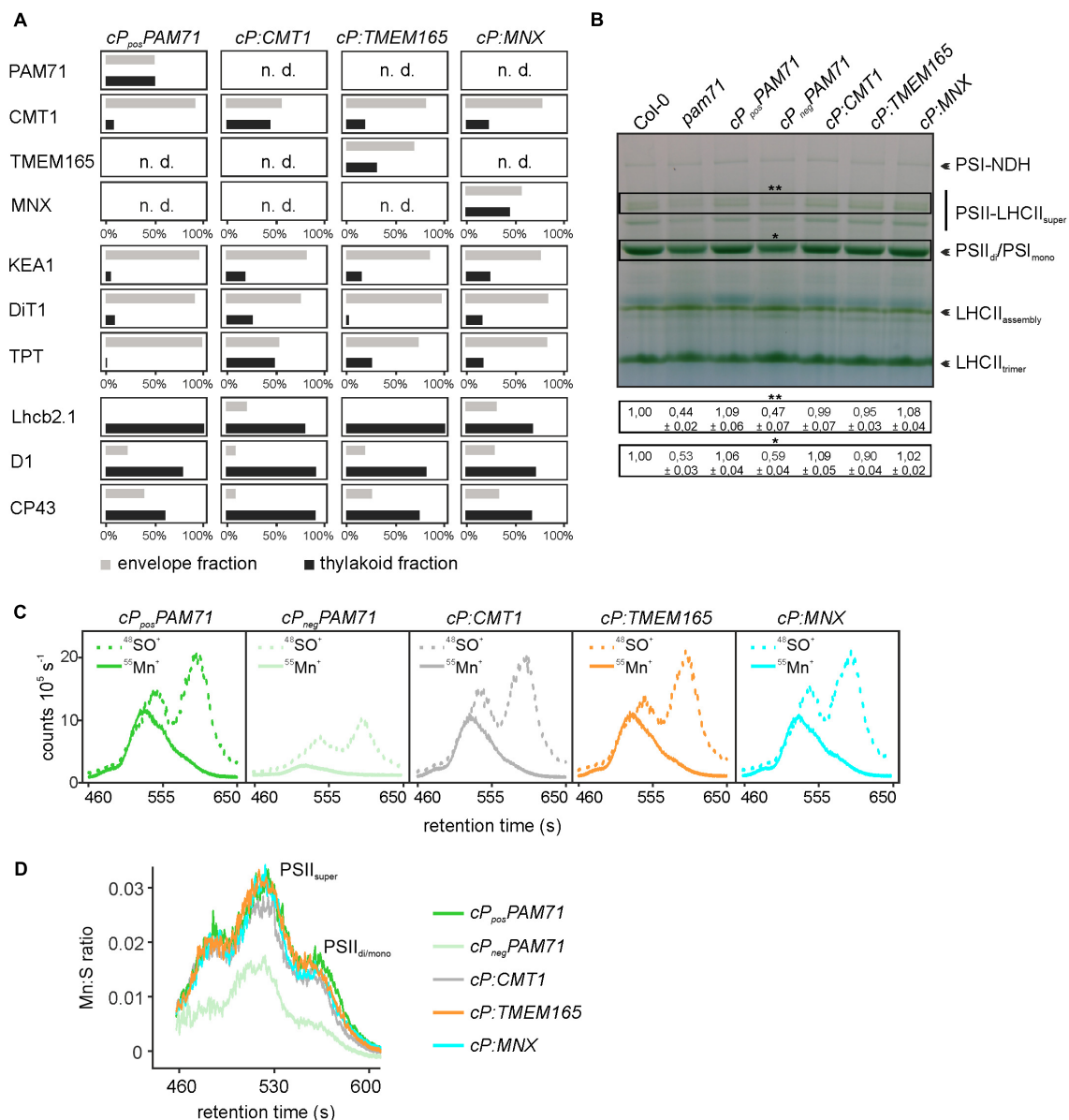


FIGURE 5 | Proteomic and ICP-MS analysis of individual transgenic lines with *pam71* genetic background. **(A)** PAM71, CMT1, TMEM165, MNX and marker proteins of envelope and thylakoid enriched fractions of the indicated plant lines. The K⁺ efflux antiporter 1 (KEA1), dicarboxylate transporter 1 (DiT1) and triosephosphate/phosphate translocator (TPT) were used as envelope marker proteins, and chlorophyll a-b binding protein 2.1 (Lhcb2.1), photosystem II protein D1 (D1) and photosystem II CP43 reaction center protein (CP43) served as thylakoid markers. The proteomic analysis is based on three independent experiments and data depicted are derived from Experiment 2 (**Supplementary Tables 3–6**). n.d., not detected. **(B)** Accumulation of thylakoid photosynthetic complexes in transgenic lines in comparison to levels in Col-0 and *pam71*. Thylakoid membrane samples (equivalent to 18 μ g of protein) were solubilized with 1% (w/v) β -dodecyl-maltoside, and protein complexes were fractionated by Blue-Native gel electrophoreses. NDH, NADH dehydrogenase-like; PSI, photosystem I; PSII, photosystem II; LHCII, light-harvesting complex of photosystem II. The different assembly states are indicated. Quantification of the indicated complexes (**PSII-LHCII supercomplexes and *PSII dimer/PSI monomer complexes) is based on intensity levels in Col-0 (=1,00). Mean values \pm SD ($n = 3$) are shown. **(C)** Size-exclusion chromatograms depicting the relative intensities of the non-oxide ion $^{55}\text{Mn}^{+}$ and the oxide ion $^{48}\text{SO}^{+}$ in the transgenic lines. Thylakoid membranes (equivalent to 50 μ g of protein) were solubilized with 1% (w/v) α -dodecyl-maltoside, and protein complexes were fractionated on a size-exclusion column. Analysis was performed with two independent experiments. **(D)** Quantification of the Mn:S ratios in the transgenic lines. Mn:S ratios are shown for the fractionated photosynthetic complexes from the samples analyzed in panel **(C)**. PSII, Photosystem II; different assembly states are indicated. The data are based on two independent experiments.

lines resembled that of *cmt1* mutant plants (**Figure 6D**). Because subtle effects might not be detectable in the T1 generation, we selected two lines per group for closer inspection. The

lines chosen exhibited the highest Fv/Fm values within their group in the respective T1 plant, carried a single-copy transgene insertion, and the magnitude of transgene expression was at

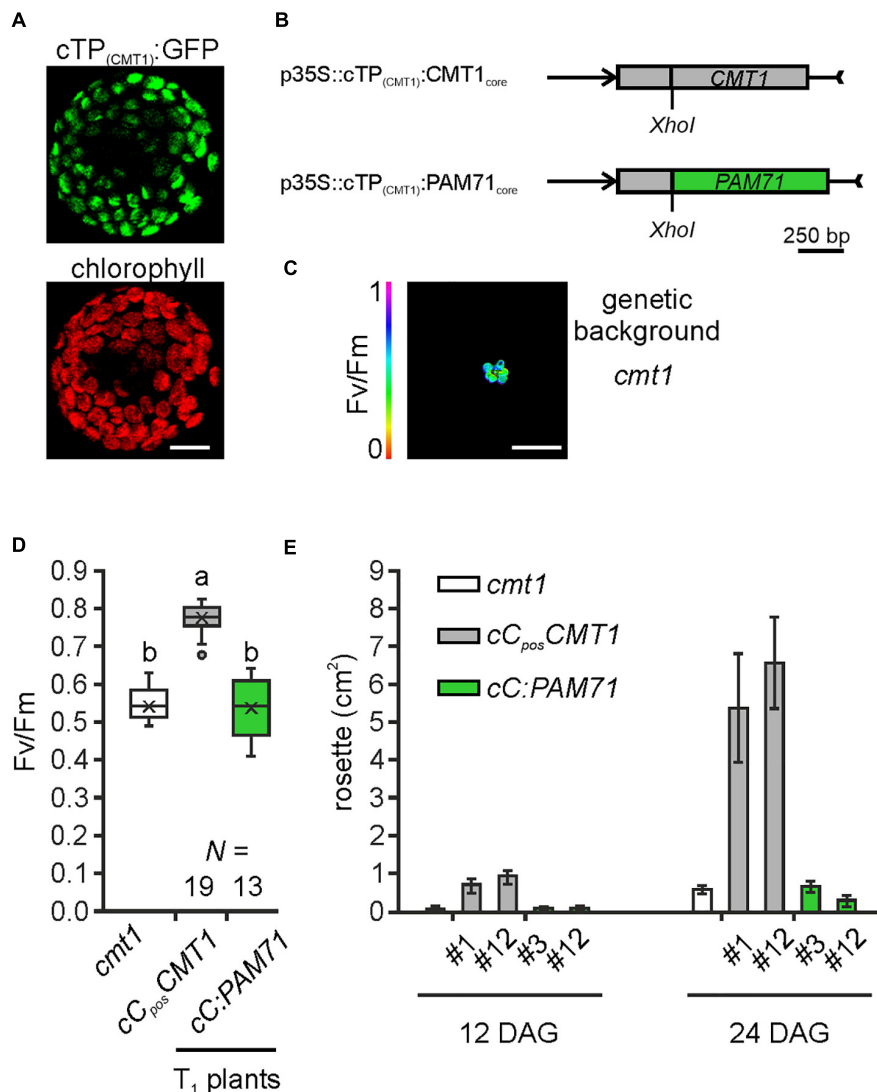


FIGURE 6 | Experimental setup for gene replacement assay and analysis of individual transgenic lines in the *cmt1* genetic background. **(A)** Verification of the N-terminal CMT1 sequence as a chloroplast-targeting peptide. *Nicotiana benthamiana* leaves were infiltrated with the Agrobacterium strain containing p35S::cTP_(CMT1):GFP; protoplasts were isolated after 48 h and analyzed by confocal microscopy. Scale bar = 12.5 μ m. **(B)** Schematic depiction of the chimeric constructs used for transformation of *cmt1*. **(C)** The *cmt1* mutant as genetic background. The maximum quantum yield of PSII (Fv/Fm) of a 4-week-old plant is shown. Scale bar = 1 cm. **(D)** Photosynthetic activity of BASTA resistant T₁ transgenic plants in comparison to *cmt1*. The maximum quantum yield of PSII (Fv/Fm) of T₁ plants is depicted as box plots representing the range of values, the exclusive median and the mean, indicated as x. The number of independent plant lines is given (N). Outliers are indicated as dots. Different letters indicate statistical significance according to ANOVA ($p < 0.01$, Tukey's HSD test). **(E)** Quantification of growth phenotypes of the indicated genotypes. Leaf areas of selected transgenic lines in comparison to *cmt1* were determined from photographs taken 12 days after germination (DAG) and 24 days after germination (DAG). Mean values \pm SD ($n = 10$) are shown.

least 10 times higher than the wild-type level (Supplementary Figures 5A,B). A re-examination of Fv/Fm values in subsequent generations revealed that, in both selected *cC:PAM71* lines, the Fv/Fm values were not significantly different from those of *cmt1* mutant plants, whereas Fv/Fm recovered to almost 0.8 in both positive control lines (Supplementary Figure 5C). In addition, growth of both *cC:PAM71* lines was markedly retarded, as in the case of *cmt1* mutant plants (Figure 6E). Taken together, these data showed that PAM71 cannot substitute CMT1 in the envelope membrane.

DISCUSSION

Our phylogenetic analysis indicates that eukaryotic and cyanobacterial members of the UPF0016 transporter family share a common ancestor, which is reflected in their functional conservation. A gene-replacement analysis was conducted in the *Arabidopsis* mutant *pam71* (Figure 3), which is characterized by diminished growth. This phenotype is readily discernible under standard cultivation conditions, and *pam71* is accessible to genetic manipulations resulting in inheritable traits. For our

purposes, these features make it more suitable than systems in which the knock-out mutation generates a conditional phenotype. For instance, a conditional phenotype has been found in the yeast UPF0016 mutant *gdt1*, which is sensitive to high concentrations of Ca^{2+} (Demaegd et al., 2013). However, its growth rate is otherwise unaffected, i.e., similar to that of wild-type strains. It has been shown that sensitivity to excess Ca^{2+} can be suppressed by transient expression of TMEM165 (Demaegd et al., 2013).

As targets for our analysis, we selected the *Synechocystis* gene *MNX*, the *Arabidopsis* gene *CMT1* and the human gene *TMEM165*. Their protein products share with PAM71 the predicted topology of two clusters of three transmembrane domains, including the consensus motifs (Supplementary Figure 2). Variations at the N-terminus are assumed to be required for correct membrane targeting (Hoecker et al., 2017), and indeed the N-terminal portion of PAM71 is sufficient for targeting to chloroplasts (Figure 3A). Notably, a derivative of PAM71 lacking the chloroplast targeting signal peptide is incapable of complementing the *pam71* phenotype (Figures 3D, 4, 5B–D), indicating that the cTP is specifically required for correct targeting. Thus, the proteins MNX, CMT1 and TMEM165 could be successfully targeted to the thylakoid membrane of *pam71* plants by equipping them with the cTP of PAM71 (Figure 5A) and overexpressed from the respective transgenes (Figure 4D). We demonstrate that the paralog CMT1, as well as both orthologs SynMNX and HsTMEM165, are functional in *Arabidopsis* thylakoid membranes when introduced into the *Arabidopsis pam71* mutant background. These findings show that all four proteins have retained the ancestral function. Like PAM71, CMT1, MNX and TMEM165 are capable of transporting Mn^{2+} into the thylakoid lumen for efficient reconstitution of inorganic Mn clusters in photosystem II (Figures 5C,D)—as demonstrated by the recovery of photosystem II efficiency (Figure 4C), which eventually increased plant growth (Figure 4B). A strong proton gradient across the thylakoid membrane (Hohner et al., 2016; Pottosin and Shabala, 2016) is established upon illumination, which presumably energizes Mn^{2+} uptake into the acidic thylakoid lumen, in accordance with the current model of a cation/proton antiport mechanism for the UPF0016 protein family (Thines et al., 2020). In this respect, it is interesting to note that CMT1 can functionally replace PAM71 at the thylakoid membrane, but not *vice versa* (Figure 6 and Supplementary Figure 5). It is tempting to speculate that CMT1 has acquired additional features that allow it to cope with the conditions prevailing at the envelope membrane, where the proton gradient is much weaker (Hohner et al., 2016).

Our findings indicate that UPF0016 members function independently of additional factors and/or of the lipid composition of the membrane. It is particularly remarkable that the human ortholog TMEM165 can replace PAM71 in the thylakoid membrane, which is rich in monogalactosyldiacylglycerol and digalactosyldiacylglycerol (Li-Beisson et al., 2013; Rocha et al., 2018), in contrast to the Golgi membrane. TMEM165 (Foulquier et al., 2012; Potelle et al., 2016; Dulary et al., 2017; Lebredonchel et al., 2019; Foulquier and Legrand, 2020), like its plant counterpart PML3

(Hoecker et al., 2020; Yang et al., 2021), naturally resides in the Golgi membrane, where the Mn^{2+} imported into the Golgi lumen acts as an essential cofactor in the synthesis of N-glycans. In the present study an LC_MS/MS-based approach was employed to gain insight into the partitioning of overexpressed TMEM165, MNX, PAM71, and CMT1 between the envelope and thylakoid membranes, because quantitative proteomics studies on purified chloroplast membranes and their subfractions have been shown in the past to be an efficient method for this purpose (Ferro et al., 2010). The expected enrichment of marker proteins in the two membrane fractions allowed us to conclude that the method is reliable (Figure 5A). As observed in the past (Ferro et al., 2010), it was not possible to identify the endogenous PAM71 in wild-type samples (Supplementary Table 2); only in the overexpressor line *cP_{pos}PAM71* could it be successfully identified (Figure 5A). Clearly, fractions of the overexpressed TMEM165, MNX, and PAM71 proteins were retained in the envelope membrane. However, at least in the case of PAM71, presumably non-functional (Figure 6).

UPF0016 proteins are of interest not only because of their conserved ability to facilitate Mn^{2+} transport, but also in terms of their evolutionary history—given that members have been identified across Archaea, Bacteria, and Eukaryota (Supplementary Figure 1). Small UPF0016 gene/protein families exist in plants, and in *Arabidopsis* the genes that code for both ER-localized proteins (PML4/PML5) are derived from a chromosomal duplication event in the progenitor of *Arabidopsis* (Hoecker et al., 2017)—indeed, these two share the highest similarity (Figure 2). This study suggests that the genes coding for the chloroplast-localized proteins CMT1 and PAM71 arose during the establishment of endosymbiosis, after the cyanobacterial precursor of chloroplasts contributed its gene copy to the eukaryotic host genome, which then gave rise to a gene duplication that is widely conserved in Viridiplantae (Figure 1). In green algae, the PAM71 homolog CGLD1 (conserved in the green lineage and diatoms 1) maintained the structure and function of PSII, and contributed to its protection under photo-oxidative stress conditions (Xing et al., 2017). It is well established that genes of the cyanobacterial ancestor have been transferred to the nucleus, that many of the proteins they encode are rerouted to the chloroplast (Leister, 2003, 2016; Lee and Hwang, 2018) and that numerous proteins can functionally replace each other (Savidge et al., 2002; Sattler et al., 2003; Lv et al., 2009; Armbruster et al., 2013; Proctor et al., 2018; Yoon et al., 2019). Yet, what makes the evolution of the UPF0016 family particularly interesting is that it suggests all members of Eukaryota and Cyanobacteria (Figure 1) might have a common ancestor, which would explain why human TMEM165 can functionally substitute for PAM71 in chloroplast membranes. We suggest that plants received UPF0016 gene copies *via* two independent events. Although speculative, lateral gene transfer, perhaps involving Cyanobacteria, could be at the origin of subgroup one proteins, which are present in all Eukaryota, as there is no indication of an archaeal and/or protobacterial origin of this subgroup (Figure 1). In a second event, through cyanobacterial endosymbiotic gene transfer, subgroup two proteins were then introduced into the green

lineage. We have not succeeded in tracing UPF0016 protein members to the last common ancestor of all cells, which is proposed to have lived about 3.8 billion years ago and to have had 355 protein clusters (Weiss et al., 2016, 2018). Thus, it is reasonable to assume that UPF0016 genes spread extensively by lateral gene transfer later in evolution.

It has also been suggested that PAM71 acquired an additional Ca^{2+} transport function (Wang et al., 2016; Frank et al., 2019). In this study, we have shown that the cyanobacterial MNX protein is functional in *pam71* plants and fully complements all aspects of the latter's mutant phenotype (Figure 5). This enables us to conclude that only the Mn^{2+} transport activity of PAM71 plays a significant physiological role in chloroplasts. At the thylakoid membrane it can be replaced by its paralog (CMT1) and by its orthologs from *Zea mays* (Wang et al., 2020), cyanobacteria and human, yet there is no indication that PAM71 can function at the envelope membrane. A future challenge is to determine the molecular basis for the adaptation of CMT1 to the conditions prevailing in the envelope membrane of chloroplasts, and this study opens the door to further investigations of how far proteins can diverge without losing their ancient function.

DATA AVAILABILITY STATEMENT

The mass spectrometry proteomics data have been deposited at <https://www.ebi.ac.uk/pride> under the accession number PXD022763.

REFERENCES

- Armbruster, U., Labs, M., Pribil, M., Viola, S., Xu, W., Scharfenberg, M., et al. (2013). *Arabidopsis* curvature thylakoid1 proteins modify thylakoid architecture by inducing membrane curvature. *Plant Cell* 25, 2661–2678. doi: 10.1105/tpc.113.113118
- Bammens, R., Mehta, N., Race, V., Foulquier, F., Jaeken, J., Tiemeyer, M., et al. (2015). Abnormal cartilage development and altered N-glycosylation in Tmem165-deficient zebrafish mirrors the phenotypes associated with TMEM165-CDG. *Glycobiology* 25, 669–682. doi: 10.1093/glycob/cwv009
- Brandenburg, F., Schoffman, H., Kurz, S., Kramer, U., Keren, N., Weber, A. P., et al. (2017). The *Synechocystis* manganese exporter Mnx is essential for manganese homeostasis in cyanobacteria. *Plant Physiol.* 173, 1798–1810. doi: 10.1104/pp.16.01895
- Clough, S. J., and Bent, A. F. (1998). Floral dip: a simplified method for *Agrobacterium*-mediated transformation of *Arabidopsis thaliana*. *Plant J.* 16, 735–743. doi: 10.1046/j.1365-3113x.1998.00343.x
- Colinet, A. S., Sengottaiyan, P., Deschamps, A., Colsoul, M. L., Thines, L., Demaegd, D., et al. (2016). Yeast Gdt1 is a Golgi-localized calcium transporter required for stress-induced calcium signaling and protein glycosylation. *Sci. Rep.* 6:24282.
- Cox, J., and Mann, M. (2008). MaxQuant enables high peptide identification rates, individualized p.p.b.-range mass accuracies and proteome-wide protein quantification. *Nat. Biotechnol.* 26, 1367–1372. doi: 10.1038/nbt.1511
- Cox, J., Neuhauser, N., Michalski, A., Scheltema, R. A., Olsen, J. V., and Mann, M. (2011). Andromeda: a peptide search engine integrated into the MaxQuant environment. *J. Proteome Res.* 10, 1794–1805. doi: 10.1021/pr101065j
- Demaegd, D., Colinet, A. S., Deschamps, A., and Morsomme, P. (2014). Molecular evolution of a novel family of putative calcium transporters. *PLoS One* 9:e100851. doi: 10.1371/journal.pone.0100851

AUTHOR CONTRIBUTIONS

AS: conceptualization. NH, YH, SS, GM, and SBS: investigation and analysis of data. DL and AS: resources. SBS and AS: funding acquisition and writing—review and editing. NH and AS: writing—original draft. All authors contributed to manuscript revision, read, and approved the submitted version.

FUNDING

This research was supported by the German Science Foundation (SCHN560/4-1 to AS) and by the Independent Research Fund Denmark—Technology and Production Sciences (Grant No. DFF-5054-00042 to SBS).

ACKNOWLEDGMENTS

We would like to thank Sabine Jarzombski for excellent technical assistance, Serena Schwenkert for *Nicotiana benthamiana* seeds and support with confocal microscopy, and Paul Hardy for critical reading of the manuscript.

SUPPLEMENTARY MATERIAL

The Supplementary Material for this article can be found online at: <https://www.frontiersin.org/articles/10.3389/fpls.2021.697848/full#supplementary-material>

- Demaegd, D., Foulquier, F., Colinet, A. S., Gremillon, L., Legrand, D., Mariot, P., et al. (2013). Newly characterized Golgi-localized family of proteins is involved in calcium and pH homeostasis in yeast and human cells. *Proc. Natl. Acad. Sci. U.S.A.* 110, 6859–6864. doi: 10.1073/pnas.1219871110
- Dulavy, E., Potelle, S., Legrand, D., and Foulquier, F. (2017). TMEM165 deficiencies in congenital disorders of glycosylation type II (CDG-II): clues and evidences for roles of the protein in Golgi functions and ion homeostasis. *Tissue Cell* 49, 150–156. doi: 10.1016/j.tice.2016.06.006
- Eisenhut, M. (2019). Manganese homeostasis in cyanobacteria. *Plants* 9:18. doi: 10.3390/plants9010018
- Eisenhut, M., Hoecker, N., Schmidt, S. B., Basgaran, R. M., Flachbart, S., Jahns, P., et al. (2018). The plastid envelope chloroplast manganese transporter1 is essential for manganese homeostasis in *Arabidopsis*. *Mol. Plant* 11, 955–969. doi: 10.1016/j.molp.2018.04.008
- Ferro, M., Brugiere, S., Salvi, D., Seigneurin-Berny, D., Court, M., Moyet, L., et al. (2010). AT_CHLORO, a comprehensive chloroplast proteome database with subplastidial localization and curated information on envelope proteins. *Mol. Cell. Proteomics* 9, 1063–1084. doi: 10.1074/mcp.m900325-mcp200
- Fisher, C. R., Wyckoff, E. E., Peng, E. D., and Payne, S. M. (2016). Identification and characterization of a putative manganese export protein in *Vibrio cholerae*. *J. Bacteriol.* 198, 2810–2817. doi: 10.1128/jb.00215-16
- Foulquier, F., Amyere, M., Jaeken, J., Zeevaert, R., Schollen, E., Race, V., et al. (2012). TMEM165 deficiency causes a congenital disorder of glycosylation. *Am. J. Hum. Genet.* 91, 15–26. doi: 10.1016/j.ajhg.2012.05.002
- Foulquier, F., and Legrand, D. (2020). Biometals and glycosylation in humans: congenital disorders of glycosylation shed lights into the crucial role of Golgi manganese homeostasis. *Biochim. Biophys. Acta Gen. Subj.* 1864:129674. doi: 10.1016/j.bbagen.2020.129674
- Frank, J., Happeck, R., Meier, B., Hoang, M. T. T., Stribny, J., Hause, G., et al. (2019). Chloroplast-localized BICAT proteins shape stromal calcium signals

- and are required for efficient photosynthesis. *New Phytol.* 221, 866–880. doi: 10.1111/nph.15407
- Gandini, C., Schmidt, S. B., Husted, S., Schneider, A., and Leister, D. (2017). The transporter SynPAM71 is located in the plasma membrane and thylakoids, and mediates manganese tolerance in *Synechocystis* PCC6803. *New Phytol.* 215, 256–268. doi: 10.1111/nph.14526
- Hanikenne, M., and Baurain, D. (2013). Origin and evolution of metal P-type ATPases in Plantae (Archaeplastida). *Front. Plant Sci.* 4:544. doi: 10.3389/fpls.2013.00544
- Hoecker, N., Honke, A., Frey, K., Leister, D., and Schneider, A. (2020). Homologous proteins of the manganese transporter PAM71 are localized in the Golgi apparatus and endoplasmic reticulum. *Plants* 9:239. doi: 10.3390/plants9020239
- Hoecker, N., Leister, D., and Schneider, A. (2017). Plants contain small families of UPF0016 proteins including the photosynthesis affected MUTANT71 transporter. *Plant Signal. Behav.* 12:e1278101. doi: 10.1080/15592324.2016.1278101
- Hohner, R., Aboukila, A., Kunz, H. H., and Venema, K. (2016). Proton gradients and proton-dependent transport processes in the chloroplast. *Front. Plant Sci.* 7:218. doi: 10.3389/fpls.2016.00218
- Huber, M., Bienvenut, W. V., Linster, E., Stephan, I., Armbruster, L., Sticht, C., et al. (2020). NatB-mediated N-terminal acetylation affects growth and biotic stress responses. *Plant Physiol.* 182, 792–806. doi: 10.1104/pp.19.00792
- Janowski, M., Zoschke, R., Scharff, L. B., Martinez Jaime, S., Ferrari, C., Proost, S., et al. (2018). AtRsgA from *Arabidopsis thaliana* is important for maturation of the small subunit of the chloroplast ribosome. *Plant J.* 96, 404–420. doi: 10.1111/tj.14040
- Jha, S. G., Larson, E. R., Humble, J., Domozych, D. S., Barrington, D. S., and Tierney, M. L. (2018). Vacuolar protein sorting 26C encodes an evolutionarily conserved large retromer subunit in eukaryotes that is important for root hair growth in *Arabidopsis thaliana*. *Plant J.* 94, 595–611. doi: 10.1111/tj.13880
- Karimi, M., Inze, D., and Depicker, A. (2002). GATEWAY vectors for *Agrobacterium*-mediated plant transformation. *Trends Plant Sci.* 7, 193–195. doi: 10.1016/s1360-1385(02)02251-3
- Krzewinski-Recchi, M. A., Potelle, S., Mir, A. M., Vicogne, D., Dulary, E., Duvet, S., et al. (2017). Evidence for splice transcript variants of TMEM165, a gene involved in CDG. *Biochim. Biophys. Acta Gen. Subj.* 1861, 737–748. doi: 10.1016/j.bbagen.2017.01.011
- Kumar, S., Stecher, G., Li, M., Knyaz, C., and Tamura, K. (2018). MEGA X: molecular evolutionary genetics analysis across computing platforms. *Mol. Biol. Evol.* 35, 1547–1549. doi: 10.1093/molbev/msy096
- Le, S. Q., and Gascuel, O. (2008). An improved general amino acid replacement matrix. *Mol. Biol. Evol.* 25, 1307–1320. doi: 10.1093/molbev/msn067
- Lebedonchel, E., Houdou, M., Potelle, S., De Bettignies, G., Schulz, C., Krzewinski Recchi, M. A., et al. (2019). Dissection of TMEM165 function in Golgi glycosylation and its Mn(2+) sensitivity. *Biochimie* 165, 123–130. doi: 10.1016/j.biochi.2019.07.016
- Lee, D. W., and Hwang, I. (2018). Evolution and design principles of the diverse chloroplast transit peptides. *Mol. Cells* 41, 161–167.
- Leister, D. (2003). Chloroplast research in the genomic age. *Trends Genet.* 19, 47–56. doi: 10.1016/s0168-9525(02)00003-3
- Leister, D. (2016). Towards understanding the evolution and functional diversification of DNA-containing plant organelles. *F1000Res.* 5:F1000FacultyRev-330.
- Li-Beisson, Y., Shorrosh, B., Beisson, F., Andersson, M. X., Arondel, V., Bates, P. D., et al. (2013). Acyl-lipid metabolism. *Arabidopsis Book* 11:e0161.
- Lv, H. X., Guo, G. Q., and Yang, Z. N. (2009). Translocons on the inner and outer envelopes of chloroplasts share similar evolutionary origin in *Arabidopsis thaliana*. *J. Evol. Biol.* 22, 1418–1428. doi: 10.1111/j.1420-9101.2009.01755.x
- Maxwell, K., and Johnson, G. N. (2000). Chlorophyll fluorescence—a practical guide. *J. Exp. Bot.* 51, 659–668. doi: 10.1093/jxb/51.345.659
- Morelle, W., Potelle, S., Witters, P., Wong, S., Climer, L., Lupashin, V., et al. (2017). Galactose supplementation in patients with TMEM165-CDG rescues the glycosylation defects. *J. Clin. Endocrinol. Metab.* 102, 1375–1386. doi: 10.1210/je.2016-3443
- Potelle, S., Morelle, W., Dulary, E., Duvet, S., Vicogne, D., Spriet, C., et al. (2016). Glycosylation abnormalities in Gdt1p/TMEM165 deficient cells result from a defect in Golgi manganese homeostasis. *Hum. Mol. Genet.* 25, 1489–1500. doi: 10.1093/hmg/ddw026
- Pottosin, I., and Shabala, S. (2016). Transport across chloroplast membranes: optimizing photosynthesis for adverse environmental conditions. *Mol. Plant* 9, 356–370. doi: 10.1016/j.molp.2015.10.006
- Proctor, M. S., Chidgey, J. W., Shukla, M. K., Jackson, P. J., Sobotka, R., Hunter, C. N., et al. (2018). Plant and algal chlorophyll synthases function in *Synechocystis* and interact with the YidC/Alb3 membrane insertase. *FEBS Lett.* 592, 3062–3073. doi: 10.1002/1873-3468.13222
- Rappsilber, J., Ishihama, Y., and Mann, M. (2003). Stop and go extraction tips for matrix-assisted laser desorption/ionization, nanoelectrospray, and LC/MS sample pretreatment in proteomics. *Anal. Chem.* 75, 663–670. doi: 10.1021/ac026117i
- Rocha, J., Nitenberg, M., Girard-Egrot, A., Jouhet, J., Marechal, E., Block, M. A., et al. (2018). Do galactolipid synthases play a key role in the biogenesis of chloroplast membranes of higher plants? *Front. Plant Sci.* 9:126. doi: 10.3389/fpls.2018.00126
- Rosnoblet, C., Legrand, D., Demaegd, D., Hacine-Gherbi, H., De Bettignies, G., Bammens, R., et al. (2013). Impact of disease-causing mutations on TMEM165 subcellular localization, a recently identified protein involved in CDG-II. *Hum. Mol. Genet.* 22, 2914–2928. doi: 10.1093/hmg/ddt146
- Sattler, S. E., Cahoon, E. B., Coughlan, S. J., and Dellapenna, D. (2003). Characterization of tocopherol cyclases from higher plants and cyanobacteria. Evolutionary implications for tocopherol synthesis and function. *Plant Physiol.* 132, 2184–2195. doi: 10.1104/pp.103.024257
- Savidge, B., Weiss, J. D., Wong, Y. H., Lassner, M. W., Mitsky, T. A., Shewmaker, C. K., et al. (2002). Isolation and characterization of homogentisate phytyltransferase genes from *Synechocystis* sp. PCC 6803 and *Arabidopsis*. *Plant Physiol.* 129, 321–332. doi: 10.1104/pp.010747
- Schmidt, S. B., Eisenhut, M., and Schneider, A. (2020). Chloroplast transition metal regulation for efficient photosynthesis. *Trends Plant Sci.* 25, 817–828. doi: 10.1016/j.tplants.2020.03.003
- Schmidt, S. B., Persson, D. P., Powikrowska, M., Frydenvang, J., Schjoerring, J. K., Jensen, P. E., et al. (2015). Metal binding in photosystem II super- and subcomplexes from barley thylakoids. *Plant Physiol.* 168, 1490–1502. doi: 10.1104/pp.15.00559
- Schmittgen, T. D., and Livak, K. J. (2008). Analyzing real-time PCR data by the comparative C-T method. *Nat. Protoc.* 3, 1101–1108. doi: 10.1038/nprot.2008.73
- Schneider, A., Steinberger, I., Herdean, A., Gandini, C., Eisenhut, M., Kurz, S., et al. (2016). The evolutionarily conserved protein photosynthesis affected MUTANT71 is required for efficient manganese uptake at the thylakoid membrane in *Arabidopsis*. *Plant Cell* 28, 892–910.
- Schneider, C. A., Rasband, W. S., and Eliceiri, K. W. (2012). NIH image to ImageJ: 25 years of image analysis. *Nat. Methods* 9, 671–675. doi: 10.1038/nmeth.2089
- Schulte Althoff, S., Gruneberg, M., Reunert, J., Park, J. H., Rust, S., Muhlhausen, C., et al. (2016). TMEM165 deficiency: postnatal changes in glycosylation. *JIMD Rep.* 26, 21–29. doi: 10.1007/8904_2015_455
- Schwanhauser, B., Busse, D., Li, N., Dittmar, G., Schuchhardt, J., Wolf, J., et al. (2011). Global quantification of mammalian gene expression control. *Nature* 473, 337–342. doi: 10.1038/nature10098
- Schweiger, R., and Schwenkert, S. (2014). Protein-protein interactions visualized by bimolecular fluorescence complementation in tobacco protoplasts and leaves. *J. Vis. Exp.* 9:51327. doi: 10.3791/51327
- Stribny, J., Thines, L., Deschamps, A., Goffin, P., and Morsomme, P. (2020). The human Golgi protein TMEM165 transports calcium and manganese in yeast and bacterial cells. *J. Biol. Chem.* 295, 3865–3874. doi: 10.1074/jbc.ra119.012249
- Thines, L., Stribny, J., and Morsomme, P. (2020). From the uncharacterized protein family 0016 to the GDT1 family: molecular insights into a newly-characterized family of cation secondary transporters. *Microb. Cell* 7, 202–214. doi: 10.15698/mic2020.08.725
- Vizcaino, J. A., Csordas, A., Del-Toro, N., Dienes, J. A., Griss, J., Lavidas, I., et al. (2016). 2016 update of the PRIDE database and its related tools. *Nucleic Acids Res.* 44, D447–D456.
- Wang, C., Ou, D., Wang, C., Lu, X., Du, J., Li, J., et al. (2020). Functional characterization of a chloroplast-localized Mn(2+)(Ca(2+))/H(+) antiporter, ZmmCCHA1 from *Zea mays* ssp. mexicana L. *Plant Physiol. Biochem.* 155, 396–405. doi: 10.1016/j.plaphy.2020.08.002

- Wang, C., Xu, W., Jin, H., Zhang, T., Lai, J., Zhou, X., et al. (2016). A putative chloroplast-localized Ca(2+)/H(+) antiporter CCHA1 is involved in calcium and pH homeostasis and required for PSII function in *Arabidopsis*. *Mol. Plant* 9, 1183–1196. doi: 10.1016/j.molp.2016.05.015
- Weiss, M. C., Preiner, M., Xavier, J. C., Zimorski, V., and Martin, W. F. (2018). The last universal common ancestor between ancient Earth chemistry and the onset of genetics. *PLoS Genet.* 14:e1007518. doi: 10.1371/journal.pgen.1007518
- Weiss, M. C., Sousa, F. L., Mrnjavac, N., Neukirchen, S., Roettger, M., Nelson-Sathi, S., et al. (2016). The physiology and habitat of the last universal common ancestor. *Nat. Microbiol.* 1:16116.
- Xing, J., Liu, P., Zhao, L., and Huang, F. (2017). Deletion of CGLD1 impairs PSII and increases singlet oxygen tolerance of green alga *Chlamydomonas reinhardtii*. *Front. Plant Sci.* 8:2154. doi: 10.3389/fpls.2017.02154
- Yang, C. H., Wang, C., Singh, S., Fan, N., Liu, S., Zhao, L., et al. (2021). Golgi-localised manganese transporter PML3 regulates *Arabidopsis* growth through modulating Golgi glycosylation and cell wall biosynthesis. *New Phytol.* doi: 10.1111/nph.17209 [Epub ahead of print].
- Yoon, J., Han, Y., Ahn, Y. O., Hong, M. K., and Sung, S. K. (2019). Characterization of HemY-type protoporphyrinogen IX oxidase genes from cyanobacteria and their functioning in transgenic *Arabidopsis*. *Plant Mol. Biol.* 101, 561–574. doi: 10.1007/s11103-019-00925-8
- Zeevaert, R., De Zegher, F., Sturiale, L., Garozzo, D., Smet, M., Moens, M., et al. (2013). Bone dysplasia as a key feature in three patients with a novel congenital disorder of glycosylation (CDG) type II due to a deep intronic splice mutation in TMEM165. *JIMD Rep.* 8, 145–152. doi: 10.1007/8904_2012_172
- Zeinert, R., Martinez, E., Schmitz, J., Senn, K., Usman, B., Anantharaman, V., et al. (2018). Structure-function analysis of manganese exporter proteins across bacteria. *J. Biol. Chem.* 293, 5715–5730. doi: 10.1074/jbc.m117.790717
- Zhang, B., Zhang, C., Liu, C., Jing, Y., Wang, Y., Jin, L., et al. (2018). Inner envelope chloroplast manganese transporter 1 supports manganese homeostasis and phototrophic growth in *Arabidopsis*. *Mol. Plant* 11, 943–954. doi: 10.1016/j.molp.2018.04.007

Conflict of Interest: The authors declare that the research was conducted in the absence of any commercial or financial relationships that could be construed as a potential conflict of interest.

Copyright © 2021 Hoecker, Hennecke, Schrott, Marino, Schmidt, Leister and Schneider. This is an open-access article distributed under the terms of the Creative Commons Attribution License (CC BY). The use, distribution or reproduction in other forums is permitted, provided the original author(s) and the copyright owner(s) are credited and that the original publication in this journal is cited, in accordance with accepted academic practice. No use, distribution or reproduction is permitted which does not comply with these terms.

8 Discussion

Arabidopsis thaliana mutant lines which have growth and developmental defects are challenging to work with. Albinotic, chlorotic or even embryonic lethal phenotypes make it often complicated to detect the underlying primary effect that is caused by the loss of function of the gene of interest. Secondary effects that sometimes are not easy to distinguish from primary defects can occur as well. For example, many loss-of function mutations result in growth defects but are due to disturbed plastid morphology and photosynthesis performance (Lanquar et al., 2010; Schneider et al., 2016; Schneider et al., 2014). In the case of metal transporters - which are required in every membrane of each cell type - the same difficulties apply. In addition, there are many transport proteins that can transport a wide range of metal substrates like the IRT1 or members of the CAX family (Korshunova et al., 1999; Pittman et al., 2004) leading to overlapping functions. Therefore, it is known that the excess of several metals can lead to deficiency of others as they compete for transporter binding sites and displace them.

In chloroplasts, ion homeostasis is tightly linked to photosynthesis performance. Transition metals like Mn, Fe and Cu are of utmost importance for proper electron transfer during photosynthesis as they perform the necessary redox reactions (Schmidt et al., 2020). Chloroplasts derived from an ancient endosymbiotic event. Over the span of a billion of years, eukaryotic plant cells derived from an archaeon ancestor that engulfed an α -proteobacterium. The generated heterotrophic eukaryotic host cell contained mitochondria and a nucleus, and evolved further into a green cell by the uptake of an early-cyanobacterium (Maréchal, 2018; Martin et al., 2015). The endosymbiotic event by which the early-cyanobacterium was engulfed lead to the evolution of the semiautonomous chloroplast organelle (Martin et al., 2015). Cyanobacteria are gram-negative, which means they have an inner, as well as an outer membrane separated by a periplasmic space (Liberton, 2008). The chloroplast membranes are supposed to be the ancient membranes of the up taken early-cyanobacterium (Keeling, 2004; Maréchal, 2018). Thus, in plants, chloroplasts are surrounded by two membranes and thus metal ions need to pass those two chloroplast envelope membranes. Furthermore, some metals, like Mn and Cu additionally need to pass the thylakoid membrane to enter the lumen. Such a system is for example described for the Cu transporters HMA6 and HMA8 (also PAA1 and PAA2), that reside in the inner envelope of chloroplasts and the thylakoid membrane, respectively (Abdel-Ghany et al., 2005; Boutigny et al., 2014; Catty et al., 2011; Shikanai et al., 2003). Mitochondria and chloroplasts still harbor parts of their original genome, but additionally, massive gene transfers, gene loss and rearrangements occurred. In comparisons, the modern time cyanobacteria such as *Synechocystis* possess 3168 protein-coding genes (Kaneko & Tabata, 1997) while the chloroplast genome of the model plant *Arabidopsis thaliana* harbors only 87 (Sato et al., 1999). Altogether, roughly 4500 genes were supposed to be transferred from the chloroplast to the nuclear genome of *Arabidopsis thaliana*, but only one third of the corresponding proteins are predicted to be retargeted into the chloroplast (Leister, 2003). The remaining proteins underwent redirections into other compartments (Leister, 2003). As a result of the outsourcing to the nuclear genome, the host gained control over the chloroplast function, which is regulated by retrograde (from chloroplast to nucleus)

and anterograde (from nucleus to chloroplast) signaling (Börner, 2017). In chloroplasts, the composition of photosynthetic complexes is a mixture of chloroplast genome and nucleus genome encoded proteins that consequently requires accurate regulation for correct formation (Leister, 2003).

Furthermore, the genes rearranged to the nuclear genome needed to acquire so-called N-terminal target sequences, which direct the encoded proteins post-translationally into the respective compartments and membranes (Smeekens et al., 1986).

PAM71 and CMT1 are chloroplast localized members of UPF0016

Two of the five *Arabidopsis thaliana* UPF0016 members, PAM71 and its closest homolog CMT1 (Chloroplast Mn²⁺ transporter 1) - also called BICAT2, for Bivalent cation transporter 2 (Frank et al., 2019), or PAM71-HL (Hoecker et al., 2017) harbor such cTP sequences (Hoecker et al., 2017). The PAM71 cTP directs the protein solely into the thylakoid membrane, where the protein is important for proper Mn loading of the OEC at PSII (Schneider et al., 2016). In contrast, CMT1 resides solely in the inner envelope of chloroplasts (Eisenhut et al., 2018; Zhang et al., 2018), which is in accordance with proteomic studies (Ferro et al., 2010; Ferro et al., 2003). In our proteomic analysis we verified the endogenous CMT1 protein in the envelope membrane, however endogenous PAM71 levels were below the limit of detection (Hoecker et al., 2021). The CMT1 cTP has a predicted size of 66 aa (amino acids) and the one from PAM71 of 73 aa (ChloroP, <http://www.cbs.dtu.dk/services/ChloroP/>, accessed 01.07.2021) while both do not have any significant similarities when aligned (BLASTp, <https://blast.ncbi.nlm.nih.gov/Blast.cgi>, accessed 01.07.2021). This phenomenon is also found when performing BLAST searches of the cTP of the Cu transporters HMA6 (envelope) and HMA8 (thylakoid membrane) where the former is 14 aa and the latter 63 aa (ChloroP, <http://www.cbs.dtu.dk/services/ChloroP/>, BLASTp, <https://blast.ncbi.nlm.nih.gov/Blast.cgi>, accessed 01.07.2021. Protein Sequences attached in Appendix). Thus, cTPs are very variable, can span between 20 aa and 100 aa and are largely unstructured (Bruce, 1998; Krimm et al., 1999; Wienk et al., 1999). One major protein import machinery of the chloroplast is the TIC/TOC (translocon inner/outer envelope) complex residing in the chloroplast envelope (Soll, 2002). After being imported through these complexes, the cTP gets directly cut off by so called SPP (stromal processing peptidase). In our case, CMT1 resides in the inner envelope while PAM71 needs to be transported further into the thylakoid lumen. Therefore, the cTP of PAM71 might possess a second cTP for targeting to the thylakoid membrane. However, 83 aa of the N-terminus are sufficient for directing homologous proteins of PAM71 (TMEM165, CMT1, MNX) into the thylakoid membrane, indicating that a second cTP might not be absolutely required for functionality (Hoecker et al., 2021). It is worth noting, that we used a prolonged version of the PAM71 cTP for the *Synechocystis* MNX in our experiments as this protein is lacking the 7th putative TM domain which may play an important role in proper orientation in the membrane. Thylakoid import can happen through the SEC (secretion route), TAT (twin-arginine translocation) or SRP (signal recognition proteins) pathway. It was shown that the transit peptide indicating the protein to be a substrate of the SEC or TAT pathway

consists of two arginine, followed by a hydrophobic domain (Wang & Dalbey, 2011). So far it is unclear which pathway is used by PAM71, in addition there is also the option of spontaneous insertion. Investigating how insertion of CMT1 and PAM71 into the respecting membrane is mediated, is a challenging task for future studies.

PAM71 and CMT1 managing chloroplast Mn homeostasis

The Mn transport ability of PAM71 and CMT1 was demonstrated, as both proteins can complement the *Δpmr* yeast mutant sensitivity to high Mn concentrations (Eisenhut et al., 2018; Schneider et al., 2016). In addition, an independent study used the yeast mutant *Δsmf1*, lacking a Mn^{2+} -only importer at the plasma membrane, which displays reduced growth under Mn deficiency. Expression of CMT1 in this yeast mutant also rescues the Mn deficiency phenotype as it restores the intracellular Mn^{2+} levels (Zhang et al., 2018), confirming CMT1 to be a Mn^{2+} transporter. The impact and importance of CMT1 for Mn homeostasis in the chloroplasts is supported by the drastical reduction of Mn concentrations in the chloroplasts of *cmt1* leading to reduced Mn binding in PSII complexes (Eisenhut et al., 2018; Zhang et al., 2018). A different study mentioned PAM71 and CMT1 to be Ca^{2+} importers into the thylakoid lumen and stroma, respectively (Frank et al., 2019). However, chloroplast Ca levels were even slightly increased in the *cmt1* mutant and CMT1 was not able to rescue the Ca^{2+} sensitive phenotype of the *Δgdt1* yeast mutant and therefore Zhang and colleagues concluded that CMT1 is specific for Mn transport (Zhang et al., 2018). Regarding PAM71 we showed that supplementing the growth media with Ca did not rescue the *pam71* phenotype and moreover the thylakoid lumen of *pam71* accumulated more radiolabelled Ca than the WT, indicating that the effect on Ca homeostasis might represent secondary effects. Furthermore, Mn supply to the growth media was able to restore the *pam71* phenotype back to WT phenotype - including its PSII performance. This suggests that phenotypic alterations in *pam71* are exclusively due to reduced Mn^{2+} transport into the thylakoid lumen and let us conclude that PAM71 acts as Mn^{2+} transporter (Figure 5). Nevertheless, the idea that CMT1 and PAM71 are unspecific bivalent cation transporter with a preference for Ca still persists in the literature. If the plant UPF0016 transporters are Ca^{2+}/Mn^{2+} transporter, it would be very difficult to transport enough Mn^{2+} to meet the high requirement of the OEC for this metal. To enable sufficient Mn^{2+} transport, the transport of Ca^{2+} would have to be tightly regulated. That is for example reported for a mitochondrial Ca uniporter, which changes its substrate specificity to Mn^{2+} when the regulatory interaction partner is missing (Kamer et al., 2018). There is no indication that PAM71 is dependent on a regulatory interaction partner (Hoecker et al., 2021). Furthermore, the difference in Mn^{2+} and Ca^{2+} concentration in chloroplast, with at least tenfold higher Ca^{2+} amounts (Zhang et al., 2018) would prefer PAM71 and CMT1 to transport Ca^{2+} instead of Mn^{2+} .

For *cmt1* and *pam71* it was shown that as a result of Mn^{2+} deficiency in the thylakoid lumen less Mn is incorporated into the OECs of PSII (Eisenhut et al., 2018; Schneider et al., 2016). As a consequence, the oxygen evolution reflecting the activity of PSII, is reduced as well as the electron transport rate through PSII and PSI (Eisenhut et al., 2018; Zhang et al., 2018).

Correspondingly, regulated energy dissipation, non-photochemical quenching (NPQ) of PSII and non-regulated energy dissipation (NO) of PSI increases in *cmt1*. If the electron transport through PSII and PSI is disturbed, it is likely that more ROS are produced and indeed, more superoxide anion radicals were detected in the *cmt1* mutant (Eisenhut et al., 2018).

The very severe phenotype of *cmt1* - compared to *pam71* - underlines the importance of Mn^{2+} for chloroplast development and also for Mn-dependent reactions in the stroma (Figure 5). Loss-of-function of both CMT1 and PAM71 did not result in a seedling lethal phenotype, but resembled more the one of *cmt1*, even being slightly better (Eisenhut et al., 2018). This observation confirms that the proteins are not redundant in function, but the effect of the loss of PAM71 in the background of *cmt1* possibly generates a moderate level of Mn^{2+} in the stroma which might keep Mn-dependent reactions there active/possible. Consequently, CMT1 is the limiting step in Mn^{2+} delivery into the chloroplast. Although nothing is known about the communication between chloroplast and nucleus - regarding sensing and regulating Mn homeostasis it is speculative, that mechanisms in the double mutant could have a positive effect in this communication. Conceivably, an unbalanced Mn^{2+} ratio between chloroplast stroma and thylakoid lumen in *cmt1* can result in higher amounts of superoxide anion radicals which may send stronger signal to cope with oxidation processes. The levels of MnSOD - residing in mitochondria - decreased under standard growth conditions in *cmt1* mutant plants (Eisenhut et al., 2018). A similar regulatory mechanism in *Chlamydomonas* might help to reduce MnSOD activity to promote PSII performance under Mn deficiency (Allen et al., 2007). In *cmt1* chloroplasts Zn levels seemed slightly higher than in WT or the complemented line (Eisenhut et al., 2018; Zhang et al., 2018). This might be explained by a higher requirement of Zn for the chloroplast Cu/Zn-dependent SOD. Although this only seems to help marginally, as *cmt1* and the double mutant *cmt1xpam71* accumulate superoxide anion radicals. Analyzing the amount of chloroplast localized SOD levels in *cmt1*, *pam71* and *cmt1xpam71* would therefore be interesting for future studies.

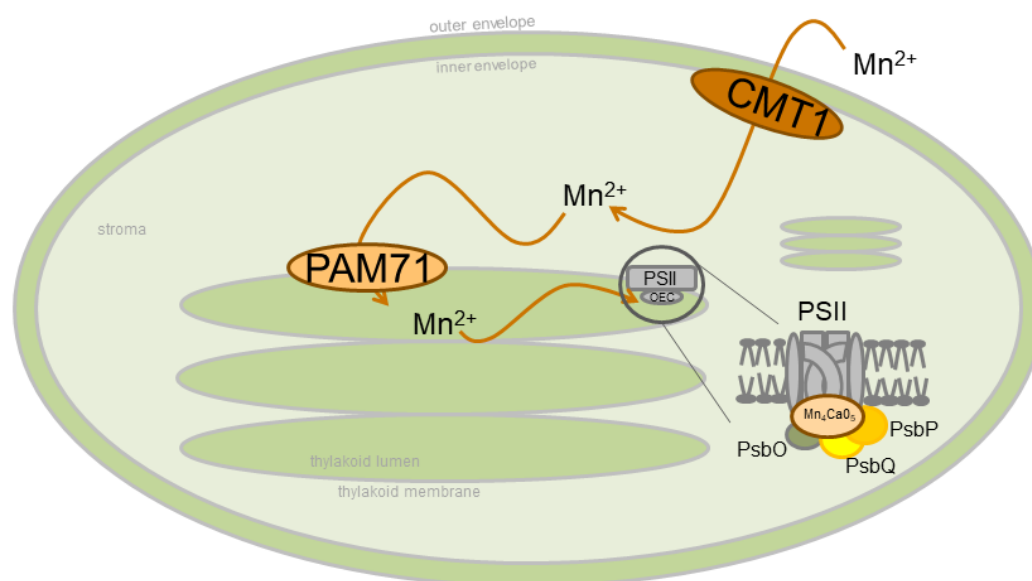


Figure 5 Schematic model for the Mn transport in chloroplasts by the proteins CMT1 and PAM71. CMT1 is transporting Mn^{2+} from the cytosol into the chloroplast stroma where it is then transported into the thylakoid lumen by PAM71. Afterwards, Mn^{2+} is incorporated into the OEC of PSII. In the stroma Mn^{2+} can be used for Mn-dependent reactions. Modified from (Schmidt et al., 2020; Zhang et al., 2018).

PML3, PML4 and PML5 as secretory pathway localized plant members of UPF0016

In plants, the UPF0016 family comprises mostly two chloroplast localized members as well as a variable number of proteins which are predicted to be substrates of the secretory pathway (Hoecker et al., 2017; Schneider et al., 2016). In *Arabidopsis thaliana*, the latter proteins are encoded by three genes, *At5g36290* (*GDT1-like 3*, renamed in *PML3*), *At1g25520* (*GDT1-like 4*, renamed in *PML4*) and *At1g68650* (*GDT1-like 5*, renamed in *PML5*). The genes coding for *PML4* and *PML5* are supposed to originate from a segmental chromosome duplication event in a progenitor of *Arabidopsis thaliana* (Hoecker et al., 2017). Localization studies revealed *PML4* and *PML5* to be localized in the ER membrane (Hoecker et al., 2020). The single mutant, as well as the double mutant did not display any altered phenotype under standard Mn or higher Mn concentrations (Hoecker et al., 2020), suggesting *PML4* and *PML5* being dispensable for proper plant metabolism. They both were expressed in the same organs, but slightly differ in their cell type expression as for example *PML4* was expressed in root hairs while *PML5* was expressed in the root stele (Hoecker et al., 2020). While knock-out of *ECA1*, coding for an ER localized Mn^{2+} transporter, resulted in defects in root hair elongation under Mn excess (Wu et al., 2002) neither *pml4*, *pml5* nor the *pml4xpml5* double mutant did show any alterations. This led to the idea of *PML4* and *PML5* being rather responsible for fine tuning of Mn allocation into the ER compartment, as *ECA1* can still supply enough Mn^{2+} for Mn-dependent enzymes - like for example the auxin amidohydrolases (LeClere et al., 2002). For further investigation of the role of *PML4* and *PML5*, it would be interesting to generate and test *pml4xpml5xeca1* triple mutants and double mutants of *pml4xeca1* and *pml5xeca1*. Additionally, the specificity towards Mn^{2+} of *PML4* and *PML5* needs to be analyzed.

The remaining protein, PML3, was localized in the Golgi membrane system - more precisely in the *cis*-Golgi (Hoecker et al., 2020; Yang et al., 2021; Zhang et al., 2021). Mn²⁺ transport ability was explored by Zhang et al. (2021). Because PML3 complements the Mn-associated phenotypes of Δpmr and $\Delta smf1$ yeast mutant strains, it can be regarded as Mn transporter (Yang et al., 2021; Zhang et al., 2021). *PML3* was expressed in all organs, but the highest expression was found in roots and Mn deficiency resulted in increased expression while other ion deficiencies (Fe, Zn) had no influence (Hoecker et al., 2020; Yang et al., 2021; Zhang et al., 2021). Several *pm13* alleles displayed reduced growth of roots and shoots under Mn deficiency conditions, which could be restored gradually by Mn supply (Yang et al., 2021; Zhang et al., 2021). Additionally, one study discovered curled leaves and brown spots in *pm13* mutant raised on Mn-deficient media which could be a result of disturbed Mn distribution inside the cells causing altered cell wall biosynthesis (Zhang et al., 2021). Pollen germination was affected, and pollen tube elongation was slower in *pm13* mutants leading to reduction in siliques size and seed fertility and pollen tubes display abnormal morphologies like swelling and branching (Zhang et al., 2021). Yang et al. suggested PML3 to play an important role in Golgi Mn homeostasis that can affect cell wall biosynthesis, for example the cellulose content was reduced in *pm13* under Mn deficiency, and could be reversed by adding Mn (Yang et al., 2021). Pollen tube elongation requires rapid biosynthesis and removal of cell wall components, that is why disturbance in those processes can affect pollen tube growth (Zhang et al., 2021). Enzymes regulating *N*-glycosylation, for example the α -mannosidases (MNS1, MNS2, MNS3), had decreased activity in the *pm13* mutant under Mn deficiency (Yang et al., 2021). Additionally, the RSW2 enzyme that regulates cell wall biosynthesis was reduced in *pm13* (Yang et al., 2021). It was suspected that the reduced cellulose amount under Mn deficiency was a consequence of reduced RSW2 protein and altered *N*-glycosylation of RSW2 in *pm13* plants (Yang et al., 2021). Overexpression of *PML3* in WT plants led to wrinkled leaves (Hoecker et al., 2020) which might indicate a disturbed cell wall composition as well. Overexpression of *PML3* might cause Mn²⁺ excess in the Golgi, which could affect *N*-glycosylation and hence cell wall biosynthesis. Like PML3, the human and yeast homologs influence Golgi Mn²⁺ levels and downstream Mn-dependent reactions (Potelle et al., 2016). The transporter NRAMP2 - also localized in the Golgi membrane - is releasing Mn²⁺ into the cytosol and is also required for proper plant growth and Mn distribution (Alejandro et al., 2017; Gao et al., 2018). Interestingly though, compared to *pm13* single mutant, the double knock out of *NRAMP2* and *PML3* were able to rescue the Mn deficiency phenotype (Yang et al., 2021). It was supposed, that reduced Mn release into the cytosol by loss of function of *NRAMP2* prevents high *pm13*-induced Mn deficiency in the Golgi (Yang et al., 2021). These findings solidified the impact of PML3 on Golgi Mn homeostasis and Mn-dependent reactions.

Taken all these together, PML3 is hypothesized to transport Mn²⁺ from the cytosol into the Golgi lumen, managing Mn homeostasis for proper cell wall biosynthesis and glycosylation which is especially important for rapid growing tissue (Yang et al., 2021; Zhang et al., 2021).

Manganese transport of UPF0016 proteins as an ancient feature

PAM71, CMT1 and PML3 are characterized as Mn^{2+} transporters of the thylakoid membrane, the inner envelope and the Golgi membrane, respectively. The human (TMEM165) and yeast (GDT1) homologs are supposed to have an extra function in Ca^{2+} transport - with GDT1 having higher affinity to Ca^{2+} - which gave rise to the suggestion that members of the UPF0016 are involved in Ca^{2+} transport as well. Several complementation studies - introducing truncated versions of TMEM165 (Stribny et al., 2020), PAM71 (Wang et al., 2016) into $\Delta gdt1$ and CMT1 into $\Delta pmr1\Delta gdt1$ (Frank et al., 2019) - suppressed their conditional phenotype when grown on high concentrations of Ca^{2+} . However, it is not clear whether the Ca^{2+} sensitivity of $\Delta gdt1$ mutants is only a result of Mn deficiency and introducing heterologous genes into the $\Delta gdt1$ mutant background might rescue Mn transport.

In the present work, complementation assays employing *pam71* and fusion proteins of the cTP from PAM71 with the (core)protein of the human TMEM165, the *Arabidopsis thaliana* CMT1 and the *Synechocystis* MNX were conducted. It turned out that all three proteins were able to completely rescue the *pam71* mutant phenotype (Hoecker et al., 2021). Mn binding in the OEC of PSII was restored in all three overexpressor lines, which resulted in the rescue of protein levels of photosynthetic complexes and ultimately in photosynthetic performance. For the *Synechocystis* Δmnx strain, it was shown that the intracellular Mn pool increased, while other ion pools - including Ca^{2+} - were nearly unaffected (Brandenburg et al., 2017; Gandini et al., 2017). It was concluded that MNX is a specific Mn transporter, like the only other - to date - characterized bacterial UPF0016 member from *Vibrio cholerae* MneA (Fisher et al., 2016). In $\Delta mneA$ strains an increased sensitivity to high extracellular Mn levels, as well as increased internal Mn pools, can be found (Fisher et al., 2016). In conclusion, this suggests a specific Mn-only transport function for bacterial members of the UPF0016 family. Because MNX was able to complement the *pam71* phenotype to wildtype levels the hypothesis of PAM71 to work as specific Mn^{2+} transporter is strengthened. In case that Ca^{2+} transport of PAM71 plays a significant physiological role, we would not have expected MNX to fully complement the plant phenotypes.

Taken together, *Synechocystis* MNX can functionally complement *pam71* and it is therefore obvious that the functionality of both proteins remained conserved since the endosymbiotic event. TMEM165 and plant secretory proteins seem to be introduced during an earlier gene transfer event (discussed in the following paragraph). Thus we concluded, the common functionality of UPF0016 transporter was established predating the endosymbiotic event, because even TMEM165 was able to substitute for PAM71 in *Arabidopsis thaliana* (Hoecker et al., 2021). Consequently, Mn^{2+} transport is an ancient feature of UPF0016 proteins.

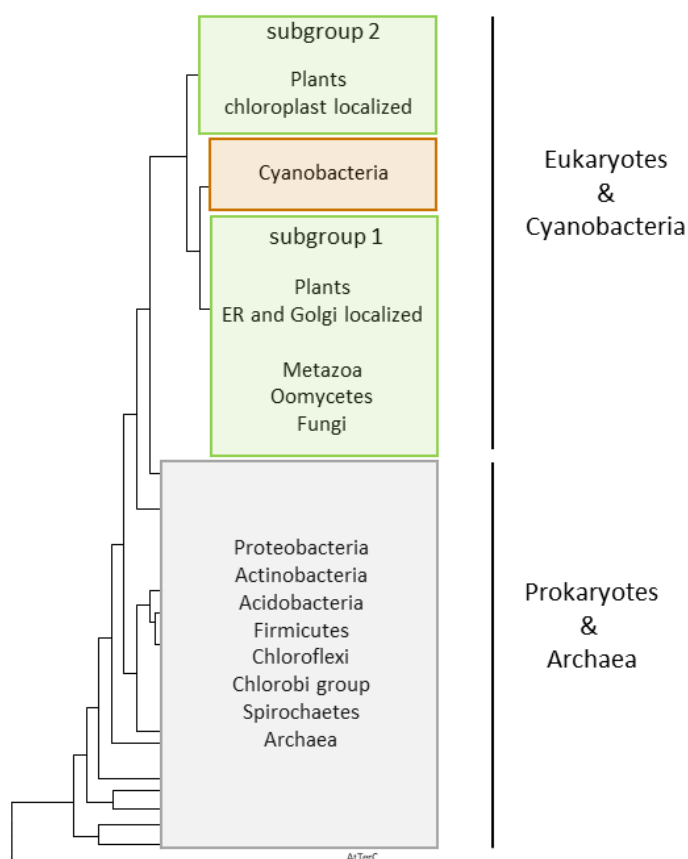


Figure 6 Schematic illustration of the phylogenetic analysis including two-clustered topology proteins of the UPF0016, modified from (Hoecker et al., 2021). Eukaryotes and cyanobacteria are more closely related than cyanobacteria to other prokaryotes and archaea (lower part, grey box).

If we take a closer look at the phylogeny of UPF0016, we can find interesting points regarding their evolution. Demaegd et al. (2014), separated the UPF0016 gene family into twelve subgroups (Figure 2) with two main groups - bacteria & archaea as the first and eukaryotes & cyanobacteria as the second group (Demaegd et al., 2014). They found cyanobacteria proteins of two-cluster topology - (corresponding to 6 TM domains) group VI - to be closer related to the ones of eukaryotes than to other bacteria and archaea proteins. The single-cluster cyanobacteria proteins (corresponding to 3 TM domains; group II and III, Figure 2) are closer related to prokaryotes and archaea (Demaegd et al., 2014). In our phylogenetic study we included all plant paralogs of *Arabidopsis thaliana* and *Oryza sativa* as representatives as well as other eukaryotic proteins (in total 24 eukaryotic proteins from 10 species), including human HsTMEM165 and yeast ScGDT1. Additionally, 33 proteins of prokaryotes which encompass only two-cluster topology proteins encoded by a single gene were included, and we rooted the tree on *Arabidopsis thaliana* TerC, which is also part of the LysE transporter superfamily. The two closely related chloroplast localized UPF0016 members - in *Arabidopsis thaliana* PAM71 and CMT1 - clustered together with their counterparts from other plant species - for example rice - which was referred to subgroup VII according to Demaegd et al. (2014). Our analysis returned the same tree with all chloroplast localized members clustered in subgroup 2 (See Figure 6, according to (Hoecker et al., 2021). The remaining plant homologs, as well as

the human and yeast ones were combined in subgroup 1. Both subgroups (1 and 2) were closely related to the cyanobacterial group and not to any other investigated bacterial phyla (see Figure 6) in accordance with the tree obtained by Demaegd et al. (2014) (Figure 2). Differences to the former classification according to Demaegd et al. (2014), appeared in our subgroup 1. We did not observe clear phylogenies among the eukaryotic members, for instance clustering of Golgi membrane localized proteins. Instead, the ER membrane localized homologs from plants (e.g., PML4 and PML5) seem to be closer related to the human TMEM165 and yeast GDT1, than to the Golgi membrane localized plant PML3 versions. This might indicate that the ancestral gene is the one coding for a protein directed to the ER membrane as it also represents the simplest version lacking a target peptide (e.g., PML4 or PML5). It could be that in the green lineage further duplication events evolved the gene *PML3*, coding for the Golgi membrane localized homolog, represented by its conservation from mosses to higher plants. Recently in evolution, *PML5* was generated from *PML4* by a segmental chromosome duplication in a progenitor of *Arabidopsis thaliana*.

With respect to the chloroplast localized proteins of subgroup 2 (containing AtCMT1 and AtPAM71) we postulate the respective gene arose from cyanobacteria through endosymbiotic gene transfer (EGT). During the endosymbiotic event that led to the implementation of chloroplasts in plants, this gene was transferred into the nuclear genome and duplicated later. It is well established that genes from the cyanobacteria ancestor were transferred to the nucleus and that the proteins they code for can replace each other (Leister, 2003, 2016; Savidge et al., 2002). This is further supported by the fact that *Synechocystis* MNX can replace PAM71 at the thylakoid membrane.

Manganese/Proton Antiport

UPF0016 members are hypothesized to work as secondary transporter (Thines et al., 2020). Loss of TMEM165 leads to an acidification of the human Golgi lumen due to reduced H⁺ transport into the cytoplasm (H. Wang et al., 2020). In addition, transport by GDT1 depends on the pH gradient between the cytosol and the Golgi lumen in yeast (Thines et al., 2020). In chloroplasts, usually, a strong proton gradient is generated across the thylakoid membrane during illumination (Höhner et al., 2016; Pottosin & Shabala, 2016). This proton gradient could be used to drive the Mn²⁺ uptake into the acidic thylakoid lumen via PAM71 (Schneider et al., 2016; Thines et al., 2020). With the cross-species complementation assays we could demonstrate that TMEM165, MNX and CMT1 are able to complement *pam71* (Hoecker et al., 2021), in addition to its ortholog from *Zea mays* (C. Wang et al., 2020). Consequently, if PAM71 is performing Mn²⁺/H⁺ antiport, the other proteins should have the same transport mechanism even though the precise transport mechanism of CMT1 is still far from being understood. Across the envelope membrane there is a proton gradient from the cytosol (pH 7) to the stroma (pH 8) during illumination (Höhner et al., 2016). Due to this, the situation at the envelope membrane is more complex and for example would require a local microenvironment, where the proton gradient is inversed to allow CMT1 to act in a Mn²⁺/H⁺ antiport mechanism. PAM71 cannot substitute CMT1 in *cmt1* mutant plants, thus it might not

be able to cope with the conditions prevailing at the envelope membrane or it simply might be not present in sufficient amounts (Hoecker et al., 2021).

In summary, it seems most likely that the UPF0016 proteins perform Mn^{2+} transport in exchange of protons. It is possible that several members, for example CMT1, gained specific features to influence the surrounding pH in order to make Mn^{2+} transport in exchange for protons possible. The fact that, for example, TMEM165 can replace PAM71 makes this even more interesting, as human Golgi membrane composition differs from the thylakoid membrane, indicating that - at least - the influence of the lipid composition might be negligible. To further confirm the substrate specificity and the H^+ antiport mechanism, direct transport assays will have to be performed in future.

Regulated Mn homeostasis is crucial for plant growth

Mn is the second most abundant trace metal in Earth's crust and it is widespread in soils, sediments and other biological materials (Geszvain et al., 2012). For plants, Mn availability depends on the pH and redox conditions of the soil (Geszvain et al., 2012; Sparrow & Uren, 2014). Mentioned and explained in the introduction, there are many enzymes using Mn as cofactor or as activator. Therefore, to be able to face Mn excess or deficiency, plants need a tightly regulated Mn homeostasis. High Mn levels can additionally cause ROS formation and for some species, for example perennial ryegrass, there is a sophisticated active antioxidation system reported (Ribera-Fonseca et al., 2013). Interestingly, *cmt1* had an overall reduction of Mn concentration in shoots, which could explain the observed smaller amounts of mitochondrial MnSOD which could have led to the accumulation of superoxide anion radicals (Eisenhut et al., 2018). Additionally, decreased Fe amounts in *cmt1* chloroplasts may result in a decreasing activity and/or amount of chloroplast localized FeSOD. Therefore, it would be interesting to further examine the antioxidation systems. To prevent high cytosolic Mn accumulation, a regulated Mn transport is of utmost importance for plant Mn homeostasis. This already starts with the uptake of Mn from roots, followed by the translocation and distribution into most plant organs and cell compartments. There are many protein families involved in this process, for example members of the ECA/NRAMP/CCX and CAX family, as well as the UPF0016 protein family (Figure 7). Some members of ECA, MTP, CAX, CCX are organizing the intracellular distribution into several (storage) compartments to prevent cytosol toxification. NRAMP family proteins are involved in releasing Mn from vacuoles and the Golgi apparatus into the cytosol to supply other compartments with Mn under Mn deficiency. All proteins of the UPF0016 family are hypothesized to act as Mn transporter. The two chloroplast localized members are the solely described Mn transporter importing Mn into the stroma (CMT1) and into the thylakoid lumen (PAM71, see Figure 5). Disturbing their functionality led to detrimental effects in chloroplast development (*cmt1*) and photosynthetic performance (*cmt1* and *pam71*) (Eisenhut et al., 2018; Schneider et al., 2016). The remaining members, localize in the ER membrane (PML4/PML5) (Hoecker et al., 2020) and the Golgi membrane localized PML3 is important for proper Mn supply into this compartment (Yang et al., 2021; Zhang et al., 2021).

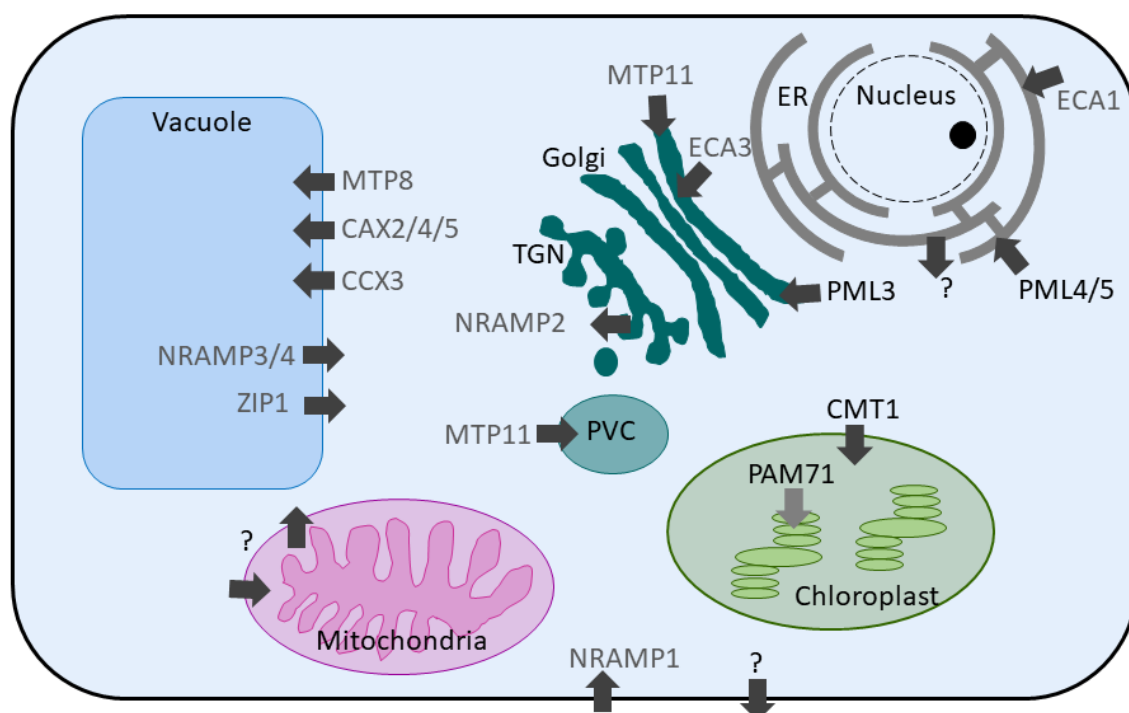


Figure 7 Characterized Mn^{2+} transporter of mesophyll cells in plants. Loading of mesophyll cells is performed by NRAMP1. Loading of Mn^{2+} into vacuoles by MTP8, CAX2/4/5, CCX3 and release by NRAMP3/4 and ZIP1. Members of the ECA and MTP family import Mn^{2+} into the ER lumen (ECA1) and Golgi lumen (ECA3, MTP8). The recently described UPF0016 members PML4/PML5 are supposed to be involved in ER loading and PML3 is crucial for Mn^{2+} transport into the Golgi apparatus. CMT1 and PAM71 are mediating chloroplast and thylakoid Mn uptake, respectively. Modified from (Alejandro et al., 2020).

In summary, we characterized the UPF0016 as Mn transport family, and Mn transport can be regarded as ancient feature of this protein family. There are still many open questions regarding regulation of Mn homeostasis, Mn sensing and signaling of the Mn status within a specific compartment. Future perspectives include investigation of the transport mechanisms, possibly Mn^{2+}/H^{+} antiport. This will contribute to a deeper understanding of Mn homeostasis in plants. Additionally, it would be important to identify proteins mediating mitochondrial Mn transport to improve the understanding of subcellular Mn distribution and possible crosslink between Mn transport and Mn-dependent antioxidation. How plants sense Mn deficiency or excess and send responding signals to the nucleus is unknown to date. Determining the underlying mechanisms in response to environmental changes and the interplay of different metal homeostasis could help speeding crop development. Crops that can quickly adapt to drought, heat stress and fluctuating nutrient availabilities are of great desire in the face of climate change and rising population.

9 References

- Abdel-Ghany, S. E., Müller-Moulé, P., Niyogi, K. K., Pilon, M., & Shikanai, T. (2005). Two P-type ATPases are required for copper delivery in *Arabidopsis thaliana* chloroplasts. *The Plant Cell*, 17(4), 1233-1251.
- Alejandro, S., Cailliatte, R., Alcon, C., Dirick, L., Domergue, F., Correia, D., Castaings, L., Briat, J.-F., Mari, S., & Curie, C. (2017). Intracellular distribution of manganese by the trans-Golgi network transporter NRAMP2 is critical for photosynthesis and cellular redox homeostasis. *The Plant Cell*, 29(12), 3068-3084.
- Alejandro, S., Höller, S., Meier, B., & Peiter, E. (2020). Manganese in plants: from acquisition to subcellular allocation. *Frontiers in plant science*, 11.
- Allen, M. D., Kropat, J., Tottey, S., Del Campo, J. A., & Merchant, S. S. (2007). Manganese deficiency in *Chlamydomonas* results in loss of photosystem II and MnSOD function, sensitivity to peroxides, and secondary phosphorus and iron deficiency. *Plant physiology*, 143(1), 263-277.
- Barker, A., Bloem, E., Brown, P., Bryson, G., Datnoff, L., De Kok, L., Drihem, K., Dunn, M., Gorham, J., & Graham, R. (2007). Handbook of Plant Nutrition; Barker, AV, Pilbeam, JD, Eds. In: Taylor and Francis CRC: Boca Raton, FL, USA.
- Barker, A. V., & Pilbeam, D. J. (2015). *Handbook of plant nutrition*. CRC press.
- Borgstahl, G. E., Parge, H. E., Hickey, M. J., Beyer Jr, W. F., Hallewell, R. A., & Tainer, J. A. (1992). The structure of human mitochondrial manganese superoxide dismutase reveals a novel tetrameric interface of two 4-helix bundles. *Cell*, 71(1), 107-118.
- Börner, T. (2017). The discovery of plastid-to-nucleus retrograde signaling—a personal perspective. *Protoplasma*, 254(5), 1845-1855.
- Boutigny, S., Sautron, E., Finazzi, G., Rivasseau, C., Frelet-Barrand, A., Pilon, M., Rolland, N., & Seigneurin-Berny, D. (2014). HMA1 and PAA1, two chloroplast-envelope PIB-ATPases, play distinct roles in chloroplast copper homeostasis. *Journal of Experimental Botany*, 65(6), 1529-1540.
- Bowler, C., Van Camp, W., Van Montagu, M., Inzé, D., & Asada, K. (1994). Superoxide dismutase in plants. *Critical Reviews in Plant Sciences*, 13(3), 199-218.
- Brandenburg, F., Schoffman, H., Kurz, S., Krämer, U., Keren, N., Weber, A. P., & Eisenhut, M. (2017). The *Synechocystis* MANGANESE EXPORTER Mnx is essential for manganese homeostasis in cyanobacteria. *Plant physiology*, 173(3), 1798-1810.
- Broadley, M., Brown, P., Cakmak, I., Rengel, Z., & Zhao, F. (2012). Function of nutrients: micronutrients. In *Marschner's mineral nutrition of higher plants* (pp. 191-248). Elsevier.
- Bruce, B. D. (1998). The role of lipids in plastid protein transport. *Protein trafficking in plant cells*, 223-246.
- Burnap, R. L. (2004). D1 protein processing and Mn cluster assembly in light of the emerging photosystem II structure. *Physical Chemistry Chemical Physics*, 6(20), 4803-4809.

- Cai, X., & Lytton, J. (2004). The cation/Ca²⁺ exchanger superfamily: phylogenetic analysis and structural implications. *Molecular biology and evolution*, 21(9), 1692-1703.
- Cailliatte, R., Schikora, A., Briat, J.-F., Mari, S., & Curie, C. (2010). High-affinity manganese uptake by the metal transporter NRAMP1 is essential for Arabidopsis growth in low manganese conditions. *The Plant Cell*, 22(3), 904-917.
- Cao, F.-Q., Werner, A. K., Dahncke, K., Romeis, T., Liu, L.-H., & Witte, C.-P. (2010). Identification and characterization of proteins involved in rice urea and arginine catabolism. *Plant physiology*, 154(1), 98-108.
- Castaigns, L., Caquot, A., Loubet, S., & Curie, C. (2016). The high-affinity metal transporters NRAMP1 and IRT1 team up to take up iron under sufficient metal provision. *Scientific reports*, 6(1), 1-11.
- Catty, P., Boutigny, S., Miras, R., Joyard, J., Rolland, N., & Seigneurin-Berny, D. (2011). Biochemical characterization of AtHMA6/PAA1, a chloroplast envelope Cu (I)-ATPase. *Journal of Biological Chemistry*, 286(42), 36188-36197.
- Chu, H.-H., Car, S., Socha, A. L., Hindt, M. N., Punshon, T., & Guerinot, M. L. (2017). The Arabidopsis MTP8 transporter determines the localization of manganese and iron in seeds. *Scientific reports*, 7(1), 1-10.
- Colinet, A.-S., Sengottaiyan, P., Deschamps, A., Colsoul, M.-L., Thines, L., Demaegd, D., Duchêne, M.-C., Foulquier, F., Hols, P., & Morsomme, P. (2016). Yeast Gdt1 is a Golgi-localized calcium transporter required for stress-induced calcium signaling and protein glycosylation. *Scientific reports*, 6(1), 1-11.
- Collin, S., Justin, A. M., Cantrel, C., Arondel, V., & Kader, J. C. (1999). Identification of AtPIS, a phosphatidylinositol synthase from Arabidopsis. *European journal of biochemistry*, 262(3), 652-658.
- Corpas, F. J., Barroso, J. B., Palma, J. M., & Rodriguez-Ruiz, M. (2017). Plant peroxisomes: a nitro-oxidative cocktail. *Redox Biology*, 11, 535-542.
- Curie, C., Alonso, J. M., JEAN, M. L., Ecker, J. R., & Briat, J.-F. (2000). Involvement of NRAMP1 from Arabidopsis thaliana in iron transport. *Biochemical Journal*, 347(3), 749-755.
- Dasgupta, J., Ananyev, G. M., & Dismukes, G. C. (2008). Photoassembly of the water-oxidizing complex in photosystem II. *Coordination chemistry reviews*, 252(3-4), 347-360.
- Delhaize, E., Gruber, B. D., Pittman, J. K., White, R. G., Leung, H., Miao, Y., Jiang, L., Ryan, P. R., & Richardson, A. E. (2007). A role for the AtMTP11 gene of Arabidopsis in manganese transport and tolerance. *The Plant Journal*, 51(2), 198-210.
- Demaegd, D., Colinet, A.-S., Deschamps, A., & Morsomme, P. (2014). Molecular evolution of a novel family of putative calcium transporters. *PloS one*, 9(6), e100851.
- Demaegd, D., Foulquier, F., Colinet, A.-S., Gremillon, L., Legrand, D., Mariot, P., Peiter, E., Van Schaftingen, E., Matthijs, G., & Morsomme, P. (2013). Newly characterized Golgi-localized family of proteins is involved in calcium and pH homeostasis in yeast and human cells. *Proceedings of the National Academy of Sciences*, 110(17), 6859-6864.
- Dulary, E., Potelle, S., Legrand, D., & Foulquier, F. (2017). TMEM165 deficiencies in Congenital Disorders of Glycosylation type II (CDG-II): Clues and evidences for roles of the protein

- in Golgi functions and ion homeostasis. *Tissue Cell*, 49(2 Pt A), 150-156. <https://doi.org/10.1016/j.tice.2016.06.006>
- Dulary, E., Yu, S. Y., Houdou, M., de Bettignies, G., Decool, V., Potelle, S., Duvet, S., Krzewinski-Recchi, M. A., Garat, A., Matthijs, G., Guerardel, Y., & Foulquier, F. (2018). Investigating the function of Gdt1p in yeast Golgi glycosylation. *Biochim Biophys Acta Gen Subj*, 1862(3), 394-402. <https://doi.org/10.1016/j.bbagen.2017.11.006>
- Durr, G., Strayle, J., Plemper, R., Elbs, S., Klee, S. K., Catty, P., Wolf, D. H., & Rudolph, H. K. (1998). The medial-Golgi ion pump Pmr1 supplies the yeast secretory pathway with Ca²⁺ and Mn²⁺ required for glycosylation, sorting, and endoplasmic reticulum-associated protein degradation. *Molecular biology of the cell*, 9(5), 1149-1162.
- Edmond, C., Shigaki, T., Ewert, S., Nelson, M. D., Connorton, J. M., Chalova, V., Noordally, Z., & Pittman, J. K. (2009). Comparative analysis of CAX2-like cation transporters indicates functional and regulatory diversity. *Biochemical Journal*, 418(1), 145-154.
- Eisenhut, M., Hoecker, N., Schmidt, S. B., Basgaran, R. M., Flachbart, S., Jahns, P., Eser, T., Geimer, S., Husted, S., Weber, A. P. M., Leister, D., & Schneider, A. (2018). The Plastid Envelope CHLOROPLAST MANGANESE TRANSPORTER1 Is Essential for Manganese Homeostasis in Arabidopsis. *Mol Plant*, 11(7), 955-969. <https://doi.org/10.1016/j.molp.2018.04.008>
- Engelsma, G. (1972). A possible role of divalent manganese ions in the photoinduction of phenylalanine ammonia-lyase. *Plant physiology*, 50(5), 599-602.
- Entus, R., Poling, M., & Herrmann, K. M. (2002). Redox regulation of Arabidopsis 3-deoxy-D-arabino-heptulosonate 7-phosphate synthase. *Plant physiology*, 129(4), 1866-1871.
- Eppstein, E. (1972). Mineral nutrition of plants and perspectives.
- Eroglu, S., Giehl, R. F., Meier, B., Takahashi, M., Terada, Y., Ignatyev, K., Andresen, E., Küpper, H., Peiter, E., & Von Wiren, N. (2017). Metal tolerance protein 8 mediates manganese homeostasis and iron reallocation during seed development and germination. *Plant physiology*, 174(3), 1633-1647.
- Ferro, M., Brugière, S., Salvi, D., Seigneurin-Berny, D., Court, M., Moyet, L., Ramus, C., Miras, S., Mellal, M., & Le Gall, S. (2010). AT_CHLORO, a comprehensive chloroplast proteome database with subplastidial localization and curated information on envelope proteins. *Molecular & Cellular Proteomics*, 9(6), 1063-1084.
- Ferro, M., Salvi, D., Brugière, S., Miras, S., Kowalski, S., Louwagie, M., Garin, J., Joyard, J., & Rolland, N. (2003). Proteomics of the chloroplast envelope membranes from Arabidopsis thaliana. *Molecular & Cellular Proteomics*, 2(5), 325-345.
- Fisher, C. R., Wyckoff, E. E., Peng, E. D., & Payne, S. M. (2016). Identification and characterization of a putative manganese export protein in Vibrio cholerae. *Journal of bacteriology*, 198(20), 2810-2817.
- Foulquier, F. (2009). COG defects, birth and rise! *Biochimica et Biophysica Acta (BBA)-Molecular Basis of Disease*, 1792(9), 896-902.
- Foulquier, F., Amyere, M., Jaeken, J., Zeevaert, R., Schollen, E., Race, V., Bammens, R., Morelle, W., Rosnoblet, C., & Legrand, D. (2012). TMEM165 deficiency causes a congenital disorder of glycosylation. *The American Journal of Human Genetics*, 91(1), 15-26.

- Foulquier, F., Ungar, D., Reynders, E., Zeevaert, R., Mills, P., García-Silva, M. T., Briones, P., Winchester, B., Morelle, W., & Krieger, M. (2007). A new inborn error of glycosylation due to a Cog8 deficiency reveals a critical role for the Cog1–Cog8 interaction in COG complex formation. *Human molecular genetics*, 16(7), 717-730.
- Foulquier, F., Vasile, E., Schollen, E., Callewaert, N., Raemaekers, T., Quelhas, D., Jaeken, J., Mills, P., Winchester, B., & Krieger, M. (2006). Conserved oligomeric Golgi complex subunit 1 deficiency reveals a previously uncharacterized congenital disorder of glycosylation type II. *Proceedings of the National Academy of Sciences*, 103(10), 3764-3769.
- Frank, J., Happeck, R., Meier, B., Hoang, M. T. T., Stribny, J., Hause, G., Ding, H., Morsomme, P., Baginsky, S., & Peiter, E. (2019). Chloroplast-localized BICAT proteins shape stromal calcium signals and are required for efficient photosynthesis. *New Phytologist*, 221(2), 866-880.
- Gandini, C., Schmidt, S. B., Husted, S., Schneider, A., & Leister, D. (2017). The transporter SynPAM71 is located in the plasma membrane and thylakoids, and mediates manganese tolerance in *Synechocystis* PCC6803. *New Phytol*, 215(1), 256-268. <https://doi.org/10.1111/nph.14526>
- Gao, H., Xie, W., Yang, C., Xu, J., Li, J., Wang, H., Chen, X., & Huang, C. F. (2018). NRAMP2, a trans-Golgi network-localized manganese transporter, is required for Arabidopsis root growth under manganese deficiency. *New Phytologist*, 217(1), 179-193.
- Geszvain, K., Butterfield, C., Davis, R. E., Madison, A. S., Lee, S.-W., Parker, D. L., Soldatova, A., Spiro, T. G., Luther III, G. W., & Tebo, B. M. (2012). The molecular biogeochemistry of manganese (II) oxidation. *Biochemical Society Transactions*, 40(6), 1244-1248.
- Hebert, D. N., Lamriben, L., Powers, E. T., & Kelly, J. W. (2014). The intrinsic and extrinsic effects of N-linked glycans on glycoproteostasis. *Nature chemical biology*, 10(11), 902-910.
- Hoecker, N., Hennecke, Y., Schrott, S., Marino, G., Schmidt, S. B., Leister, D., & Schneider, A. (2021). Gene replacement in Arabidopsis reveals manganese transport as an ancient feature of human, plant and cyanobacterial UPF0016 proteins. *Frontiers in plant science*, 12, 1157.
- Hoecker, N., Honke, A., Frey, K., Leister, D., & Schneider, A. (2020). Homologous Proteins of the Manganese Transporter PAM71 Are Localized in the Golgi Apparatus and Endoplasmic Reticulum. *Plants*, 9(2), 239.
- Hoecker, N., Leister, D., & Schneider, A. (2017). Plants contain small families of UPF0016 proteins including the PHOTOSYNTHESIS AFFECTED MUTANT71 transporter. *Plant Signal Behav*, 12(2), e1278101. <https://doi.org/10.1080/15592324.2016.1278101>
- Höhner, R., Aboukila, A., Kunz, H.-H., & Venema, K. (2016). Proton gradients and proton-dependent transport processes in the chloroplast. *Frontiers in plant science*, 7, 218.
- Hood, M. I., & Skaar, E. P. (2012). Nutritional immunity: transition metals at the pathogen–host interface. *Nature Reviews Microbiology*, 10(8), 525-537.

- Huda, K. M. K., Yadav, S., Banu, M. S. A., Trivedi, D. K., & Tuteja, N. (2013). Genome-wide analysis of plant-type II Ca²⁺ ATPases gene family from rice and Arabidopsis: potential role in abiotic stresses. *Plant Physiology and Biochemistry*, 65, 32-47.
- Hüttner, S., Veit, C., Vavra, U., Schoberer, J., Liebminger, E., Maresch, D., Grass, J., Altmann, F., Mach, L., & Strasser, R. (2014). Arabidopsis class I α -mannosidases MNS4 and MNS5 are involved in endoplasmic reticulum-associated degradation of misfolded glycoproteins. *The Plant Cell*, 26(4), 1712-1728.
- Ingle, R. A. (2011). Histidine biosynthesis. *The Arabidopsis Book/American Society of Plant Biologists*, 9.
- Irving, H., & Williams, R. (1948). Order of stability of metal complexes. *Nature*, 162(4123), 746-747.
- Jaeken, J., Hennet, T., Matthijs, G., & Freeze, H. H. (2009). CDG nomenclature: time for a change! *Biochimica et biophysica acta*, 1792(9), 825-826.
- Jaeken, J., & Matthijs, G. (2007). Congenital disorders of glycosylation: a rapidly expanding disease family. *Annu. Rev. Genomics Hum. Genet.*, 8, 261-278.
- Kamer, K. J., Sancak, Y., Fomina, Y., Meisel, J. D., Chaudhuri, D., Grabarek, Z., & Mootha, V. K. (2018). MICU1 imparts the mitochondrial uniporter with the ability to discriminate between Ca²⁺ and Mn²⁺. *Proceedings of the National Academy of Sciences*, 115(34), E7960-E7969.
- Kaneko, T., & Tabata, S. (1997). Complete genome structure of the unicellular cyanobacterium *Synechocystis* sp. PCC6803. *Plant and Cell Physiology*, 38(11), 1171-1176.
- Keeling, P. J. (2004). Diversity and evolutionary history of plastids and their hosts. *American journal of botany*, 91(10), 1481-1493.
- Kern, J., Chatterjee, R., Young, I. D., Fuller, F. D., Lassalle, L., Ibrahim, M., Gul, S., Fransson, T., Brewster, A. S., & Alonso-Mori, R. (2018). Structures of the intermediates of Kok's photosynthetic water oxidation clock. *Nature*, 563(7731), 421-425.
- Kok, B., Forbush, B., & McGloin, M. (1970). Cooperation of charges in photosynthetic O₂ evolution—I. A linear four step mechanism. *Photochemistry and Photobiology*, 11(6), 457-475.
- Köllner, T. G., Held, M., Lenk, C., Hiltbold, I., Turlings, T. C., Gershenzon, J., & Degenhardt, J. (2008). A maize (E)- β -caryophyllene synthase implicated in indirect defense responses against herbivores is not expressed in most American maize varieties. *The Plant Cell*, 20(2), 482-494.
- Koren'kov, V., Park, S., Cheng, N.-H., Sreevidya, C., Lachmansingh, J., Morris, J., Hirschi, K., & Wagner, G. (2007). Enhanced Cd²⁺-selective root-tonoplast-transport in tobaccos expressing Arabidopsis cation exchangers. *Planta*, 225(2), 403-411.
- Kornak, U., Reynders, E., Dimopoulou, A., Van Reeuwijk, J., Fischer, B., Rajab, A., Budde, B., Nürnberg, P., Foulquier, F., & Lefeber, D. (2008). Impaired glycosylation and cutis laxa caused by mutations in the vesicular H⁺-ATPase subunit ATP6V0A2. *Nature genetics*, 40(1), 32-34.

- Korshunova, Y. O., Eide, D., Clark, W. G., Guerinot, M. L., & Pakrasi, H. B. (1999). The IRT1 protein from *Arabidopsis thaliana* is a metal transporter with a broad substrate range. *Plant molecular biology*, 40(1), 37-44.
- Krimm, I., Gans, P., Hernandez, J. F., Arlaud, G. J., & Lancelin, J. M. (1999). A coil-helix instead of a helix-coil motif can be induced in a chloroplast transit peptide from *Chlamydomonas reinhardtii*. *European journal of biochemistry*, 265(1), 171-180.
- Lane, D. R., Wiedemeier, A., Peng, L., Höfte, H., Vernhettes, S., Desprez, T., Hocart, C. H., Birch, R. J., Baskin, T. I., & Burn, J. E. (2001). Temperature-sensitive alleles of RSW2 link the KORRIGAN endo-1, 4- β -glucanase to cellulose synthesis and cytokinesis in *Arabidopsis*. *Plant physiology*, 126(1), 278-288.
- Lanquar, V., Lelièvre, F., Bolte, S., Hamès, C., Alcon, C., Neumann, D., Vansuyt, G., Curie, C., Schröder, A., & Krämer, U. (2005). Mobilization of vacuolar iron by AtNRAMP3 and AtNRAMP4 is essential for seed germination on low iron. *The EMBO journal*, 24(23), 4041-4051.
- Lanquar, V., Ramos, M. S., Lelièvre, F., Barbier-Brygoo, H., Krieger-Liszkay, A., Krämer, U., & Thomine, S. (2010). Export of vacuolar manganese by AtNRAMP3 and AtNRAMP4 is required for optimal photosynthesis and growth under manganese deficiency. *Plant physiology*, 152(4), 1986-1999.
- Lebredonchel, E., Houdou, M., Potelle, S., De Bettignies, G., Schulz, C., Recchi, M.-A. K., Lupashin, V., Legrand, D., Klein, A., & Foulquier, F. (2019). Dissection of TMEM165 function in Golgi glycosylation and its Mn²⁺ sensitivity. *Biochimie*, 165, 123-130.
- LeClere, S., Tellez, R., Rampey, R. A., Matsuda, S. P., & Bartel, B. (2002). Characterization of a family of IAA-amino acid conjugate hydrolases from *Arabidopsis*. *Journal of Biological Chemistry*, 277(23), 20446-20452.
- Leister, D. (2003). Chloroplast research in the genomic age. *TRENDS in Genetics*, 19(1), 47-56.
- Leister, D. (2016). Towards understanding the evolution and functional diversification of DNA-containing plant organelles. *F1000Research*, 5.
- Liberton, M. (2008). Membrane systems in cyanobacteria.
- Liebming, E., Hüttner, S., Vavra, U., Fischl, R., Schoberer, J., Grass, J., Blaukopf, C., Seifert, G. J., Altmann, F., & Mach, L. (2009). Class I α -mannosidases are required for N-glycan processing and root development in *Arabidopsis thaliana*. *The Plant Cell*, 21(12), 3850-3867.
- Lisher, J. P., & Giedroc, D. P. (2013). Manganese acquisition and homeostasis at the host-pathogen interface. *Frontiers in cellular and infection microbiology*, 3, 91.
- Liu, C., Niu, G., Zhang, H., Sun, Y., Sun, S., Yu, F., Lu, S., Yang, Y., Li, J., & Hong, Z. (2018). Trimming of N-glycans by the Golgi-localized α -1, 2-mannosidases, MNS1 and MNS2, is crucial for maintaining RSW2 protein abundance during salt stress in *Arabidopsis*. *Molecular plant*, 11(5), 678-690.
- Lovley, D. R., Ueki, T., Zhang, T., Malvankar, N. S., Shrestha, P. M., Flanagan, K. A., Aklujkar, M., Butler, J. E., Giloteaux, L., & Rotaru, A.-E. (2011). Geobacter: the microbe electric's physiology, ecology, and practical applications. *Advances in microbial physiology*, 59, 1-100.

- Lynch, J. P., & Clair, S. B. S. (2004). Mineral stress: the missing link in understanding how global climate change will affect plants in real world soils. *Field Crops Research*, 90(1), 101-115.
- Maréchal, E. (2018). Primary endosymbiosis: emergence of the primary chloroplast and the chromatophore, two independent events. *Plastids*, 3-16.
- Marschner, H. (1995). Mineral nutrition of higher plants. *Mineral nutrition of higher plants*. (Ed. 2).
- Marschner, H., & Marschner, P. (2012). *Marschner's mineral nutrition of higher plants/Mineral nutrition of higher plants* (0123849055).
- Martin, W. F., Garg, S., & Zimorski, V. (2015). Endosymbiotic theories for eukaryote origin. *Philosophical Transactions of the Royal Society B: Biological Sciences*, 370(1678), 20140330.
- Merchant, S. S. (2007). Trace metal utilization in chloroplasts. In *The structure and function of plastids* (pp. 199-218). Springer.
- Mittler, R. (2017). ROS are good. *Trends in Plant Science*, 22(1), 11-19.
- Nowicki, M., Müller, F., & Frentzen, M. (2005). Cardiolipin synthase of *Arabidopsis thaliana*. *FEBS letters*, 579(10), 2161-2165.
- Nunan, K. J., & Scheller, H. V. (2003). Solubilization of an arabinan arabinosyltransferase activity from mung bean hypocotyls. *Plant Physiol*, 132(1), 331-342. <https://doi.org/10.1104/pp.102.019406>
- Peiter, E., Montanini, B., Gobert, A., Pedas, P., Husted, S., Maathuis, F. J., Blaudez, D., Chalot, M., & Sanders, D. (2007). A secretory pathway-localized cation diffusion facilitator confers plant manganese tolerance. *Proceedings of the National Academy of Sciences*, 104(20), 8532-8537.
- Petersen, T. N., Brunak, S., Von Heijne, G., & Nielsen, H. (2011). SignalP 4.0: discriminating signal peptides from transmembrane regions. *Nature methods*, 8(10), 785-786.
- Pittman, J. K. (2011). Vacuolar Ca²⁺ uptake. *Cell calcium*, 50(2), 139-146.
- Pittman, J. K., Shigaki, T., Marshall, J. L., Morris, J. L., Cheng, N.-H., & Hirschi, K. D. (2004). Functional and regulatory analysis of the *Arabidopsis thaliana* CAX2 cation transporter. *Plant molecular biology*, 56(6), 959-971.
- Potelle, S., Dulary, E., Climer, L., Duvet, S., Morelle, W., Vicogne, D., Lebredonchel, E., Houdou, M., Spriet, C., Krzewinski-Recchi, M. A., Peanne, R., Klein, A., de Bettignies, G., Morsomme, P., Matthijs, G., Marquardt, T., Lupashin, V., & Foulquier, F. (2017). Manganese-induced turnover of TMEM165. *Biochem J*, 474(9), 1481-1493. <https://doi.org/10.1042/BCJ20160910>
- Potelle, S., Morelle, W., Dulary, E., Duvet, S., Vicogne, D., Spriet, C., Krzewinski-Recchi, M.-A., Morsomme, P., Jaeken, J., & Matthijs, G. (2016). Glycosylation abnormalities in Gdt1p/TMEM165 deficient cells result from a defect in Golgi manganese homeostasis. *Human molecular genetics*, 25(8), 1489-1500.
- Pottosin, I., & Shabala, S. (2016). Transport across chloroplast membranes: optimizing photosynthesis for adverse environmental conditions. *Molecular plant*, 9(3), 356-370.

- Pribil, M., Pesaresi, P., Hertle, A., Barbato, R., & Leister, D. (2010). Role of plastid protein phosphatase TAP38 in LHCII dephosphorylation and thylakoid electron flow. *PLoS Biol*, 8(1), e1000288.
- Rawson, S., Bisson, C., Hurdiss, D. L., Fazal, A., McPhillie, M. J., Sedelnikova, S. E., Baker, P. J., Rice, D. W., & Muench, S. P. (2018). Elucidating the structural basis for differing enzyme inhibitor potency by cryo-EM. *Proceedings of the National Academy of Sciences*, 115(8), 1795-1800.
- Reinhardt, T. A., Lippolis, J. D., & Sacco, R. E. (2014). The Ca²⁺/H⁺ antiporter TMEM165 expression, localization in the developing, lactating and involuting mammary gland parallels the secretory pathway Ca²⁺ ATPase (SPCA1). *Biochemical and biophysical research communications*, 445(2), 417-421.
- Rengel, Z. (2000). Manganese uptake and transport in plants. *Metal ions in biological systems*, 37, 57-87.
- Reynders, E., Foulquier, F., Annaert, W., & Matthijs, G. (2011). How Golgi glycosylation meets and needs trafficking: the case of the COG complex. *Glycobiology*, 21(7), 853-863.
- Reynders, E., Foulquier, F., Leão Teles, E., Quelhas, D., Morelle, W., Rabouille, C., Annaert, W., & Matthijs, G. (2009). Golgi function and dysfunction in the first COG4-deficient CDG type II patient. *Human molecular genetics*, 18(17), 3244-3256.
- Ribera-Fonseca, A., Inostroza-Blancheteau, C., Cartes, P., Rengel, Z., & Mora, M. (2013). Early induction of Fe-SOD gene expression is involved in tolerance to Mn toxicity in perennial ryegrass. *Plant Physiology and Biochemistry*, 73, 77-82.
- Romero, P., & Herscovics, A. (1989). Glycoprotein biosynthesis in *Saccharomyces cerevisiae*: characterization of α -1, 6-mannosyltransferase which initiates outer chain formation. *Journal of Biological Chemistry*, 264(4), 1946-1950.
- Rosnoblet, C., Legrand, D., Demaegd, D., Hacine-Gherbi, H., De Bettignies, G., Bammens, R., Borrego, C., Duvet, S., Morsomme, P., & Matthijs, G. (2013). Impact of disease-causing mutations on TMEM165 subcellular localization, a recently identified protein involved in CDG-II. *Human molecular genetics*, 22(14), 2914-2928.
- Rudolph, H. K., Antebi, A., Fink, G. R., Buckley, C. M., Dorman, T. E., LeVitre, J., Davidow, L. S., Mao, J.-i., & Moir, D. T. (1989). The yeast secretory pathway is perturbed by mutations in PMR1, a member of a Ca²⁺ ATPase family. *Cell*, 58(1), 133-145.
- Sato, S., Nakamura, Y., Kaneko, T., Asamizu, E., & Tabata, S. (1999). Complete structure of the chloroplast genome of *Arabidopsis thaliana*. *DNA research*, 6(5), 283-290.
- Savidge, B., Weiss, J. D., Wong, Y.-H. H., Lassner, M. W., Mitsky, T. A., Shewmaker, C. K., Post-Beittenmiller, D., & Valentin, H. E. (2002). Isolation and characterization of homogentisate phytyltransferase genes from *Synechocystis* sp. PCC 6803 and *Arabidopsis*. *Plant physiology*, 129(1), 321-332.
- Schachter, H., & Freeze, H. H. (2009). Glycosylation diseases: quo vadis? *Biochimica et Biophysica Acta (BBA)-Molecular Basis of Disease*, 1792(9), 925-930.
- Schmidt, S. B., Eisenhut, M., & Schneider, A. (2020). Chloroplast transition metal regulation for efficient photosynthesis. *Trends in Plant Science*, 25(8), 817-828.

- Schmidt, S. B., & Husted, S. (2019). The biochemical properties of manganese in plants. *Plants*, 8(10), 381.
- Schmidt, S. B., Jensen, P. E., & Husted, S. (2016). Manganese deficiency in plants: the impact on photosystem II. *Trends in Plant Science*, 21(7), 622-632.
- Schneider, A., Steinberger, I., Herdean, A., Gandini, C., Eisenhut, M., Kurz, S., Morper, A., Hoecker, N., Ruhle, T., Labs, M., Flugge, U. I., Geimer, S., Schmidt, S. B., Husted, S., Weber, A. P., Spetea, C., & Leister, D. (2016). The Evolutionarily Conserved Protein PHOTOSYNTHESIS AFFECTED MUTANT71 Is Required for Efficient Manganese Uptake at the Thylakoid Membrane in Arabidopsis. *Plant Cell*, 28(4), 892-910. <https://doi.org/10.1105/tpc.15.00812>
- Schneider, A., Steinberger, I., Strissel, H., Kunz, H. H., Manavski, N., Meurer, J., Burkhard, G., Jarzombski, S., Schünemann, D., & Geimer, S. (2014). The Arabidopsis Tellurite resistance C protein together with ALB 3 is involved in photosystem II protein synthesis. *The Plant Journal*, 78(2), 344-356.
- Schwacke, R., Schneider, A., van der Graaff, E., Fischer, K., Catoni, E., Desimone, M., Frommer, W. B., Flügge, U.-I., & Kunze, R. (2003). ARAMEMNON, a novel database for Arabidopsis integral membrane proteins. *Plant physiology*, 131(1), 16-26.
- Shikanai, T., Müller-Moulé, P., Munekage, Y., Niyogi, K. K., & Pilon, M. (2003). PAA1, a P-type ATPase of Arabidopsis, functions in copper transport in chloroplasts. *The Plant Cell*, 15(6), 1333-1346.
- Simm, S., Papasotiriou, D., Ibrahim, M., Leisegang, M., Müller, B., Schorge, T., Karas, M., Mirus, O., Sommer, M., & Schleiff, E. (2013). Defining the core proteome of the chloroplast envelope membranes. *Frontiers in plant science*, 4, 11.
- Smeekens, S., Bauerle, C., Hageman, J., Keegstra, K., & Weisbeek, P. (1986). The role of the transit peptide in the routing of precursors toward different chloroplast compartments. *Cell*, 46(3), 365-375.
- Socha, A. L., & Gueriot, M. L. (2014). Mn-euvering manganese: the role of transporter gene family members in manganese uptake and mobilization in plants. *Frontiers in plant science*, 5, 106.
- Soll, J. (2002). Protein import into chloroplasts. *Current opinion in plant biology*, 5(6), 529-535.
- Sparrow, L., & Uren, N. (2014). Manganese oxidation and reduction in soils: effects of temperature, water potential, pH and their interactions. *Soil Research*, 52(5), 483-494.
- Strasser, R. (2014). Biological significance of complex N-glycans in plants and their impact on plant physiology. *Frontiers in plant science*, 5, 363.
- Strasser, R. (2016). Plant protein glycosylation. *Glycobiology*, 26(9), 926-939.
- Stribny, J., Thines, L., Deschamps, A., Goffin, P., & Morsomme, P. (2020). The human Golgi protein TMEM165 transports calcium and manganese in yeast and bacterial cells. *Journal of Biological Chemistry*, 295(12), 3865-3874.
- Szurmak, B., Wyśłouch-Cieszyńska, A., Wszelaka-Rylik, M., Bal, W., & Dobrzańska, M. (2008). A diadenosine 5', 5''-P1P4 tetraphosphate (Ap4A) hydrolase from Arabidopsis thaliana that is activated preferentially by Mn²⁺ ions. *Acta Biochimica Polonica*, 55(1), 151-160.

- Takahashi, S., Sakamoto, A. N., Tanaka, A., & Shimizu, K. (2007). AtREV1, a Y-family DNA polymerase in Arabidopsis, has deoxynucleotidyl transferase activity in vitro. *Plant physiology*, 145(3), 1052-1060.
- Thines, L., Deschamps, A., Sengottaiyan, P., Savel, O., Stribny, J., & Morsomme, P. (2018). The yeast protein Gdt1p transports Mn²⁺ ions and thereby regulates manganese homeostasis in the Golgi. *Journal of Biological Chemistry*, 293(21), 8048-8055.
- Thines, L., Stribny, J., & Morsomme, P. (2020). From the Uncharacterized Protein Family 0016 to the GDT1 family: Molecular insights into a newly-characterized family of cation secondary transporters. *Microbial Cell*, 7(8), 202.
- Thomine, S., Lelièvre, F., Debarbieux, E., Schroeder, J. I., & Barbier-Brygoo, H. (2003). AtNRAMP3, a multispecific vacuolar metal transporter involved in plant responses to iron deficiency. *The Plant Journal*, 34(5), 685-695.
- Tsu, B. V., & Saier Jr, M. H. (2015). The LysE superfamily of transport proteins involved in cell physiology and pathogenesis. *PloS one*, 10(10), e0137184.
- Vinothkumar, K. R., & Henderson, R. (2010). Structures of membrane proteins. *Quarterly reviews of biophysics*, 43(1), 65-158.
- von Heijne, G. (2006). Membrane-protein topology. *Nature reviews Molecular cell biology*, 7(12), 909-918.
- Waight, A. B., Pedersen, B. P., Schlessinger, A., Bonomi, M., Chau, B. H., Roe-Zurz, Z., Risenmay, A. J., Sali, A., & Stroud, R. M. (2013). Structural basis for alternating access of a eukaryotic calcium/proton exchanger. *Nature*, 499(7456), 107-110.
- Wang, C., Ou, D., Wang, C., Lu, X., Du, J., Li, J., Lai, J., Zhang, S., & Yang, C. (2020). Functional characterization of a chloroplast-localized Mn²⁺ (Ca²⁺)/H⁺ antiporter, ZmmCCHA1 from Zea mays ssp. mexicana L. *Plant Physiology and Biochemistry*, 155, 396-405.
- Wang, C., Xu, W., Jin, H., Zhang, T., Lai, J., Zhou, X., Zhang, S., Liu, S., Duan, X., & Wang, H. (2016). A putative chloroplast-localized Ca²⁺/H⁺ antiporter CCHA1 is involved in calcium and pH homeostasis and required for PSII function in Arabidopsis. *Molecular plant*, 9(8), 1183-1196.
- Wang, H., Yang, Y., Huang, F., He, Z., Li, P., Zhang, W., Zhang, W., & Tang, B. (2020). In situ fluorescent and photoacoustic imaging of Golgi pH to elucidate the function of transmembrane protein 165. *Analytical chemistry*, 92(4), 3103-3110.
- Wang, P., & Dalbey, R. E. (2011). Inserting membrane proteins: the YidC/Oxa1/Alb3 machinery in bacteria, mitochondria, and chloroplasts. *Biochimica et Biophysica Acta (BBA)-Biomembranes*, 1808(3), 866-875.
- Waters, B. M., Chu, H.-H., DiDonato, R. J., Roberts, L. A., Eisley, R. B., Lahner, B., Salt, D. E., & Walker, E. L. (2006). Mutations in Arabidopsis yellow stripe-like1 and yellow stripe-like3 reveal their roles in metal ion homeostasis and loading of metal ions in seeds. *Plant physiology*, 141(4), 1446-1458.
- Waters, L. S., Sandoval, M., & Storz, G. (2011). The Escherichia coli MntR miniregulon includes genes encoding a small protein and an efflux pump required for manganese homeostasis. *Journal of bacteriology*, 193(21), 5887-5897.

- Wei, X., Guo, J., Li, M., & Liu, Z. (2015). Structural mechanism underlying the specific recognition between the Arabidopsis state-transition phosphatase TAP38/PPH1 and phosphorylated light-harvesting complex protein Lhcb1. *The Plant Cell*, 27(4), 1113-1127.
- Werner, A. K., Sparkes, I. A., Romeis, T., & Witte, C.-P. (2008). Identification, biochemical characterization, and subcellular localization of allantoate amidohydrolases from Arabidopsis and soybean. *Plant physiology*, 146(2), 418-430.
- White, A. R., Xin, Y., & Pezeshk, V. (1993). Xyloglucan glucosyltransferase in Golgi membranes from *Pisum sativum* (pea). *Biochemical Journal*, 294(1), 231-238.
- Wienk, H. L., Czisch, M., & de Kruijff, B. (1999). The structural flexibility of the preferredoxin transit peptide. *FEBS letters*, 453(3), 318-326.
- Wu, X., Steet, R. A., Bohorov, O., Bakker, J., Newell, J., Krieger, M., Spaapen, L., Kornfeld, S., & Freeze, H. H. (2004). Mutation of the COG complex subunit gene COG7 causes a lethal congenital disorder. *Nature medicine*, 10(5), 518-523.
- Wu, Z., Liang, F., Hong, B., Young, J. C., Sussman, M. R., Harper, J. F., & Sze, H. (2002). An endoplasmic reticulum-bound $\text{Ca}^{2+}/\text{Mn}^{2+}$ pump, ECA1, supports plant growth and confers tolerance to Mn^{2+} stress. *Plant physiology*, 130(1), 128-137.
- Xing, J., Liu, P., Zhao, L., & Huang, F. (2017). Deletion of CGLD1 impairs PSII and increases singlet oxygen tolerance of green alga *Chlamydomonas reinhardtii*. *Frontiers in plant science*, 8, 2154.
- Yang, C. H., Wang, C., Singh, S., Fan, N., Liu, S., Zhao, L., Cao, H., Xie, W., Yang, C., & Huang, C. F. (2021). Golgi-localised manganese transporter PML3 regulates Arabidopsis growth through modulating Golgi glycosylation and cell wall biosynthesis. *New Phytologist*.
- Zeinert, R., Martinez, E., Schmitz, J., Senn, K., Usman, B., Anantharaman, V., Aravind, L., & Waters, L. S. (2018). Structure–function analysis of manganese exporter proteins across bacteria. *Journal of Biological Chemistry*, 293(15), 5715-5730.
- Zhang, B., Zhang, C., Liu, C., Fu, A., & Luan, S. (2021). A Golgi-localized manganese transporter functions in pollen tube tip growth to control male fertility in Arabidopsis. *Plant communications*, 2(3), 100178.
- Zhang, B., Zhang, C., Liu, C., Jing, Y., Wang, Y., Jin, L., Yang, L., Fu, A., Shi, J., & Zhao, F. (2018). Inner envelope CHLOROPLAST MANGANESE TRANSPORTER 1 supports manganese homeostasis and phototrophic growth in Arabidopsis. *Molecular plant*, 11(7), 943-954.
- Zhu, W., & Richards, N. G. (2017). Biological functions controlled by manganese redox changes in mononuclear Mn-dependent enzymes. *Essays in biochemistry*, 61(2), 259-270.

10 Appendix

10.1 List of Protein Sequences

Sequences from: <http://aramemnon.uni-koeln.de/> Accessed: 01.07.2021

PAM71 (At1g64150.1):

MLSLNLSESLRIPFQNPRPPKSDFSSTSSSPSSSSRRRCVSAYPIPIGFSVRNQYFSRCLTQLRRNESQQLGFRCL
FQRNDAACYLEKAEESEHNRNLDVLVESSIAHSRREIQRVLMFLAVSGSVALLGTDPAFAASSIPNVTQSLV
TSFGDLGDISSGFASAFLLIFFSELGDKTFFIAALLAARNSAATVFGTFGALGIMTIISVVLGRTFHYVDEV
L PFRFGGTDLPIDDIAAVCLLVYFGVSTLLDAVSDEGKADEEQKEAELAVSELGNGAGIVAAANTIISTFALV
FVAEWGDKSFFSTIALAAASSPLGVIAGALAGHGAATLLAVLGGSLGNFLSEKAIAYVGGVLFVFAAVTV
AEIVT

CMT1 (At4g13590.1):

MKLTSLSKNANSTATAVTVSSIQKLPFLSLSETLPCPKSSRKPTFLPLRCRRRPKDLLWGKFRVRASDAGV
GSGSYSGGEEDGSQSSSLDQSPATSSSELKPRGPFYPYLSIALVLLSCGLVFSLITFVKGGPSSVLA AVAKSGF
TAAFSILFVSEIGDKTFFIAALLAMQYEKTLVLLGSMGALSMTILSVVIGKIFQSVPAQFQTTLPIGEYAAIAL
LMFFGLKSIKDAWDLPPVEAKNGEETGIELGEYSEAEELVKEKASKKLTNPLEILWKSFSLSLVFFAEWGD
RSLATVALGAAQSPGLGVASGAIAAGHLVATVLAIMGGAFLANYISEKLVGVVGGALFLVFAAATFFGVF

HMA6 (At4g33520.1):

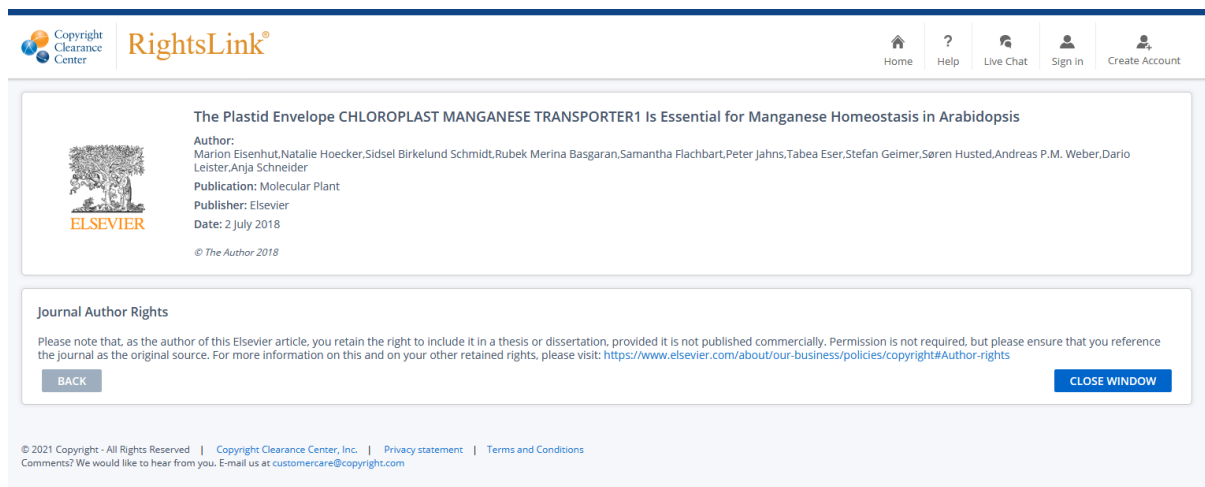
MESTLSAFSTVKATAMARSSGGPSLPLLTISKALNRHFTGARHLHPLLLARCSPSVRRLLGGFHGSRFTSSNS
ALRSLGAAVLPVIRHRLECLSSSSPSFRSISSSGGSGFGGYNGGSGGGGGGGSES GDSKSKLGANASDGV
SVPSSDIILDVGGMTCGGCSASVKKILESQPQVASASVNLTTETAIVWPVPEAKSVPDWQKSLGETLANHL
TNCGFQSTPRGEVPEDIAGEFAP

HMA8 (At5g21930.1):

MASNLLRFPLPPSSLHIRPSKFLVNRCFPLRRSRIRRHCSRPFLLVSNVSEISTQSFESTE SIESVKSITS
DTPILLDVSGMMCGGCVARVKSVMSSDDRVASAVVNMLTETA AVKFKPEVEVTADTAESLAKRLTESGFEA
KRRVSGMGVAENVKKWKEMVSKKEDLLVKSRRNVAFAWTLVALCCGSHTSHILHSLGIHIAHGGIWDLL
HNSYVKGGGLAVGALLGPGRELLFDGIKAFGKRSPNMNSLVGLGSMAAFSISLISLVNPELEWDASFFDEPV
MLLGFVLLGRSLEERAKLQASTDMNELLSLISTQSRLVITSSDNNTPVDSVLSSDSICINVSVD DIRVGD
SLLVLPGETFPVDGSLVLAGRSVVD ESMLTGESLPVFKEEGCSVSAGTINWDGPLRIKASSTGSNSTISKIVRMV
EDAQGNAAAPVQRLADAIAGPFVYTIMSLSAMTFAFWYYYVGS HIFPDVLLNDIAGPDGDALALSLKLA
VDV LVVSCPCALGLATPTAILIGTSLGAKRGYLIRGGDVLERLASIDCV ALDKTGTLTEGRPVVSGVASLG
YEEQE VLKMAAAVEKTATHPIAKAIVNEAESLNLKTPETRGQLTEPGFGLAEIDGRFVAVGSLEWVSDRFLK
KND SSDMVKLESLLDHKLSNTSSTSRYSKTVVYVGREGEGIIGAIAISDCLRQDAEFTVARLQEKGIKTVLLS
GDR EGAVATVAKNVGIKSESTNYSLSPEKKFEFISNLQSSGHRVAMVGDGINDAPSLAQADVGIALKIEAQENA
ASNAASVILVRNKL SHVVDALSLAQATMSKVYQNLAWAIAYNVISIPIAAGVLLPQYDFAMTPSLSGGLM
ALSSIFVVSNSLLLQLHKSETSKNSL

10.2 Permission for republication

10.2.1 Publication I: The Plastid Envelope CHLOROPLAST MANGANESE TRANSPORTER1 Is Essential for Manganese Homeostasis in *Arabidopsis*



The Plastid Envelope CHLOROPLAST MANGANESE TRANSPORTER1 Is Essential for Manganese Homeostasis in *Arabidopsis*

Author:
Marion Eisenhut, Natalie Hoecker, Sidsel Birkelund Schmidt, Rubek Merina Basgaran, Samantha Flachbart, Peter Jahns, Tabea Eser, Stefan Geimer, Søren Husted, Andreas P.M. Weber, Dario Leister, Anja Schneider

Publication: Molecular Plant

Publisher: Elsevier

Date: 2 July 2018

© The Author 2018

Journal Author Rights

Please note that, as the author of this Elsevier article, you retain the right to include it in a thesis or dissertation, provided it is not published commercially. Permission is not required, but please ensure that you reference the journal as the original source. For more information on this and on your other retained rights, please visit: <https://www.elsevier.com/about/our-business/policies/copyright#author-rights>

[BACK](#) [CLOSE WINDOW](#)

© 2021 Copyright - All Rights Reserved | Copyright Clearance Center, Inc. | [Privacy statement](#) | [Terms and Conditions](#)
Comments? We would like to hear from you. E-mail us at customer-care@copyright.com

Can I use material from my Elsevier journal article within my thesis/dissertation? –

As an Elsevier journal author, you have the right to Include the article in a thesis or dissertation (provided that this is not to be published commercially) whether in full or in part, subject to proper acknowledgment; see [the Copyright page](#) for more information. No written permission from Elsevier is necessary.

This right extends to the posting of your thesis to your university's repository provided that if you include the published journal article, it is embedded in your thesis and not separately downloadable.

Figure 8 <https://www.elsevier.com/about/policies/copyright/permissions> (accessed: 04.07.2021)

Information gained from the two websites (both accessed on 04.07.2021):

https://www.elsevier.com/_data/assets/pdf_file/0007/55654/AuthorUserRights.pdf

<https://www.elsevier.com/about/policies/copyright/permissions>

10.2.2 Publication II: Homologous Proteins of the Manganese Transporter PAM71 Are Localized in the Golgi Apparatus and Endoplasmic Reticulum

© 2020 by the authors (Hoecker, Honke, Frey, Leister, Schneider). Licensee MDPI, Basel, Switzerland. This article is an open access article distributed under the terms and conditions of the Creative Commons Attribution (CC BY) license (<http://creativecommons.org/licenses/by/4.0/>) (<https://www.mdpi.com/2223-7747/9/2/239/htm>, accessed 11.06.2021).

10.2.3 Publication III: Gene Replacement in Arabidopsis Reveals Manganese Transport as an Ancient Feature of Human, Plant and Cyanobacterial UPF0016 Proteins

© 2021 Hoecker, Hennecke, Schrott, Marino, Schmidt, Leister and Schneider. This is an open-access article distributed under the terms of the Creative Commons Attribution License (CC BY). The use, distribution or reproduction in other forums is permitted, provided the original author(s) and the copyright owner(s) are credited and that the original publication in this journal is cited, in accordance with accepted academic practice. No use, distribution or reproduction is permitted which does not comply with these terms (<https://www.frontiersin.org/articles/10.3389/fpls.2021.697848/abstract>, accessed 11.06.2021).

11 Acknowledgement

First, I want to express my thanks to my supervisor Anja Schneider for the interesting and promising projects I was able to work on since my bachelor thesis. I am deeply thankful for all the progress we successfully published in several papers and the continuous support for letting me turn into an autonomous scientist.

My special thanks go to Gabriele Burkhard, who taught me a lot since the very beginning and Sabine Jarzombski, for endowing in my projects and keeping a great and funny working atmosphere. I also want to thank Cordelia Bolle and Lisa-Marie for correcting this thesis.

I want to thank Prof. Dr. D. Leister for providing laboratory space and access to all the technical devices to perform my research. Additionally, I want to thank the DFG for funding my work.

Many heartfelt thanks to my collaboration partner, Marion Eisenhut and Sidsel Birkelund Schmidt, as well as Simon, Yvonne, Anna and Katharina and all the other people contributing to the projects. Thank you for your support.

I further want to thank my TAC committee for their great input and ideas to promote my projects. Additionally, I want to thank my graduate school LSM for accompany my journey and providing helpful workshops to educate myself in different fields.

Thanks to the whole AG Leister for critical discussion and their support.

I am deeply thankful for my former colleagues, Lisa-Marie, Anna and Alex. Thank you for all the affable discussions, more important for all the coffee and cookie breaks and most importantly for becoming good friends.

Finally, my special ones. I am very grateful for my boyfriend Moritz for keeping me on track and helping me through phases where the progress was stagnating. And then a huge thank you to my whole family for unconditionally supporting me and giving me the opportunity to study and graduate. You are the best.